CHARACTERISING SUN1 MITOTIC PHOSPHORYLATION AND ITS EFFECTS ON LINC COMPLEX INTERACTIONS

Thesis submitted for the degree of

Doctor of Philosophy

at the University of Leicester

by

Jennifer Tulsi Patel BSc (Hons) (Nottingham Trent)

Department of Biochemistry

University of Leicester

September 2012

DECLARATION

The accompanying thesis submitted for the degree of Doctor of Philosophy, entitled "Characterising SUN1 mitotic phosphorylation and its effects on LINC complex interactions" is based on work conducted by the author in the Department of Biochemistry at the University of Leicester during the period between October 2008 and September 2012. All work in this thesis is original unless otherwise acknowledged in the text or by references. None of the work has been submitted for another degree in this, or any other University.

Signed:

Date:

Department of Biochemistry
University of Leicester
Lancaster Road
Leicester
LE1 9HN

ABSTRACT

Characterising SUN1 mitotic phosphorylation and its effects on LINC complex interactions

Jennifer Tulsi Patel

Mammalian inner nuclear membrane (INM) proteins, SUN1 and SUN2, interact with nesprins located on the outer nuclear membrane to form the linker of nucleoskeleton to cytoskeleton (LINC) complex. The complex acts as a molecular bridge connecting the cytoskeleton to the nuclear lamina. At its nucleoplasmic N-terminus, SUN1 interacts with lamin A/C, emerin and small nesprin isoforms, strengthening LINC complex anchorage at the NE and contributing to attachment of the nuclear lamina to the NE.

At the onset of mitosis, the nuclear envelope (NE) disassembles to allow chromosome segregation. Nuclear envelope breakdown (NEBD) is induced by partial disassembly of nuclear pore complexes and depolymerisation of the nuclear lamina, which weakens the NE allowing microtubule-dependent forces to physically tear open the NE. This process is initiated by phosphorylation of NPC components, the nuclear lamina and INM proteins by mitotic kinases.

This thesis aimed to determine whether SUN1 undergoes mitotic phosphorylation and to assess how phosphorylation impacts upon LINC complex interactions.

I found that SUN1 is phosphorylated specifically during mitosis at serines 48, 138 and 333. Furthermore, CDK1 is responsible for phosphorylation of S48 and S333, whilst PLK1 phosphorylates S138. Use of phospho-deficient mutants and kinase inhibitors supports these findings and indicates that additional kinases, particularly Aurora A, may also phosphorylate SUN1. Importantly, I showed loss of SUN1 interaction with N-terminal but not C-terminal binding partners in mitotic extracts. A triple phospho-mimetic mutant also displayed increased solubility and reduced retention at the NE. My data demonstrate that mitotic SUN1 phosphorylation does not disrupt the LINC complex itself but is required for its dissociation from the nuclear lamina, presumably promoting NEBD.

In addition, by implementing an immunoprecipitation-mass spectrometry approach, I identified numerous potential binding partners for SUN1. My data suggest that SUN1 may be involved in many other protein networks beyond the LINC complex.

ACKNOWLEDGEMENTS

First and foremost I would like to thank my supervisor Dr Sue Shackleton for giving me the opportunity to pursue a PhD as part of her laboratory group. The combination of Sue's subject knowledge, guidance and support over the past four years has given my research direction and equipped me with the skills necessary to become an independent researcher.

I would also like to thank Professor Andrew Fry for being a fountain of knowledge on my PhD journey. His insightful comments and drive for scientific discovery helped shape my research.

Thank you to past and present members of the Shackleton and Fry laboratories for their support and friendship, especially Dr Farhana Haque, Dr Suzy Prosser and Dr Laura O'Regan.

A special thanks goes to Lindsey Smith, Alice Barkell and Sheree Purmessur. We started our PhD journey's together and have supported each other ever since. My final year would have been impossible without the help of some truly wonderful friends, thank you Jesvin Samuel, Emma Kelsall, Sarah Sabir and Navdeep Sahota.

I want to thank my family who never lost faith and encouraged me to be the best I can be. Mum and dad, thank you for the spur-of-the-moment trips to see me and bringing me back to earth when things got too much. Jason-bhai and Mamta-bhabi, thank you for your constant encouragement and belief in me when I felt the odds were stacked against me. Justin-bhai and Pinky-bhabi, thank you for always being there and raising my spirits. Thank you to my nieces, Sakshi, Mili and Rishi for your unconditional love.

I reserve my biggest expression of gratitude for Steven Cairns, my fiancé. He has been my tower of strength, supporting me through the highs and lows that a PhD brings. His patience and blind faith in my ability to achieve in life is the reason I have got this far.

CONTENTS

ABBREVIATIONS

^{o}C	degrees Celsius
%	percentage
^{32}P	^{32}phosphorus
^{35}S	^{35}sulphur
AEBSF	4-(2-aminoethyl)-benzenesulphonyl fluoride
ANC-1	Nuclear anchorage defect gene 1
APC/C	Anaphase promoting complex/cyclosome
APS	ammonium persulphate
ARVC	Arrhythmogenic ventricular cardiomyopathy
ATCC	American type culture collection
ATP	adenosine triphosphate
At	*Arabidopsis thaliana*
A.thaliana	*Arabidopsis thaliana*
AtRanGAP1	*Arabidopsis thaliana* RanGTPase activating protein 1
AtSUN	*Arabidopsis thaliana* SUN-domain protein
AtWIP	*Arabidopsis thaliana* WPP domain-interacting protein
BAF	Barrier of autointegration factor
Bqt	Bouquet
BrdU	bromodeoxyuridine
BSA	bovine serum albumin
Btf	BCL1-associated transcription factor
C-	carboxy-
CAAX	cysteine–aliphatic residue–aliphatic residue–any residue
Ca^{2+}	calcium ion
$CaCl_2$	calcium chloride
Cdc	Cell division cycle
CDK	Cyclin-dependent kinase
cDNA	complementary DNA
Ce	*Caenorhabditis elegans*
C.elegans	*Caenorhabditis elegans*

CH	Calponin homology
ChIP	chromatin-immunoprecipitation
cm	centimetre
CMT	Charcot-Marie-Tooth disease
cNLS	classical NLS
Co-IP	co-immunoprecipitation
CO_2	carbon dioxide
DAPI	4',6-diamidino-2-phenylindole
DCM	Dialated cardiomyopathy
D.discoideum	*Dictyostellium discoideum*
DHC-1	Dynein heavy chain-1
dH_20	distilled water
Dm	*Drosophila melanogaster*
D.melanogaster	*Drosophila melanogaster*
DMEM	Dulbecco's modified eagle medium
DMSO	dimethylsulfoxide
DNA	deoxyribonucleic acid
dsDNA	double stranded DNA
DTT	dithiothreitol
ECL	enhanced chemiluminescence
E.coli	*Escherichia coli*
EMD	Emerin gene (human)
EDMD	Emery Dreifuss muscular dystrophy
EDTA	ethylene diamine tetra acetic acid
e.g.	exempli gratia
ER	endoplasmic reticulum
et al.	et alia (and others)
EtBr	ethidium bromide
FACE-1	Farnesylated protein-converting enzyme-1
FACS	fluorescence activated cell sorting
FBS	fetal bovine serum

FG	phenylalanine-glycine
FHL	Four and a half LIM domain protein
FL	full-length
FPLD	Familial partial lipodystrophy
FRAP	fluorescence recovery after photo-bleaching
g	gram
G0	G zero
G1	gap 1
G2	gap 2
GAPDH	glyceraldehyde-3-phosphate dehydrogenase
GCL	Germ cell less
GE	glycine eluate
GFP	green fluorescent protein
Gp210	Glycoprotein 210 kDa
GTP	guanosine triphosphate
H	hour
HA	Hemagglutinin
hALP	Human acetyltransferase-like protein
HAT1	Histone acetyltransferase 1
HCl	hydrochloric acid
HDAC 10	Histone deacetylase 10
HeLa	Henrietta Lack
HEPES	4-(2-hydroxyethyl)-1-piperazineethanesulfonic acid
HGPS	Hutchinson-Gilford progeria syndrome
HP1	Heterochromatin protein 1
HRP	horse-radish peroxidase
hSUN	human SUN-domain protein
ICMT	Isoprenylcysteine carboxyl methyltransferase
Ig	immunoglobulin
IgG	immunoglobulin G
Ima1	Integral membrane protein 1

IMAC	immobilised metal affinity chromatography
INM	inner nuclear membrane
IP	immunoprecipitation
IPTG	isopropyl-β-D-thiogalactopyranoside
IVT	*in vitro* translation
KASH	Klarsicht, ANC-1, Syne-1 homology
Kb	kilo base
KCl	potassium chloride
kDa	kilo Daltons
KDP-1	KASH-domain protein 1
KH_2PO_4	potassium di-hydrogen orthophosphate
KIF20A	Kinesin family member 20A
L	litre
LAP1	Lamin-associated protein
LB	Luria broth
LBR	Lamin B receptor
LC-MS/MS	liquid chromatography-mass spectrometry/mass spectrometry
LEM	LAP, emerin, MAN1
LGMD-1B	Limb girdle muscular dystrophy-1B
LINC	Linker of nucleoskeleton to cytoskeleton
LMNA	Lamin A/C gene (human)
Lmna$^{-/-}$	Lamin A/C gene (mouse) null
LMNB1	Lamin B1 gene (human)
LMNB2	Lamin B2 gene (human)
M	mitosis
M	molar
mA	milli-ampheres
MBP	maltose binding protein
MDa	mega Daltons
MEFs	mouse embryonic fibroblast
mg	milli-gram

$MgCl_2$	magnesium chloride
Mg^{2+}	magnesium ion
min	minutes(s)
ml	milli-litre
mM	milli-molar
mRNA	messenger ribonucleic acid
MS	mass spectrometry
MTOC	Microtubule organising centre
Mps3	Monopolor spindle 3
Msp-300	Muscle-specific protein 300 kDa
mSUN1	mouse SUN-domain protein
Myne	Myocyte nuclear envelope
µg	micro-gram
µl	micro-litre
µm	micro-meter
µM	micro-molar
N-	amino-
NaCl	sodium chloride
NaF	sodium fluoride
NaH_2PO_4	sodium di-hydrogen orthophosphate
NaOAc	sodium acetate
NaOH	sodium hydroxide
Na_2HPO_4	di-sodium hydrogen orthophosphate
NE	nuclear envelope
NEBD	nuclear envelope breakdown
NES	nuclear export signal
Nesprin	Nuclear envelope spectrin repeat proteins
NET	nuclear envelope transmembrane protein
NETN	nonident P-40, EDTA, Tris-HCl, NaCl buffer
ng	nano-gram

NIH 3T3	National institute of health (3-day transfer, inoculum 3 x 10^5 cells) mouse fibroblast cell line
NIMA	Never in mitosis A
NLS	nuclear localisation signal
nm	nano-meter
nM	nano-molar
Noc	nocodazole
NP-40	nonident P-40
NPC	nuclear pore complex
NUANCE	Nucleus and actin connecting element
Nup	nucleoporin
Nurim	nuclear rim
OD_{600}	optical density (absorbance) at 600 nm
ONM	outer nuclear membrane
PBD	Plectin binding domain
PBS	phosphate-buffered saline
PCNA	Proliferating cell nuclear antigen
PFA	paraformaldehyde
pH	potential of hydrogen
PI	propidium iodide
PKA	Protein kinase A
PKC	Protein kinase C
PLK	Polo-like kinase
PMSF	phenylmethylsulfonyl fluoride
PNACL	Protein Nucleic Acid Chemistry Laboratory
PNS	perinuclear space
POM	pore membrane
PP1	Protein phosphatase 1
PP2A	Protein phosphatase 2A
pS48	human SUN1 serine 48 phospho-specific antibody
PROTEX	Protein Expression laboratory

RanBP1	Ran binding protein 1
RanGAP1	RanGTPase activating protein 1
RanGDP	Ran guanosine diphosphate
RanGEF	Ran guanine exchange factor
RanGTP	Ran guanosine triphosphate
Rb	Retinoblastoma protein
RBBP4	Retinoblastoma binding protein 4
RCC1	Regulator of chromosome condensation 1
RCC2	Regulator of chromosome condensation 2
RCE1	Ras-converting enzyme-1
RFC	Replication factor C
RNA	ribonucleic acid
RNAi	ribonucleic acid interference
rpm	revolutions per minute
RT	room temperature
RT-PCR	reverse-transcriptase polymerase chain reaction
s	second(s)
S	synthesis
SAC	Spindle assembly checkpoint
Sad1	Spindle architecture disrupted 1
SAF	Spindle assembly factor
SAMP1	Spindle-associated membrane protein 1
S.cerevisiae	*Saccharomyces cerevisiae*
SDEL	serine-aspartic acid-glutamic acid-leucine
SDS-PAGE	sodium dodecyl sulphate-polyacrylamide gel electrophoresis
siRNA	small interfering RNA
SPAG-4	Sperm associated antigen-4
SPAG-4L	Sperm associated antigen-4-like
SPB	Spindle pole body
S.pombe	*Saccharomyces pombe*
SR	spectrin repeat

SREBP1	Sterol regulatory element binding protein-1
SUN	Sad1, Unc-84 homology
Syne	Synaptic nuclear envelope
TAE	tris, acetic acid, EDTA buffer
TAN	Transmembrane actin-associated
TBS	tris-buffered saline
TD-60	Telophase disc-60
TEA	triethylammonium chloride
TEMED	N,N,N',N'-tetramethylethylethylenediamine
TMD	transmembrane domain
TMEM43	Transmembrane protein 43
TGF-β	Transforming growth factor-β
TNT®	transcription and translation
U	untransfected
UNC	Uncoordinated
U2OS	human Osteosarcoma cell line
V	voltage
v/v	volume/volume
WB	western blot
WT	wild-type
w/v	weight/volume
X-EDMD	X-linked Emery Dreifuss muscular dystrophy
xg	gravity force
ZMPSTE24	Zinc metalloprotease related to yeast Ste24p
ZYG-12	Zygote defective-12

FIGURES AND TABLES

CHAPTER 1
Introduction

Chapter 1 Introduction

1.1 Nuclear Envelope

The eukaryotic nucleus houses the genetic material and is the site of DNA replication, RNA transcription and processing, as well as ribosome subunit assembly. During interphase, the DNA is enclosed in the nucleus by a structure known as the nuclear envelope (NE) which serves to segregate the cytoplasmic and nuclear compartments of the eukaryotic cell. In addition to its role as a barrier and structural support for the nucleus, the NE also provides anchorage sites for chromatin at the nuclear periphery. This allows the temporal control of nuclear events such as DNA replication, gene expression and mitotic entry (Dechat *et al.*, 2008; Mekhail & Moazed, 2010).

The NE is comprised of an outer nuclear membrane (ONM) and an inner nuclear membrane (INM). The ONM is continuous with, and has similar biochemical properties to the endoplasmic reticulum (ER), as both have ribosomes embedded on their surface. The INM differs in that it harbours a distinct set of integral membrane proteins, many of which have not been fully characterised (Dreger *et al.*, 2001; Schirmer *et al.*, 2003). They are generally anchored at the INM through interactions with the nuclear lamina and/or chromatin. The two membranes are fused at the periphery by nuclear pore complexes (NPCs) (Dechat *et al.*, 2008; Broers *et al.*, 2006; Foisner, 2003; Gruenbaum *et al.*, 2005) (**Figure 1.1**). The NPC allows the bi-directional transport of macromolecules in and out of the nucleus and helps maintain the 100 nm lumenal spacing between the INM and the ONM, known as the perinuclear space (PNS) (Tran & Wente, 2006).

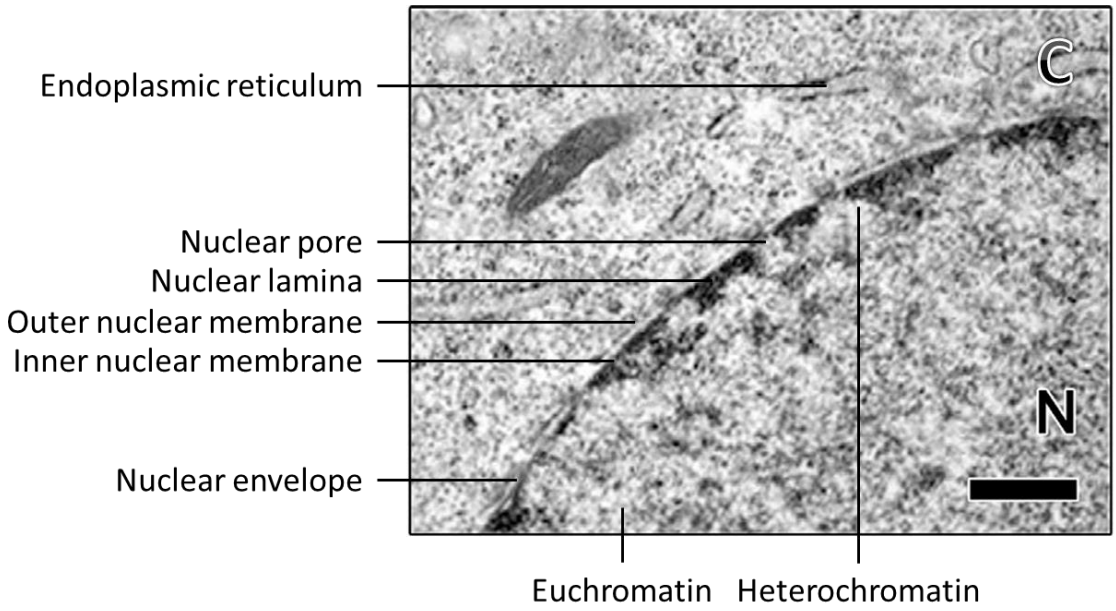

Figure 1.1. Electron micrograph of a mammalian cell nucleus in cross-section.

Transmission electron microscopy image of a HeLa cell. The nucleoplasm (N) and cytoplasm (C) are segregated into two compartments by the presence of the nuclear envelope (NE). The NE is a double membrane structure composed of the outer (ONM) and inner nuclear membranes (INM) which are fused together at the site of nuclear pores. The ONM is continuous with the endoplasmic reticulum (ER) while the INM harbours a unique set of integral proteins. These proteins interact with components of the nuclear lamina and chromatin. The nuclear lamina is a filamentous network underlying the INM. It anchors integral membrane proteins at the INM and provides docking sites for chromatin. Scale bar 0.5 µm. Adapted from (Mitchell *et al.*, 2010). Full re-use permission granted.

1.1.1 Nuclear pore complex (NPC)

The ONM and INM of the NE are separated by the lumenal PNS but are fused together at certain points in the membrane to form channels where NPCs are inserted (D'Angelo *et al.*, 2006). The NE is embedded with thousands of NPCs as seen in **Figure 1.2** and **Figure 1.5**. NPCs are large multi-protein complexes that range in size from 60-125 MDa depending on the species (D'Angelo & Hetzer, 2008). The NPC mediates the flow of macromolecules between the cytoplasm and nucleus (Tran & Wente, 2006). The site of ONM and INM fusion at the NPC is known as the pore membrane (POM) domain.

1.1.1.1 NPC structure

The NPC is comprised of multiple copies of approximately 30 nuclear pore proteins otherwise known as nucleoporins or Nups (Cronshaw *et al.*, 2002). Most nucleoporins are organised into subcomplexes with copies or multiples of eight owing to its octagonal arrangement as described below (**Figure 1.3**).

The eight-fold rotational symmetry of the NPC complex transpires through a scaffold structure anchored to the annular fenestrations of the NE that surround the central transport channel. Two ring structures are bound to the scaffold, one either side of the channel in the nucleus and cytoplasm. Filaments (fibrils) are attached to each ring, the cytoplasmic filaments are loose, while the nuclear filaments are bound at the distal end to another ring in a nuclear basket formation (D'Angelo & Hetzer, 2008) (**Figure 1.2** and **Figure 1.5**).

Figures 1.2A and 1.2B have been omitted for copyright reasons. Please refer to Fahrenkrog & Aebi (2003) box 1c and box 1b, respectively, or the hard copy version of this thesis for the images.

Figure 1.2. Visualisation of the nuclear pore complex from various angles.

(A) Thin sections of embedded *Xenopus* nuclear envelopes. Cross-section image shows the nuclear pore complexes with the nuclear basket and the cytoplasmic filaments. **(B)** Transmission electron micrographs of nuclear pore complexes from *Xenopus* nuclear envelope samples show a clear basket formation on the nuclear face and the tips of the cytoplasmic filaments on the cytoplasmic face. Scale bar 100 nm. Adapted from (Fahrenkrog & Aebi, 2003). Restricted re-use permission granted.

Figures 1.3A and 1.3B have been omitted for copyright reasons. Please refer to D'Angelo & Hetzer (2008) figures 1a and 1b, respectively, or the hard copy version of this thesis for the images.

Figure 1.3. Schematic representation of the nuclear pore complex structure.

(A) Schematic representation of a cross-section of a nuclear pore complex (NPC) showing the nuclear ring attached to the basket structure in the nucleoplasm and the cytoplasmic ring with the attached cytoplasmic filaments. The central scaffold at the interface of the nuclear and cytoplasmic rings anchors the NPC in place and the central channel mediates movement across the nuclear envelope. **(B)** Possible localisation of the 30 different nucleoporins that make up the NPC in an eight-fold symmetry manner. The NPC consists of individual proteins and subcomplexes. The central scaffold is anchored through transmembrane nucleoporins gp210, POM121 and Ndc1 embedded in the pore membrane domain. Adapted from (D'Angelo & Hetzer, 2008). Restricted re-use permission granted.

Anchorage of the NPC scaffold to the POM domain of the NE is mediated through transmembrane nucleoporins, only three of which are known in vertebrates: gp210, POM121 and Ndc1 (Gerace *et al.*, 1982; Greber *et al.*, 1990; Hallberg *et al.*, 1993; Stavru *et al.*, 2006). All three are involved in post-mitotic NPC assembly but gp210 is dispensable for this function, instead gp210 has a key role in NPC disassembly and nuclear envelope breakdown (NEBD) (Galy *et al.*, 2008).

1.1.1.2 Nucleo-cytoplasmic transport

The main function of the NPC is to maintain controlled nucleo-cytoplasmic transport across the NE. Proteins with a mass less than 40 kDa may be transported by passive diffusion through the central aqueous channel of the NPC. Those of a larger molecular weight require active transport (Paine *et al.*, 1975; Bonner, 1975).

The passage of large molecules is conducted through the energy-dependent RanGTPase system (**Figure 1.4**). Ran exists in two guanine nucleotide-bound conformations, RanGTP and RanGDP. In mammals, these states are controlled through Ran specific regulatory proteins RanGAP1 and RCC1. RanGAP1 is a cytoplasmic GTPase activating protein, aided by RanBP1 and RanBP2/Nup358 that help to maintain high concentrations of RanGDP in the cytoplasm. In contrast, chromatin-bound RCC1, a Ran guanine nucleotide exchange factor (RanGEF) maintains high levels of RanGTP in the nucleus. The gradient of the two Ran conformations across the NE drives nuclear transport (Fried & Kutay, 2003). Proteins destined for the nucleus contain a nuclear localisation signal (NLS) within their protein sequence. The classical NLS (cNLS) is comprised of one or two short stretches of sequence rich in positively charged amino acids lysine and arginine (Lange *et al.*, 2007). Likewise, proteins targeted to the

Figure 1.4 has been omitted for copyright reasons. Please refer to Clarke & Zhang (2004) figure 1, or the hard copy version of this thesis for the image.

Figure 1.4. Energy-dependent Ran GTPase nucleo-cytoplasmic transport system.

Proteins are actively transported in and out of the nucleus via components of the RanGTPase system. In the nucleus high levels of RanGTP are sustained while in the cytoplasm high levels of RanGDP are found. These gradients are maintained by Ran specific regulatory proteins RCC1 (RanGEF) and RanGAP1 (RanGTPase activating protein), respectively. Importins recognise and bind the nuclear localisation signal (NLS) on a protein surface and mediate its passage through the NPC. In the nucleus importins release the cargo by preferentially binding to RanGTP and both are transported back into the cytoplasm. Here, hydrolysis of RanGTP to RanGDP occurs with the help of accessory proteins RanGAP1, RanBP1 and RanBP2. In a similar way, in the nucleus RanGTP binds exportins such as Crm1 bind the nuclear export signal (NES) of a protein cargo for transportation into the cytoplasm. In the cytoplasm the accessory proteins hydrolyse RanGTP to RanGDP disassembling the export complex. RanGDP and exportins are translocated back to the nucleus separately where RCC1 exchanges the GDP for a GTP. Adapted from (Clarke & Zhang, 2004). Restricted re-use permission granted.

cytoplasm exhibit a nuclear export signal (NES), the best characterised is a short sequence rich in leucine residues (Wen *et al.*, 1995). The NLS and NES sequences are recognised by carrier proteins known as karyopherins. The two types of karyopherins are importins, which transport protein cargos into the nucleus, and exportins, which move protein to the cytoplasm (Lange *et al.*, 2007).

Importin-α binds the NLS sequence of proteins and importin-β to mediate transport through the NPC. The cargo goes through a series of associations and disassociations with nucleoporins rich in phenylalanine-glycine (FG) motifs to travel through the pore channel. Once in the nucleus, RanGTP binds importin-β, releasing importin-α from the protein load. RanGTP bound to the importins are recycled back to the cytoplasm where RanGTP is hydrolysed to RanGDP by RanGAP1 assisted by accessory proteins RanBP1 and RanBP2/Nup358 (Fried & Kutay, 2003) (**Figure 1.4**).

Transfer of proteins to the cytoplasm works in a similar but reverse manner. In the nucleus RanGTP binds exportins, which increases the affinity of exportins for the NES-containing protein cargo. These are transported across the NE through NPCs to the cytoplasm where hydrolysis of the RanGTP to RanGDP by RanGAP1, causes the export complex to disassemble. Exportins and RanGDP are then transported back separately to the nucleus where RCC1 promotes the exchange of GDP to GTP (Fried & Kutay, 2003) (**Figure 1.4**).

1.1.2 Nuclear Lamina

Located at the interface between the INM and chromatin is the nuclear lamina. The nuclear lamina is a highly insoluble filamentous meshwork of type V intermediate

filaments and lamin-binding proteins (**Figure 1.5**). It structurally supports the nucleus and ensures mechanical stability as well as maintaining nuclear shape in interphase. The nuclear lamina is connected to the NE via interactions with INM proteins and together they provide anchorage sites for heterochromatin at the nuclear periphery. The lamina is also involved in many nuclear functions such as DNA replication and RNA polymerase II-dependent transcription (Foisner, 2003; Gruenbaum *et al.*, 2005).

The major components of the nuclear lamina are A-type and B-type lamins, which are grouped according to their biochemical properties and behaviour in mitosis (Gerace & Blobel, 1980; Stuurman *et al.*, 1998). A-type lamins are encoded by a single gene, *LMNA,* which produces the alternatively mRNA spliced isoforms lamins A, AΔ10, C and C2. Lamins A and C are the major A-type isoforms and are expressed at approximately equal levels in most somatic cells. They differ due to alternative splicing in exon 10 of the 12 exon *LMNA* gene. Lamins A and C are identical from amino acid residues 1-566 (Dechat *et al.*, 2008). However, lamin C lacks exons 11 and 12 and also has five distinctive amino acids at its N-terminus (Fisher *et al.*, 1986). Lamin AΔ10 lacks exon 10 while lamin C2 is germline-specific (Machiels *et al.*, 1996; Furukawa *et al.*, 1994) (**Figure 1.6**). A-type lamins are developmentally regulated and are expressed in differentiated cells but absent from early embryos, suggesting tissue-specific functions (Lin & Worman, 1993). B-type lamins are essential for cell viability and are encoded by two genes, *LMNB1,* which encodes lamin B1, and *LMNB2,* which encodes lamins B2 and B3 (Lin & Worman, 1995; Hoger *et al.*, 1988; Hoger *et al.*, 1990; Furukawa & Hotta, 1993) (**Figure 1.6**). All nucleated somatic cells express at least one of the B-type lamins

Figure 1.5 has been omitted for copyright reasons. Please refer to Stuurman *et al.* (1998) figure 2, or the hard copy version of this thesis for the image.

Figure 1.5. Electron micrograph of *Xenopus laevis* oocyte nuclear lamina.

Transmission electron microscopy of nuclear envelope prepared from *Xenopus laevis* oocytes shows the nuclear lamina meshwork partially perforated by nuclear pore complexes. Inset shows a higher magnification of the nuclear lamina with particular emphasis on the net-like structure. Scale bar 1 µm. Taken from (Stuurman *et al.*, 1998). Restricted re-use permission granted.

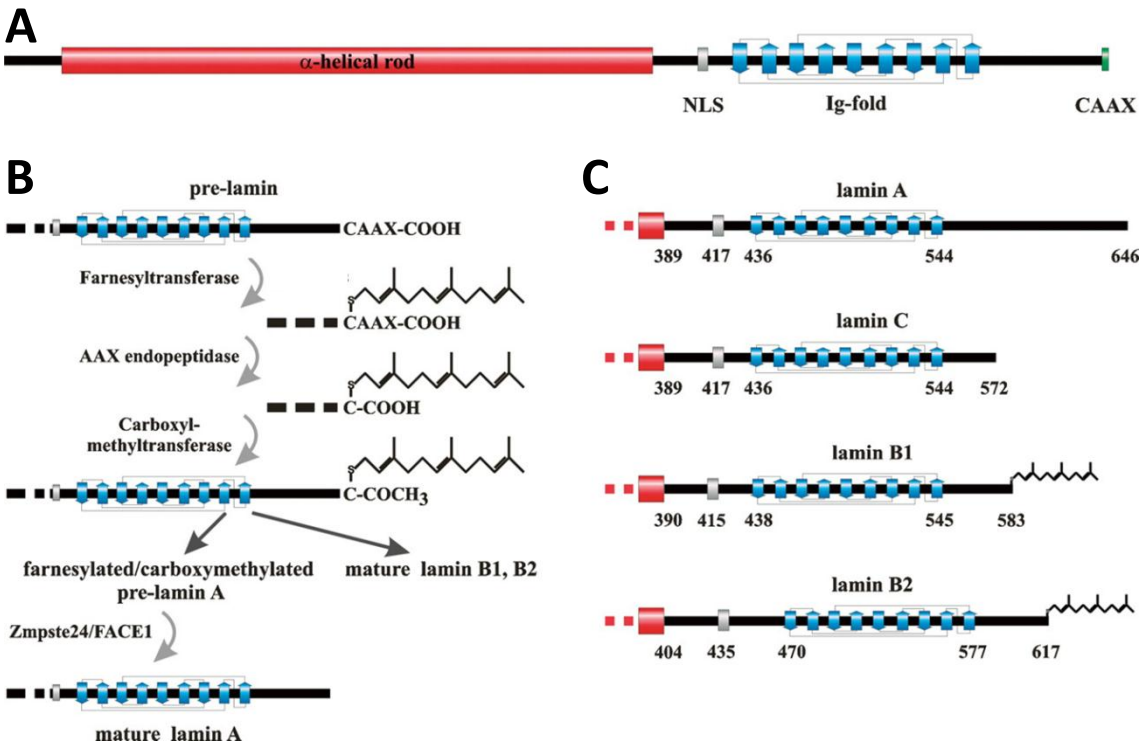

Figure 1.6. Nuclear lamin isoforms, structures and processing.

(A) Schematic representation depicting the N-terminal α-helical rod-domain (red), nuclear localisation signal (NLS) (grey), immunoglobulin (Ig) fold (blue) and the C-terminal CAAX motif (green). **(B)** Processing of nascent lamins to mature lamins requires farnesylation of the cysteine residue in the CAAX motif, which induces the proteolytic cleavage of the AAX residues by an endopeptidase. The cysteine is then carboxy-methylated producing mature lamin B1 and lamin B2. Lamin A is further processed by cleavage of an additional 15 amino acids including the farnesylated and carboxy-methylated cysteine by ZMPSTE24/FACE-1 to form the mature protein. **(C)** Schematics of the C-terminal domains of the mature lamin isoforms after processing. Lamin A does not retain the farnesyl group while lamin B1 and B2 do. Various amino acid boundaries for each of the isoforms are indicated. Adapted from (Dechat *et al.*, 2008). Full re-use permission granted.

during development, although lamin B3 is only expressed in spermatocytes (Broers *et al.*, 2006).

Vertebrates have multiple lamin isoforms whereas arthropods and invertebrates may possess one or two. *Caenorhabditis elegans (C.elegans)* has a single lamin protein, lmn-1, which is expressed in all cells except mature sperm, and is thought to behave in a similar manner to B-type lamins. *Drosophila melanogaster (D.melanogaster)* possesses two lamins, Dm_o expressed in all cells throughout development and DmC expressed in late embryonic stages and differentiated cells. Yeast and plants do not have lamins (Goldman *et al.*, 2002).

As well as residing at the nuclear periphery, lamins have also been observed in the nucleoplasm through the use of immunofluorescence microscopy and live-cell imaging with GFP-lamins. They present as well-defined foci or general fluorescence (Shumaker *et al.*, 2003).

1.1.2.1 Lamin structure

The general lamin structure consists of a central rod-domain flanked by a short N-terminal head domain and a C-terminal globular tail domain (Gerace & Burke, 1988; Dechat *et al.*, 2009) (**Figure 1.6**).

The central rod-domain is composed of four coiled-coiled regions, 1A, 1B, 2A and 2B separated by linker regions L1, L2 and L3. The rod-domain promotes dimerization of lamin polypeptide chains. The head and tail regions of these dimers mediate head-to-tail polymer assembly and higher order assembly to form 10 nm filaments (Stuurman *et al.*, 1998). Between the central α-helical rod-domain and the tail region is a NLS

sequence responsible for targeting lamins to the nucleus (Fisher *et al.*, 1986). Structural studies have shown that lamins harbour an immunoglobulin-like fold (Ig-fold) within the C-terminal domain (Dhe-Paganon *et al.*, 2002; Krimm *et al.*, 2002). All lamins, with the exception of lamin C, have a CAAX box motif at the extreme C-terminus where the C refers to cysteine, A represents an aliphatic residue and X denotes any residue. This sequence is required for processing of lamins to their mature forms (Rusinol & Sinensky, 2006).

1.1.2.2 Lamin processing

After synthesis, all lamins, except lamin C, undergo a series of post-translational modifications to form the mature lamin polypeptides. The cysteine of the CAAX motif is first farnesylated to aid its membrane association with the NE. This is followed by C-terminal cleavage of the C-terminal three residues of the CAAX motif by endopeptidase zinc metalloprotease related to yeast Ste24p (ZMPSTE24)/farnesylated protein-converting enzyme-1 (FACE-1) for lamin A or Ras-converting enzyme-1 (RCE-1) for lamin B. Finally, the cysteine residue undergoes methyl esterification, which helps target the lamins to the INM. At this stage B-type lamins are ready for incorporation into the nuclear lamina but lamin A is processed further. An extra 15 amino acids, including the farnesylated cysteine residue, are cleaved from the C-terminus by ZMPSTE24/FACE-1 to form mature lamin A (Rusinol & Sinensky, 2006) (**Figure 1.6**). It is currently not known why lamin A undergoes transient farnesylation at its C-terminus but defects in this process, leading to premature ageing disorders have sparked huge interest in this area (**section 1.3**).

1.1.2.3 Functions of the nuclear lamina

The major roles of the nuclear lamina are to establish nuclear integrity and resistance to mechanical stress (Sullivan *et al.*, 1999; Broers *et al.*, 2004). Lamins are type V intermediate filaments whose principle property and function is to provide tensile strength to the NE through its rope-like structure (Alberts, 2002). The nuclei of *Lmna* wild-type mouse embryonic fibroblasts (MEFs) are roughly circular or oval shaped while *Lmna*$^{-/-}$ MEFs display elongated and highly irregular nuclear morphology (Sullivan *et al.*, 1999). These cells were co-stained with LAP2, Nup153 and lamin B, and all were lost from one pole of the nucleus. The nuclei remained intact but the nuclear membranes were herniated. NE herniation's coincided with regions showing loss or thinning of heterochromatin (Sullivan *et al.*, 1999). *Lmna* wild-type and *Lmna*$^{-/-}$ MEFs subjected to controlled mechanical stress by a compression device show that the nuclei have reduced resistance to mechanical strain (Broers *et al.*, 2004).

The lamin proteins are also involved in many other cellular roles, from maintenance of nuclear shape and size, to organisation of the nuclear architecture. Mouse spermatocytes exhibit a hook-shaped NE morphology which can be reproduced in spherical somatic COP5 cells upon expression of germline specific lamin B3 (Furukawa & Hotta, 1993). Cells from patients with the accelerated ageing disease Hutchinson-Gilford progeria syndrome (HGPS) show NE blebbing and thickening of the nuclear lamin due to accumulation of a truncated and farnesylated lamin A mutant (Goldman *et al.*, 2004). *In vitro* studies, where lamins were immuno-depleted from a cell-free nuclear assembly extract derived from *Xenopus* egg extract show that nuclei are fragile

and small (Newport *et al.*, 1990). Collectively, these studies support the idea that the nuclear lamina regulates the nuclear morphology.

The nuclear lamina forms connections with the integral membrane proteins of the INM and with chromatin and so has a major role in organisation of nuclear architecture. The nuclear lamina provides anchorage sites for chromatin and, in the absence of A-type lamins or overexpression of mutants, there is a thinning/loss of heterochromatin from the nuclear periphery and a clumping or loss of NPCs (Sullivan *et al.*, 1999; Goldman *et al.*, 2004). The lack of lamins in *Lmna*$^{-/-}$ MEFs prevents immobilisation of some of the integral membrane proteins such as emerin, SUN2, nesprin-1 and nesprin-2 which are mislocalised to the cytoplasm (Sullivan *et al.*, 1999; Crisp *et al.*, 2006; Libotte *et al.*, 2005). These examples highlight the importance of the nuclear lamina in NE architectural organisation.

Lamins are also key to nuclear processes such as chromatin organisation, transcription, DNA replication and splicing. Within the nucleus, chromatin is arranged in a highly organised manner through its connections with the nuclear lamina (Goldman *et al.*, 2002; Sullivan *et al.*, 1999). Chromatin exists in two forms, active euchromatin and inactive heterochromatin. Transcriptionally active genes generally localise to the nuclear interior while transcriptionally repressed genes are often silenced at the nuclear periphery (Croft *et al.*, 1999). In the absence of A-type lamins, there is a loss of heterochromatin from the NE periphery (Sullivan *et al.*, 1999). Some lamin-binding proteins also interact with chromatin (**Table 1.1**).

Table 1.1. Properties of mammalian integral membrane proteins.

Adapted mainly from (Burke & Stewart, 2006), further references indicated.

Name	Molecular weight	Lamin binding	Characteristics/functions
LAP1A	75 kDa	A-type B-type	LAP1 has three splice variants LAP1A, LAP1B and LAP1C. Splice variants share the same transmembrane and lumenal domain. Splice variants bind TorsinA via lumenal domain.
LAP1B	68 kDa	A-type B-type	
LAP1C	57 kDa	A-type B-type	
LAP2β	50 kDa	B-type	LEM domain. **DNA/Chromatin binding partners:** BAF (via LEM domain), HA95, HP1 (Ye & Worman, 1996) Directly to DNA (Furukawa *et al.*, 1997) Binds transcriptional regulator GCL (Nili *et al.*, 2001)
LAP2ε, δ, γ	38-46 kDa	Most likely A-types and B-types	Splice variants of LAP2β containing a transmembrane domain. LAP2α and LAP2ζ lack are soluble proteins (Foisner, 2003). **DNA/Chromatin binding partners:** BAF
Emerin	34 kDa (Bione *et al.*, 1994)	A-type B-type	LEM domain ONM and INM (Salpingidou *et al.*, 2007) Binds SUN1, SUN2, nesprins, MAN1 (Haque *et al.*, 2010; Wheeler *et al.*, 2007; Mansharamani & Wilson, 2005) Emerin defects lead to EDMD **DNA/Chromatin binding partners:** BAF (via LEM domain) Binds transcriptional regulator GCL and transcription factor Btf (Bengtsson & Wilson, 2004)
MAN1	82 kDa	A-type B-type	LEM domain N- and C-termini in nucleoplasm (Wu *et al.*, 2002) Binds emerin (Mansharamani & Wilson, 2005) **DNA/Chromatin binding partners:** BAF (via LEM domain) Binds transcriptional regulator GCL and transcription factor Btf (Mansharamani & Wilson, 2005) Binds SMAD protein inhibiting TGF-β signalling pathway
LBR	70 kDa	B-type	Multi-spanning protein Defects associated with Pelger-Huet and Greenberg skeletal dysplasia (Waterham *et al.*, 2003) Sequence homology with sterol reductase enzymes **DNA/Chromatin binding partners:** HP1, HA95, Histone H3 and H4 tetramers (Polioudaki *et al.*, 2001) Directly to DNA (Ye & Worman, 1994)

Nurim	29 kDa		Multi-spanning protein Unknown function Very short N-terminus Majority of protein embedded in NE Sequence homology with ICMT enzymes (Rolls *et al.*, 1999; Hofemeister & O'Hare, 2005)
TMEM43/ LUMA	45 kDa	A-type	Multi-spanning protein N- and C-termini in nucleoplasm Binds emerin and SUN2 Defects associated with ARVC and EDMD (Dreger *et al.*, 2001; Bengtsson & Otto, 2008; Liang *et al.*, 2011)
SAMP1	43 kDa		Multi-spanning protein Four CAAX motifs Spindle-associated in mitosis (Buch *et al.*, 2009)
SUN1	102 kDa	A-type Possible B-types	C-terminal SUN-domain Seven potential splice variants (Gob *et al.*, 2011) Component of LINC complex Binds emerin, nesprins and NPC components (Haque *et al.*, 2010; Liu *et al.*, 2007; Talamas & Hetzer, 2011) Aids decondensation of chromosomes in anaphase (Chi *et al.*, 2007) Telomere anchorage and homologous pairing in meiotic cells (Ding *et al.*, 2007)
SUN2	80 kDa	A-type Possible B-types	C-terminal SUN-domain Component of LINC complex Component of TAN lines (Luxton *et al.*, 2011) Binds emerin, nesprins and TMEM43 (Haque *et al.*, 2010; Liang *et al.*, 2011) Telomere anchorage and homologous pairing in meiotic cells (Schmitt *et al.*, 2007)
Nesprin-1	100-1000 kDa	A-type	C-terminal KASH-domain, spectrin repeats Some isoforms have CH domains which binds actin Component of LINC complex Many splice variants
Nesprin-2	50-800 kDa	A-type	C-terminal KASH-domain, spectrin repeats Some isoforms have CH domains which binds actin Component of LINC complex Many splice variants Component of TAN lines (Luxton *et al.*, 2011)
Nesprin-3	108 kDa (α) 99 kDa (β)		2 splice variants α and β Component of LINC complex Binds indirectly to intermediate filaments via plectin (Wilhelmsen *et al.*, 2005; Ketema *et al.*, 2007)
Nesprin-4	42 kDa		Expressed in secretory epithelium Kinesin-1 adaptor protein Binds indirectly to microtubules (Roux *et al.*, 2009)

Changes in lamin expression coincide with variations in gene expression patterns and suggest that the nuclear lamina may regulate transcription. It is thought that the expression of A-type lamins in differentiated cells promotes permanent changes in chromatin organisation, securing the cell in a modified state (Peter & Nigg, 1991).

The nuclear lamina associates with a wide range of transcription factors, below are just a few examples. The transcription repressor Oct-1, which represses the collagenase gene, localises with lamin B1 at the nuclear periphery. The repressive activity is only maintained while Oct-1 is associated with lamin B1 (Imai *et al.*, 1997). Retinoblastoma (Rb) protein binding to A-type lamins coincides with its transcriptional activity (Mancini *et al.*, 1994; Ozaki *et al.*, 1994). Sterol regulatory element binding protein-1 (SREBP1), binds A-type lamins and is involved in adipocyte differentiation (Lloyd *et al.*, 2002). The lamin-binding protein LAP2β interacts with transcription factor germ cell less (GCL) required for germline formation. Overexpression of either protein alone, or in combination, represses genes under the regulatory control of E2F-DP (Nili *et al.*, 2001).

Studies in support of the role of lamins in transcription show that ectopic expression of dominant-negative lamin mutants lacking the N-terminus in mammalian cells and *Xenopus laevis* embryonic nuclei, disrupts the organisation of the nuclear lamina. In turn this alters the distribution of basal transcription factors and prevents synthesis of RNA polymerase II-dependent transcripts (Spann *et al.*, 2002).

Research has shown that lamins are also essential for DNA replication. NIH 3T3 cells stained with lamin B antibody show lamin B at nuclear foci which colocalise with sites of bromodeoxyuridine (BrdU) incorporation and replication foci containing

proliferating cell nuclear antigen (PCNA) in late S phase (Moir *et al.*, 1994). In contrast, it appears that in primary cells, replication foci colocalise with A-type lamins in the early stages of DNA synthesis (Kennedy *et al.*, 2000). Experiments using *in vitro* assembled nuclei from *Xenopus* egg interphase extract immuno-depleted of lamins, failed to replicate DNA (Newport *et al.*, 1990). Moreover, PCNA was much more readily extracted, indicating it is lamin-associated in the nucleus (Jenkins *et al.*, 1993). Further support from studies in *Xenopus* and mammalian cells show dominant-negative lamin mutants disrupted the nuclear lamina causing redistribution of endogenous lamins to intracellular foci and inevitably blocked DNA synthesis. These foci also contained PCNA and replication factor C (RFC) replication elongation factors (Spann *et al.*, 1997). It has thus been proposed that the nuclear lamina acts as a platform for the assembly and stabilisation of transcription factor and DNA replication machinery (Dechat *et al.*, 2008; Goldman *et al.*, 2002).

Of particular interest in this thesis is the function of the nuclear lamina in mitotic events which will be discussed with in **section 1.4**.

1.1.3 Integral nuclear membrane proteins

The NE harbours many integral membrane proteins on both the ONM and INM most of which are poorly characterised and their functions unclear (Dreger *et al.*, 2001; Schirmer *et al.*, 2003). The majority are localised at the INM through interactions with the nuclear lamina/chromatin (**Figure 1.7A**).

Recent proteomics studies by E.Schirmer and colleagues observed the global effects of nuclear envelope transmembrane (NET) proteins on chromosome organisation and

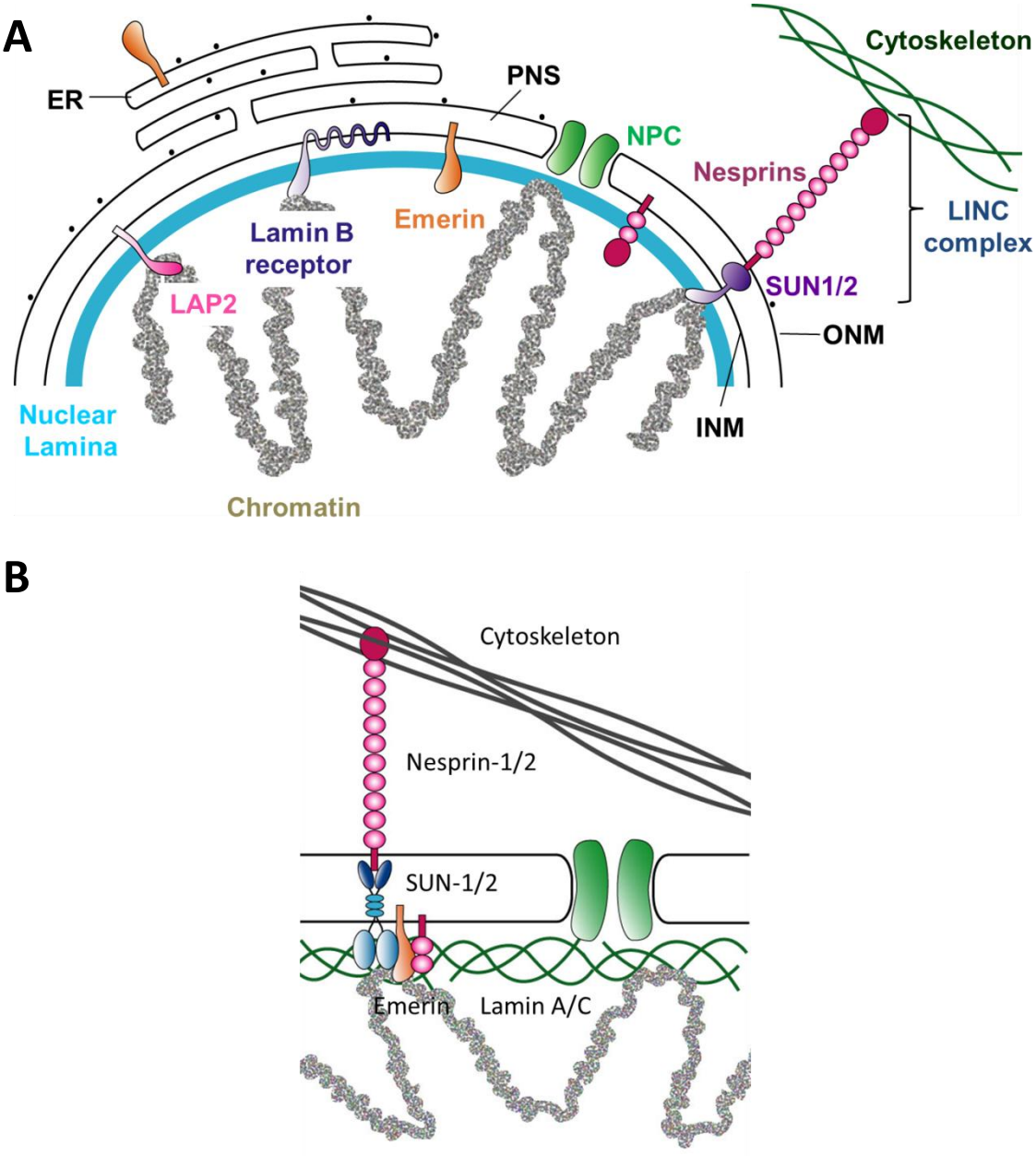

Figure 1.7. Schematic representation of the nuclear envelope and the LINC complex.

(A) Diagram illustrating the nuclear envelope (NE) acting as a barrier to compartmentalise the cytoplasm from the genetic material. The NE is double membrane structure composed of an outer (ONM) and inner nuclear membrane (INM) fused at points occupied by nuclear pore complexes. The ONM is biochemically similar to and continuous with the endoplasmic reticulum (ER) while the INM contains a distinct set of integral membrane proteins, a selection are shown. These proteins are anchored at the INM through interactions with the nuclear lamina and/or chromatin. The nuclear lamina is a filamentous network of lamin proteins underlying the INM which provides anchorage sites for chromatin. **(B)** Diagram illustrating the interaction between the SUN-domain of SUN1/2 and the KASH-domain of nesprins-1/2 in the perinuclear space (PNS) that connect the nucleoskeleton to the cytoskeleton, otherwise known as the LINC complex. The nucleoplasmic domain of SUN1/2 binds lamin A/C, emerin and nesprins as some nesprin isoforms can localise to both sides of the NE. These interactions stabilise the LINC complex to the nuclear lamina. Images courtesy of S.Shackleton. Full re-use permission granted.

gene expression and have revealed that they may be expressed in a tissue-specific, cell cycle-related or state-related manner (Schirmer *et al.*, 2003; Schirmer & Gerace, 2005; Malik *et al.*, 2010; Korfali *et al.*, 2010; Wilkie *et al.*, 2011). In one study of rat liver NE, 80 proteins were identified; of these, 13 were already known whilst the remaining 67 proteins were novel (Schirmer *et al.*, 2003). This demonstrates how little is known about the NE structure and function.

Another study examining resting and active leukocytes discovered 87 more NETs than the previous liver proteome study, highlighting the fact that many NE proteins are tissue specific (Schirmer *et al.*, 2003; Korfali *et al.*, 2010). The majority of NETs identified are expressed in both resting and active states but 25% are unique to one state. Of the 12 confirmed integral membrane proteins in this study, two are capable of inducing movement of chromatin from the active central location to the nuclear periphery and one is involved in chromosome condensation (Korfali *et al.*, 2010).

A few selected proteins, that are relevant to this thesis, are discussed in this section. **Table 1.1** provides a summary of some of the integral membrane proteins. The majority of INM proteins are type II integral membrane proteins with a nucleoplasmic N-terminal domain and a short C-terminal domain. These proteins are localised at the INM through their interactions with the nuclear lamina and/or chromatin/DNA through their N-terminal domains (Burke & Stewart, 2006). Retention at the INM renders them immobile, demonstrated by fluorescence recovery after photo-bleaching (FRAP) experiments (Ostlund *et al.*, 2009), and these proteins are highly insoluble shown by their ability to resist extraction in buffers containing non-ionic detergent or high-salt (Foisner, 2003; Burke & Stewart, 2002).

Some of the integral membrane proteins share common features. For example, INM proteins, lamin-associated protein 2 (LAP2), emerin and MAN1 all share a nucleoplasmic 43 residue motif in their N-terminus. This region was named the LEM domain after the three proteins and since, further LEM proteins have been identified (Foisner, 2003; Gruenbaum *et al.*, 2005). The LEM domain binds a highly conserved chromatin-associated protein called barrier to autointegration factor (BAF), which in turn binds DNA (Segura-Totten & Wilson, 2004). SUN-domain and KASH-domain proteins reside at the INM and ONM, respectively, and are discussed in **sections 1.2.2** and **1.2.3,** respectively.

1.1.3.1 Lamin B receptor (LBR)

LBR was the first integral membrane protein of the NE to be identified (Worman *et al.*, 1988). It is unusual as it is a multi-membrane-spanning protein with eight transmembrane domains orientated so that both termini are in the nucleoplasm (Worman *et al.*, 1990). Its C-terminal domain shares homology with sterol reductases suggesting that LBR has enzyme activity involved in sterol-dependent signalling (Holmer *et al.*, 1998). Its 200 amino acid N-terminus binds to B-type lamins, histones H3 and H4 tetramers, chromatin-associated protein HA95 and heterochromatin protein 1 (HP1) (Ye & Worman, 1994; Polioudaki *et al.*, 2001; Martins *et al.*, 2000; Ye *et al.*, 1997). It also binds directly to double stranded DNA (dsDNA) (Ye & Worman, 1994). Its close interactions with DNA and chromatin emphasise its significant role in chromatin organisation.

LBR is essential for development as homozygous mutations can be lethal. Mutations in LBR can manifest as two different diseases. Homozygous mutations result in

Greenberg skeletal dysplasia, an embryonic lethal disease (Waterham *et al.*, 2003). Heterozygous mutations cause Pelger-Huet anomaly, which is a silent phenotype with abnormal chromatin organisation in granulocytes and nuclei, show less lobulation suggesting LBR is involved in nuclear shape architecture in granulocytes (Hoffmann *et al.*, 2002).

1.1.3.2 Lamin-associated protein 2 (LAP2)

LAP2 formerly known as thymopoietin produces six alternatively spliced variants: LAP2α, β, γ, δ, ε and ζ. Of these, LAP2β, γ, δ and ε are type II integral membrane proteins whereas LAP2α and ζ lack a transmembrane domain hence are soluble proteins (Foisner, 2003; Harris *et al.*, 1995; Berger *et al.*, 1996; Dechat *et al.*, 2000).

LAP2β is a 50 kDa protein while LAP2γ, δ and ε range in molecular mass from 38-46 kDa (Burke & Stewart, 2006). LAP2β binds B-type lamins supported by studies in cells where, in the absence of lamin A/C, LAP2β did not mislocalise to the ER but did in the presence of dominant mutant lamin B1 through disruption of lamin B filaments (Furukawa & Hotta, 1993; Foisner & Gerace, 1993; Vaughan *et al.*, 2001; Schirmer *et al.*, 2001). In addition to binding to chromatin-associated proteins HA95 and HP1, LAP2β has a unique DNA binding region (Foisner, 2003; Martins *et al.*, 2000; Ye *et al.*, 1997). LAP2β also binds transcriptional regulator GCL (Nili *et al.*, 2001).

1.1.3.3 Emerin

Emerin is another member of the LEM-domain family and is encoded by the *EMD* gene, located on the human X chromosome. The protein sequence is 254 amino acids in length translating to a 34 kDa protein (Bione *et al.*, 1994). Emerin is composed of a

nucleoplasmic N-terminus containing the LEM domain followed by an unstructured region and a single transmembrane domain anchoring the short lumenal C-terminus (Foisner, 2003; Bione *et al.*, 1994; Manilal *et al.*, 1996). Emerin binds both A-type and B-type lamins with a particular preference for lamin C (Vaughan *et al.*, 2001; Ellis *et al.*, 1997). Unlike LAP2β, emerin requires A-type lamins for its retention at the INM (Sullivan *et al.*, 1999; Vaughan *et al.*, 2001). A population of emerin has also localises on the ONM where it is believed to interact with the centrosome through β-tubulin to anchor the centrosome at the ONM (Salpingidou *et al.*, 2007). Emerin interacts with a range of proteins including components of the LINC complex (**section 1.2**), transcriptional repressors BAF and GCL and gene expression protein BCL2-associated transcription factor (Btf) (Haque *et al.*, 2010; Wheeler *et al.*, 2007; Zhang *et al.*, 2005; Bengtsson & Wilson, 2004). This host of connections suggest that emerin plays a key role in organisation of the NE architecture. Despite these findings, the precise role of emerin at the NE is still poorly understood.

Emerin mutations cause X-linked Emery-Dreifuss muscular dystrophy (EDMD) as discussed in **section 1.3.1** but emerin in not essential for cell survival and development (Harris *et al.*, 1995). *EMD*$^{-/-}$ mouse models do not display the EDMD phenotype seen in patients to its full extent (Ozawa *et al.*, 2006). However, emerin$^{-/-}$ MEFs show altered nuclear morphology which leads to changes in gene expression. Under mechanical stress, these cells undergo apoptosis suggesting emerin has a potential role in regulating mechanosensitive gene transcription (Lammerding *et al.*, 2005).

1.1.3.4 Transmembrane protein 43 (TMEM43)/LUMA

TMEM43/LUMA is highly conserved across several species. Mammalian LUMA consists of 12 exons equating to 400 amino acids in the mouse sequence with a molecular weight of 45 kDa (Dreger *et al.*, 2001; Bengtsson & Otto, 2008). There are four confirmed transmembrane domains, which are required to target LUMA to the NE. Most of the sequence is of a hydrophilic nature and is situated between transmembrane domains one and two in the ER/NE lumen, the N- and C-terminus lie on the nucleoplasmic face (Bengtsson & Otto, 2008).

Analysis of mRNA expression of LUMA in mouse tissues shows that LUMA transcripts are highly expressed in placenta while other tissues such as testes, prostate, thymus, small intestine and spleen are low expressing, no expression was detected in skeletal muscle (Bengtsson & Otto, 2008).

LUMA binds to both A-type and B-type lamins, preferentially to lamin B2, as well as emerin and SUN2 (Bengtsson & Otto, 2008; Liang *et al.*, 2011). It controls emerin distribution across the NE and is assumed to spatially and functionally organise complexes at the INM (Bengtsson & Otto, 2008).

The protein is encoded by the gene *TMEM43* and a missense mutation in this gene resulting in amino acid substitution S358L causes arrhythmogenic right ventricular cardiomyopathy (ARVC) (Merner *et al.*, 2008). The E85K LUMA mutation prevents LUMA from oligomerising and contributes to the pathological mechanism seen in EDMD (Liang *et al.*, 2011).

1.1.3.5 Nurim

Nurim exclusively localises to the nuclear rim of mammalian cells hence its name. The protein sequence is 262 amino acids in length with a molecular weight of 29 kDa. Initial research showed that nurim had five transmembrane domains with short intervening loops while another group argued that there are six transmembrane domains as the fifth transmembrane domain spans the membrane twice with a hairpin turn in the middle. Both papers agree that the incredibly short N-terminus of four or five residues faces the nucleoplasm but they differ in opinion as to where the C-terminus lies, the nucleoplasm or PNS (Rolls *et al.*, 1999; Hofemeister & O'Hare, 2005).

Nurim is quite distinct from other INM proteins in that it has a very short N-terminus as many INM proteins have a significant hydrophilic N-terminus which is required for targeting to the INM. Also, nurim is extremely insoluble, so much so, that even under conditions that completely solubilise other INM proteins and lamins, nurim is only partially extracted and is still visible at the NE showing that it is not anchored by the lamina (Rolls *et al.*, 1999). However, mutations in the protein mislocalise the protein to the ER where it is easily extractable suggesting that its strong NE attachment is due to multiple regions for targeting to the NE (Rolls *et al.*, 1999).

There is no evidence of binding partners and its function remains unknown but sequence analysis shows similarity to isoprenylcysteine carboxyl methyltransferase (ICMT) enzymes involved in processing proteins with a CAAX motif (Hofemeister & O'Hare, 2005).

1.1.3.6 Spindle-associated membrane protein 1 (SAMP1)

SAMP1 is a recently discovered INM protein and is the human orthologue of rat NET5 and fission yeast Ima1 (Integral membrane protein 1) (Schirmer *et al.*, 2003; King *et al.*, 2008). The protein has a mass of 43 kDa consisting of a 392 amino acid protein sequence which contains five hydrophobic regions predicted to correspond to five transmembrane domains, with a large conserved nucleoplasmic loop between the first and second transmembrane domains. Four CXXC motifs lie within that loop organised in such a way that suggests the presence of two zinc finger motifs. SAMP1 maybe orientated so that the N-terminus is in the PNS while the C-terminus resides in the nucleoplasm (Buch *et al.*, 2009).

In interphase cells, in the absence of SAMP1, the distance between the NE and the centrosomes significantly increases, suggesting a functional connection between SAMP1, centrosomes and the cytoskeleton (Buch *et al.*, 2009). This is supported by studies with the *Saccharomyces pombe (S.pombe)* orthologue Ima1 where Ima1 contributes to coupling of the spindle pole body (SPB) to the NE by indirectly mediating heterochromatin and Sad1 (SUN orthologue, see **section 1.2.2.1**) interactions (King *et al.*, 2008). SAMP1 was named so due to its localisation at the polar regions of the mitotic spindle during mitosis (Buch *et al.*, 2009).

1.1.4 Targeting of proteins to the INM

As discussed in **section 1.1.1.2**, soluble proteins can be actively transported in and out of the nucleus via the NPC. Integral membrane proteins are thought to be targeted to the INM by a slightly different mechanism, known as the diffusion-retention model (**Figure 1.8**). INM proteins are initially synthesised on the rough ER where they become

inserted into the ER membrane. As the ER is continuous with the ONM and INM, proteins laterally diffuse from the ONM to the INM via the lateral POM located at the interface of the NPC and NE. These proteins are immobilised at the INM through interactions with the nuclear lamins and/or chromatin (Ellenberg *et al.*, 1997; Holmer & Worman, 2001). Evidence for this idea comes from studies with LBR and emerin. FRAP studies with LBR and emerin show the highly mobile state of integral membrane proteins in the ER compared to their immobilisation at the INM (Ostlund *et al.*, 2009; Ellenberg *et al.*, 1997).

There is also strong evidence that the NPC plays a role in regulating access of proteins to the INM. Firstly, all known INM proteins have a nucleoplasmic domain of less than 60 kDa (Holmer & Worman, 2001), which is approximately the maximum size of proteins able to diffuse passively to the NPC. Secondly, experiments with LBR show it contains two independent sequences that target it to the INM (Ellenberg *et al.*, 1997; Soullam & Worman, 1993; Soullam & Worman, 1995; Smith & Blobel, 1993). The N-terminal domain of LBR has a mass of 22.5 kDa and can gain access to the INM as can an LBR chimeric protein with two N-terminal nucleoplasmic domains. However, increasing the molecular weight to 67 kDa, by adding a third copy, prevents LBR reaching the INM (Soullam & Worman, 1995).

Integral membrane proteins are usually targeted to the INM by their N-terminus nucleoplasmic domain and, in some cases, their transmembrane domains. To date, a motif universal to INM proteins has not been found to target INM proteins directly to the INM.

Figure 1.8 has been omitted for copyright reasons. Please refer to Voeltz *et al.* (2002) figure 2, or the hard copy version of this thesis for the image.

Figure 1.8. Diffusion-retention model.

The model proposes a mechanism for targeting integral membrane proteins to the inner nuclear membrane (INM). **(A)** The INM protein is synthesised on the ribosome and is then inserted into the endoplasmic reticulum (ER). **(B** and **C)** As the ER is continuous with the nuclear envelope, the integral membrane protein laterally diffuses from the ER, to the outer nuclear membrane (ONM) reaching the INM via movement through the pore membrane. **(D)** Integral membrane proteins are retained at the INM retained through interactions with the nuclear lamina and/or chromatin. Taken from (Voeltz *et al.*, 2002). Restricted re-use permission granted.

Models incorporating the diffusion-retention theory with an energy-dependent transport system are perceived as more realistic (Ohba *et al.*, 2004). Sequence analysis of some INM proteins in yeast and mammalian systems show they have predicted regions resembling NLS sequences. Yeast INM proteins Heh1p and Heh2p are orthologues of mammalian MAN1 and experiments show that they are transported by the yeast equivalent receptor specific pathway as previously discussed in **section 1.1.2.2** (**Figure 1.4**). The suspected NLS sequences in Heh1 and Heh2 are required to bind transport receptor karyopherin α/β1 mediating transport of membrane proteins through the NPC. Furthermore, mutations in the RanGTPase pathway disrupts transport (King *et al.*, 2006). Interestingly, a study in HeLa cells shows that an NLS sequence is not compulsory for energy-dependent transport (Ohba *et al.*, 2004). Interestingly, SUN2 is targeted to the INM through multiple elements. A cNLS sequence in its nucleoplasmic N-terminus, a golgi retrieval signal proximal to the former and the C-terminal SUN-domain all contribute to targeting of SUN2 to the INM (Turgay *et al.*, 2010).

A set of guidelines has been put forward for the transport of proteins to INM depending on size (Lusk *et al.*, 2007). Based on current research it proposes that firstly, proteins with a nucleoplasmic domain smaller than 25 kDa laterally diffuse across interconnecting ER, ONM and INM membranes and are anchored at the INM through chromatin and/or nuclear lamina interactions (diffusion-retention model). Secondly, proteins with nucleoplasmic domains between 25-75 kDa should bear an NLS for energy-dependent mechanism travel across the as the NPC may require remodelling to facilitate transport of larger proteins. Finally, proteins in excess of 75 kDa should be

incorporated into the INM through interactions with nuclear components prior to post-mitotic NE reassembly (Lusk *et al.*, 2007).

1.2 Linker of nucleoskeleton and cytoskeleton (LINC) complex

1.2.1 Nuclear envelope bridging model

The nucleus and cytoplasm do not exist in isolation, in fact physical connection between the two compartments is vital to numerous cellular processes, in particular nuclear positioning and migration. Early research showing that the cytoskeleton and nucleoskeleton are connected involved microbeads attached to integrins on the plasma membrane. When the microbeads were pulled, it caused the nucleoskeleton and cytoskeleton to become distorted and move in the direct of the force. In doing so, the nucleoli experienced some rearrangement too (Maniotis *et al.*, 1997). It is now known that SUN-domain and KASH-domain NE proteins mediate this connection.

Studies in *C.elegans*, initially identified three genes, *unc-83, unc-84* and *anc-1*, that appeared to be required for nuclear migration and anchorage. Mutations in the *unc-83* and *unc-84* genes lead to uncoordinated movement and nuclear anchorage defects while mutations in *anc-1* also manifest as nuclear anchorage impairment but not nuclear migration defects (Horvitz & Sulston, 1980; Sulston & Horvitz, 1981; Hedgecock & Thomson, 1982). Protein sequence analysis of the three proteins show that UNC-84 contains a conserved SUN-domain at its C-terminus while UNC-83 and ANC-1 both have a KASH-domain at their C-terminus (Malone *et al.*, 1999; Starr & Han, 2002) (see **section 1.2.2** and **section 1.2.3**).

UNC-84 localises at the NE in a Ce-lamin-dependent manner (Malone *et al.*, 1999; Lee *et al.*, 2002; McGee *et al.*, 2006). In turn, ANC-1 is dependent upon UNC-84 for NE localisation. ANC-1 is a giant protein (950 kDa) with a C-terminal KASH-domain and two N-terminal calponin homology (CH) domains which bind actin (Starr & Han, 2002). From these studies it was postulated that the SUN-domain protein UNC-84 at the INM tethers KASH-domain protein ANC-1 to the ONM, forming a molecular chain spanning the PNS. This interaction connects the actin cytoskeleton to the nuclear lamina (Starr & Han, 2002) (**Figure 1.9**).

This NE bridging complex is not exclusive to *C.elegans* but is highly conserved in yeast, flies, mammals and even plants (Razafsky & Hodzic, 2009). The specific term LINC complex was coined by Crisp *et al.* (2006) when they described the mammalian SUN and KASH protein interaction, involving SUN proteins SUN1 and SUN2 and KASH-domain proteins nesprin-1 and nesprin-2. Since then, other nesprin isoforms at the ONM have emerged that connect the nucleus to the cytoplasmic microtubule and intermediate filament networks (Wilhelmsen *et al.*, 2005; Roux *et al.*, 2009) (**Figure 1.9**). The formation of these physical connections not only gives strength and integrity to the nucleus and cell as a whole, but also provides potential routes for signal transduction pathways.

However, the LINC complex is not essential for every cell. Granulocytes have lobulated nuclei and lack many of the components of the LINC complex in comparison to macrophages. Their flexible nature aids quick passage through blood vessels and tissues to sites of infection. It is thought that the presence of the LINC complex may stiffen granulocytes impairing their function (Olins *et al.*, 2009).

Figure 1.9 has been omitted for copyright reasons. Please refer to Burke & Roux (2009) figure 2, or the hard copy version of this thesis for the image.

Figure 1.9. Mammalian LINC complex isoforms.

The SUN-domain of SUN1 and SUN2 interacts with the nuclear lamina at their N-termini while tethering the KASH-domain of nesprin isoforms to the ONM at their C-termini. Nesprins bind to all three cytoskeletal networks via different isoforms, connecting between the cytoskeleton and the nucleoskeleton. The SUN-KASH interaction which makes the connection possible has been coined the linker of nucleoskeleton to cytoskeleton (LINC) complex. The illustration depicts the different isoforms of mammalian LINC complexes and the connections with all three cytoskeletal networks. Taken from (Burke & Roux, 2009). Restricted re-use permission granted.

1.2.2 SUN-domain proteins

SUN proteins are defined by their C-terminal SUN-domain, which is highly conserved in all eukaryotes. Malone *et al.* (1999) coined the term SUN-domain after discovering that the *C.elegans* protein UNC-84 possessed a 200 amino acid C-terminal sequence that bore remarkable homology to the Sad1 protein of *S.pombe* (Sad1p UNC-84). It has also been shown that other species have proteins containing the SUN-domain, indicating that the SUN proteins are an evolutionarily conserved family (Malone *et al.*, 1999; Padmakumar *et al.*, 2005) as shown in **Figure 1.10**. Mammals have a repertoire of SUN-domain proteins while other eukaryotes such as *S.pombe* (Sad1), *C.elegans* (UNC-84 and matefin/Sun-1) and *D.melanogaster* (klaroid and giacomo) possess one or two (Tzur *et al.*, 2006; Kracklauer *et al.*, 2007).

SUN-domain containing proteins are type II integral membrane proteins localised at the INM and orientated so that the N-terminus is at the nucleoplasmic face and the C-terminus resides within the PNS. Most have a large nucleoplasmic N-terminal domain and a central transmembrane domain that are responsible for its localisation, this is followed by a coiled-coil region for oligomerisation and the conserved C-terminal SUN-domain (Tzur *et al.*, 2006).

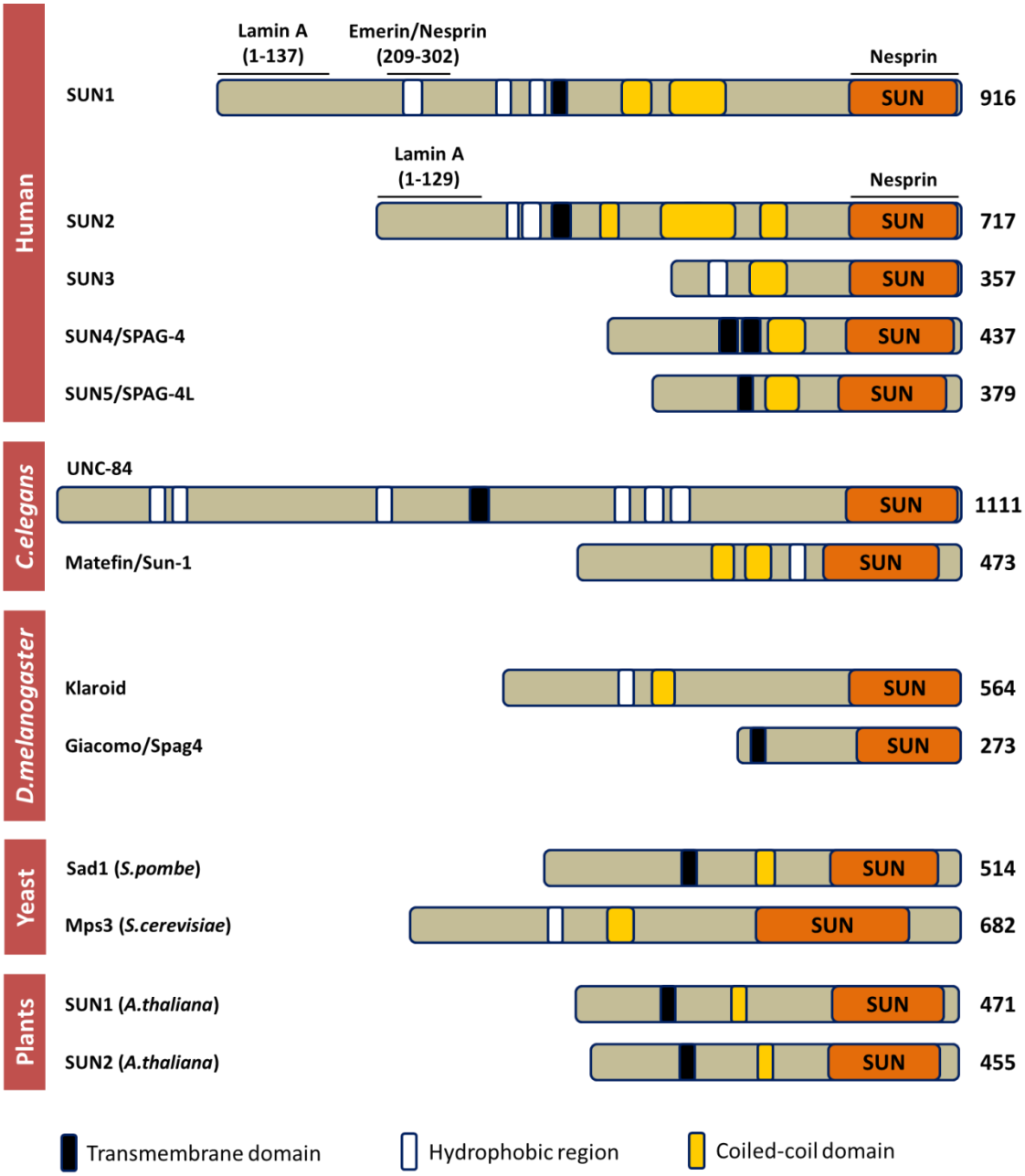

Figure 1.10. Schematic representation of SUN-domain proteins from various species.

Information from UniProtKB and Pfam proteomic databases has been used to construct each of the SUN proteins, with the exception of human SUN1 (hSUN1). The hSUN1 structure displayed represents the full-length isoform not available on UniProtKB. The closest protein available is hSUN1 1-812, this lacks exons 7 and 8 corresponding to residues 220-286. The hSUN1 isoform above is based on that entry but takes into account the additional protein sequence from data generated in the Shackleton laboratory (Haque *et al.*, 2010; Haque *et al.*, 2006). For the two NE-associated hSUN proteins, binding sites for interacting partners have been labelled accordingly. Hydrophobic regions for the SUN proteins have been highlighted and suggest potential transmembrane domains. Accession numbers: human SUN1 (O94901), SUN2 (Q9UH99), SUN3 (Q8TAQ9), SUN4/SPAG-4 (Q9NPE6) and SPAG-4L (Q8TC36), *C.elegans* UNC-84 (Q20745), matefin/Sun-1 (Q20924), *D.melanogaster* klaroid (A1Z6Q1) (Hiraoka & Dernburg, 2009), giacomo (Q9VKG2) (Kracklauer *et al.*, 2010), *S.pombe* Sad1 (Q09825), *S.cerevisiae* Mps3 (P47069), *A.thaliana* AtSUN1 (Q9FF75), AtSUN2 (Q9SG79).

1.2.2.1 Non-mammalian SUN-domain proteins

Sad1 (spindle architecture disrupted) in *S.pombe* is one of the founding members of the SUN-protein family (Hagan & Yanagida, 1995). Sad1 mutants affect spindle formation and function, and a deletion of the gene is lethal. It localises to the NE periphery in interphase but during mitotic and meiotic phases it is solely associated with the SPB. Sad1 interacts with KASH-domain proteins kms1 and kms2 located on the ONM (King *et al.*, 2008) tethering the SPB to the ONM in interphase, which is then inserted into the NE upon mitosis (Ding *et al.*, 1997).

Mps3 (monopolar spindle) *in Saccharomyces cerevisiae (S.cerevisiae)* has roles in nuclear organisation, specifically, tethering of chromosomes and gene silencing which are regulated through acetylation (Ghosh *et al.*, 2012). Interestingly, no KASH-domain proteins have yet been identified in *S.cerevisiae.*

Sad1 and Mps3 have roles in meiotic cells aiding the anchorage of telomeres to the INM. Telomeres of meiotic chromosomes adopt a bouquet arrangement which is important for homologous chromosome pairing and progression through the meiotic cycle (Antoniacci *et al.*, 2007; Bupp *et al.*, 2007; Conrad *et al.*, 2007; Chikashige *et al.*, 2006).

UNC-84 in *C.elegans* is the other founding member of the SUN family discussed previously in **section 1.2.1**. Another SUN protein, matefin/Sun-1 is expressed in all embryonic nuclei but, from mid-embryogenesis to adulthood, matefin expression is exclusive to the germline. Collectively, matefin has essential roles in embryogenesis, germ cell line proliferation and survival (Fridkin *et al.*, 2004). It binds ZYG-12 (zygote

defective) anchoring it to the ONM through its small KASH-domain. The matefin-ZYG-12 interaction secure the centrosome to the NE (Malone *et al.*, 2003; Minn *et al.*, 2009). Like yeast SUN proteins, matefin also has meiotic roles in homologous chromosome pairing and reorganisation of chromatin in early meiosis (Penkner *et al.*, 2007).

Klaroid in *D.melanogaster* tethers KASH-domain protein Klarsicht at the nuclear periphery in the eye. Composite mutations in the klaroid and klarsicht genes result in rough eye morphological defect. The klaroid-klarsicht interaction is required for nuclear migration in differentiating neurons and in non-neuronal cells (Kracklauer *et al.*, 2007). In the germline, klaroid tethers two KASH-domain proteins, klarsicht and Msp-300 to the NE but appears to have no tissue-specific function in oogenesis (Technau & Roth, 2008).

Giacomo is the orthologue of mammalian sperm-associated antigen-4 (SPAG-4) (Shao *et al.*, 1999; Kennedy *et al.*, 2004). Giacomo is testis-specific and localises to the spermatid nucleus but is highly concentrated at the nucleus-spermatid centriole interface (Kracklauer *et al.*, 2007; Technau & Roth, 2008). In the absence of giacomo, the nucleus and centrioles/basal bodies disconnect from each other post-meiosis and giacomo null mutants are sterile. Tethering of the centriole to the nucleus is not a LINC complex-dependent interaction (Kracklauer *et al.*, 2010). This suggests that SUN isoforms are involved in complexes other than the LINC complex.

Sun-1 and ***SunB*** in *Dictyostellium discoideum* (*D.discoideum*) are unique in comparison to other SUN-domain containing proteins. Sun-1 has an SDEL ER retention signal at its

extreme C-terminus (Xiong *et al.*, 2008). It competes with the KASH-domain protein interaptin for localisation at the NE (Schulz *et al.*, 2009). Expression of a dominant-negative Sun-1 mutant or depletion of Sun-1 promotes the separation of the INM and ONM resulting in deformation in nuclear morphology and dissociation of the centrosome form the nucleus. The latter causes centrosome hyperamplification leading to impaired spindle function, aneuploidy and inevitably cell death (Xiong *et al.*, 2008). Hence, Sun-1 is a scaffold protein required for anchoring the centrosome to the nucleus in interphase and mitosis. In addition, Sun-1 is also essential for maintaining genome stability and ensuring correct segregation of chromosomes (Xiong *et al.*, 2008; Schulz *et al.*, 2009). SunB is unusual as it has a central SUN-domain. It is found in a region around the nucleus in the vegetative cell and is involved in cytokinesis, cell proliferation and differentiation (Shimada *et al.*, 2010). Despite having SUN-domain and KASH-domain proteins, there is no evidence of a LINC complex in *D.discoideum*.

There is emerging evidence for the presence of SUN proteins in the plant kingdom, demonstrating the high evolutionary conservation of SUN-domain proteins. *Arabidopsis thaliana* (*A.thaliana)* has two SUN-domain proteins, ***AtSUN1*** and ***AtSUN2*** while maize has 5 different genes (***ZmSUN 1-5***) (Graumann *et al.*, 2010; Murphy *et al.*, 2010). Their characteristics suggest that the LINC complex may exist in the plant kingdom (Graumann *et al.*, 2010).

1.2.2.2 Mammalian SUN-domain proteins

There are currently five known mammalian SUN-domain proteins encoded by different genes. ***SUN1*** and ***SUN2*** are ubiquitously expressed, ***SUN3***, ***sperm-associated antigen-4 (SPAG4)*** and ***sperm-associated antigen-4-like (SPAG4L)*** are exclusively expressed in

testis (Crisp *et al.*, 2006; Tzur *et al.*, 2006; Shao *et al.*, 1999; Frohnert *et al.*, 2011). SUN1 and SUN2 were initially identified by proteomic screening for NE components (Dreger *et al.*, 2001; Schirmer *et al.*, 2003). Although SUN3 is very similar in domain organisation to SUN1 and SUN2, it has a distribution pattern typical of an ER protein and is primarily expressed in the germline (Crisp *et al.*, 2006). INM proteins SUN1 and SUN2 are the focus of this research hence further discussion will be based on these two proteins only (**Figure 1.10**).

SUN1 and SUN2 have a large N-terminal nucleoplasmic domain and the C-terminal SUN-domain is located in the PNS (Crisp *et al.*, 2006; Padmakumar *et al.*, 2005; Hodzic *et al.*, 2004; Haque *et al.*, 2006). SUN1 and SUN2 are targeted to the INM by slightly different mechanisms Unusually, the SUN1 nucleoplasmic domain is sufficient for NE localisation perhaps due to the presence of the three hydrophobic regions at its distal end. Interestingly, the transmembrane and C-terminal domain are also able to localise to the NE, potentially through dimerization with full-length SUN proteins or interactions with nesprins (Crisp *et al.*, 2006; Liu *et al.*, 2007; Hasan *et al.*, 2006). SUN2 has an N-terminal NLS sequence which binds importins-α/β and is actively transported to the INM. The SUN2 C-terminus also contributes to its NE localisation (Turgay *et al.*, 2010; Hodzic *et al.*, 2004).

Studies have shown SUN1 and SUN2 form homodimers and heterodimers via their coiled-coil domains as well as tetramers and higher oligomers (Liu *et al.*, 2007; Lu *et al.*, 2008). The N-terminus may also contribute to SUN1 and SUN2 oligomerisation (Haque *et al.*, 2006). However, two recent structural studies reveal that the crystal

structure of the SUN2 SUN-domain is in fact a homotrimer and binds three KASH-domain peptides (Zhou *et al.*, 2012b; Sosa *et al.*, 2012).

SUN1 and SUN2 form multiple protein interactions at the INM. SUN1 and SUN2 appear to act redundantly to tether the KASH-domain of nesprin-1 and nesprin-2 to the ONM. Only co-depletion of SUN1 and SUN2 releases nesprin-2 giant from the NE (Crisp *et al.*, 2006). More recently, SUN1 and SUN2 have been shown to interact with nesprins-3 and nesprin-4 connecting the nucleus to intermediate filament and microtubule networks, respectively (**section 1.2.3.2**).

Both SUN1 and SUN2 bind lamin A/C via their N-terminus but differ in INM retention patterns. In *Lmna*$^{-/-}$ MEFs, SUN1 remains bound at the INM whereas SUN2 mislocalises to the ER, moreover, re-introduction of lamins back into the cells fails to recruit SUN2 to the NE. This indicates that A-type lamins partially contribute to SUN2 INM localisation but are not required for SUN1 INM retention (Crisp *et al.*, 2006; Haque *et al.*, 2006; Hasan *et al.*, 2006). Interestingly, SUN1 has a particular preference for prelamin A binding and so is thought to be involved in A-type lamin processing. This interaction has also been shown to play a role in lamin A-linked premature ageing disorders (**section 1.3.4**) (Crisp *et al.*, 2006; Haque *et al.*, 2010; Chen *et al.*, 2012). At the N terminus, SUN1 and SUN2 also interact with emerin and small nesprin isoforms that localise to the INM. However, SUN1 does not rely on emerin or nesprins for its NE localisation indicating other anchorage mechanisms for SUN1 (Haque *et al.*, 2010). The SUN1 lamin-binding region is at the extreme N-terminus (amino acids 1-138) while, at a distinct region (amino acids 209-302), the emerin and small nesprin isoform binding sites overlap (**Figure 1.10**). Whether these proteins compete for SUN1 binding is

unknown. Collectively, this research shows that SUN proteins are part of multiple complexes at the INM (Haque *et al.*, 2010).

SUN1, but not SUN2, associates with NPCs and requires both its nucleoplasmic and lumenal domains for this interaction. Depletion of SUN1 by RNAi or overexpression of SUN1 dominant-negative mutants results in NPC clustering and suggests that SUN1 is vital to efficient NPC distribution across the NE (Liu *et al.*, 2007). Furthermore, SUN1 co-localises with to POM121 in interphase and is required for NPC assembly (Talamas & Hetzer, 2011).

SUN1 has seven alternatively spliced variants (α, β, γ, δ, ε, ζ and η), each has a deletion of one or more exons ranging from exon 7-10, which encodes regions of the N-terminus (Gob *et al.*, 2011; Liu *et al.*, 2007). RT-PCR with mRNA from different tissues shows expression of the different isoforms is often tissue-specific. The shortest isoform, SUN1η is testis-specific both at the mRNA and protein level. However, existence and functionality of other isoforms at the protein level is still required and the predominant isoform in most tissues is full-length (Crisp *et al.*, 2006; Gob *et al.*, 2011). SUN2 antibody detects three bands by western blotting with molecular weights of 65, 75 and 85 kDa (Hodzic *et al.*, 2004). It is not known whether all three are SUN2 isoforms or if some are the result of non-specific binding by the antibody.

During mitosis SUN1 and SUN2 display very different localisation patterns with respect to the chromatin mass. Although initially both are dispersed in the ER, in late anaphase to early telophase when the NE starts to reform, SUN2 localises to the longitudinal region of the chromatin mass which is devoid of NPCs. SUN1 is not present in this

region but instead localises to the lateral poles of the chromatin mass where NPC assembly is initiated (Liu *et al.*, 2007) (**Figure 1.11**). This further supports research showing that SUN1 but not SUN2 is associated with NPC such as POM121 (Liu *et al.*, 2007; Talamas & Hetzer, 2011). Furthermore, SUN1 binds chromatin at its N-terminus and chaperones human acetyltransferase-like protein (hALP) for chromosome decondensation in anaphase on the reforming daughter NE (Chi *et al.*, 2007). Lu *et al.* (2008) also found SUN1 binds chromatin through chromatin-immunoprecipitation (ChIP) assays. In addition to their mitotic roles, both SUN1 and SUN2 associate with telomeres during meiotic prophase I and are crucial for telomere anchorage, dynamic movement and homologous chromosome pairing (Ding *et al.*, 2007; Schmitt *et al.*, 2007). In support of a role in meiosis, SUN1 knockout mice are sterile, due to defects in telomere attachment to the NE periphery (Ding *et al.*, 2007).

1.2.3 KASH-domain proteins

Another major group of proteins that bridge the NE are the KASH-domain proteins which are the only known integral membrane proteins residing mainly at the ONM. Their N-terminus lies in the cytoplasm whereas their C-terminus is within the PNS (Razafsky & Hodzic, 2009). KASH (klarsicht, ANC-1, syne homology) proteins are defined by a short sequence in their C-terminus of approximately 60 residues composed of a transmembrane domain and 30 residues that project into the PNS (Starr & Han, 2002). Four residues rich in proline (PPPX) at the extreme C-terminus of the KASH-domain are crucial for the KASH-SUN interaction (Padmakumar *et al.*, 2005).

The KASH-domain is highly conserved in *D.melanogaster*, *C.elegans* and humans hence the origin of its name (Starr & Han, 2002). Several KASH proteins have a very large N-

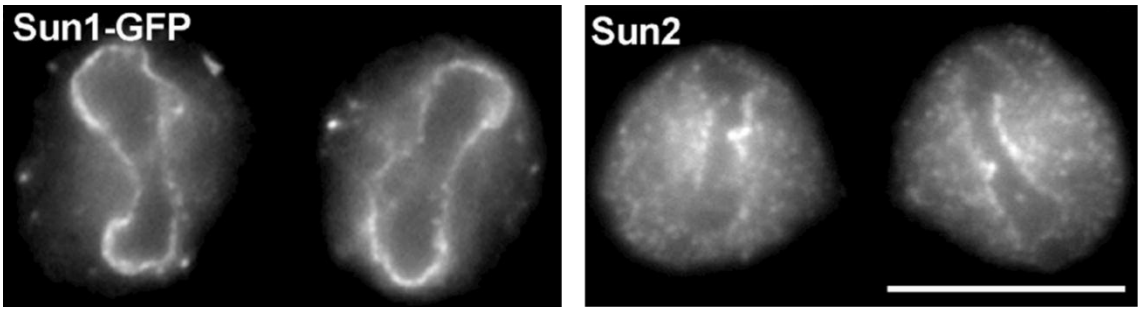

Figure 1.11. Mammalian SUN1 and SUN2 show distinct localisation patterns in mitosis.

HeLa cells in late anaphase/early telophase shows SUN1-GFP predominant localisation at the lateral margins of the chromatin mass while SUN2 appears exclusively at the longitudinal core region. Scale bar 4 µm. Adapted from (Liu *et al.*, 2007). Full re-use permission granted.

terminus with two CH domains at the extreme N-terminus, which are capable of binding to actin, while other KASH proteins can bind to the intermediate filaments and microtubules (Wilhelmsen *et al.*, 2005; Roux *et al.*, 2009; Starr & Han, 2002). The large mass of these proteins can be attributed to its N-terminal domain which contains coiled-coil regions. The KASH-domain is highly conserved across species but the N-terminus is quite divergent suggesting that different KASH-domain proteins have varying functions or that the sequence itself is not important, but act as an extended linker (Razafsky & Hodzic, 2009).

While the KASH-domain alone is sufficient to target the protein to the ONM, anchorage at the ONM requires the SUN-domain family members positioned on the INM, an interaction termed the LINC complex (Starr, 2011; Burke, 2012). Therefore KASH-domain proteins function to connect the cytoskeleton to the nucleus.

1.2.3.1 Non-mammalian KASH-domain proteins

C.elegans encodes four KASH-domain proteins; ANC-1, UNC-83, ZYG-12 and KDP-1. ***ANC-1*** was the first KASH protein to be characterised as described earlier in **section 1.2.1**.

UNC-83 is an ONM protein expressed in cells with migrating nuclei (Starr *et al.*, 2001). UNC-83 KASH-domain interactions with the SUN-domain of UNC-84 anchors it to the ONM (McGee *et al.*, 2006; Starr *et al.*, 2001). The importance of UNC-83 in nuclear anchorage and migration was noted over 30 years ago (Horvitz & Sulston, 1980; Sulston & Horvitz, 1981) but the mechanistic function has only just been discovered. UNC-83 recruits both kinesin-1 and dynein to the cytoplasmic face of the nucleus

where they collectively mediate the migration of the nucleus on microtubule tracks. Microtubules are highly dynamic and polarise in the direction of movement, kinesin-1 aids forward movement while dynein mediates backwards movement or nuclear rolling to avoid cellular obstacles (Meyerzon *et al.*, 2009; Fridolfsson & Starr, 2010; Fridolfsson *et al.*, 2010).

ZYG-12 is a KASH-domain protein expressed in the germline and in early embryonic cells. It is also part of the Hook protein family, which are regarded as protein linkers of membrane organelles with the microtubule cytoskeleton (Gruenbaum *et al.*, 2005). ZYG-12 has three isoforms, ZYG-12A, ZYG-12B and ZYG-12C. ZYG-12A is localised exclusively at the centrosomes, in a microtubule-dependent manner, and lacks the KASH-domain therefore is not membrane-associated. ZYG-12B and ZYG-12C are found at the centrosome as well as the NE. The C-terminus interaction with matefin is responsible for ZYG-12B and ZYG-12C anchorage at the ONM, while the N-terminus binds the dynein heavy chain 1 (DHC-1). ZYG-12, along with matefin and dynein, are crucial for the attachment of the centrosome to the nucleus. The mechanism involves ZYG-12 B/C recruiting the dynein complex to the NE through its interaction with DHC-1. This binds the centrosome via the microtubules and pulls the centrosome towards the nucleus. Once within range, the ZYG-12A isoform on the centrosome and the ZYG-12B and ZYG-12C at the NE dimerise and so connect the centrosome and the nucleus (Malone *et al.*, 2003; Minn *et al.*, 2009). In addition, the ZYG-12 interaction with dynein has a role in maintaining gonad architecture in nematodes (Zhou *et al.*, 2009). Moreover, binding of matefin and ZYG-12 functions to reorganise the chromosomes and promote homologous pairing in meiosis (Penkner *et al.*, 2007; Labella *et al.*, 2011).

KDP-1 (KASH-domain protein-1) is a small protein with only 145 amino acid residues and a mass of 15 kDa. Like other *C.elegans* KASH proteins it interacts with UNC-84 and matefin. KDP-1 is crucial for survival, larval growth and development and also, has a role in promoting timely cell cycle progression from S phase to mitotic entry (Mcgee *et al.*, 2009).

Msp-300 (muscle specific protein 300 kDa) in *D.melanogaster* is a giant protein with a mass of 300 kDa which binds the actin cytoskeleton at its cytoplasmic N-terminus. It is expressed in somatic, visceral and heart embryonic muscles, and contributes to proper myotube formation during development (Volk, 1992; Rosenberg-Hasson *et al.*, 1996). In the germline, SUN-domain protein klaroid tethers Msp-300 to the ONM (Technau & Roth, 2008) and in turn it anchors nuclei to the actin cytoskeleton (Xie & Fischer, 2008).

Klarsicht in *D.melanogaster* is one of the three founding members of the KASH-domain family (Starr & Han, 2002). There are three isoforms of klarsicht, α, β and γ. Klarsicht α (251 kDa) and γ (62 kDa) localise to the NE while β is not membrane bound and has no KASH-domain (Guo *et al.*, 2005). The protein requires SUN-domain klaroid and nuclear lamin Dm_0 for its ONM localisation (Kracklauer *et al.*, 2007; Patterson *et al.*, 2004). At its cytoplasmic N-terminus klarsicht binds to microtubules, possibly through dynein interactions, hence connecting the microtubule organising centre (MTOC) to the nucleus to mediate nuclear migration (Patterson *et al.*, 2004; Fischer *et al.*, 2004). Klarsicht is necessary to position the photoreceptor and cone cell nuclei in the developing eye, failure to reposition the nuclei from the basal to the apical side of the eye presents as oddly shaped photoreceptors (Xie & Fischer, 2008; Fischer-Vize &

Mosley, 1994; Mosley-Bishop *et al.*, 1999). Klarsicht null mutants are viable and fertile indicating that the function is only important for specific motor protein function. It is also required for transport of lipid droplets along microtubule tracks in the eye (Mosley-Bishop *et al.*, 1999).

Interaptin is the only KASH protein found in *D.discoideum* and binds to the actin network (Rivero *et al.*, 1998). KASH-domains in other species tend to interact with SUN-domain proteins promoting their localisation at the ONM, but this is not the case for interaptin. Interaptin remains at the NE in the absence of Sun-1 and vice versa, moreover, interaptin overexpression displaces Sun-1 from the NE indicating that the two proteins compete with each other for localisation or a common binding partner.

Recently, *A.thaliana* WPP domain interacting proteins (AtWIPs) have been identified as plant KASH-domain proteins (Graumann *et al.*, 2010; Murphy *et al.*, 2010). There are three AtWIPs, ***AtWIP 1***, ***2*** and ***3*** which all localise to the ONM through interactions with AtSUN1 and AtSUN2. They also interact with *A.thaliana* RanGAP1 (AtRanGAP1) in their N-terminus and both AtWIPs and AtRanGAP1 require AtSUN proteins for localisation at the NE (Zhou *et al.*, 2012a). This reiterates the fact that the LINC complex is conserved outside of the animal kingdom.

1.2.3.2 Mammalian KASH-domain proteins

The major KASH-domain proteins found in mammals are called nesprins (nuclear envelope spectrin repeat proteins) and the four forms, nesprin-1, -2, -3 and -4 are encoded by different genes (Wilhelmsen *et al.*, 2005; Roux *et al.*, 2009; Zhang *et al.*,

2001) (**Figure 1.12**). The identification of nesprin isoforms by various groups at roughly the same time has led to the existence of many names for the same proteins.

Like all KASH proteins, nesprins are composed of a cytoplasmic N-terminal domain, and a lumenal C-terminal KASH-domain localised to the NE via a transmembrane domain and anchored to the ONM by SUN1 and SUN2. The N- and C-termini are separated by a series of spectin repeats, which resemble the globular domains of spectrins (Zhang *et al.*, 2001) (**Figure 1.12**).

Nesprin-1 and nesprin-2 undergo extensive alternative splicing as illustrated in **Figure 1.12.** The genes are huge, 147 exons and 115 exons, respectively, and alternative splicing leads to isoforms that vary massively in size (40 -1000 kDa) due to the number of spectrin repeats. Nesprins-3 and nesprin-4 are much smaller with 1-3 spectrin repeats and have little or no alternative splicing (Wilhelmsen *et al.*, 2005; Roux *et al.*, 2009; Rajgor *et al.*, 2012; Padmakumar *et al.*, 2004; Zhen *et al.*, 2002). Nesprin-1 and -2 isoforms also differ in subcellular localisation. Not all isoforms are integral membrane proteins as some do not have a KASH-domain (Padmakumar *et al.*, 2004). Their subcellular location depends on their protein domains and the cell type (Zhang *et al.*, 2001; Rajgor *et al.*, 2012; Zhang *et al.*, 2002). Most isoforms have been identified only at the mRNA level and it is not clear whether all are translated into functional proteins.

Nesprins form connections with all three cytoskeletal networks through N-terminal interactions. Nesprin-1 and -2 associate with the actin cytoskeleton while nesprins-3 and -4 indirectly bind intermediate filaments and microtubules, respectively (Wilhelmsen *et al.*, 2005; Roux *et al.*, 2009; Zhang *et al.*, 2002) (**Figure 1.9**). At the NE,

Figure 1.12 has been omitted for copyright reasons. Please refer to Mellad *et al.* (2011) figure 2, or the hard copy version of this thesis for the image.

Figure 1.12. Mammalian nesprin isoforms and splice variants.

Schematic representation of the four nesprin isoforms and their splice variants. Nesprin-1 and -2 undergo extensive splicing which adds to the complexity of LINC complex isoforms. Giant nesprins contain two calponin homology (CH) domain which bind actin whereas, features like the spectrin repeats (SR) and KASH-domain are common to a lot of the splice variants. Some isoforms lack the KASH-domain. This illustration is not a complete picture, more isoforms are being discovered and characterised. Taken from (Mellad *et al.*, 2011). Restricted re-use permission granted.

the C-terminal KASH-domain of nesprins interacts with the SUN-domain of SUN1 and SUN2 in the ER/NE lumen and forms a protein bridge over the PNS. The KASH-SUN interaction was termed the LINC complex and demonstrates the coupling of the cytoskeleton to the nucleus (Crisp *et al.*, 2006; Padmakumar *et al.*, 2005; Haque *et al.*, 2006).

Nesprin isoforms remain poorly understood because of the many technical difficulties encountered when trying to detect the individual nesprin variants. The majority of the isoforms have the same general protein structure altering only in the spectrin repeat rod-domain making it hard to distinguish specific isoforms (**Figure 1.12**). However, isoform expression does exhibit some tissue specificity (Zhang *et al.*, 2001; Randles *et al.*, 2010).

Nesprin-1 and ***nesprin-2*** isoforms are known by a few different names. The first group to identify (what is now more commonly known as nesprin-1) in mice named this protein synaptic nuclear envelope-1 (Syne-1) because it was the first protein to be concentrated at synaptic nuclei (Apel *et al.*, 2000). Another group also isolated the same protein but felt the name did not reflect the widespread tissue pattern where the protein was localised to the NE in skeletal, cardiac and smooth muscle cells. In light of this, the protein was re-named myocyte nuclear envelope-1 (Myne-1) (Mislow *et al.*, 2002a). The characterisation of this protein in human muscle tissue led to the name nesprin-1 (nuclear envelope spectrin repeat proteins) owing to its cellular localisation and protein domain structure (Zhang *et al.*, 2001). The name nesprin has since been generally adopted.

Nesprin-2 was first identified from database searches by two independent groups and was given the name syne-2 because of its close homology with syne-1 by one group (Apel *et al.*, 2000), whilst the other group named it nesprin-2 (Zhang *et al.*, 2001). As nesprin-1 and -2 giants are highly homologous, they show a degree of redundancy in function as will become apparent in this section.

The major, full-length nesprin-1 isoform (formerly known as enaptin) consists of 8749 amino acids with a predicted molecular weight of 1 MDa and so is one of the largest proteins in the cell. Syne-1, myne-1 and nesprin-1 are all in fact alternative splice variants of enaptin, which is now called nesprin-1 giant (Padmakumar *et al.*, 2004; Zhang *et al.*, 2002). The largest, full-length nesprin-2 isoform has a molecular weight of 796 kDa and was originally named nucleus and actin connecting element (NUANCE) but has now been re-named as nesprin-2 giant (Zhen *et al.*, 2002).

Nesprin-1 giant and nesprin-2 giant tethers nuclei to the actin cytoskeleton (Starr & Han, 2002; Padmakumar *et al.*, 2004; Zhen *et al.*, 2002). In support of this, genetically modified knockout mice lacking the nesprin-1 KASH-domain show that myonuclei are not anchored in position and therefore float freely (Zhang *et al.*, 2007). Nesprin-2 giant and SUN2 have been shown to be components of TAN (transmembrane actin-associated) lines which couple the nucleus to the actin cytoskeleton to facilitate the actin-dependent nuclear movement in migrating fibroblasts (Luxton *et al.*, 2011). This is another example of how elements of the LINC complex are involved in the cytoskeleton to nucleoskeleton connection.

Nesprin-1 giant and nesprin-2 giant are ubiquitously expressed across a wide range of human tissues including neurological gastro-intestinal muscular, genito-urinary, lymphoid and haemopoietic, pulmonary, fetal and placental as well as a range of cancer cell lines. Particular high expression was noted in kidney, liver, stomach, placenta whilst skeletal muscle and brain were lowly expressed. Interestingly, cancer cell lines, with the exception of Daudi Burkitt's lymphoma cells were absence or mere trace expression of nesprin-2 suggesting that like nesprin-1, nesprin-2 may have a role in chromatin organisation (Zhen *et al.*, 2002).

Nesprin-1α, -1β, -2α and -2β isoforms are all known to localise at the NE (Zhang *et al.*, 2001) via a KASH-dependent mechanism (Zhang *et al.*, 2001; Zhang *et al.*, 2002). In addition, they all interact with emerin and nesprin-1α, -2α and -2β bind lamin A/C (Wheeler *et al.*, 2007; Zhang *et al.*, 2001; Mislow *et al.*, 2002b). This suggests that these nesprin isoforms are also located at the INM. In support of this, evidence from immuno-gold EM studies in HaCat cells shows that nesprin-2 isoforms are located at both the ONM and INM. Moreover, nesprin-2 KASH-containing isoforms are required for proper emerin localisation at the INM (Libotte *et al.*, 2005; Wheeler *et al.*, 2007; Zhang *et al.*, 2005).

In nesprin-2 knockout mice both synaptic and non-synaptic nuclei are correctly positioned and mice are viable, however, nesprin-1 and nesprin-2 double knockout mice die shortly after birth. In the time between birth and death they are capable of moving their legs in response to pain but not their ribcage (Zhang *et al.*, 2007). This research shows that either nesprin-1 or nesprin-2 are required for survival and echoes

previous comments on nesprin-1 and -2 having a high degree of functional redundancy.

Nesprin-3 is ubiquitously expressed and possesses two alternatively spliced variants, nesprin-3α (108 kDa) and 3β (99 kDa). Unlike nesprin-1 and -2, nesprin-3α and -3β lack the N-terminal CH domains but nesprin-3α has a plectin binding domain (PBD). Plectin is a member of the plakin family of diverse cytolinkers (Wiche, 1998). Nesprin-3α interacts with dimerised plectin promoting its localisation at the ONM (Ketema *et al.*, 2007). Plectin in turn binds the intermediate filament network (Wilhelmsen *et al.*, 2005; Ketema *et al.*, 2007). Thus, nesprin-3α indirectly connects intermediate filaments to the nucleus (**Figure 1.9**).

Nesprin-4 is an epithelial-specific KASH-domain protein. It is expressed in secretory epithelium such as salivary glands, exocrine pancreas, bulbourethral gland and mammary tissues. Kinesin was identified as a nesprin-4 binding partner following IP of GFP-tagged nesprin-4 lacking the KASH-domain coupled with mass-spectrometry (MS). Kinesin is a plus-end-directed microtubule motor protein. Nesprin-4 is thus a kinesin-1 adapter protein and provides a docking site for the protein at the NE. Together they promote positioning of the nucleus towards the basal membrane in secretory cells (Roux *et al.*, 2009).

1.2.4 Functions of the LINC complex

The importance of the LINC complex is evident from its highly conserved nature in both the animal and plant kingdoms hence, the purpose of this connection must be universal. Here I discuss LINC complex functions and the evidence supporting these ideas.

1.2.4.1 Nuclear migration and positioning

Nuclei are far from static in a eukaryotic cell, on the contrary the nucleus is a dynamic organelle, repositioning itself in response to cellular requirements. Cellular processes such as fertilisation, embryogenesis, cell polarisation, cell migration and cell division require movement of the nucleus to specific regions in the cell (Reinsch & Gonczy, 1998; Burke & Roux, 2009). Nuclear migration requires crosstalk between the cytoskeleton and the nucleus, and the LINC complex couples the two compartments for this purpose. The identification of the LINC complex has furthered research in the nuclear migration field and shows that the divergent N-terminus of the SUN proteins interacts with the nuclear lamina and/or chromatin while the variable N-termini of the nesprin proteins bind to all three cytoskeletal networks, actin, microtubules and intermediate filaments. The constant factor is the SUN-KASH interaction at the NE (Burke & Roux, 2009) (**Figure 1.9**).

Nuclear movement requires force generated by the cytoskeleton and the majority of nuclear migration is microtubule-dependent, but some actin-dependent mechanisms have started to emerge. An example of microtubule-driven nuclear positioning involves the nesprin-4 isoform and the plus-end microtubule motor protein kinesin-1. Together the two proteins move the nucleus towards the microtubule plus-end and the basal membrane in secretory epithelial cells. Similarly, in *C.elegans* ZYG-12 and matefin mediate the coupling of the centrosome to the nucleus by recruiting the dynein complex to the ONM which in turn pulls the nucleus towards the centrosome located at the microtubule minus-end (Malone *et al.*, 2003).

Emerging research highlights the role of actin-dependent nuclear migration. Cell polarisation prior to migration in fibroblasts requires the movement of the nuclei away from the leading edge while centrosomes remain stationary, leading to overall repositioning of centrosomes and golgi towards the leading edge (Gomes *et al.*, 2005). The LINC complex is now thought to be involved in this process. Recently, two specific components of the LINC complex, nesprin-2 giant and SUN2, have been shown to form TAN lines on the NE. These proteins form linear arrays on the NE that coincide with cytoplasmic actin cables attached to the outer surface of the NE and facilitate nuclear movement in fibroblasts by transmitting force generated from retrograde actin flow to the nucleus. Lamin A/C is not concentrated at these TAN lines but acts to anchor them to the nucleus (Luxton *et al.*, 2011).

1.2.4.2 Mechanotransduction

For some time it has been known that the cell is hard-wired from the receptors on plasma membrane to the nuclear interior and the LINC complex explains how the various cytoskeletal networks connect to the nucleus via the SUN-KASH interaction.

Mechanotransduction is the cellular response to external mechanical stimuli. Studies have shown that by attaching integrin beads to the surface of cells and creating tension by movement in a certain direction, the nucleus also realigns in the same direction (Maniotis *et al.*, 1997). Mechanical stress generated from the cytoskeletal networks is transferred to the nucleus and can induce changes in gene expression (Andres & Gonzalez, 2009).

To assess the role of the LINC complex in intracellular force transmission, a recent study used biophysical assays where MEFs were placed under cytoskeletal stress through computer controlled microneedle manipulation and the cytoskeletal displacement was observed. In wild-type cells, the nucleus and regions of cytoplasm distant from the microneedle showed high degree of displacement, confirming strong connection between the cytoskeleton and the nucleus. However, in the presence of dominant-negative SUN or nesprin mutants that disrupt the LINC complex, this displacement was significantly reduced. MEFs transiently expressing mini nesprin-2 giant showed major nuclear and cytoskeletal displacement. This suggests that the LINC complex not only couples the cytoskeleton to the nucleus but transfers motion generated by tension across the NE (Lombardi *et al.*, 2011). In addition, wound-healing migration assays show diminished cell polarisation in cells expressing the dominant-negative nesprin mutant (Lombardi *et al.*, 2011). Similarly, overexpression of dominant-negative nesprin mutants in *Lmna*$^{-/-}$ MEFs disrupts the LINC complex and leads to reduced cellular mechanical stiffness, this supports the fact that the LINC complex is important for cell rigidity (Stewart-Hutchinson *et al.*, 2008).

1.2.4.3 Chromosome reorganisation in meiosis

In meiosis, genetic variation is achieved by exchange of genetic material between homologous chromosomes. The three key events during first meiotic division are homologous pairing of duplicated chromosomes, synapsis, where the synaptonemal complex forms between the homologous pairs along their entire length, and crossover of genetic material between the homologues. The pairing of homologues requires

sequestering homologues to the NE to find matching pairs, and this involves dynamic movement of chromosomes.

Emerging research has shown that the LINC complex facilitates tethering of telomeres at the nuclear periphery and movement of chromatin for homologue pairing. First noted in *S.pombe*, SUN-domain protein Sad1 is required for bundling meiotic telomeres to form a 'bouquet' structure. Bouquet proteins, Bqt1 and Bqt2, connect the SPB-localised Sad1 to Rap1, a telomere-associated protein (Chikashige *et al.*, 2006). Similarly in *S.cerevisiae*, SUN-domain protein Mps3 appears to anchor telomeres at the NE through its association with Ndj1 and is necessary for bouquet formation (Conrad *et al.*, 2007). Moreover, Mps3 is critical for chromosome movement in meiosis. An Mps3 mutant lacking the SUN-domain still localised correctly to the NE and did not affect SPB duplication, however, defects arose in meiotic prophase I where chromosomes experienced decreased chromosomal movement and premature synaptonemal complex formation (Rao *et al.*, 2011).

In *C.elegans*, each chromosome has a pairing centre, a region which facilitates homologue pairing and connects to the microtubule network. The matefin and ZYG-12 SUN-KASH complex transfers microtubule-generated forces from the cytoskeleton to the nucleus to reorganise meiotic chromosomes and promote homologue pairing (Penkner *et al.*, 2007). Depolymerisation of microtubules with colchicine disrupts microtubule networks and inevitably inhibits chromosome pairing (Sato *et al.*, 2009). Interestingly, the dynamic nature of this particular LINC complex requires meiosis-specific phosphorylation of matefin by Polo-like kinase 2 (PLK2) for homologous

pairing. The absence of PLK2 prevents homologue pairing but leads to non-homologue synapsis (Labella *et al.*, 2011).

Mammalian SUN1 and SUN2 also play a role in telomere attachment to the NE (Ding *et al.*, 2007; Schmitt *et al.*, 2007). SUN1 knockout mice display severe disruptions to homologue pairing, synapsis and crossover, in both spermatocytes and oocytes, due to an inability of SUN1 to anchor telomeres to the nuclear periphery, which leads to sterility (Ding *et al.*, 2007). The same group also found that SUN2 is not expressed in spermatocytes and concluded that SUN2 is not important for meiosis. In contrast, another group have shown that SUN2 is found at telomere attachment sites and is involved in telomere dynamics in meiotic cells (Schmitt *et al.*, 2007). This research highlights the conserved role of the LINC complex in telomere anchorage to the NE periphery in meiotic cells and dynamic chromosomal movement aiding homologue pairing and meiotic progression.

1.3 Laminopathies and nuclear envelopathies

Laminopathies are defined as a group of inherited diseases arising from mutations in the genes that encode nuclear lamins. These can be sub-divided into primary and secondary laminopathies where the former is concentrates on mutations of the lamins genes *LMNA*, *LMNB1*, *LMNB2,* while the later focuses on genes such as *FACE-1/ZMPSTE24,* which are involved in the maturation of prelamin A (Broers *et al.*, 2006). In recent years, additional mutations have been found in genes encoding NE proteins and the term nuclear envelopathies now encompasses diseases associated with both mutations of NE proteins and the nuclear lamina (Worman & Bonne, 2007).

Laminopathies encompass a range of diseases with varying clinical phenotypes but surprisingly, the majority of laminopathies are a result of mutations in a single gene, *LMNA*. To date, over 200 mutations have been recorded in the *LMNA* gene resulting in an array of laminopathies (http://www.umd.be). Laminopathies affect mainly mesenchymal tissues and can be divided into categories based on tissue specificity; striated muscle, peripheral nerves, adipose tissue or systemic involvement such as accelerated ageing disease (Broers *et al.*, 2006). Furthermore, the findings that mutations in other NE proteins can lead to similar disease phenotypes is beginning to shed light on potential disease mechanisms and also advance our understanding of these NE proteins.

1.3.1 Striated muscle diseases

To date, diseases affecting striated muscle account for approximately 60% of laminopathies (Burke & Stewart, 2006). Emery Dreifuss muscular dystrophy (EDMD) is a muscle-wasting disease of the upper and lower limbs accompanied by weakness, contractures of the tendons restricting movement of the joints, cardiomyopathy and cardiac conduction defects (Emery, 1989).

Lamin A/C mutations cause autosomal-dominant and occasionally recessive forms of EDMD (Vigouroux *et al.*, 2000). Dominant *LMNA* mutations cause a range of phenotypes, with different clinical names, but these are probably just variations of the same overall disease. For example, EDMD and limb girdle muscular dystrophy 1B (LGMD-1B) involves different skeletal muscle groups whereas dilated cardiomyopathy (DCM) only affects the heart (Gruenbaum *et al.*, 2005).

Interestingly, mutations in integral proteins of the NE have also been implicated in EDMD. Mutations in the X-linked *EMD* gene, which encodes the INM protein emerin, has also been shown to cause EDMD (Sullivan *et al.*, 1999). SUN and nesprin mutation are also associated with EDMD (Zhang *et al.*, 2007) (S.Shackleton and M.Wehnert unpublished data). Furthermore, four and a half LIM domain protein 1 (FHL1), although not an INM protein, has been identified as another gene responsible for EDMD (Gueneau *et al.*, 2009). Thus, mutations in multiple genes are associated with EDMD. Most of them have been shown to interact which each other, suggesting that they all function in the same pathway and support a common disease mechanism.

1.3.2 Peripheral neuropathy

Charcot-Marie-Tooth type 2b (CMT2B) disease is a laminopathy which affects peripheral nerves. Among other mutations, a missense mutation in the *LMNA* gene at R298C commonly causes an autosomal recessive form of the disease (De Sandre-Giovannoli *et al.*, 2002). Patients exhibit clinical features such as loss of reflexes in lower limbs, weakness and wasting of muscles due to enervation and motor defects (Chaouch *et al.*, 2003). Tissues from patients display a loss of large myelinated nerve fibres, while the sciatic nerve of *Lmna*$^{-/-}$ mice shows demyelination (De Sandre-Giovannoli *et al.*, 2002; Chaouch *et al.*, 2003). It is currently not known why mutations in lamin A/C should specifically result in neuropathy.

1.3.3 Lipodystrophies

LMNA mutations affecting adipose tissue cluster within the C-terminal tail domain of lamin A/C and result in Dunnigan-type familial partial lipodystrophy (FPLD) where the autosomal dominant *LMNA* missense mutation R482W is the most frequent

(Shackleton *et al.*, 2000). At birth, patients have normal fat distribution but at the onset of puberty, subcutaneous adipose tissue is lost from the upper and lower extremities, gluteal region and areas of the trunk with sparing of the neck and face area (Dunnigan *et al.*, 1974). This is associated with insulin resistance, type-2 diabetes and increased risk of heart disease.

1.3.4 Accelerated aging disorders

LMNA mutations are also involved in systemic syndromes such as the premature ageing laminopathy Hutchinson-Gilford progeria syndrome (HGPS). In addition to *LMNA* mutations, mutations in ZMPSTE24, an enzyme involved in post-translational processing of lamin A also causes HGPS (Worman & Bonne, 2007). This is a devastating disease in which children show signs of premature ageing. As well as this, they experience loss of subcutaneous fat, growth retardation, atherosclerosis, sclerodermatous skin and bone deformations (Sarkar & Shinton, 2001). Most patients die in their early teens due to heart complications. The lamin A/C mutation most commonly associated with HGPS is G608G point mutation which creates a cryptic splice site resulting in the permanent farnesylation of mutant prelamin A, otherwise known as progerin (Eriksson *et al.*, 2003; De Sandre-Giovannoli *et al.*, 2003). Accumulation of this protein to toxic levels is reflected in the disease phenotype (Goldman *et al.*, 2004; Dechat *et al.*, 2007). Other premature ageing conditions caused by *LMNA* mutations are atypical HGPS and atypical Werner's syndrome (Gruenbaum *et al.*, 2005).

1.3.5 Possible disease mechanisms

The question perplexing the laminopathy field is how can mutations, which are spread along the whole *LMNA* gene, give rise to an array of disease phenotypes across a variety of tissues? Several mechanisms have been proposed.

The 'structural' hypothesis speculates that mutations in components of the NE such as lamin A/C, emerin, nesprins and now possibly SUN proteins disrupts connections at the NE hence compromising the structural integrity of nucleus. These variations weaken the NE and are inadequate to withstand mechanical forces upon the NE. This model provides a possible explanation for laminopathies affecting striated muscle as muscle cells are under constant stress from contraction (Capell & Collins, 2006). In support of this theory, evidence already shows that some mutations in components of the LINC complex disrupt the binding and localisation of others (Zhang *et al.*, 2007; Ostlund *et al.*, 2001; Holt *et al.*, 2003) and disruption of the nuclear lamina or LINC complex results in reduced resistance of the NE to mechanical force (Broers *et al.*, 2004; Lombardi *et al.*, 2011; Stewart-Hutchinson *et al.*, 2008).

The gene expression hypothesis is based on the fact that A-type lamins and associated proteins regulate gene expression through interactions in signal transduction pathways with transcription factors and chromatin-associated proteins (Andres & Gonzalez, 2009). Therefore, mutations in the lamin genes are thought to alter binding to chromatin with subsequent effects on transcription and gene expression, potentially explaining the vast variation in laminopathy phenotypes and tissue specificities (Andres & Gonzalez, 2009; Capell & Collins, 2006).

1.4 Nuclear envelope dynamics in mitosis

Cell reproduction is comprised of a series of events collectively known as the cell cycle whereby components of the cell, including the genetic material, are duplicated and then divided equally between two daughter cells. There are four phases in the eukaryotic cell cycle, G1, S, G2 and M. The first three stages are collectively known as interphase. There is an additional phase called G0 where cells exit the cell cycle and no longer proliferate but are still metabolically active, this occurs upon terminal differentiation. Some cells are capable of re-entering the cell cycle under the instruction of extracellular signals.

G1 (gap phase 1) is the growth phase immediately after M phase where the cell forms new organelles, hence a great deal of protein synthesis takes place in a highly metabolic cell. This is followed by S (synthesis) phase and is the stage where DNA is replicated. The identical replicated chromosomes are bound to each other at a region called the centromere; at this point they are known as sister chromatids. The cell then enters a second growth phase, G2 (gap phase 2), in preparation for M phase. Entry into M phase commits the cell to divide into two identical daughter cells (Johnson & Walker, 1999; Nigg, 2001).

1.4.1 Mitosis

M (mitotic) phase is where sister chromatid separation and cell division are achieved. Mitosis itself is an elaborate series of events that brings about dramatic changes in the architecture of the interphase cell (Morgan, 2006). It can occur in an open or closed manner; this refers to the whether the organism requires NE disassembly for mitosis or not. Yeast proceed by closed mitosis while higher eukaryotes, such as nematodes,

arthropods and mammals, require NEBD for mitotic progression (Foisner, 2003). There are six distinct stages of eukaryotic open mitosis: prophase, prometaphase, metaphase, anaphase, telophase and cytokinesis (**Figure 1.13**).

Prophase is characterised by the condensation of chromosomes into a densely coiled and folded structure which is visible under a light microscope (Hirano, 2000). Simultaneously, the duplicated centrosomes, located in the cytoplasm, start to move apart to promote spindle assembly outside the nucleus (Crasta *et al.*, 2008). Prometaphase is the defining moment when the cell undergoes NEBD (**section 1.4.3.2**). Sister chromatids now have access to the spindle, composed of microtubules nucleated from the centrosomes (spindle poles). They attach to the mitotic spindle via the kinetochore, a protein structure that assembles on the centromere. Once attached, chromosomes are pulled to the central region of the cell by tension in the spindle apparatus. In metaphase, the sister chromatids are fully aligned on the mitotic spindle equator, or metaphase plate, between the two poles, awaiting signals for chromosome segregation (Salaun *et al.*, 2008).

The appropriate signals in anaphase dissolve the cohesion ring between the two sister chromatids and separate the centromeres in order to segregate each of the sister chromatids to opposite poles of the mitotic spindle. The spindle poles also move further apart to maximise chromosome separation (Salaun *et al.*, 2008; Pines, 2011). In telophase, the reforming NE encloses the two sets of decondensing chromosomes, along with other nuclear components, forming two identical daughter nuclei (Morgan, 2006). The mitotic spindle is no longer required and so is disassembled and each daughter nucleus is associated with one centrosome. In cytokinesis, a contractile ring

Figure 1.13 has been omitted for copyright reasons. Please refer to Pines (2011) figure 1, or the hard copy version of this thesis for the image.

Figure 1.13. The cell cycle, checkpoints and regulation by cyclin-dependent kinases.

The four phases of the cell cycle, G1, S, G2 and M are governed by cyclin-dependent kinases (CDKs) and their regulatory cyclin subunit as indicated. The cell is assessed at three stages of the cell cycle known as checkpoints for DNA damage and to see if the cell has met the criteria required for entry into the next phase/stage. If the cell is not satisfied it is halted at that checkpoint until the necessary repairs have been conducted. Alternatively, cells can exit the cell cycle and enter a quiescent stage known as G0. The three checkpoints are at the G1/S boundary, G2/M boundary and at the metaphase-to-anaphase transition indicated by the green bars. Mitosis consists of six stages, prophase (chromosome condensation), prometaphase (attachment of chromosomes to mitotic spindle), metaphase (alignment of chromosomes on metaphase plate), anaphase (sister chromatids separation to opposite poles) and telophase (NE reforms). These are followed by cytokinesis (separation of the cytoplasm to form two identical daughter cells). Adapted from (Pines, 2011). Restricted re-use permission granted.

of actin and myosin filaments creates the cleavage furrow which pinches the cell in two. The equal distribution of the cytoplasm between the two identical daughter cells marks the end of cell division (Salaun *et al.*, 2008).

1.4.2 Cell cycle regulation

There are approximately 500 protein kinases encoded by the human genome which makes them one of the largest protein families (Hanks, 2003). Their function is to modify proteins by phosphorylation which involves targeting of substrates by the addition of a phosphate group on serine, threonine or tyrosine residues. This induces changes in the biochemical nature of the substrate altering protein charge and conformation. Phosphorylation can result in changes in the activation state of a protein, modulate protein interactions and alter complex formation. The majority of protein kinases are cell cycle regulators.

Progression through the cell cycle relies on a family of enzymes, named the cyclin-dependent kinases (CDKs), and their regulatory subunits called cyclins. Together they form the core component of cell cycle control and drive the unidirectional progression of the cell cycle. CDKs are expressed at a constant level throughout the cell cycle and remain inactive until bound to a cyclin subunit, at which point they become activated with the capacity to phosphorylate target substrates (Malumbres & Barbacid, 2005).

CDK activity oscillates throughout the cell cycle and these spikes in activity are due to cell cycle-dependent expression of the different cyclins (Morgan, 1997). Distinct CDK-cyclin complexes phosphorylate components of the cell cycle machinery in a cell cycle-dependent manner, promoting progression through a cell cycle phase or transition into

the next. CDK-cyclin complexes are regulated by degradation of the cyclin regulatory subunit, rendering the CDK inactive. Different CDK-cyclin combinations drive phosphorylation events at certain stages of the cell cycle (Morgan, 1997) (**Figure 1.13**). For example, cyclin A levels peak in G2 and its binding to CDK1 is essential for mitotic entry and activation of CDK1-cyclin B. The CDK1-cyclin B complex then phosphorylates proteins required for mitotic entry and the early stages of mitosis such as disassembly of the nuclear lamina and chromatin condensation (Nigg, 2001; Pagano *et al.*, 1992; Lindqvist *et al.*, 2009).

The cell cycle is a complex series of events that are prone to mistakes. Accumulation of mistakes and incompletion of phases can lead to aneuploidy and ultimately cancer. The cell safeguards against errors by assessing the genomic and physiological state at cell cycle checkpoints. These are significant control points which can temporarily halt the cell in a particular phase until the appropriate processes have been fully and accurately completed. The eukaryotic cell cycle has three particular checkpoints that operate at the G1/S boundary, G2/M boundary and the metaphase/anaphase transition (**Figure 1.13**).

The G1/S checkpoint ensures that the cell has the relevant growth factors and nutrients required and that the cell has reached critical mass to enter S phase. The DNA is also examined for damage and repaired prior to DNA replication in S phase. The G2/M checkpoint ensures the genome has been completely replicated and is damage-free. It also determines whether the cell is large enough to divide (Alberts, 2002; Morgan, 2006). The third checkpoint, occurring in mitosis between metaphase and anaphase, and also known as the spindle assembly checkpoint (SAC), makes sure that

all the sister chromatids have attached to the mitotic spindle and are aligned on the metaphase plate (Rieder & Salmon, 1998).

Up to this point, the sister chromatids are encircled by cohesin rings around the centromere and the arms of the chromosomes to bind them together. The mitotic kinase polo-like kinase 1 (PLK1) removes the cohesion rings around the sister chromatid arms through phosphorylation (Sumara *et al.*, 2002) but the cohesion associated with the centrosome is removed by a different mechanism. This involves the protease separase which is associated with the centrosome and remains in an inactive state bound to securin and phosphorylated by CDK1-cyclin B until the cell is ready to progress to anaphase (Chestukhin *et al.*, 2003; Zou *et al.*, 1999; Stemmann *et al.*, 2001). The metaphase-anaphase transition involves a series of activation and inactivation events starting with the release of cell division cycle 20 (cdc20) from centrosomes and spindle poles, this activates the anaphase promoting complex/cyclosome (APC/C) and resulting in targeting securin for ubiquitinylation and degradation (Liu *et al.*, 2010; Fang *et al.*, 1998; Glotzer *et al.*, 1991; Hagting *et al.*, 2002). This in turn triggers separase to cleave the cohesion ring around the centromere (Uhlmann *et al.*, 1999). The mitotic spindle can now segregate the sister chromatids to opposite ends of the cell through rapid depolymerisation of the spindle microtubules. In addition, the APC/C signals for cyclin B degradation, inactivating CDK1 and promoting progression to mitotic exit (Glotzer *et al.*, 1991).

1.4.3 Regulation of mitotic protein phosphorylation

Regulation of M phase progression relies on three post-translational mechanisms: protein phosphorylation, degradation and dephosphorylation. A vast number of

phosphorylation events occur at the onset of mitosis and persist at a high level until the metaphase-to-anaphase transition. The major mitotic kinase responsible for initiating the majority of these phosphorylation events is CDK1, bound to cyclin A or cyclin B. In addition to this particular kinase, other mitotic kinases play major roles throughout mitosis including members of the Polo, Aurora and NIMA (never in mitosis A) families (Nigg, 2001) (reviewed in **Table 1.2**).

CDK1 activation does not depend on binding to cyclin B alone but also dephosphorylation of two threonine residues in its ATP-binding active site, T14 and T15. In interphase, Wee1 and Myt1 kinases constitutively phosphorylate these residues preventing activity but, at the G2/M transition, protein phosphatase cdc25 removes the phosphate groups at a faster rate than the opposing kinases, thereby activating CDK1-cyclin B. In turn, CDK1 and PLK1 phosphorylate Wee1 and Myt1 for their proteosomal degradation and inhibition, respectively (Morgan, 1995). Rapid activation leads to phosphorylation of serine and threonine residues on numerous substrates for entry into mitosis. A few examples are the phosphorylation of nuclear lamins to depolymerise the nuclear lamina network (Gerace & Blobel, 1980; Heald & Mckeon, 1990; Luscher *et al.*, 1991; Peter *et al.*, 1990), phosphorylation of nucleoporins to dissociate from the NPC complex leading to permeabilisation of the NE (Laurell *et al.*, 2011) and phosphorylation of histone H1 to promote chromosome condensation (Doree & Galas, 1994). At the SAC, CDK1 is inactivated by degradation of the cyclin B regulatory subunit by APC/C. This drives the cell towards mitotic exit and cytokinesis (Glotzer *et al.*, 1991).

Table 1.2. Properties of major mammalian mitotic kinases.

Information in this table has been adapted from the following reviews (Nigg, 2001; Salaun *et al.*, 2008; Pines, 2011; Wurzenberger & Gerlich, 2011; Ferrari, 2006; Luo & Liu, 2012).

Mitotic Kinase	Subcellular localisation	Mitotic functions
CDK1	Centrosome (*interphase*) Nucleus (*interphase/prophase*) Cytoplasm (*prometaphase/metaphase*) Spindle microtubules (*prometaphase/metaphase*)	G2/M transition Centrosome separation Spindle assembly Nuclear lamina depolymerisation and disassembly Chromatin condensation Regulation of APC/C
PLK1	Nucleus (*interphase*) Centrosome (*prophase/metaphase/cytokinesis*) Kinetochore (*prometaphase/metaphase*) Central spindle region (*anaphase*) Midbody (*telophase/cytokinesis*)	G2/M transition Regulation of CDK1-cyclin B Centrosome maturation Microtubule dynamics Localisation of spindle checkpoint proteins to kinetochore Sister chromatid separation Contributes to APC/C activation Activates kinesins for cytokinesis
Aurora A	Centrosome Spindle microtubules	G2/M transition Centrosome separation Centrosome maturation Recruits protein involved in microtubule nucleation Bipolar spindle assembly Cytokinesis
Aurora B	Kinetochore (*metaphase-anaphase transition*) Spindle midzone (*anaphase/telophase*)	Promotes chromatin condensation SAC activation Correct kinetochore to spindle attachment Cytokinesis
Nek 2	Centrosome (*prophase/metaphase/cytokinesis*) Condensing chromosomes (*prophase*) Kinetochore (*metaphase*) Midbody (*cytokinesis*)	Centrosome splitting

The massive structural and architectural changes that the eukaryotic cell experiences to facilitate chromosome segregation and cell division in early mitosis need to be reversed for the cell to function in interphase. APC/C targeting and destruction of cyclins to inactivate CDK1-cyclin B is not sufficient, since the phosphate group still remains on substrates, preventing their interphase functions. The activation of protein phosphatases is therefore required for the removal of phosphate groups from the substrates, in order to exit mitosis and rebuild the interphase cell. Much work has been carried out in yeast to understand this process, where cdc14 is the key mitotic phosphatase (Visintin *et al.*, 1998; Wurzenberger & Gerlich, 2011). Initial findings on mammalian protein phosphatases place emphasis on protein phosphatases PP1 and PP2A (Wurzenberger & Gerlich, 2011; Barr *et al.*, 2011). Recently, studies observing mitotic exit found that PP1 and PP2A were required for lamin dephosphorylation and NE reassembly suggesting that these are the major mitotic phosphatases (Thompson *et al.*, 1997; Tseng & Chen, 2011).

1.4.3.1 Disassembly of NE protein complexes

In interphase, the NE of eukaryotic cells consists of the nuclear lamina, NPCs and the ONM and INM. Protein-protein interactions within and between the structures form many networks and complexes that ensure structural stability and protect against mechanical stress. At the onset of mitosis, the cell undergoes profound structural reorganisation to accommodate the needs of chromosome segregation and cell division. Higher eukaryotes proceed by open mitosis, which requires NE disassembly as the MTOC is positioned in the cytoplasm and therefore cannot gain access to the

chromosomes. Yeast cell division is carried out in a closed mitosis as the SPB, the yeast equivalent of the MTOC is inserted into the NE at mitosis (Guettinger *et al.*, 2009).

NEBD defines the transition between prophase and prometaphase and requires depolymerisation of the nuclear lamina, detachment from the chromatin and disassembly of the NPCs (Foisner, 2003). These events occur in a timely fashion and are a prerequisite to NEBD. Phosphorylation of components of the nuclear lamina, nucleoporins and INM proteins modulates these interactions by changing their structural conformation, thereby destabilising the NE (Foisner, 2003). The fragility of the NE is thought to aid a microtubule-dependent mechanism that tears open the NE (Beaudouin *et al.*, 2002; Salina *et al.*, 2002).

The higher order structure of the nuclear lamina is composed of A-type and B-type filamentous lamin networks, which becomes hyperphosphorylated at the onset of mitosis primarily by the serine/threonine mitotic kinase CDK1 (Gerace & Blobel, 1980; Luscher *et al.*, 1991; Peter *et al.*, 1990; Ottaviano & Gerace, 1985; Ward & Kirschner, 1990). These events induce depolymerisation of the nuclear lamina, disrupting its attachment to the INM and interactions with chromatin and may be a trigger for chromatin condensation (Heald & Mckeon, 1990; Peter *et al.*, 1990; Ward & Kirschner, 1990; Kuga *et al.*, 2010; Pfaller *et al.*, 1991). The two lamin networks are independent of each other as A-type lamins are shown to depolymerise in prophase, whilst B-type lamins depolymerise in metaphase (Georgatos *et al.*, 1997). Lamin phosphorylation sites are situated in the N-terminal head and C-terminal globular tail domains to depolymerise the nuclear lamina although some sites have been identified in the α-helical rod-domain. Phospho-deficient mutations in these sites prevent disassembly

(Heald & Mckeon, 1990; Kuga *et al.*, 2010). Data so far have shown that CDK1 is the major mitotic kinase phosphorylating lamins (Heald & Mckeon, 1990; Peter *et al.*, 1990). There is limited evidence showing that lamin B is also a substrate for protein kinase C (PKC) in mitosis (Thompson & Fields, 1996) but is also phosphorylated in interphase by PKA and PKC (Peter *et al.*, 1990).

Integral membrane proteins residing at the INM are also phosphorylated at the onset of mitosis predominantly by CDK1. LBR, LAP1, LAP2, emerin, MAN1 and p54 mitotic phosphorylation further disrupts protein networks and associations with chromatin promoting NE fragility in preparation for eventual NEBD (Foisner & Gerace, 1993; Courvalin *et al.*, 1992; Hirano *et al.*, 2005; Hirano *et al.*, 2009; Bailer *et al.*, 1991). LBR mitotic phosphorylation causes loss of chromatin binding but not lamin B (Courvalin *et al.*, 1992; Nikolakaki *et al.*, 1997; Meier & Georgatos, 1994). This is to disassemble the NE structure and also inhibits ER attachment to chromatin until required for NE reassembly (Tseng & Chen, 2011; Nikolakaki *et al.*, 1997; Takano *et al.*, 2004).

Phosphorylated LAP2, but not LAP1, loses its ability to bind lamin B, furthermore, mitotic LAP2 does not interact with mitotic chromosomes (Foisner & Gerace, 1993). Mitotic phosphorylation of LEM-domain proteins emerin and MAN1 initiates dissociation away from BAF, which mediates binding to DNA in interphase (Hirano *et al.*, 2005; Hirano *et al.*, 2009). Much of this work was conducted 10-20 years ago and so the molecular details are not fully elucidated due to technical limitations at that time.

Dissociation of the NPC is a key event for NEBD and requires phosphorylation of nucleoporins to promote subcomplex disassembly (Laurell *et al.*, 2011; Dultz *et al.*, 2008). Hyperphosphorylation of the nucleoporin Nup98 by CDK1, PLK1 and Nek kinases promotes its dissociation from the NPC in prophase, allowing the NE to become more permeable hence, permitting entry of cytoplasmic components into the nucleus. Furthermore, expression of mutant phospho-deficient Nup98 delays NEBD by slowing downs its disassociation from the NPC (Laurell *et al.*, 2011). Other NPC components, for example, those that lie within the Nup107-160 subcomplex, are specifically phosphorylated in mitosis, including Nup96, Nup107, Nup133 and Nup160. These phosphorylation events do not disassemble interactions within the subcomplex but disrupt interactions with other subcomplexes of the NPC (Glavy *et al.*, 2007).

1.4.3.2 Nuclear envelope breakdown (NEBD)

NEBD is the crucial moment when the NE loses its integrity. This allows the capture of the sister chromatids by the mitotic spindle and chromosome segregation. Two elegant studies have demonstrated that NEBD is promoted by microtubule-generated forces mediated by the motor protein dynein (Beaudouin *et al.*, 2002; Salina *et al.*, 2002).

A major component of the dynein/dynactin complex, $p150^{Glued}$, firstly establishes itself at the NE in prophase following phosphorylation by PLK1 (Li *et al.*, 2010). However, the mechanism anchoring dynein to the NE remains elusive. In prophase duplicated centrosomes form newly nucleated spindle microtubules which bind to dynein on the NE surface. The spindle microtubules project into the NE forming invaginations, and it is thought that this is due to minus-end-directed movement of dynein, which

generates tension by pulling the attached nuclear membranes towards the centrosome (Salina *et al.*, 2002). The stretching and pulling of the already fragile NE causes it to become weak and tear at the surface distal to the centrosomes, this moment defines NEBD. NE membrane fragments are then pulled away from chromosomes towards the separating poles and are thought to retract into the ER where the integral membrane proteins disperse throughout the ER in the cytoplasm. Removal of the NE allows mitosis to progress (Beaudouin *et al.*, 2002; Salina *et al.*, 2002) (**Figure 1.14**). Interestingly, NEBD can still occur in the absence of dynein action but is delayed demonstrated by overexpression of p62 dynactin subunit which induces dissociation of dynein from the membrane without hindering the centrosome function (Salina *et al.*, 2002). The concerted actions of protein depolymerisation and microtubule-induced tension are thought to induce timely breakdown of the NE.

1.4.3.3 Nuclear envelope reassembly

After the SAC in anaphase when the sister chromatids have segregated to opposite spindle poles, the cell has to reform the NE around each set of chromosomes to complete nuclear division. The profound architectural changes imposed at the onset of mitosis must be reversed, which involves dephosphorylation of mitotically phosphorylated substrates, recruitment of nuclear membranes to the chromosomes, membrane fusion, followed by insertion of NPCs, nucleus enlargement and reformation of the nuclear lamina (Margalit *et al.*, 2005).

Inactivation of CDK1 activity occurs through cyclin B degradation, allows protein phosphatases such as PP1 and PP2A to prevail. Although they have not been directly linked to any particular substrate, PP1 and PP2A have been shown to be required for

Figures 1.14A, 1.14B, 1.14C, 1.14D and 1.14E have been omitted for copyright reasons. Please refer to Burke & Ellenberg (2002) figures 3a, 3b, 3c, 3d and 3e, respectively, or the hard copy version of this thesis for the images.

Figure 1.14. Model of nuclear envelope breakdown.

The simplified schematic illustration shows a cross-section of a nucleus including the centrosomes (orange), microtubules (red), endoplasmic reticulum/nuclear envelope (yellow), nuclear lamina (green) and the chromosomes (purple). **(A)** In interphase, the nuclear envelope segregates the nucleus form the cytoplasm. The chromosomes are housed in the nucleus. In G2, the duplicated centrosomes start to form newly nucleated microtubules. **(B)** In prophase, the microtubules project into the NE forming invaginations and the chromatin condenses. Progression in this manner causes stretching of the NE and weakness in the distal region due to the pulling forces of the motor protein dynein which localises at the NE and binds the microtubules. **(C)** Prometaphase is defined by the tearing of the nuclear lamina causing an influx of cytoplasmic factors into the nucleus and collapse of the NE. **(D)** Progressive fragmentation and **(E)** retraction of the membranes away from the chromosomes towards the centrosomes allows microtubules to capture chromosomes for segregation. Adapted from (Burke & Ellenberg, 2002). Restricted re-use permission granted.

dephosphorylation of CDK1 substrates in order to bind chromatin (Tseng & Chen, 2011; Pfaller *et al.*, 1991; Ito *et al.*, 2007). Chromosome decondensation is also required for mitotic exit. PP1γ is recruited to chromatin at anaphase by its regulatory subunit Repo-Man and dephosphorylates histone H3 (Vagnarelli *et al.*, 2006; Trinkle-Mulcahy *et al.*, 2006; Qian *et al.*, 2011). The INM protein SUN1 in conjunction with hALP also contributes to mitotic chromosome decondensation (Chi *et al.*, 2007).

Reassembly of the NE has been mostly studied in *in vitro* systems using *Xenopus* egg extracts. These experiments show that two distinct populations of precursor membrane vesicles are recruited to the surface of decondensing chromatin where they undergo fusion to form the membranes, followed by insertion of the NPCs (Vigers & Lohka, 1991; Drummond *et al.*, 1999; Sasagawa *et al.*, 1999). Mitotic cells in vertebrates do not appear to vesicularise the NE, instead the NE is retracted back into the ER after NEBD (Ellenberg *et al.*, 1997; Yang *et al.*, 1997). Time-lapse experiments show that NE reassembly begins by recruiting ER tubular ends to chromatin where they are anchored to the chromatin. This results in expansion and formation of ER sheets on the chromatin surface encasing the DNA. Reticulon and DP1 aid the process through their ability to reshape the ER (Anderson & Hetzer, 2007; Anderson & Hetzer, 2008).

How the ER is initially recruited to the chromatin can be partly explained by the actions of the INM proteins at the end of mitosis. INM proteins all remain within the ER during mitosis but studies show LBR, emerin and LAP2β are all recruited to chromatin in very early telophase (Foisner & Gerace, 1993; Furukawa *et al.*, 1997; Haraguchi *et al.*, 2000). Furthermore, LBR, MAN1, LAP2β and transmembrane nucleoporins Ndc1 and POM121

are all believed to drive NE expansion after initial ER tubular end contact. Depletion of these proteins delays NE reassembly, whilst this was not true for SUN1 (Anderson *et al.*, 2009). This may be due to redundancy with SUN2.

Live-cell imaging shows that LBR and emerin localise to the chromatin at the same time, approximately 5 minutes post-anaphase. Initially, both are found at distinct locations, LBR is mainly at the lateral ends of the chromatin, while emerin is situated at the longitudinal core region. Soon after, the two integral membrane populations merge showing a uniform distribution (Haraguchi *et al.*, 2000). Furthermore, phosphorylated LBR in mitosis binds importin-β for its role in targeting nuclear membranes to the chromatin surface. Once within close proximity, importin-β dissociates by switching binding preference to RanGTP. Dephosphorylation of LBR by PP1 has shown to promote chromatin binding (Lu *et al.*, 2010). Thus, the action of protein phosphatases in anaphase is likely to be the trigger for NE reassembly.

1.5 Research aims

In order for mitosis to proceed in higher eukaryotes, the NE has to be disassembled to allow segregation of the chromosomes. NE disassembly is initiated through phosphorylation of the NPC and nuclear lamina. Nucleoporin Nup98 is phosphorylation causes permeabilisation of the NE (Laurell *et al.*, 2011) while A-type and B-type lamin phosphorylation results in the depolymerisation of the nuclear lamina (Heald & Mckeon, 1990; Peter *et al.*, 1990). Phosphorylation of INM proteins LBR, LAP1, LAP2, emerin, and MAN1 disrupts their attachment to the nuclear lamina and chromatin (Foisner & Gerace, 1993; Courvalin *et al.*, 1992; Hirano *et al.*, 2005; Hirano *et al.*, 2009). Collectively, these events weaken the NE hence preparing it for NEBD. Since the

early studies on phosphorylation of INM proteins, many additional INM proteins have been identified and are likely to also play roles in NEBD in mitosis. One of these is SUN1, which plays a key role in NE interactions with the nuclear lamina and, through nesprins, to the cytoskeleton.

Investigations into SUN1 phosphorylation are limited. Meiosis-specific phosphorylation of *C.elegans* matefin at serine 12 promotes homologue pairing (Labella *et al.*, 2011). A single broad phospho-proteomic study highlighting global mitotic substrates and phosphorylation sites identified human SUN1 (hSUN1) as a substrate, which was shown by MS to be phosphorylated at serine S138 (Dephoure *et al.*, 2008).

I propose that, like other INM proteins, hSUN1 is phosphorylated in mitosis and that the protein conformation is altered to such a degree, it loses its interactions with lamin A/C, emerin and nesprins. These events could release hSUN1 from its immobile state at the INM for possible roles in mitotic progression and exit. In the course of my research, I hoped to fully characterise SUN1 and possibly SUN2 phosphorylation and also determine the role of such events in mitosis.

SUN1 is a core component of the LINC complex, its function ensures structural stability and protects against mechanical stress. SUN1 interacts with lamin A/C, emerin and nesprin isoforms yet not all SUN1 binding partners have been determined. For instance, SUN1 is anchored at the INM not through lamin A/C, emerin or small nesprins but through an unknown mechanism (Crisp *et al.*, 2006; Haque *et al.*, 2010). I therefore propose that hSUN1 has many more binding partners than identified so far and that it is not just a core component of the LINC complex, but also part of other

complexes and pathways. Some of these binding partners will most probably be NE integral membrane proteins or nucleoporins but other transient interactions from protein modifiers or cytoplasm to nucleus shuttling proteins are likely too. My research aim is to identify further hSUN1 interacting partners.

CHAPTER 2
Materials and Methods

Chapter 2 Materials and methods

2.1 Materials

2.1.1 Reagents

All chemicals were of analytical grade or higher. **Table 2.1** contains a list of general reagents used and their suppliers. Other reagents are specified in text with the relevant supplier.

Table 2.1. General reagents.

Table of routinely used reagents and their suppliers.

Reagent	Supplier
Bromophenol blue	Acros Organics (Geel, Belgium) – Part of Thermo Scientific® (Waltham, USA)
DMEM **FBS EU approved origin** **GlutaMAX™-1** **OPTI-MEM®1** **Penicillin Streptomycin** **Sodium Pyruvate** **0.5% Trypsin. Trypsin-EDTA**	Gibco® – Part of Life Technologies™ (Paisley, UK)
6x DNA loading dye **GeneRuler™ 1Kb DNA ladder** **PageRuler™ Plus prestained protein ladder**	Fermentas (York, UK) – Part of Thermo Scientific® (Waltham, USA)
Acetic acid glacial. **Coomassie Blue G250** **Ethanol** **Ethidium bromide** **Isopropanol, Methanol** **$CaCl_2$, HCl, KH_2PO_4, KCl, $MgCl_2$, $MnCl_2$, Na_2HPO_4, NaH_2PO_4, NaCl, NaF, NaOAc, NaOH**	Fisher Scientific (Loughborough, UK) – Part of Thermo Fisher Scientific (Waltham, USA)
Lipofectamine® 2000 reagent	Invitrogen™ – Part of Life Technologies™ (Paisley, UK)
AEBSF, Ampicillin **DTT** **EDTA** **Glycerol, Glycine** **HEPES** **IPTG** **Kanamycin** **SDS** **Trytone** **Yeast extract**	Melford (Suffolk, UK)
Ultra Pure ProtoGel® 30% (w/v) Acrylamide: **0.8% (w/v) Bis-Acrylamide**	National Diagnostics (Hull, UK)
RNASE A	Omega Bio-Tek (Norcross, USA)
PBS (Dulbecco A) **Agar Bacteriological**	Oxoid (Basingstoke, UK) – Part of Thermo Scientific® (Waltham, USA)
ATP lithium salt 100mM pH7 **Complete protease inhibitor cocktail tablets** **Protein A Sepharose™ CL-4B**	Roche (Lewes, UK)
ProTran Nitrocellulose membrane	Schleicher and Schuell (Dassell, Germany)
Brilliant Blue G-Colloidal stain, BSA **Casein, Coomassie Plus™ protein assay reagent** **DMSO HYBRI-MAX®** **β-Glycerophosphate** **30% Hydrogen peroxide** **β-Mercaptoethanol** **Nonidet P-40** **PMSF, N-propylgallate, Ponceau S** **Sodium azide, Sodium Orthovanadate** **TEMED, Tris base, Triton® X-100, Tween®20**	Sigma-Aldrich® (Dorset, UK)
Coomassie Plus™ protein assay reagent	Fisher Scientific (Loughborough, UK) – Part of Thermo Fisher Scientific (Waltham, USA)

2.1.2 Vectors

Table 2.2. Vectors.

List of vectors for constructs mentioned in **Table 2.5**. Vectors were used for protein expression in bacterial and mammalian systems.

Vector	Application	Supplier
pLEICS10	Bacterial protein expression	PROTEX (University of Leicester, UK)
pLEICS20	Mammalian protein expression	PROTEX (University of Leicester, UK)
pLEICS21	Mammalian protein expression	PROTEX (University of Leicester, UK)
pCI neo	Mammalian protein expression	Promega (Southampton, UK)
pEGFP-C1	Mammalian protein expression	ClonTech (Saint-Germain-en-Laye, France)
pCMV-Tag3B	Mammalian protein expression	Stratagene now Agilent technologies (Cheshire, UK)
pMAL-c2G	Bacterial protein expression	New England Biolabs® Inc. (Hitchin, UK)

2.1.3 Oligonucleotides and plasmids

All oligonucleotides were purchased from Sigma-Aldrich® (Dorset, UK) or Invitrogen™ (Paisley, UK).

Table 2.3. Mutagenesis and cloning oligonucleotides.

Oligos and their sequences used in mutagenesis and cloning reactions to create plasmids (**Table 2.5**). Service carried out by Protein Expression laboratory (PROTEX) at the University of Leicester.

Name	Primer sequence 5'-3'
hSUN1 RecA-F	GTATTTTCAGGGCGCCGATTTTTCTCGGCTTCACATGT
hSUN1 RecA-R	GACGGAGCTCGAATTTCATCACTTGACAGGTTCGCCAT
hSUN1 RecA-R 1-217	GACGGAGCTCGAATTTCACTAATTCCTGTCCCTAGAATAAACTCTCG
hSUN1 RecA-R 1-362	GACGGAGCTCGAATTTCACTATCCGATCCTGCGCAAGATCTGCA
hSUN1 RecE-F	TCCGGACTCAGATCTGATTTTTCTCGGCTTCACATG
hSUN1 RecE-R	TCGACTGCAGAATTTCACTTGACAGGTTCGCCATG
hSUN1 S48A-F	CTGTATTTGATGCTCCACGGATG
hSUN1 S48A-R	CATCCGTGGAGCATCAAATACAG
hSUN1 S48D-F	CTGTATTTGATGATCCACGGATG
hSUN1 S48D-R	CATCCGTGGATCATCAAATACAG
hSUN1 S52A-F	TTGATTCTCCACGGATGGCCCGCCGTAGTTTGCGC
hSUN1 S52A-R	GCGCAAACTACGGCGGGCCATCCGTGGAGAATCAA
hSUN1 S52D-F	TTTGATTCTCCACGGATGGACCGCCGTAGTTTGCGCC
hSUN1 S52D-R	GGCGCAAACTACGGCGGTCCATCCGTGGAGAATCAAA
hSUN1 S138A-F	ATTGGACGAGGCTTGGATTCG
hSUN1 S138A-R	CGAATCCAAGCCTCGTCCAAT
hSUN1 S138D-F	CCTCCTGTATTGGACGAGGATTGGATTCGTGAACAGAC
hSUN1 S138D-R	GTCTGTTCACGAATCCAATCCTCGTCCAATACAGGAGG
hSUN1 T144A-F	TTCGTGAACAGGCCACAGTGGAC
hSUN1 T144A-R	GTCCACTGTGGCCTGTTCACGAA
hSUN1 T144D-F	TTCGTGAACAGGACACAGTGGAC
hSUN1 T144D-R	GTCCACTGTGTCCTGTTCACGAA
hSUN1 T144E-F	TTCGTGAACAGGAGACAGTGGAC
hSUN1 T144E-R	GTCCACTGTCTCCTGTTCACGAA
hSUN1 S333A-F	CCGCCCACTCGCAGGCGCCACGGCTGCCC
hSUN1 S333A-R	GGGCAGCCGTGGCGCCTGCGAGTGGGCGG
hSUN1 S333D-F	CACAGCCGCCCACTCGCAGGATCCACGGCTGCCCGGTCGGG
hSUN1 S333D-R	CCCGACCGGGCAGCCGTGGATCCTGCGAGTGGGCGGCTGTG
3NLS-EF	TCCGGACTCAGATCTGATCCAAAAAAGAAGAGAAAGGTAGATCCAAAAAAGAAGAG AAAGGTAGATCCAAAAAAGAAGAGAAAGGTATGAAATTCTGCAGTCGAC
3NLS-ER	GTCGACTGCAGAATTTCATACCTTTCTCTTCTTTTTTGGATCTACCTTTCTCTTCTTTTTT GGATCTACCTTTCTCTTCTTTTTTGGATCAGATCTGAGTCCGGA

Table 2.4. Oligonucleotides used for Sanger sequencing.

DNA plasmid sequences were confirmed by Sanger sequencing. This service was carried out by Protein Nucleic Acid Chemistry Laboratory (PNACL) at the University of Leicester.

Name	Primer sequence 5'-3'
pLEICS10-F	AGACTAATTCGAGCTCGAACA
pLEICS10-R	CCCAGTCACGACGTTGTAAAACG
pLEICS19-F	CTGTACGGAAGTGTTACTT
pLEICS19-R	CATCACAAATTTCACAAATA
pLEICS21-F	CACATGGTCCTGCTGGAGTT
pLEICS21-R	GCTGATTATGATCAGTTAT
hSUN1 F	GAGCGCAAGGACGTGCTCACG
hSUN1 F2	AGGCAGCCTCTGGAGTGTTC
hSUN1 F3	CGAGGGAGACTGACTTTATGG

Table 2.5. DNA plasmids.

Plasmids generated by past members of the Shackleton laboratory and myself in conjunction with PROTEX. Other plasmids were kindly given by collaborators. AMP - ampicillin, KAN - kanamycin.

Plasmid DNA name	Antibiotic resistance	Generated by/obtained from
pCMV3B hSUN1 (1-916) Bgl	AMP	Shackleton lab
pMAL hSUN1 455-916	AMP	Shackleton lab
pLEICS20 hSUN1 WT myc	AMP	Shackleton lab/PROTEX
pLEICS20 hSUN1 S48A myc	AMP	Shackleton lab/PROTEX
pLEICS20 hSUN1 S48D myc	AMP	Shackleton lab/PROTEX
pLEICS20 hSUN1 S52A myc	AMP	Shackleton lab/PROTEX
pLEICS20 hSUN1 S52D myc	AMP	Shackleton lab/PROTEX
pLEICS20 hSUN1 S138A myc	AMP	Shackleton lab/PROTEX
pLEICS20 hSUN1 S138D myc	AMP	Shackleton lab/PROTEX
pLEICS20 hSUN1 T144A myc	AMP	Shackleton lab/PROTEX
pLEICS20 hSUN1 T144E myc	AMP	Shackleton lab/PROTEX
pLEICS20 hSUN1 S333A myc	AMP	Shackleton lab/PROTEX
pLEICS20 hSUN1 S333D myc	AMP	Shackleton lab/PROTEX
pLEICS20 hSUN1 S48A/S138A myc	AMP	Shackleton lab/PROTEX
pLEICS20 hSUN1 S48D/S138D myc	AMP	Shackleton lab/PROTEX
pLEICS20 hSUN1 S48A/S333A myc	AMP	Shackleton lab/PROTEX
pLEICS20 hSUN1 S48D/S333D myc	AMP	Shackleton lab/PROTEX
pLEICS20 hSUN1 S48A/S138A/S333A myc	AMP	Shackleton lab/PROTEX
pLEICS20 hSUN1 S48D/S138D/S333D myc	AMP	Shackleton lab/PROTEX
pLEICS21 hSUN1 WT GFP	KAN	Shackleton lab/PROTEX
pLEICS21 hSUN1 S48A GFP	KAN	Shackleton lab/PROTEX
pLEICS21 hSUN1 S48D GFP	KAN	Shackleton lab/PROTEX
pLEICS21 hSUN1 S138A GFP	KAN	Shackleton lab/PROTEX
pLEICS21 hSUN1 S138D GFP	KAN	Shackleton lab/PROTEX
pLEICS21 hSUN1 T144E GFP	KAN	Shackleton lab/PROTEX
pLEICS21 hSUN1 S333A GFP	KAN	Shackleton lab/PROTEX
pLEICS21 hSUN1 S333D GFP	KAN	Shackleton lab/PROTEX
pLEICS21 hSUN1 S48A/S333A GFP	KAN	Shackleton lab/PROTEX
pLEICS21 hSUN1 S48D/S333D GFP	KAN	Shackleton lab/PROTEX
pLEICS21 hSUN1 S48A/S138A/S333A GFP	KAN	Shackleton lab/PROTEX
pLEICS21 hSUN1 S48D/S138D/S333D GFP	KAN	Shackleton lab/PROTEX
pLEICS10 hSUN1 WT 1-217 MBP	AMP	Shackleton lab/PROTEX
pLEICS10 hSUN1 WT 1-362 MBP	AMP	Shackleton lab/PROTEX
pLEICS10 hSUN1 WT 455-916 MBP	AMP	Shackleton lab/PROTEX
pLEICS10 hSUN1 S48A 1-217 MBP	AMP	Shackleton lab/PROTEX
pLEICS10 hSUN1 S48A 1-362 MBP	AMP	Shackleton lab/PROTEX
pLEICS10 hSUN1 S48D 1-362 MBP	AMP	Shackleton lab/PROTEX
pLEICS10 hSUN1 S52A 1-362 MBP	AMP	Shackleton lab/PROTEX
pLEICS10 hSUN1 S52D 1-362 MBP	AMP	Shackleton lab/PROTEX
pLEICS10 hSUN1 S138A 1-217 MBP	AMP	Shackleton lab/PROTEX
pLEICS10 hSUN1 S138A 1-362 MBP	AMP	Shackleton lab/PROTEX
pLEICS10 hSUN1 S138D 1-362 MBP	AMP	Shackleton lab/PROTEX
pLEICS10 hSUN1 T144A 1-217 MBP	AMP	Shackleton lab/PROTEX
pLEICS10 hSUN1 T144E 1-362 MBP	AMP	Shackleton lab/PROTEX
pLEICS10 hSUN1 S333A 1-362 MBP	AMP	Shackleton lab/PROTEX

pLEICS10 hSUN1 S333D 1-362 MBP	AMP	Shackleton lab/PROTEX
pLEICS10 hSUN1 S48A/S333A MBP	AMP	Shackleton lab/PROTEX
pLEICS10 hSUN1 S138A/T144A MBP	AMP	Shackleton lab/PROTEX
pLEICS10 hSUN1 S48A/S138A/S333A MBP	AMP	Shackleton lab/PROTEX
pLEICS10 hSUN1 S48D/S138D/S333D MBP	AMP	Shackleton lab/PROTEX
pEGFP NET5 ΔN	KAN	E.Schirmer (Edinburgh University)
pEGFP NET5 FL	KAN	E.Schirmer (Edinburgh University)
pEGFP Nesprin-2α	KAN	C.Shanahan (King's College London)
pEGFP Nesprin-2α KASH	KAN	C.Shanahan (King's College London)
pEGFP Nesprin-2α ΔTM	KAN	C.Shanahan (King's College London)
pLEICS10 GFP 3NLS GFP	KAN	Shackleton lab/PROTEX

2.1.4 RNA interference

Table 2.6. siRNAs.

List of siRNAs targeted to human SUN1 (hSUN1) or glyceraldehyde 3-phosphate dehydrogenase (GAPDH) and the oligo sequences.

siRNA	Oligo sequence	Supplier
hSUN1 oligo 1	CAGGACGTGTTTAAACCCACCACTT	Invitrogen™ (Paisley, UK).
hSUN1 oligo 2	ACGTGCAAGTCAGAGAAATGGTGAA	Invitrogen™ (Paisley, UK).
GAPDH	Not available	Life Technologies™ (Paisley, UK).

2.1.5 Cells

Table 2.7. Cell lines.

List of cell lines and supplier.

Cell line	Supplier
NIH 3T3 (mouse fibroblasts)	American Type Culture Collection (ATCC)
U2OS (human osteosarcoma)	American Type Culture Collection (ATCC)
HeLa (human cervical cancer cells)	American Type Culture Collection (ATCC)

2.1.6 Drugs

Table 2.8. Drugs.

A list of drugs, their full chemical names, as well as the corresponding suppliers. Drugs were solubilised in DMSO and then used in various assays at the concentrations given.

Drug	Chemical name	[Stock]	[Final]	Supplier
Aphidicolin	(3*R*,4*R*,4a*R*,6a*S*,8*R*,9*R*,11a*S*,11b*S*)-4,9-bis(hydroxymethyl)-4,11b-dimethyltetradecahydro-8,11a-methanocyclohepta[*a*]naphthalene-3,9-diol	1.6 mg/ml	1.6 µg/ml	Sigma-Aldrich® (Dorset, UK)
MG132	benzyl N-[(2S)-4-methyl-1-[[(2S)-4-methyl-1-[[(2S)-4-methyl-1-oxopentan-2-yl] amino]-1-oxopentan-2-yl]amino]-1-oxopentan-2-yl]carbamate	10 mM	10 µM	Calbiochem® (Darmstadt, Germany)
Nocodazole	Methyl-(5-[2-thienylcarbonyl]-1H-benzinidazol-2-yl)carbamate	500 µg/ml	500 ng/ml	Sigma-Aldrich® (Dorset, UK)
RO-3306	5-(6-Quinolinylmethylene)-2-[(2-thienylmethyl)amino]-4(5*H*)-thiazolone	10 mM	10 µM	Calbiochem® (Darmstadt, Germany)
Roscovitine	2-(R)-(1-ethyl-2-hydroxyethylamino)-6-benzylamino-9-isopropylpurine	100 mM	100 µM	Calbiochem® (Darmstadt, Germany)
BI2536	(R)-4-[(8-Cyclopentyl-7-ethyl-5,6,7,8-tetrahydro-5-methyl-6-oxo-2-pteridinyl)amino]-3-methoxy-N-(1-methyl-4-piperidinyl)benzamide	100 µM	100 nM	Axon MedChem (Groningen, Netherlands)
MLN 8054	4-[[9-chloro-7-(2,6-difluorophenyl)-5H-pyrimido[5, 4-d][2]benzazepin-2-yl]amino]benzoic acid	1 mM	1 µM	SelleckChem (Houston, USA)
UO126	1,4-diamino-2,3-dicyano-1,4-bis[2-aminophenylthio] butadiene	10 mM	10 µM	Cell Signalling Technology® (Beverly, USA)

2.1.7 Antibodies

Table 2.9. Primary antibodies.

List of primary antibodies and the corresponding suppliers. Target epitopes and concentrations are given where known. Dilutions used for western blots and indirect immunofluorescence are shown as well as amounts of antibody used for immunoprecipitation (IP).

Primary antibody	[antibody]	Dilution for WB	Dilution for IF	Amount for IP	Supplier
Mouse anti-c-myc	0.5 µg/µl	1:500	1:200	2 µg	Invitrogen™ (Paisley, UK)
Goat anti-lamin A/C	200 µg/ml	1:2000	1:200	-	Santa Cruz (California, USA)
Rabbit anti-hSUN1 Atlas	0.11 mg/ml	1:500	-	2 µg	Sigma-Aldrich®, Atlas (Dorset, UK)
Rabbit anti-GFP	0.5 mg/ml	1:8000	1:500	2 µg	Abcam® (Cambridge)
Mouse anti-GAPDH	1 mg/ml	1:10000	-	-	Millipore (Darmstadt, Germany)
Mouse anti-β-actin	-	1:50000	-	-	Sigma-Aldrich®, Atlas (Dorset, UK)
Mouse anti-cyclin A	200 µg/ml	1:200	-	-	Santa Cruz (California, USA)
Mouse anti-cyclin B	200 µg/ml	1:200	-	-	Santa Cruz (California, USA)
Rabbit anti-hSUN2 (262-492 C-terminus)	-	1:1000	-	-	D.Hodzic (Washington University in St. Louis) (Hodzic *et al.* 2004)
Rabbit anti-emerin (1-188 N terminus)	-	1:2000	-	-	G.Morris (Center for Inherited Neuromuscular Disease, Oswestry, UK)
SSHR1/0545 rabbit anti-mSUN1 (450-913 C-terminus)	-	1:500	-	-	In house (Haque *et al.* 2006)
2294 rabbit anti-mSUN2 (1-18 N terminus)	-	1:1000	-	-	In house (Haque *et al.* 2010)
2383 GE 1 rabbit-anti hSUN1 (450-913 C-terminus)	0.22 mg/ml	1:200	-	-	In house
2383 GE 2 rabbit-anti hSUN1 (450-913 C-terminus)	0.51 mg/ml	1:200	-		In house
2853 anti-hSUN2 (1-18 N terminus)	-	1:200	-	-	In house (Haque *et al.* 2010)
Rabbit anti-pS48 (phospho antibody) 42-pS48-54 (N terminus region)	-	1:50	-	-	Antibody generation by Eurogentec (Seraing, Belgium)

Table 2.10. Secondary antibodies.

List of secondary antibodies and the corresponding suppliers. Dilutions for western blotting or indirect immunofluorescence are as shown.

Secondary antibody	Dilution	Supplier
Goat anti mouse HRP	1:6000	Sigma-Aldrich® (Dorset, UK)
Goat anti rabbit HRP	1:3000	Sigma-Aldrich® (Dorset, UK)
Rabbit anti goat HRP	1:5000	Sigma-Aldrich® (Dorset, UK)
Alexa Fluor® 488 donkey anti mouse	1:500	Molecular Probes® - Part of Life Technologies™ (Paisley, UK)
Alexa Fluor® 594 donkey anti goat	1:500	Molecular Probes® - Part of Life Technologies™ (Paisley, UK)

2.1.8 Purified kinases

Table 2.11. Kinases.

List of active kinases used in *in vitro* kinase assays.

Kinase	Concentration of active kinase	Supplier
CDK1/cyclin B	10 µg in 4.3 µl	Merck Millipore (Watford. UK)
PLK1	10 µg in 2.9 µl	Merck Millipore (Watford. UK)
Aurora A	10 µg in 34.6 µl	Merck Millipore (Watford. UK)

2.1.9 Radioisotopes

Table 2.12. Radioisotopes.

Isotope used in radiolabelled *in vitro* translation and *in vitro* kinase assays with the specific activity values.

Isotope	Specific Activity	Supplier
[^{35}S]-methionine	43.5 Tbq/mmol	Perkin Elmer (Cambridge, UK)
[γ-^{32}P]-ATP	167 Tbq/mmol	Perkin Elmer (Cambridge, UK)

2.2 Molecular Biology Techniques

2.2.1 Mutagenesis and cloning

Primers required for mutagenesis and cloning reactions were designed by Dr Sue Shackleton or myself. See **Table 2.3** for a list of primers and the sequences. Relevant primers and templates were sent to the Protein Expression (PROTEX) cloning service at the University of Leicester to be processed for mutagenesis and cloning reactions. **Appendix B** and **Appendix C** details primers and templates used for cloning of each construct. Generation of the mutant constructs was carried out by recombination of

PCR-generated inserts using BD In-Fusion™ (ClonTech, France) recombinase. Inserts were cloned into one of three vectors, pLEICS10 MBP fusion for bacterial protein expression, pLEICS20 myc-tag and pLEICS21 GFP-tag for overexpression of tagged protein in mammalian cells.

Clones received back from PROTEX were validated for the desired mutation(s) and correct sequence by Sanger sequencing. This was performed by Protein Nucleic Acid Chemistry Laboratory (PNACL) sequencing facility at the University of Leicester. Successful clones were then transformed into DH5α for myc- and GFP-tagged constructs and BL21 for MBP-tagged constructs. Subsequently, large-scale DNA preparations and glycerol stocks were made.

2.2.2 DNA sequencing

A 10 µl PCR mix comprising 0.5 µl BigDye™ terminator version 3.1 (Applied Biosystem, USA), 1.75 µl BigDye™ 5x buffer (Applied Biosystem, USA), 0.75 µl 5 µM primer (see **Table 2.4** for primers used) and 200 ng plasmid was placed in a 0.2 ml PCR tube. The mix was processed through the following PCR program for 28 cycles on a thermal cycler (G-storm, UK): 96^{o}C 10 s, 50^{o}C 5 s, 60^{o}C 4 minutes (min). The sample was combined with 10 µl de-ionised water (dH_20) and 2 µl of 2.2% SDS and then incubated for 98^{o}C 5 min then 25^{o}C 10 min. Performa® gel filtration cartridges (EdgeBio, USA) were prepared by centrifuging at 3000 rpm for 3 min in a microcentrifuge. The column was transferred to a labelled 1.5 ml microcentrifuge tube and the sample was applied to the column. The sample was centrifuge once more at 3000 rpm for 3 min.

The eluate was sent to PNACL at the University of Leicester for Sanger sequencing on An Applied Biosystems 3730 sequencer. Data received from PNACL was analysed using CodonCode Aligner 3.7.1 software.

2.2.3 Generation of chemically competent bacteria

Escherichia coli (E.coli) strains (DH5α or BL21) were streaked out onto a LB (Luria broth) agar plate (1% (w/v) tryptone, 0.5% (w/v) yeast extract, 1% (w/v) NaCl, 1.5% (w/v) bacteriological agar) and incubated overnight at 37^{o}C. A volume of 25 ml of LB broth (1% (w/v) tryptone, 0.5% (w/v) yeast extract, 1% (w/v) NaCl) was inoculated with a single colony from the LB agar plate and incubated overnight at 37^{o}C in a G25 shaking incubator (New Brunswick Scientific, UK) at 220 rpm.

A volume of 100 ml of pre-warmed LB broth was inoculated with 1 ml of the overnight culture and grown at 37^{o}C for 2 hours (h) until the OD_{600} was approximately 0.2. Next, 20 mM $MgCl_2$ was added and cultures were grown to an OD_{600} of approximately 0.45-0.55. Cells were decanted into 50 ml tubes and incubated on ice for 2 h. Bacteria were pelleted by centrifugation in a 5810R refrigerated centrifuge (Eppendorf, UK) at 1811 xg 4^{o}C for 5 min. The supernatant was discarded and the pellet resuspended in 50 ml of pre-chilled $Ca^{2+}Mn^{2+}$ solution A (40 mM NaOAc, 100 mM $CaCl_2$, 70 mM $MnCl_2$, HCl pH 5.5) and incubated on ice for a further 45 min. Cells were pelleted at 1360 xg for 5 min and the supernatant was discarded. The pellet was gently resuspended in 5 ml $Ca^{2+}Mn^{2+}$ solution B (40 mM NaOAc, 100 mM $CaCl_2$, 70 mM $MnCl_2$, HCl pH 5.5, 15% (v/v) glycerol). Competent cells were quickly aliquoted into pre-chilled 1.5 ml microcentrifuge tubes on ice and snap frozen in liquid nitrogen before being stored at -80^{o}C.

2.2.4 Bacterial transformations

Purified plasmids were transformed into chemically competent *E.coli* DH5α or BL21, prepared as described in **section 2.2.3**. A volume of 50 µl competent cells were thawed on ice from storage at -80^{o}C. The bacteria were carefully combined with 50 ng of the purified plasmid and incubated on ice for 30 min. The cells were then subjected to heat-shock for 90 seconds (s) at 42^{o}C and placed back on ice for 5 min. For plasmids resistant to ampicillin, the bacteria were plated onto a LB agar plate containing 100 µg/µl ampicillin. For plasmids resistant to kanamycin, 500 µl of LB broth was added to the tube and the bacteria were grown for 1 h at 37^{o}C in a shaking incubator at 220 rpm. Bacteria were centrifuged at 4000 xg and 400 µl of the supernatant was removed. The pellet was resuspended in the remaining supernatant and transferred to an LB agar plate containing 30 µg/µl kanamycin. Plates were incubated overnight at 37^{o}C to allow colony formation and stored at 4^{o}C thereafter.

2.2.5 Bacterial growth and storage

A single colony from a transformation plate of the required plasmid was used to inoculate 5 ml of LB broth supplemented with either 100 µg/µl of ampicillin or 30 µg/µl kanamycin. This was grown overnight at 37^{o}C in a shaking incubator at 220 rpm. A glycerol stock was made from the culture by adding 750 µl of bacteria culture to 250 µl of 80% glycerol, inverting three times and storing at -80^{o}C.

2.2.6 Plasmid preparations

2.2.6.1 Miniprep

LB broth (5ml) supplemented with the appropriate antibiotic was inoculated with either, bacteria scraped from a frozen glycerol stock or, 5 µl of an overnight cultured

broth or a single colony from a transformation plate. The culture was grown overnight in a 37^{o}C shaker and then centrifuged at 3220 xg for 15 min and the supernatant discarded. Plasmid DNA was extracted and purified from the bacterial pellet using a GeneJET™ plasmid miniprep kit (Fermentas, UK) according to the manufacturer's instructions. The purified plasmid was eluted into 30 µl dH_20 and stored at -20^{o}C.

2.2.6.2 Midiprep

A single colony from a bacterial plate was used to inoculate 3 ml of LB broth supplemented with either 100 µg/µl of ampicillin or 30µg/ µl kanamycin as appropriate. The culture was grown for 8 h in a shaker at 220 rpm and subsequently used to inoculate 100ml of LB broth supplemented with the appropriate antibiotic. This was incubated at 37^{o}C in a shaking incubator overnight. The culture was centrifuged at 3220 xg for 15 min and the supernatant discarded. Plasmid DNA was extracted and purified from the bacterial pellet using a NucleoBond® Xtra Midi kit (Macherey-Nagel, Germany) according to the manufacturer's instructions. The purified plasmid was eluted into 200 µl dH_20 and stored at -20^{o}C. Plasmid concentration was determined using a ND-1000 NanoDrop® spectrophotometer at OD_{260}.

2.2.7 Agarose gel electrophoresis

Plasmid DNA was analysed by agarose gel electrophoresis to compare DNA concentrations found using the ND-1000 NanoDrop® spectrophotometer. An amount of 200 ng plasmid DNA was combined with 6x DNA loading dye in a volume ratio of 1:6 and resolved on a 1% agarose (Bioline, UK) -TAE (40 mM Tris-base, 1 mM EDTA, 0.1% (v/v) glacial acetic acid) gel supplemented with 0.4 µg/ml ethidium bromide. Gels were run at 90 V for approximately 45 min in TAE buffer. Gel images were captured using a

UV-transluminator universal hood (Biorad, UK) and analysed with Biorad Quantity 1 Version 4.2.2 software.

2.3 Cell culture

2.3.1 Cell maintenance and propagation

HeLa and U20S cells were cultured in DMEM supplemented with 10% (v/v) foetal bovine serum (FBS), 1% (v/v) GlutaMAX™-1, 10 µM (v/v) sodium pyruvate and penicillin/streptomycin solution at 100 units/ml and 100 µg/ml respectively. Cells were routinely grown in 6/10/15 cm tissue culture dishes at 37^{o}C in a 5% CO_2 atmosphere and passaged before reaching confluence. Growth medium was aspirated from the culture dish and the cells washed in phosphate buffered saline (PBS). Cells were detached from the surface of the dish using PBS containing 0.05% trypsin-EDTA and incubated at 37^{o}C in a 5% CO_2 atmosphere for 5-10 min. Trypsin-EDTA was deactivated by adding an equal or greater volume of growth medium. Cells were counted using a haemocytometer and seeded into pre-warmed growth medium at an appropriate density.

2.3.1.1 Cell counting

Cells were counted using a haemocytometer BS 748 (Hawksley, UK) by applying 10 µl of cell suspension to the device and counting as described below. The haemocytometer grid is comprised of 12 x 12 squares. The number of cells within a 4 x 4 area is equivalent to the number of cells x 10^4/ml. The number of cells per ml was calculated using the following equation:

$$Cells\ per\ ml = \left(\frac{Total\ number\ of\ cells\ from\ four\ 4x4\ corners}{4}\right) \times 10^4$$

Appropriate numbers of cells were seeded into suitable culture dishes.

2.3.2 Cell storage and recovery

Growth medium was aspirated from a confluent tissue culture dish of cells and washed in PBS. Cells were trypsinised as described in **section 2.3.1** and then resuspended in growth medium. Cells were then transferred to a 15 ml centrifuge tube and pelleted by centrifugation at 200 xg for 5 min at room temperature (RT). The supernatant was aspirated and the pellet resuspended in growth medium containing 5% DMSO, cells were then transferred to cryotubes (Nunc, Denmark). Tubes were placed in an isopropanol filled cryo -1^{o}C freezing container (Nalgene, USA) and stored at -80^{o}C for at least 24 h. Tubes were then transferred to liquid nitrogen for long-term storage.

To recover cells, a cryotube was removed from the liquid nitrogen storage vessel and rapidly thawed in a 37^{o}C water bath. Cells were transferred to a 15 ml centrifuge tube containing an excess of pre-warmed medium and mixed gently. Cells were then pelleted at 200 xg for 5 min at RT. After discarding the supernatant, the pellet was resuspended in growth medium and transferred to a 10 cm culture dish for incubation at 37^{o}C, 5% CO_2.

2.3.3 Preparation of acid-etched sterile coverslips

Coverslips were placed in 1 M HCl for 30 min with gentle agitation and occasional turning with forceps. The HCl was then discarded and coverslips were rinsed in distilled water (dH_20). Coverslips were then washed in 100% ethanol for 30 min with occasional

turning before being air-dried on 3MM Whatman paper in a fume-hood. Coverslips were flamed immediately before use.

2.3.4 Transient transfection of plasmid DNA or RNAi

Cells were seeded 24 h prior to transient transfection onto either, an acid-etched coverslip at a density of 1.5 x 10^5 for indirect immunofluorescence microscopy or, 2 x 10^5 for protein extracts, in a single well of a 6-well dish. For a 10 cm or 6 cm culture dish, cells were seeded at a density of 1.8 x 10^6 or 7 x 10^5, respectively. Plasmid DNA and Lipofectamine® 2000 (Invitrogen, UK) were prepared in OPTI-MEM®-1 (serum and Penicillin/Streptomycin free) (Invitrogen, UK) according to the manufacturer's protocol.

For 6-well, 6 cm or 10 cm dishes, 1 µg, 2 µg or 4 µg of plasmid DNA was thought to be sufficient for adequate protein expression, respectively. In a microcentrifuge tube, plasmid DNA was combined with 100 µl of OPTI-MEM®-1 per µg of plasmid DNA. In a separate microcentrifuge tube, Lipofectamine® 2000 was used in a 2:1 or 3:1 ratio to the plasmid DNA. The same volume of OPTI-MEM®-1 in the first microcentrifuge tube was also applied to the second microcentrifuge tube.

For RNA interference experiments, cells were seeded 24 h prior to transient oligo transfection into a single well of a 6-well dish or 10 cm dish at a density of 2 x 10^5 or 1.8 x 10^6, respectively. Oligo transfection was carried out so that 60 pmoles (20 pmol/µl) of siRNA oligo and an equal volume of Lipofectamine® 2000 were prepared, in 100 µl OPTI-MEM®-1 (serum and Penicillin/Streptomycin free), in separate tubes as described above according to the manufacturers protocol.

These mixtures were incubated at RT for 5 min before combining the DNA or RNA with the Lipofectamine® 2000 and incubating for a further 20 min.

The standard growth medium on the cells was replaced with growth medium lacking penicillin/streptomycin. The DNA or RNA/Lipofectamine® 2000 mix was added to the dishes and incubated for 6 h at 37^{o}C, 5% $CO_{2.}$ Media was then aspirated and replaced with standard growth media. Cells were incubated at 37^{o}C for 4-24 h for plasmid DNA transfections and 48 h for RNAi before using them in subsequent assays.

2.3.5 Cell synchronisation

For analysis of endogenous hSUN1, HeLa cells were treated with aphidicolin 10 h after seeding or alternatively, 10 h after transfection with hSUN1 constructs (refer to **section 2.3.4**). Media was aspirated and replaced with standard growth medium containing 1.6 µg/ml aphidicolin and incubated at 37^{o}C, 5% CO_2 for 16 h. The drug was removed by washing the cells 3 times in PBS, followed by incubation for 4 h in pre-warmed growth medium. Growth medium was then replaced with medium containing 500 ng/ml nocodazole to arrest cells in mitosis or containing 10 µM RO-3306 to arrest cells in G2. The cells were then incubated for a further 16 h. Samples were then collected and processed as described in subsequent sections. For treatment with mitotic kinase inhibitors, 4 h prior to harvesting lysates, samples were treated with 10 µM MG132 as well as 100 µM Roscovitine, 100 nM BI2536, 1 µM MLN 8054 or 10 µM U0126.

2.3.6 Flow cytometry

Growth medium was aspirated from cells in a culture dish and washed in PBS. Asynchronous cells were trypsinised as described in **section 2.3.1** and then resuspended in growth medium. Mitotically synchronised cells were collected by vigorous shaking of the cells to detach them from the tissue culture dish surface, this is also known as mechanical shake-off. Cells were transferred to a 15 ml centrifuge tube and pelleted by centrifugation at 200 xg for 5 min at RT. The supernatant was aspirated and the cells washed in ice-cold PBS and centrifuged once more. The PBS was discarded and the cells resuspended in pre-cooled 70% ethanol with gentle pipetting to disperse any cell clumps. Fixed cells were stored at -20^{o}C for at least 24 h. Cells were then washed twice in ice-cold PBS and the pellet was resuspended in propidium iodide (PI) (Calbiochem, UK) staining solution (PI 50 µg/ml, RNase A 10 µg/ml in PBS) and transferred to round-bottomed tube (BD, UK). Samples were incubated at 37^{o}C for 1 h. The DNA profile of each sample was then measured using BD FACSCanto™ II instrument and analysed with BD FACSDiva™ software.

2.4 Analysis of proteins

2.4.1 Microscopy

2.4.1.1 Indirect immunofluorescence microscopy

Cells grown on coverslips were washed in 2 ml of PBS 24 h after transfection and then fixed in ice-cold methanol for a minimum time of 10 min at -20^{o}C. Cells were washed three times for 5 min in 1x PBS (137 mM NaCl, 2.7 mM KCl, 10 mM Na_2HPO_4, 1.8 mM KH_2HPO_4, pH 7.4) and then blocked in 1% BSA in PBS for 10 min. Coverslips were then incubated with primary antibody, diluted in 3% BSA in PBS for 1 h at RT in a dark,

humid environment (see **Table 2.9** for primary antibodies used and dilutions). Cells were washed again three times for 5 min in 1x PBS and then incubated for 1 h at RT with fluorescent secondary antibody and DAPI (Molecular Probes, UK) (50 ng/ml), diluted in 3% BSA in PBS in a dark, humid environment (see **Table 2.10** for secondary antibodies used and dilutions). Coverslips were washed four times for 5 min in 1x PBS and then inverted and mounted onto glass slides with a small drop of mounting medium (3% (v/v) n-propyl-gallate, 80% (v/v) glycerol). Excess liquid was removed from the edges of the coverslip, which was then sealed with clear nail varnish. The nail varnish was allowed to set for 30 min and slides were then stored at 4^{O}C in the dark.

All slides were analysed using a Nikon TE300 semi-automatic inverted microscope with a Plan Apo VC 60x DIC oil-immersion objective (NA 1.4). Fluorescent images were captured with an ORCA-R^2 digital camera (Hamamatsu, Japan) with Volocity® software, version 6.0.1 (Perkin Elmer, UK), and processed using Adobe Photoshop.

2.4.1.2 Fluorescence intensity measurements

Cells were processed for indirect immunofluorescence microscopy as described in **section 2.4.1.1** and imaged using an Olympus Scan^R screening platform on an IX81 microscope stand. The system was equipped with a Hamamatsu ORCA-ER camera and an Olympus MT20 illumination system using a 150W Xe arc burner. 100 images were captured per slide using an Olympus LUCPLFLN 20x/0.45 NA objective and Olympus Scan^R Acquisition software version 2.2.0.8.

After using the DAPI channel for auto-focus (excitation filter 350/50, Dichroic filter U-61002bs, emission filter U-61002m) a DAPI image (exposure time 1 s, 25% xenon bulb

output) and a GFP image (excitation filter 470/22, Dichroic 505LP, emission filter 535/50; exposure time 1 s) were captured. Also, to check the health of the cell a differential interference contrast (DIC) image was captured.

Images were analysed after background subtraction using Olympus Scan^R Analysis software version 1.2.0.4. For segmentation, nuclei were identified using edge detection in the DAPI channel and nuclei were gated to exclude extreme high and low intensities. The green fluorescence from the selected nuclei was measured. The signal 50 pixels around the nuclei was measured as signal in the cytoplasm and a ratio of hSUN1 in the cytoplasm to nucleus was calculated.

2.4.2 Cell extracts

2.4.2.1 Total cell extracts

Cells were grown to confluence in a single well of a 6-well dish. Depending on the assay, 24-48 h post-transfection, growth medium was aspirated from cells in a culture dish and washed in PBS. Cells were trypsinised as described in **section 2.3.1** and then resuspended in growth medium. Cells were transferred into a 15 ml centrifuge tube and pelleted by centrifugation at 200 xg for 5 min at RT. The supernatant was aspirated and the pellet resuspended in 50 µl PBS. An equal volume of 2x Laemmli buffer was added and samples were boiled for 5 min prior to resolving proteins by SDS-PAGE.

2.4.2.2 Soluble cell lysates

Depending on the assay, 24-48 h post transfection, growth media was aspirated from the cells and washed in PBS. Cells were collected by trypsinisation as described in

section 2.3.1, by scrapping or mechanical shake-off into pre-chilled media in 15 ml or 50 ml tubes. For cells previously treated with drugs such as nocodazole, RO-3306, MG132, Roscovitine, BI2536, MLN8054, or UO126 in a synchronisation assay, the pre-chilled media were supplemented with those drugs at the same concentration as used for incubation on the cells (**section 2.3.5**). This was to prevent the reversal of the effect of the drug. Cells were pelleted by centrifugation at 300 xg for 5 min at 4^{o}C. The supernatant was aspirated and the pellet resuspended in 2ml PBS then centrifuged once more. The supernatant was discarded and the cell pellet resuspended in lysis buffer (10 mM Hepes-KOH pH 7.4, 100 mM NaCl, 5 mM EDTA, 1% Triton® X-100, 1x protease inhibitor (PI) cocktail, 2 mM AEBSF, 5 mM NaF, 500 mM β-glycerophosphate). Samples were incubated on ice for 30 min with occasional pipetting after which they were sonicated in a sonicator using a MSE Soniprep 150, 10 mm probe amplitude 2-3 µm on ice for 3 cycles of 15 s with a 30 s interval.

Cell debris was removed by centrifuging the sample at 10000 xg for 10 min at 4^{o}C and the soluble lysate fraction was transferred to a 1.5ml microcentrifuge tube. Samples intended for the GFP-TRAP® protocol (**section 2.4.3.4**) were centrifuged at 20000 xg for 10 min. Protein concentration was measured using a comparative Bradford assay (**section 2.4.2.2.1**). Sample concentrations were adjusted with lysis buffer so that they were all equivalent. Part or all of the lysate was combined with an equal volume of 2x Laemmli buffer and boiled for 5 min. Samples were then resolved by SDS-PAGE for western blotting or Coomassie blue staining. In some instances remaining lysate was used in subsequent IP experiments (see **section 2.4.3.2** and **2.4.3.4**).

2.4.2.2.1 Comparative Bradford Assay

Protein concentrations for soluble cell lysates were determined as described below. A volume of 2 µl of lysis buffer or soluble lysate was incubated at RT with 1 ml of Coomassie Plus™ protein assay reagent for 15 min. Protein concentrations were determined using a BioPhotometer (Eppendorf, UK) spectrophotometer. The lysis buffer sample was used as a blank and the absorbance readings of the soluble lysates were measured at 595 nm. The following calculation was performed where 0.0396 is the arbitrary unit used to calculate protein concentration in a Bradford assay and x is the volume in µl of the soluble lysate:

$$\left((Absorbance\ reading\ \div 0.0396) \div x\right) = protein\ \mu g/\mu l$$

Samples were adjusted to the same concentration as the most dilute sample.

2.4.2.3 Lambda phosphatase (λ ppase) treatment

Soluble lysates prepared as described in **section 2.4.2.2** were treated with λ ppase as using a lambda phosphatase kit (Sigma, UK). The enzyme was diluted 1:100 to the soluble lysate while the 10x λ ppase buffer and 10x $MnCl_2$ were diluted down to 1x solutions according to the manufacturer's instructions. Samples were incubated at 30^{o}C for 45 min and then combined with 2x Laemmli buffer and boiled for 5 min. Samples were resolved by SDS-PAGE and analysed by western blotting.

2.4.3 Immunoprecipitation

2.4.3.1 Preparations of Protein A-sepharose C-4B beads

An amount of 0.5 g of Protein A-sepharose CL-4B was placed in a 30 ml tube. To this, 20 ml of dH_20 was added and gently mixed with the beads. The sepharose beads were

pelleted by centrifugation at 1000 xg for 5 min at 4^{o}C, discarding the dH_20 and the wash was repeated once more. Protein A-sepharose beads were resuspended in 5ml PBS/0.1% sodium azide and stored at 4^{o}C.

2.4.3.2 Immunoprecipitation (IP)

Soluble lysates, prepared as in **section 2.4.2.2**, pre-cleared by incubation for 1 h with 20 µl of Protein-A sepharose CL-4B beads at 4^{o}C with end-over-end mixing. The lysates were then centrifuged at 1000 xg, 4^{o}C for 5 min and the supernatant was transferred to a 1.5 ml microcentrifuge tube with 2 µg of antibody (see **Table 2.9** for antibodies used for IP). Samples were incubated for 2 h at 4^{o}C before adding 30 µl of Protein-A CL-4B sepharose beads and rotating for a further hour. The sepharose beads were then washed 3 times in 1 ml of wash buffer (10 mM Hepes-KOH pH 7.4, 100 mM NaCl, 5 mM EDTA, 1% Triton® X-100, 5 mM NaF, 500 mM β-glycerophosphate), centrifuging at 1000 xg, 5 min at 4^{o}C. After discarding the final wash supernatant, beads were resuspended in an appropriate volume of 2x Laemmli buffer and boiled for 5 min. Samples were then resolved by SDS-PAGE and processed for western blotting.

2.4.3.3 Preparation of GFP-TRAP® beads

GFP-TRAP® beads (Chromotek, Germany) were equilibrated in dilution buffer (10 mM Tris-HCl pH 7.5, 150 mM NaCl, 0.5 mM EDTA, 1 mM PMSF, 1x PI cocktail) immediately before adding soluble lysate. According to the manufacturer's protocol, 30-60 µl of bead slurry was resuspended in 500 µl of ice-cold dilution buffer. The beads were centrifuged at 2700 xg for 2 min at 4^{o}C and the supernatant was discarded. Beads were washed twice more then used in the GFP-TRAP® assay as described in **section 2.4.3.4**.

2.4.3.4 GFP-TRAP

GFP-tagged SUN1 or NET5 FL/Δ were purified from soluble lysates derived from transiently transfected HeLa cells by GFP-TRAP® as an alternative to IP. Soluble lysates and 30-60 µl of prepared GFP-Trap® beads were combined and incubated for 2 h at 4^{o}C with end-over-end mixing. The beads were then centrifuged at 2000 xg for 2 min at 4^{o}C. The supernatant was discarded and the GFP-Trap® beads were washed 3 times in wash buffer (10 mM Tris-HCl pH 7.5, 150 mM NaCl, 0.5 mM EDTA, 2 mM AEBSF, 1x PI cocktail, 5 mM NaF, 50 mM β-glycerophosphate, 0.2 mM Na_3VO_4) centrifuging at 2000 xg and 4^{o}C for 2 min. GFP-Trap® beads were resuspended in 20-30 µl of 2x Laemmli buffer and boiled for 10 min. Beads were pelleted by centrifugation and samples were then resolved by SDS-PAGE and processed for western blotting.

2.4.4 Bacterial protein expression and purification

2.4.4.1 Preparation of amylose resin

A volume of 1.33 ml of amylose resin (New England Biolabs, UK) which is equal to 1 ml of packed amylose beads was transferred to a 15 ml tube and centrifuged at 1000 xg for 5 min at 4^{o}C. The supernatant was removed and the amylose beads washed twice in 10 ml of cold PBS, centrifuging at 1000 xg for 5 min at 4^{o}C. The supernatant was removed and the beads resuspended in 1 ml PBS and stored at 4^{o}C for up to two months.

2.4.4.2 Bacterial expression and purification MBP fusion proteins

pMAL-c2G and pLEICS10 MBP plasmids containing the desired cDNA inserts were transformed into *E.coli* BL21 strain as described in **section 2.2.4**. A single colony from the transformation plate or alternatively a wire-loop of the glycerol stock of bacteria

containing the desired plasmid was grown in 2 ml LB broth supplemented with 100 µg/ml ampicillin at 37^{o}C in a shaking incubator at 220 rpm overnight. This culture was added to an appropriate volume of LB broth supplemented with 100 µg/ml ampicillin at a 1:20 dilution. For initial tests of protein expression, 5 ml volumes were used. Subsequently culture volumes were adjusted to yield approximately 5 µg of protein per sample. The bacteria were grown at 30^{o}C for 2 h after which protein expression was induced by adding 0.2 mM IPTG and the culture was incubated for a further 2 h at 30^{o}C. Bacteria were pelleted by centrifugation at 3220 xg and 4^{o}C for 15 min. The supernatant was discarded and pellets stored at -80^{o}C or processed immediately.

The bacterial pellet was resuspended in 1 ml 0.5% NETN buffer (1 mM EDTA, 20 mM Tris-HCl pH 8.0, 100 mM NaCl, 0.5% Nonidet P-40) and transferred to a 1.5 ml tube. Samples were sonicated in a Soniprep 150 using a 10 mm probe at amplitude 2 µm on ice for 3 cycles at 15 s, with a 30 s interval. Cell debris was removed by centrifuging the sample at 10000 xg for 10 min and transferring the supernatant to a fresh 1.5ml microcentrifuge tube. A volume of 30 µl of 50% amylose resin was added and the tube was rotated for 1 h at 4^{o}C. Amylose beads were washed three times in 0.5% NETN buffer, centrifuging at 1000 xg for 5 min. The supernatant was resolved by SDS-PAGE and Coomassie stained to observe protein expression levels (**sections 2.4.8** and **2.4.8.1.1**). Once protein levels had been equalised, MBP-fusion protein bound to amylose beads were used in *in vitro* kinase assays (**section 2.4.7**).

2.4.5 High-low salt extraction

U20S cells were seeded into 6 cm dishes and transiently transfected as described in **section 2.3.4**. Growth medium was aspirated from cells in a culture dish 24 h after

transfection and washed in PBS. Cells were trypsinised as described in **section 2.3.1**, resuspended in growth medium and divided between two 15 ml centrifuge tubes. The cells were pelleted by centrifugation at 200 xg for 5 min at RT, the supernatant aspirated and the pellet resuspended in 2 ml PBS. Tubes were centrifuged once more and the supernatant discarded.

The first cell pellet was resuspended in 100 µl of 50 mM NaCl buffer (10 mM Tris pH 7.4, 2 mM $MgCl_2$, 1% Triton® X-100, 1x PI cocktail, 1 mM PMSF, 50 mM NaCl) and the second in 500 mM NaCl buffer (10 mM Tris pH 7.4, 2 mM $MgCl_2$, 1% Triton® X-100, 1x PI cocktail, 1 mM PMSF, 500 mM NaCl). Samples were transferred to 1.5 ml microcentrifuge tube and incubated on ice for 15 min and then centrifuged for 5 min at 10000 xg at 4^{o}C. The supernatants were transferred to fresh 1.5ml micro-centrifuge tube where an equal volume of 2x Laemmli buffer was added and the samples boiled for 5 min. The pellets were resuspended in 200 µl of 2x Laemmli buffer and boiled for 5 min. Samples were resolved by SDS-PAGE (**section 2.4.8**) and analysed by western blotting (see **section 2.4.8.2**).

2.4.6 *In vitro* phosphorylation assay

The TNT® T7 Quick-Coupled transcription/translation kit (Promega, UK) was used to prepare *in vitro* translations (IVTs) of plasmids containing a T7 promoter upstream of the cDNA, according to the manufacturer's instructions. The IVT mix consisted of 1 µg of pCI-mSUN1 or pCI-mSUN2Δ154-185 (splice variant lacking exon 5) plasmid combined with 40 µl TNT® Mastermix, 2 µl [^{35}S]-methionine (Perkin Elmer, UK) and adjusted to a final volume of 50 µl with dH_20. The mix was then incubated at 30^{o}C for 1 h and used in subsequent *in vitro* phosphorylation assays as described below.

Cytostatic factor (CSF) (metaphase II-arrested) *Xenopus* egg extracts were prepared as described (Hames *et al.,* 2001; Desai *et al.,* 2001). Extracts (9 µl) were supplemented with 1 µl of *in vitro* translated protein and 0.3 µl cyclohexamide (10 mg/ml) before incubation at 22^{o}C for 30 min. Alternatively, aliquots of 2.5 µl were taken at 0, 10, 30 and 60 min. An equal volume of 2x Laemmli buffer was added to the samples, mixed and boiled for 5 min. Samples were resolved by SDS-PAGE and gels were then stained as described in **section 2.4.8.1.1** and analysed by autoradiography.

2.4.7 *In vitro* kinase assay

MBP and hSUN1 MBP-fusion proteins bound to amylose resin (**section 2.4.4.2**) and 5 µg of casein were combined with kinase buffer (50 mM Hepes-KOH pH 7.4, 5 mM $MgCl_2$, 5 mM β–glycerophosphate, 5 mM NaF, 4 µM ATP, 1 mM DTT) and 100 ng of purified CDK1, PLK1 or Aurora A (**Table 2.11**). To detect phosphorylated proteins by autoradiography the reaction was supplemented with 1 µCi of [^{32}P]-γ-ATP and incubated at 30^{o}C for 30 min. To generate phosphorylated proteins for mass spectrometry (MS) analysis, [^{32}P]-γ-ATP was omitted and reactions were incubated for 4 h at 30^{o}C. An equal volume of 50 µl of 2x Laemmli buffer was added and samples boiled for 3 min. Beads were spun down at 1000 xg for 5 min and the supernatant was resolved by SDS-PAGE. Gels were stained as described in **section 2.4.8.1** and analysed by autoradiography or further processed for MS, as appropriate.

2.4.7.1 Scintillation counts

Protein bands from the dried Coomassie gel were excised and placed in scintillation vials (SLS, UK) with 3 ml of OptiPhase HiSafe scintillation fluid (Perkin Elmer, UK). Radioactivity was measured in counts per minute (cpm) on the LS 6500 multipurpose

scintillation counter (Beckman Coulter™, UK) this measuring incorporation of the ^{32}P radiolabel. Scintillation values for the casein positive control and deletion constructs were corrected by subtracting counts derived from the MBP negative control sample. These values were used to calulate percentage phosphorylation relative to casein (see **section 2.4.7.2**).

2.4.7.2 Quantification of Coomassie stained protein bands

For *in vitro* kinase assays, protein band intensities on Coomassie stained and dried gels were quantified using ImageJ software (NIH, USA). Scanned images of the dried Coomassie gels were analysed by selecting a region of interest encompassing the largest band, calculating the mean pixel intensity for each protein band and then subtracting background levels. These densitometry values coupled with scintillation counts were then used to calculate the percentage phosphorylation for each fusion protein relative to casein. Graphs were generated using Microsoft Excel 2010.

2.4.8 Sodium dodecyl sulphate-polyacrylamide gel electrophoresis (SDS-PAGE)

Protein samples were resolved on 6%, 7.5% or 10% polyacrylamide gels that had been cast on the Mini-PROTEAN 3 polyacrylamide gel electrophoresis (PAGE) system (Bio-Rad, UK). Resolving gels (20%, 25% or 33% ProtoGel® (30% (w/v) acrylamide), 375 mM Tris-HCl pH 8.8, 0.4% (w/v) SDS, 0.12% (w/v) APS, 0.08% (v/v) TEMED) were poured, over-laid with isopropanol above to form a horizontal line, and allowed to set in 1 mm thick casting plates for 20 min over-laid with isopropanol above to form a horizontal line. The isopropanol was removed with filter paper and 4% stacking gel (13% ProtoGel® (30% (w/v) acrylamide), 125 mM Tris-HCl pH 6.8, 0.4% (w/v) SDS, 0.3% (w/v)

APS, 0.2% (v/v) TEMED) was poured on top. A comb of the appropriate thickness for the plates was inserted and allowed to set for 20 min.

Samples to be loaded onto acrylamide gels were mixed with an appropriate volume of 2x Laemmli buffer and denatured at 100^{o}C for 5 min. Combs were removed and wells washed with dH_20, then dried with filter paper. Depending on the experiment, 5-30 µl of denatured sample was loaded onto gels. Wells and the apparatus tank were filled with SDS-PAGE running buffer (25 mM Tris-base, 192 mM glycine, 0.1% (w/v) SDS) and electrophoresis was carried out at 150 V for 60-90 min. Polyacrylamide gels were then further analysed by Coomassie Blue staining or processed for western blotting.

2.4.8.1 Staining of protein gels

2.4.8.1.1 Standard Coomassie blue staining

To visualise bacterially expressed protein, resolved SDS-PAGE gels were immersed in Coomassie blue stain (0.25% (w/v) Coomassie Brilliant Blue G250, 10% (v/v) glacial acetic acid, 40% (v/v) methanol) for 20 min with gentle agitation. The Coomassie blue stain was removed and the gels were then washed several times in destain solution (10% (v/v) glacial acetic acid, 40% (v/v) methanol) to remove background staining and distinguish stained proteins. Washes were repeated until the background was clear. Gels were dried for 2 h at 80^{o}C onto 3MM filter paper (Whatman, UK) using a SUE 300 water pump (Heto, UK) fitted to a 1125B dual temperature slab dryer (Biorad, UK) and then analysed by autoradiography if appropriate.

2.4.8.1.2 Brilliant blue colloidal stain for mass spectrometry (MS)

Bacterially expressed MBP-fusion proteins or GFP-hSUN1 purified from HeLa cells were resolved by SDS-PAGE. To visualise the separated proteins for the purpose of MS analysis, it was necessary to use a stain that was designed for this application. SDS-PAGE gels were placed in fixing solution (7% (v/v) glacial acetic acid, 40% (v/v) methanol). Brilliant Blue Colloidal G was supplied as a 200 ml concentrate. This was diluted with 800ml dH_20 and mixed thoroughly by inversion to form a 1x working solution. Immediately before staining, 4 parts of the 1x working solution were combined with 1 part methanol and vortexed. The gel was placed in the staining solution for 2 h with gentle agitation. The staining solution was then discarded and the gel briefly washed in wash solution (10% (v/v) glacial acetic acid, 25% (v/v) methanol) for 30 s. The gel was washed overnight in 25% (v/v) methanol and then submitted to the University of Leicester PNACL proteomics facility for MS analysis (**section 2.4.10.1**).

2.4.8.2 Western blotting

After electrophoretic separation of proteins, the SDS-PAGE gel was detached from the electrophoresis apparatus and the stacking gel was removed. The gels were submerged in transfer buffer (25 mM Tris-base, 192 mM glycine, 20% (v/v) methanol) for 5 min. A Bio-rad semi-dry blotting system was used to transfer resolved proteins to nitrocellulose membrane. A transfer sandwich was assembled by first stacking three pieces of 3MM paper soaked in transfer buffer (10 x 7 cm) on the blotter base excluding air bubbles between layers. Then the nitrocellulose membrane, pre-incubated for 10 min in transfer buffer (9 x 6 cm), was placed on top with the gel positioned over it. A final three pieces of 3MM filter paper were used to seal the

sandwich. The semi-dry blotting machine was closed and proteins were transferred for 1 h at 1 mA/cm^2. To observe transfer efficiency and to check equal protein loading, the membrane was stained briefly with Ponceau S (0.1% (w/v), 5% (v/v) glacial acetic acid) and was washed with dH_20 to reduce background staining.

Membranes were incubated overnight at 4^oC or for 1 h at RT in 5% non-fat milk in PBST (140 mM NaCl, 10 mM Na_2HPO_4, 2.7 mM KCl, 1.8 mM KH_2PO_4, 0.1% (v/v) Tween) to block non-specific sites on the membrane. For the hSUN1 S48 phospho-antibody, 3% BSA in TBST (50 mM Tris-HCl pH 7.4, 200 mM NaCl, 0.1% (v/v) Tween) was used as a blocking agent for 1 h at RT. Blocked membranes were incubated for 1 h at RT or overnight at 4^oC with the appropriate antibody, as indicated in **Table 2.9**, diluted in 5% non-fat milk PBST or 3% BSA TBST. Membranes were washed three times for 5 min in PBST or TBST to remove unbound primary antibody. Membranes were then incubated for a further hour at RT with the appropriate horse-radish peroxidase (HRP) secondary antibody shown in **Table 2.10**. Membranes were washed again three times for 5 min in PBST or TBST to remove unbound secondary antibody and then developed using EZ-ECL chemiluminescence detection kit (Biological Industries, Israel) for HRP, according to the manufacturer's instructions. Proteins were visualised by autoradiography. Films were exposed to immuno-blots for varying lengths of time and developed using a compact X4 x-ray film processor (Xograph imaging system, UK).

2.4.8.2.1 Re-probing western blots

To detect a second protein of a different size to the first on the same membrane, after probing and developing, blots were washed for 10 min in PBST or TBST. Alternatively, if the proteins were of similar molecular weight but the secondary antibodies were

raised in different species, the HRP of the secondary antibody from the previous probing was deactivated by incubating the membrane with 15% hydrogen peroxide (H_2O_2) for 40 min at RT and washing the membrane in PBST or TBST. Otherwise, if proteins were of similar molecular weight and the secondary antibodies were the same species, the membrane was stripped of antibodies by incubating with stripping buffer (62.5 mM Tris-HCl pH 6.8, 100 mM β-mercaptoethanol, 2% (w/v) SDS) for 30 min at 60^{o}C and washing twice for 10 min in PBST or TBST. Membranes were then blocked and re-probed as described in **section 2.4.8.2**.

2.4.9 Phospho-antibody generation and purification

Eurogentec were commissioned to generate the hSUN1 S48 phospho-antibody. The peptide encompassing the S48 phosphorylation site was generated along with its modified version LDPVFD-S[PO_3H_2]-PRMSRR and incorporated into their 28-day Super Speedy polyclonal antibody protocol. Rabbits were immunised with modified peptide for phospho-specific polyclonal antibody production. Eurogentec chose the rabbit with the highest antibody titre for affinity purification of the phospho-antibody and ELISA assays. The non-modified peptide LDPVFDSPRMSRR was used to remove antibodies that recognised the non-phosphorylated form of the protein during the affinity purification procedure. Purified antibody was delivered in a buffer with PBS, 0.01% thimerosal and 0.1% BSA.

2.4.10 Large-scale GFP-TRAP® for mass spectrometry (MS)

Large-scale GFP-TRAP® experiments were carried out to identify potential binding partners of hSUN1 and phosphorylation sites in mitotic extracts. Twenty-four 10 cm dishes were transiently transfected with 5 µg of GFP-hSUN1 and twelve 10 cm dishes

with 2 µg of GFP. Of the 24 GFP-hSUN1, 12 were synchronised in mitosis (**section 2.3.5**). Cells were harvested and lysed as in **section 2.4.2.2** and 900 µl of soluble extract was added to 60 µl of GFP-Trap® beads. Samples were processed via the GFP-Trap® protocol as described in **section 2.4.3.4**. Beads were resuspended in 30 µl of 2x Laemmli buffer and boiled for 10 min. The supernatant was resolved on 10% SDS-PAGE gels and stained with Brilliant Blue Colloidal G (**section 2.4.8.1.2**).

2.4.10.1 Mass spectrometry (MS)

Appropriate gel slices were excised from the gel and subjected to digestion with trypsin (Promega, UK) or Asp-N (Roche, UK). Peptides were analysed by liquid chromatography coupled with tandem MS (LC-MS/MS) using an Ultimate 3000 RSLC nano system for HPLC (Thermo Scientific, UK) and then a LTQ-Orbitrap Velos for MS (Thermo Scientific, UK). MS proteomic data was analysed using MASCOT v2.2.04 or Scaffold 3 software.

2.4.10.2 Immobilised metal affinity chromatography (IMAC) phospho-peptide enrichment

In some instances, digested protein samples were enriched for phospho-peptides to identify phosphorylation sites using PHOS-Select™ iron affinity gel (IMAC). The PHOS-Select™ iron affinity gel beads were gently mixed to form a uniform solution and 80 µl of the 50% slurry (40% beads) was transfer to an assemble spin column with a plug. To wash the beads, 500 µl of equilibrium buffer (250 mM acetic acid, 30% (v/v) acetonitrile, HCl pH 2.5) was added, vortexed and then the plug was removed. The spin column was centrifuged at 8200 xg for 30 s, the flow-through was discarded and the wash steps repeated twice more. Digested proteins were dehydrated in a DNA

SpeedVac system (Thermo Electron Corp., USA) to remove the carbonate from the sample, preventing buffer neutralisation. Samples were resuspended in 200 µl of equilibrium buffer and vortexed. The plug was fitted to the spin column again and the sample applied. Spin columns were mixed end-over-end for 1 h at RT. The plug was removed and the sample centrifuged as before, discarding the flow-through. Samples were washed twice, firstly with equilibrium buffer, then with dH_20 to remove any residual equilibrium buffer. The plug was fitted once more and the phospho-peptides, now retained in the column were incubated with elution solution (400 mM ammonium hydroxide) for 5 min at RT with end-over end turning. The plug was removed and the phospho-peptides eluted by centrifugation. Peptides were analysed by LC-MS/MS using an Ultimate 3000 RSLC nano system for HPLC and then a LTQ-Orbitrap Velos for MS. MS proteomic data was analysed using MASCOT v2.2.04 or Scaffold 3 software.

CHAPTER 3
Characterisation of hSUN1 phosphorylation

Chapter 3 Characterisation of hSUN1 phosphorylation

3.1 Introduction

At the onset of mitosis the NE undergoes profound architectural changes where it is broken down to allow chromosome segregation and eventual cell division to occur. NEBD firstly requires depolymerisation of the lamina network, disassembly of the nuclear lamina with its associated proteins as well as dissociation of NPCs (Gerace & Blobel, 1980; Dultz *et al.*, 2008; Katsani *et al.*, 2008). Current models suggest that these events are a prerequisite to weaken the NE before it is physically torn apart by spindle microtubules that attach to the NE during prophase (Beaudouin *et al.*, 2002; Salina *et al.*, 2002).

Phosphorylation of NE-associated proteins prepares the NE for its eventual breakdown. This induces depolymerising the lamina network (Gerace & Blobel, 1980; Heald & Mckeon, 1990; Peter *et al.*, 1990), disrupting the lamina interactions with INM proteins (Foisner & Gerace, 1993) and NPCs but also impeding its interactions with chromatin, leading to chromatin condensation (Foisner & Gerace, 1993; Pfaller *et al.*, 1991).

Since the first studies on nuclear lamina disassembly and phosphorylation in the 1990s, many further NE components, in particular integral membrane proteins, have been identified (Dreger *et al.*, 2001; Schirmer *et al.*, 2003) forming large networks that appear to be more complicated than originally thought. Thus, it is likely that some of these proteins also become phosphorylated and contribute to NEBD in mitosis. This

chapter will primarily focus on the mammalian INM protein SUN1 with brief insights into its orthologue SUN2.

The SUN-domain proteins reside at the INM where they are orientated so that their C-terminus lies in the PNS while their N-terminus is located in the nucleoplasm (Crisp *et al.*, 2006). The C-terminus is where the SUN-domain is situated and this interacts with the C-terminal KASH-domain of a range of nesprin isoforms which are found on the ONM (Crisp *et al.*, 2006; Padmakumar *et al.*, 2005; Haque *et al.*, 2006). This molecular bridge spanning the PNS is known as the LINC complex (**Figure 1.7B** and **Figure 1.9**). The N-terminus of SUN1 and SUN2 binds lamin A/C (Crisp *et al.*, 2006; Haque *et al.*, 2006) while the N-terminus of giant nesprin-1 and nesprin-2 isoforms binds the actin cytoskeleton (Starr & Han, 2002). Alternatively, nesprin-3 and nesprin-4 connect with the cytoplasmic intermediate filament network (Roux *et al.*, 2009) and microtubule network, respectively (Wilhelmsen *et al.*, 2005). The LINC complex is involved in a number of roles such as nuclear anchorage and migration, cell migration, mechanical strength and cellular rigidity (Luxton *et al.*, 2011; Malone *et al.*, 2003; Lombardi *et al.*, 2011; Stewart-Hutchinson *et al.*, 2008).

Besides being a key component of the LINC complex, mammalian SUN proteins also form various interactions with other INM proteins. Emerin and small nesprin isoforms have been found to bind at the N-terminus (Haque *et al.*, 2010) and more recently, evidence for an interaction with the novel INM protein SAMP1/NET5 has emerged (Borrego-Pinto *et al.*, 2012). Certain INM proteins, in particular, LAP1/2, emerin and MAN1, are capable of binding BAF, a chromatin-associated protein, via their LEM-domain (Gruenbaum *et al.*, 2005). Not much is known about SUN interactions with

chromatin, only that the N-terminus of SUN1 is required to bind chromatin (Chi *et al.*, 2007; Lu *et al.*, 2008) and during meiosis SUN1 mediates anchorage of telomeres at the nuclear periphery (Ding *et al.*, 2007). This work is supported by similar findings in yeast (Bupp *et al.*, 2007; Schober *et al.*, 2009).

As SUN proteins bind a range of NE components in the ONM and INM, NPCs and the nuclear lamina during interphase, it is plausible to think that, at the onset of mitosis, these interactions would need to be disassembled. Research in the field to date has not looked specifically at the role of SUN1 phosphorylation in NEBD. In fact, the only research demonstrating SUN1 is phosphorylated comes from the *C.elegans* homologue matefin, where N-terminal phosphorylation is involved in meiotic homologous pairing (Penkner *et al.*, 2009).

The Universal Protein Knowledgebase (UniProtKB) proteomic database proposes that hSUN1 has three potential phosphorylation sites at serines 48, 52 and 138. The serine 48 and 52 sites are based on predictions whereby the hSUN1 sequence was cross-referenced to previously determined kinase consensus sequences for phosphorylation. However, S138 has been identified as a phosphorylation site through a combination of stable isotope labelling by amino acids in cell culture (SILAC), cation-exchange chromatography, phospho-peptide enrichment and MS (Dephoure *et al.*, 2008; Olsen *et al.*, 2006). According to global phospho-proteome analysis studies, hSUN2 has four phospho-serines; 12, 38, 54 and 116, again with experimental data to suggest that these are true phosphorylation sites (Olsen *et al.*, 2006; Gronborg *et al.*, 2002; Mayya *et al.*, 2009). Three of these four sites were identified by an alternative method where

a MS-based proteomic approach was adopted following IP with serine/threonine phospho-specific antibodies (Gronborg *et al.*, 2002).

The aim of this chapter was to determine whether mammalian SUN-domain proteins undergo phosphorylation in a cell-cycle dependent manner and to characterise the phosphorylation sites. SUN1 became the main focus of the chapter, with some experiments shedding light on possible SUN2 phosphorylation in mitosis. Confirmation of SUN1 phosphorylation in mitosis was studied using cell synchronisation assays, applying the use of cell-cycle arrest drugs in immortalised cell lines. This was considered to be a more direct approach compared to previous methods where isoelectric points or ^{32}P pulse-labelling of interphase and mitotic cells were examined (Gerace & Blobel, 1980).

Identification of specific phosphorylation sites, were initially carried out *in vivo* using an IP-MS approach but later confirmed by *in vitro* methods. This strategy was favoured over a candidate approach where serine and threonine residues from the SUN1 sequence suspected as potential phosphorylation sites would have been mutated and analysed. This was thought to be extremely time consuming way of identifying true phosphorylation sites.

Emphasis was also placed on identification of mitotic kinases as it is well documented that CDK1 is a major mitotic kinase but, emerging data highlights the importance of other kinases such as PLK1 and Aurora A for mitotic entry (Nigg, 2001).

Very few papers that focus on mitotic substrate phosphorylation provide a comprehensive characterisation of phosphorylation for a given substrate, possibly due

to the limited methods at the time of analysis. By fully characterising SUN1 phosphorylation it provides a basis on which to build, and deliberate on its functional role in the cell.

3.2 Results

3.2.1 hSUN1 undergoes a mobility shift in mitotic extracts

To investigate the possibility that mammalian SUN proteins are phosphorylated during mitosis, initial experiments first set out to determine whether a change in electrophoretic mobility of SUN1 and SUN2 could be detected in mitosis.

[^{35}S]-methionine-labelled IVTs of plasmids pCI-mSUN1 and pCI-mSUN2, producing full-length mouse SUN1 (mSUN1) and mouse SUN2 (mSUN2) splice variant lacking exon 5 (deletion within the N-terminus) (**Figure 3.1A**), respectively, were incubated with cytosolic factor (CSF) (metaphase II-arrested) *Xenopus* egg extracts. These extracts were derived from *Xenopus* toads which had been injected with hormones to stimulate release of eggs (Desai *et al.*, 1999). The eggs were all arrested in metaphase II of meiosis and so were a synchronised population rich in kinases and factors required for the progression through the second division of meiosis, which is essentially identical to mitosis. If SUN1 and SUN2 were post-translationally modified during mitosis, the 'mitotic' extract would be able to phosphorylate the substrates.

The principle of a mobility shift experiment is that proteins acquiring post-translational modifications, particularly the negative charge of a phosphate group, frequently migrate at a slower rate on a SDS-PAGE gel in comparison to the non-modified protein and therefore produce an apparent 'shift' in molecular weight.

Initially, samples were resolved on 7.5% polyacrylamide gels, but unfortunately no change in molecular weight could be seen between treated and non-treated mSUN1 or mSUN2 samples (**Figure 3.1B**). To ensure that this was not just a result of inadequate

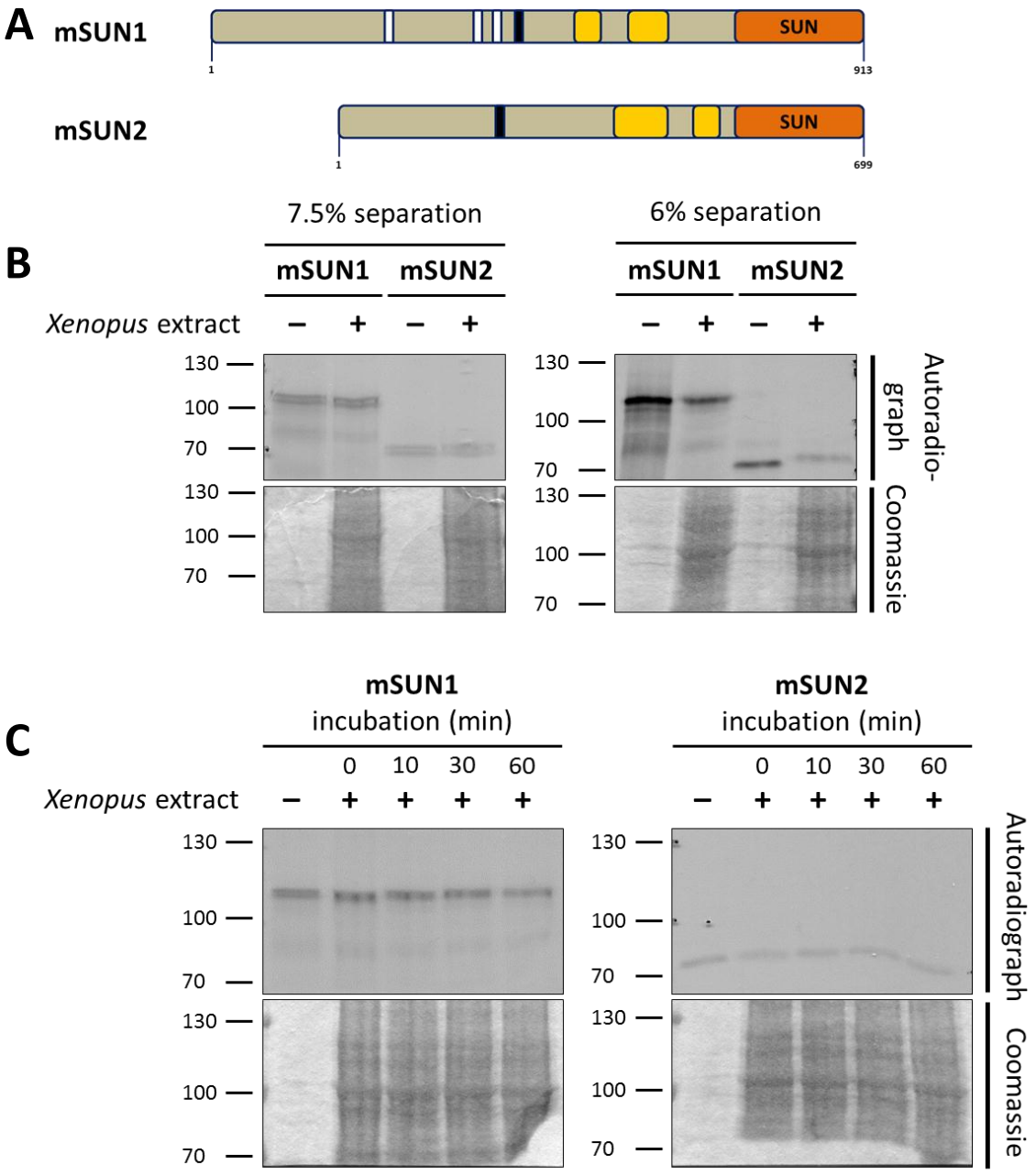

Figure 3.1. *In vitro* phosphorylation assays using *Xenopus* egg extracts.

(A) Schematic representation of *in vitro* translated mSUN1 and mSUN2 used in *in vitro* phosphorylation experiments. Hydrophobic regions (white), transmembrane domain (black) and coiled-coil domains (yellow) are indicated. **(B)** *In vitro* phosphorylation assays performed by addition of *in vitro*-translated [^{35}S]-methionine-labelled mSUN1 or mSUN2 to CSF (metaphase II-arrested) *Xenopus* egg extracts. Samples were incubated at 22^{o}C for 30 min, resolved on 7.5% or 6% SDS-PAGE gels, Coomassie stained and analysed by autoradiography. **(C)** As described in B with the exception of sample collection at the times indicated (min) and protein resolution on 6% gels only. Molecular weights (kDa) are indicated. N.B. mSUN2 is a splice variant lacking exon 5, corresponding to amino acid residues 154-185, in comparison to the full-length isoform of 729 residues.

protein separation, samples were re-run on 6% polyacrylamide gels. However, mSUN1 still did not produce a band-shift, whereas mSUN2 displayed a slight reduction in electrophoretic mobility in the sample incubated with the egg extract (**Figure 3.1B**).

Upon analysis, it was speculated that the 30 min incubation of IVTs with *Xenopus* egg extract may not have been sufficient to allow efficient phosphorylation or indeed other post-translational modifications. To address this, the same experimental design was applied with a time course up to 60 min, but no obvious band-shifts were apparent for either mSUN1 or mSUN2 (**Figure 3.1C**). Not all phosphorylated proteins undergo a change in electrophoretic mobility on a gel but before assuming that this was the case for mSUN1 and mSUN2, a different approach was taken by observing *in vivo* phosphorylation in mammalian cells.

Mouse NIH 3T3 and human U2OS and HeLa cell lines were treated with the microtubule depolymerising drug nocodazole for 16 h to arrest them in mitosis. Mitotically arrested cells were then collected by mechanical shake-off while untreated asynchronous cells were obtained by trypsinisation. Cells were counted and equivalent numbers of cells were analysed by western blot after separation on 6% gels to detect SUN1 or SUN2. **Figure 3.2** shows that mSUN1 failed to show a band-shift, consistent with results from **Figure 3.1B** and **Figure 3.1C**. In contrast, human SUN1 (hSUN1) displayed a shift in molecular weight in both U2OS and HeLa cell lines (**Figure 3.2**). This suggests that either mSUN1 is not phosphorylated (which appears to be unlikely given that the mouse and human SUN1 proteins share 66.8% homology according to UniProtKB sequence alignment) or that mSUN1 is phosphorylated but does not induce

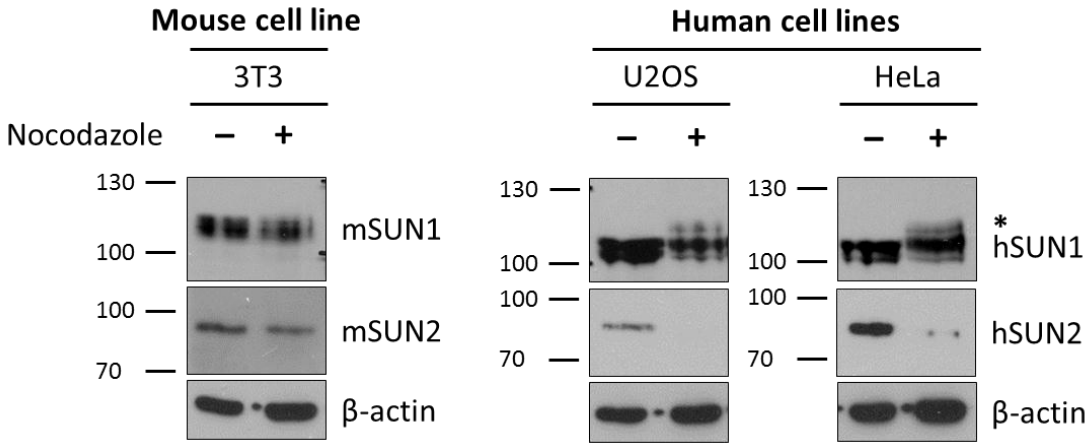

Figure 3.2. Species comparison of SUN1 and SUN2 protein expression between asynchronous and mitotic samples.

NIH 3T3, U2OS and HeLa cells were treated with nocodazole for 16 h. Total cell lysates were prepared after trypsinisation or mechanical shake-off, resolved by SDS-PAGE and immuno-blotted with anti-mSUN1 0545, anti-mSUN2 2294, anti-hSUN1 Atlas, anti-hSUN2 2853 and anti-β-actin antibodies. * represents the mobility shift seen for hSUN1. Molecular weights (kDa) are indicated.

a shift in electrophoretic mobility. Since no mSUN1 band-shift was detectable in the mouse cells, mSUN1 was not analysed in further studies.

SUN2 appeared to behave quite differently, mSUN2 showed a marginal reduction in expression level in mitotic samples from NIH 3T3 cells whilst human SUN2 (hSUN2) expression was dramatically reduced in both human cell lines (**Figure 3.2**). Possible explanations could be that hSUN2 phosphorylation in mitosis targets it for proteolytic degradation.

3.2.2 Optimisation of the synchronisation procedure

Having detected a hSUN1 band-shift in mitotic U2OS and HeLa cells, my next aim was to optimise the mitotic arrest procedure in order to maximise the band-shift. One concern with the synchronisation procedure used previously was the efficiency of cell synchronisation by a single drug treatment. It is known that cell cultures can be more efficiently enriched at certain cell cycle stages by double-drug treatments (Morgan, 2006; Bostock *et al.*, 1971). The following protocol was therefore applied to U2OS and HeLa cell lines.

Initially, cells were pre-arrested with aphidicolin for 16 h prior to mitotic arrest. This drug inhibits DNA polymerase α which is involved in DNA replication, hence arresting cells at the G1/S boundary. The reversible nature of aphidicolin allowed cells to re-enter the cell cycle upon drug removal. Cells were then washed thoroughly with PBS before releasing them into fresh medium for at least 4 h, at which point the cells would be in S/G2 phase. Cells were finally subjected to 16 h nocodazole treatment for

mitotic arrest. Samples were collected for each of the treatment stages as well as from an asynchronous sample and analysed by western blot.

Immuno-blotting with the hSUN1 antibody showed that, for both U2OS and HeLa cell lines, electrophoretic migration was retarded only in mitosis, indicating that the hSUN1 band-shift is mitosis specific (**Figure 3.3A**). Also, the shifted-band was more prominent than in the experiment using a single arrest with nocodazole, indicating that the procedure has been improved with the pre-arrest.

Samples were also probed with anti-hSUN2 2853 antibody to observe the hSUN2 profile over the cell cycle. On this occasion, two bands of different molecular weights were detected on the hSUN2 membranes, the higher molecular weight band corresponding to the one observed in **Figure 3.2**. SUN1 has seven alternatively spliced variants (Gob *et al.*, 2011) and SUN2 potentially has three splice variants detected at 85, 75 and 65 kDa (Hodzic *et al.*, 2004). It is therefore possible that the antibody is detecting more than one isoform. Alternatively, the lower band could be due to cross-reaction of the SUN2 antibody. The lower band, positioned at approximately 70 kDa, is expressed at low levels in the asynchronous lane which is confusing as, from G1 to G2, it is highly expressed and then it is virtually undetectable in mitosis (**Figure 3.3A**). In contrast, the 85 kDa band is expressed in asynchronous cells and enriched at mitosis (**Figure 3.3A**). Oddly, the 70 kDa band behaves in the same manner as bands seen in **Figure 3.2** and **Figure 3.4A** at approximately 85 kDa. Unfortunately hSUN2 expression in U2OS cells was very low in comparison to HeLa cells (**Figure 3.3B**) but expression levels appeared to correlate better with those observed in **Figure 3.2** in that the 85 kDa predominated and was significantly reduced in mitotic samples.

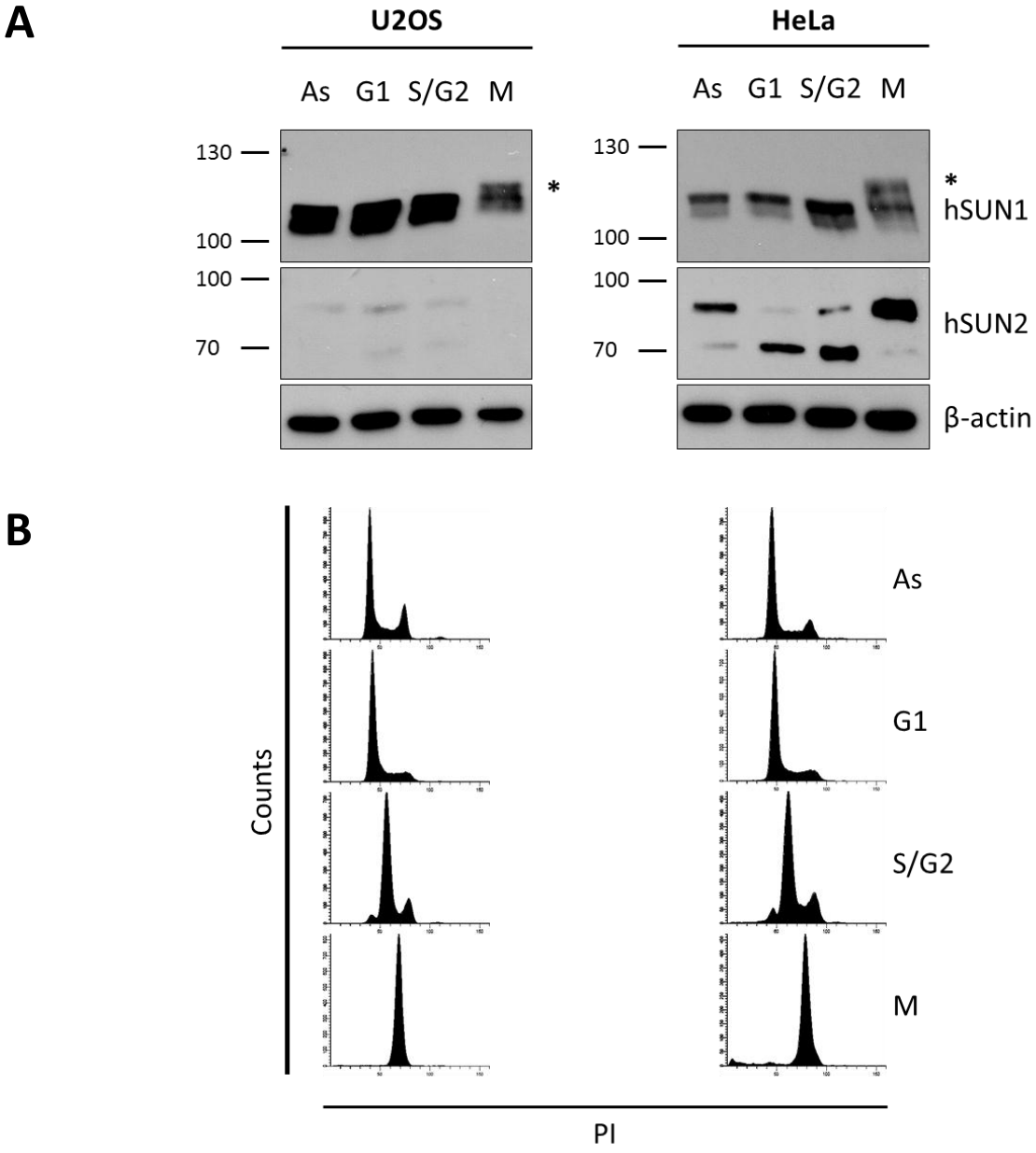

Figure 3.3. Establishing a pre-arrest mitotic synchronisation protocol in human cell lines.

(A) U2OS and HeLa cells growing in asynchronous (As) culture were treated with aphidicolin for 16 h (G1). The aphidicolin was then removed and cells were incubated in fresh medium for 4 h (S/G2) followed by a 16 h nocodazole treatment (M). As, G1 and S/G2 total cell extracts were collected by trypsinisation while M samples were collected by mechanical shake-off. Total cell extracts were resolved by SDS-PAGE and immuno-blotted with anti-hSUN1 Atlas, anti-hSUN2 2853 and anti-β-actin antibodies. * represents the mobility shift seen for hSUN1. Molecular weights (kDa) are indicated. **(B)** In parallel experiments, cells from each treatment were collected by trypsinisation and stained with propidium iodide (PI) supplemented with RNase A and analysed by FACS to determine the cell cycle profile.

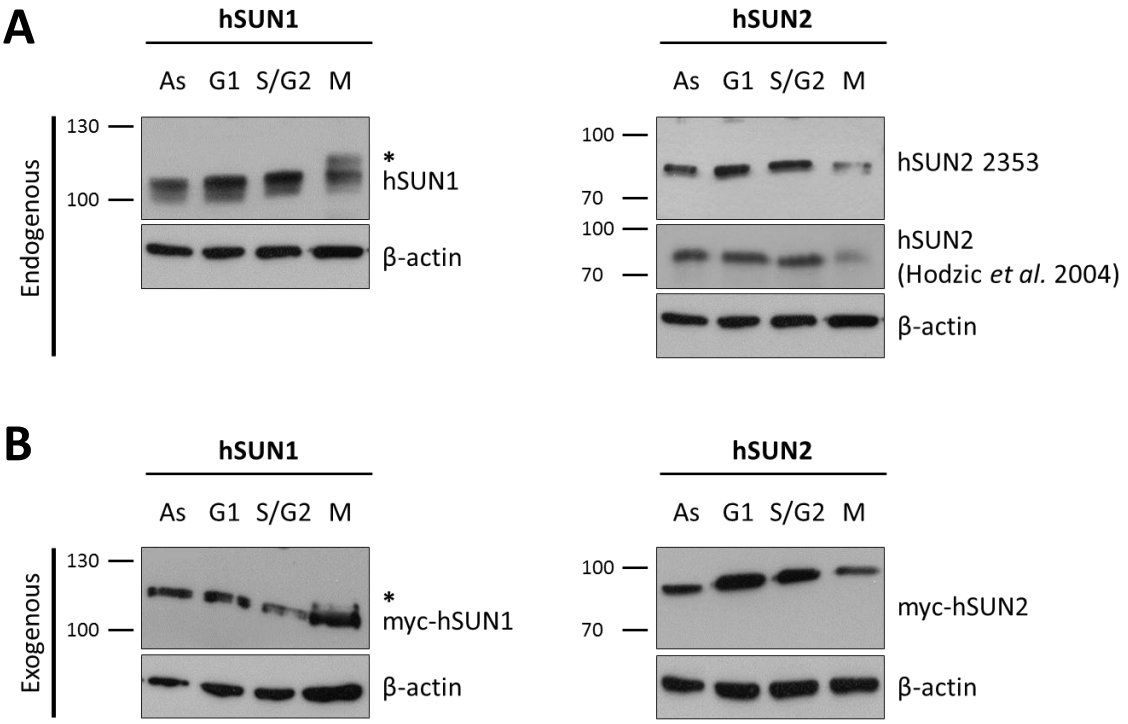

Figure 3.4. hSUN1 undergoes a mobility shift while hSUN2 has lower expression in mitotic extracts.

(A) HeLa cells growing in asynchronous (As) culture were treated with aphidicolin for 16 h (G1). The aphidicolin was then removed and cells were incubated in fresh medium for 4 h (S/G2) followed by a 16 h nocodazole treatment (M). Total cell extracts were resolved by SDS-PAGE and immuno-blotted with anti-hSUN1 Atlas, anti-hSUN2 2853, anti-hSUN2 (Hodzic *et al.* 2004) and anti-β-actin antibodies. **(B)** For exogenous myc-hSUN1 and myc-hSUN2 analysis the same protocol was applied 10 h after transfection. Total cell extracts were resolved by SDS-PAGE and immuno-blotted with anti-c-myc and anti-β-actin antibodies. * represents the mobility shift seen for hSUN1. Molecular weights (kDa) are indicated.

To confirm the cells had been arrested at the appropriate cell cycle phase, fluorescence activated cell sorting (FACS) analysis was performed. A parallel experiment was conducted and cells from the four samples were stained with PI in the presence of RNase A to detect DNA only. Samples were then loaded on to the BD FACSCanto™ II instrument and the data analysed with BD FACSDiva™ software. The asynchronous sample gave two peaks, the larger peak to the left representing cells in G1 with a diploid number of chromosomes (2n), and the smaller peak on the right representing cells where the chromosomes have been duplicated (**Figure 3.3B**). Cells arrested in G1 with aphidicolin had a single peak to the left as expected. The S/G2 sample represents cells undergoing, or completing DNA replication and can be seen by the large number of cells in the area between the two main peaks. Finally as expected, cells arrested in M phase with nocodazole have a single peak to the right indicating that all cells have undergone DNA replication (**Figure 3.3B**). This analysis confirmed that the pre-arrest synchronisation protocol was successful in mitotic synchronisation of cells in both cell lines and therefore could be applied to subsequent experiments.

3.2.3 Application of the synchronisation procedure to study transiently transfected exogenous hSUN1 and hSUN2

The data has shown that endogenous hSUN1 undergoes a mobility shift and hSUN2 predominantly shows reduced expression in mitosis. The next step was to see whether these results could be reproduced with exogenous myc-tagged hSUN1 and hSUN2 proteins. Plasmids pLEICS20 myc-hSUN1 and pLEICS20 myc-hSUN2, encoding 916 and 717 residue isoforms of each protein, respectively, were transiently transfected into HeLa cells 10 h prior to proceeding with the pre-arrest synchronisation protocol

described in **section 2.3.5**. Untransfected samples were also prepared in parallel. Analysis of samples by western blotting confirmed that exogenous hSUN1 behaved like the endogenous protein, producing a band-shift in mitotic samples only (**Figure 3.4A** and **Figure 3.4B**).

Membranes probed with anti-hSUN2 2853 antibody mirrored results shown in **Figure 3.2**, where endogenous hSUN2 expression was markedly reduced in the mitotic sample only. The anti-hSUN2 2853 antibody was raised against the extreme N-terminus of hSUN2, so to confirm that any modifications to hSUN2 in mitotic samples were not simply obstructing the anti-hSUN2 2853 antibody binding site, samples were also probed with anti-hSUN2 antibody raised against the C-terminus (Hodzic *et al.* 2004). Both antibodies produced the same pattern showing a decrease in protein expression in mitotic samples (**Figure 3.4A**). Similar to endogenous hSUN2, overexpressed myc-hSUN2, also showed reduction in protein expression in the mitotic sample relative to the other samples, suggesting that the protein maybe targeted for degradation during mitosis (**Figure 3.4B**).

3.2.4 hSUN1 is phosphorylated in mitosis

Data so far have shown that hSUN1 undergoes a post-translational modification at the onset of mitosis and that hSUN2 may be targeted for degradation. To establish whether the hSUN1 band-shift was due to phosphorylation, soluble lysates derived from mitotically arrested cells were supplemented with β-glycerophosphate to inhibit phosphatase activity. Samples were then incubated with or without λ phosphatase (λ ppase) to non-specifically dephosphorylate proteins (**Figure 3.5A**). The notion behind this experiment was that a loss of the band-shift in the presence of λ ppase would

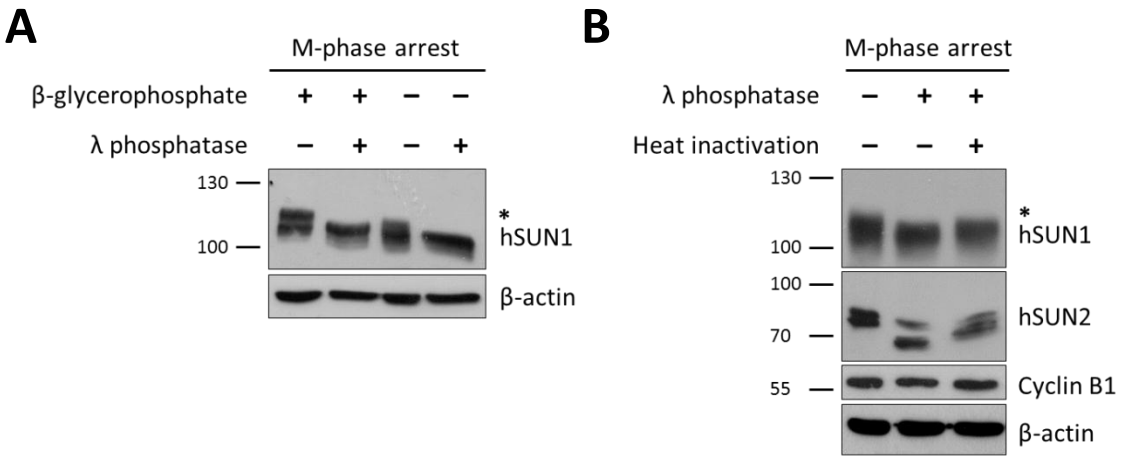

Figure 3.5. hSUN1 and hSUN2 are phosphorylated in mitotic extracts.

(A) Mitotically arrested HeLa cell lysates supplemented with β-glycerophosphate were incubated with or without λ phosphatase at 30°C for 45 min. Samples were resolved by SDS-PAGE and analysed by immuno-blotting with anti-hSUN1 Atlas and anti-β-actin antibodies. **(B)** Mitotically arrested HeLa cell lysates supplemented with β-glycerophosphate were incubated with either active λ phosphatase or heat-inactivated λ phosphatase at 30°C for 45 min. Samples were analysed by immuno-blotting with anti-hSUN1 Atlas, anti-hSUN2 2853, anti-cyclin B1 and anti-β-actin antibodies. * represents the mobility shift seen for hSUN1. Molecular weights (kDa) are indicated.

demonstrate that the post-translational modification is due to protein phosphorylation. In the absence of λ ppase, resolved proteins probed with anti-hSUN1 Atlas antibody showed that mitotic extracts supplemented with or without β-glycerophosphate both showed the characteristic band-shift, which implied that the addition of the phosphatase inhibitor was not necessary to maintain the mobility shift. Furthermore, addition of λ ppase not only caused a loss of the mobility shift but its activity was so potent that the β-glycerophosphate activity was over-hauled (**Figure 3.5A**).

To confirm that it was specifically λ phosphatase activity responsible for loss of the band-shift, mitotically arrested soluble lysates prepared as in **Figure 3.5A** were treated with either an active or a heat-inactivated form of λ phosphatase (**Figure 3.5B**). Membranes for hSUN1 showed that the band-shift was only maintained in samples lacking the phosphatase or in the presence of heat-inactivated λ phosphatase, while the sample incubated with active λ ppase was consistent with results from **Figure 3.5A**. Samples were also immuno-blotted with anti-cyclin B1 antibody as a marker of mitosis (**Figure 3.5B**). Taken together, these results indicate that hSUN1 is phosphorylated in mitotic samples and this is responsible for the band-shift.

In addition, these samples were probed with hSUN2 antibody despite previous results indicating that expression of hSUN2 was decreased in mitosis (**Figure 3.2** and **Figure 3.4**). hSUN2 membranes showed that the protein is apparently phosphorylated during mitosis (**Figure 3.5B**). The sample in the left lane did not behave as previously shown but instead exhibited a doublet and high level protein expression in mitosis. Due to the

conflicting nature of the hSUN2 data, subsequent experiments were to focus purely on hSUN1 phosphorylation.

3.2.5 hSUN1 is phosphorylated upon entry into mitosis

To establish approximate timings of the hSUN1 transient phosphorylation event, HeLa cells were pre-arrested with aphidicolin as previously described but were then synchronised in G2 with the reversible cell cycle drug RO-3306. RO-3306 inhibits CDK1 and so halts cells in G2. Samples were collected upon release from G2 at 0, 30, 60, 120 and 240 min (**Figure 3.6A**). Western blot analysis with anti-hSUN1 Atlas antibody showed that the hSUN1 band-shift appeared 30 min after drug release and was present for up to 60 min, after which the shift was lost. These data suggest that hSUN1 is phosphorylated upon entry into mitosis 30 min post G2 and continues to be phosphorylated for up to 1 h (**Figure 3.6A**). Following this, phosphorylation is lost, most likely through the action of mitotic phosphatases.

Membranes were also probed for cyclin A and cyclin B1 to confirm progression from G2 to M phase after release from RO-3306. Cyclin A peaks at G2 and is rapidly degraded before mitosis, therefore identifies samples in G2, while cyclin B1 accumulates in mitosis and therefore acts as a marker for M phase (**Figure 3.6A**). Parallel samples were also prepared for FACS analysis, as described for **Figure 3.3B**. The asynchronous sample gives the characteristic two peaks, while the time-course starting with the release from G2 exhibits a gradual shift in cells from the G2 state back to the G1 peak where the profile starts to resemble that of the asynchronous sample (**Figure 3.6B**). These analyses confirmed that the cells had been successfully released from G2 and were progressing though mitosis, back into interphase.

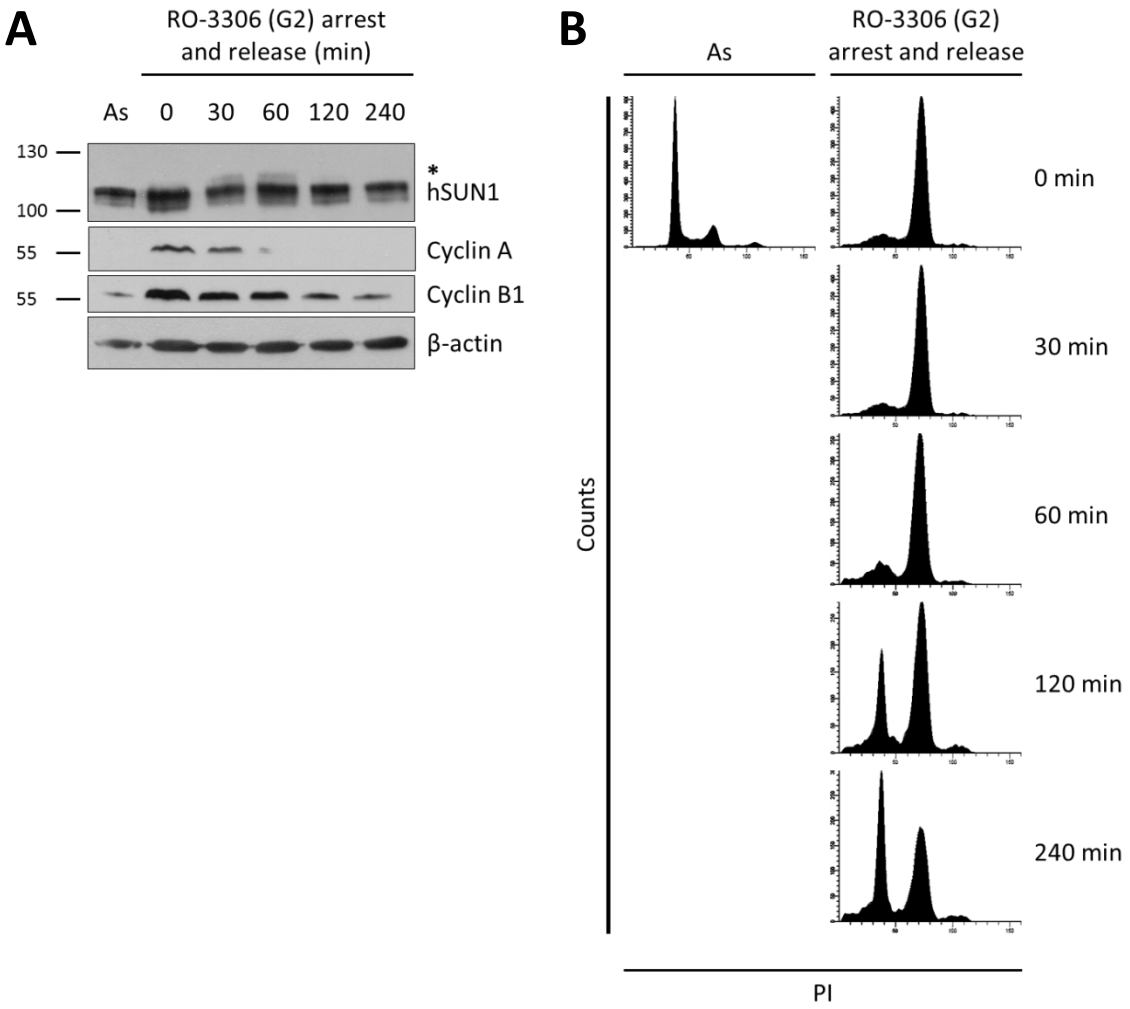

Figure 3.6. hSUN1 is phosphorylated upon entry into mitosis.

(A) HeLa cells growing in asynchronous (As) culture were treated with aphidicolin for 16 h. Aphidicolin was then removed and cells were incubated in fresh medium for 4 h followed by a 16 h RO-3306 treatment (G2 arrest). Cells were released from the block and samples collected at the time points indicated (min). Total cell extracts were resolved by SDS-PAGE and immuno-blotted with anti-hSUN1 Atlas, anti-cyclin A, anti-cyclin B1 and anti-β-actin antibodies. * represents the mobility shift seen for hSUN1. Molecular weights (kDa) are indicated. **(B)** In parallel experiments, asynchronous cells and cells from each of the time-point were stained with propidium iodide (PI) supplemented with RNase A and FACS analysed to follow the progression of cells from G2 into interphase.

3.2.6 Optimisation of large-scale hSUN1 immunoprecipitation

Having demonstrated that hSUN1 undergoes phosphorylation during mitosis, my next objective was to identify the specific residues of hSUN1 that are phosphorylated. The modern gold standard approach for the identification of *in vivo* phosphorylation sites is IP, coupled with MS. Ideally endogenous protein should be immunoprecipitated, to avoid false results due to protein overexpression. Initial experiments were therefore carried out to optimise the IP of endogenous hSUN1 from mitotic HeLa cells and scale-up for MS analysis.

Firstly, small-scale IPs were performed to assess which anti-hSUN1 antibody had the highest binding capacity and specificity for hSUN1. Soluble lysates from a 10 cm plate of asynchronously growing HeLa cells were pre-cleared with protein A-sepharose beads and then subjected to IP with 2 µg anti-hSUN1 Atlas, anti-hSUN1 2383 and anti-HA antibodies, the latter as a negative control. Despite its high binding capacity for hSUN1, the anti-hSUN1 Atlas antibody also displayed non-specific binding of other proteins whilst the anti-hSUN1 2383 antibody, even though recovered protein levels were lower, specifically identified a single band corresponding to hSUN1 (**Figure 3.7A**). Anti-HA antibody did not detect hSUN1 as expected. Since anti-hSUN1 2383 antibody had a cleaner IP result, this antibody was used for a subsequent large-scale IP.

The number of cells was then scaled up to 15 10 cm plates compared to the small-scale pilot experiment, using 7 µg anti-hSUN1 2383 antibody for IP. Soluble, insoluble and unbound fractions were resolved alongside the IP sample and bands were detected with Brilliant Blue colloidal stain. This particular stain is specifically suited for samples intended for MS analysis as it more sensitive compared to standard

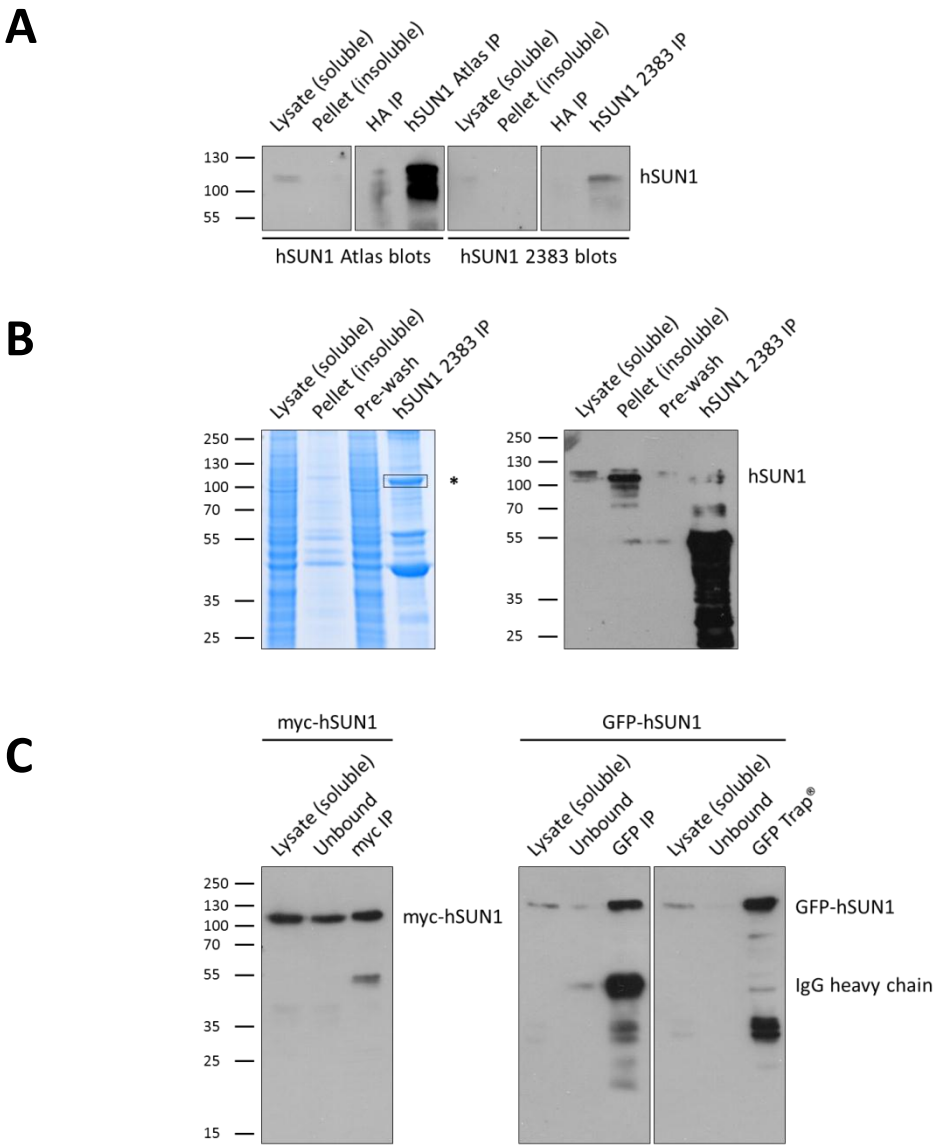

Figure 3.7. Optmisation of *in vivo* IP-MS for the identification of hSUN1 phosphorylation sites.

(A) Small-scale comparison of two hSUN1 antibodies to IP endogenous protein. Soluble lysates derived from cultured HeLa cells were subjected to IP with 2 µg of either anti-hSUN1 Atlas or anti-hSUN1 2383 antibodies as well as anti-HA antibody as a negative control. Insoluble and soluble fractions, as well as the final IP sample, were resolved by SDS-PAGE and immuno-blotted with the respective antibodies. **(B)** (Left) large-scale IP where soluble lysates derived from cultured HeLa cells were subjected to IP with 7 µg of anti-hSUN1 2383 antibody. Insoluble, soluble, un-bound fractions and the final IP sample were resolved by SDS-PAGE sent for MS analysis. The boxed band indicated with a * was excised from the gel, trypsin digested and analysed by LC-MS/MS. (Right) a second elution from the same sample was resolved by SDS-PAGE and immuno-blotted with anti-hSUN1 Atlas antibody. **(C)** Small-scale comparison of IP vs. GFP-Trap® methods. HeLa cells transiently transfected with either pLEICS20 myc-hSUN1 or pLEICS21 GFP-hSUN1 were subjected to IP with anti-c-myc and anti-GFP antibodies. Alternatively, lysates transiently transfected with pLEICS21 GFP-hSUN1 were processed using the GFP-Trap® method. Soluble, un-bound fractions and the final IP/GFP-Trap® sample were resolved by SDS-PAGE and immuno-blotted with anti-c-myc or anti-GFP antibodies. Molecular weights (kDa) are indicated.

Coomassie stain. The whole gel was sent to the University of Leicester PNACL proteomics facility where the boxed-band suspected of being hSUN1 at 100 kDa, indicated by a * in **Figure 3.7B**, **left panel,** was excised from the gel and trypsin digested ready for LC-MS/MS analysis. Data received from MS was analysed using MASCOT v2.2.04 software and identified the protein as α-actinin, which also has a molecular weight of 100 kDa.

A second elution from the same protein A-sepharose beads was re-run with samples from the other fractions and immuno-blotted for hSUN1. This revealed very low levels of hSUN1 in the IP, possibly because most of the protein still remained in the insoluble fraction (**Figure 3.7B, right panel**). It was clear that there was not enough soluble hSUN1 protein for IP and that other more abundant proteins were able to mask its presence.

To increase the expression level of the protein and therefore detection on a gel stained with Brilliant Blue colloidal stain, experiments were carried out to optimise IP of transiently expressed exogenous hSUN1. Plasmids pLEICS20 myc-hSUN1 and pLEICS21 GFP-hSUN1 were transiently transfected into one and two 10 cm plates asynchronously growing HeLa cells, respectively. Soluble, pre-cleared lysates were subjected to IP using 2 µg of anti-c-myc or anti-GFP antibodies. GFP-hSUN1 lysates were also processed via the GFP-Trap® protocol as a method comparison.

The myc-hSUN1 protein was highly expressed even in the soluble lysate fraction, so much so, that the IP fraction appeared to reach maximum binding capacity as the unbound fraction showed the same protein level as the IP sample (**Figure 3.7C, left**

panel). The GFP-hSUN1 blot showed that this protein was highly enriched in the IP sample (**Figure 3.7C, middle panel**). The GFP-Trap® method mirrored that of the GFP IP, but was even more efficient in extracting GFP-hSUN1 from the lysate (**Figure 3.7C, right panel**).

An additional factor to take into account in selecting an IP method is, not only the amount of starting material required for a large-scale IP, but also the time it takes to process such samples with minimal degradation occurring. The GFP-Trap® method is quicker than conventional IP and, because it does not use whole antibodies, but instead uses a 13 kDa GFP-binding fragment from a llama single chain antibody bound to a monovalent matrix to immunoprecipitate GFP-fused proteins (Rothbauer *et al.*, 2008), it does not exhibit a heavy chain which can often obscure other bands of a similar size on a protein gel.

The experimental design for the large-scale IP-MS hoped to encompass two objectives, the *in vivo* identification of hSUN1 phosphorylation sites but also identification of hSUN1 interacting partners (see **Chapter 4**). It was therefore important to avoid masking potential interacting partners on the gel. On the basis of these considerations and the results of the small-scale purification experiments, the following procedure was planned. HeLa cells would be transiently transfected with pEGFP C1 and pLEICS21 GFP-hSUN1, where the former would act as a negative control for non-specific binding interactions. These cells would be applied to the optimised mitotic synchronisation protocol followed by isolation of GFP-hSUN1 using the GFP-Trap® system. This was thought to be the best method to identify mitotic hSUN1 phosphorylation sites *in vivo*.

3.2.7 hSUN1 is phosphorylated *in vivo* at multiple sites within its nucleoplasmic N-terminal domain.

The large-scale IP for MS analysis of hSUN1 phosphorylation sites involved transiently transfecting 12 and 24 10 cm plates of asynchronously growing HeLa cells with pEGFP C1 and pLEICS21 GFP-hSUN1, respectively. Half of the cells transiently transfected with pLEICS21 GFP-hSUN1 were the asynchronous sample, and the other half were processed via the optimised mitotic synchronisation protocol outlined in **section 2.4.10**. Final GFP-Trap® samples were resolved by SDS-PAGE and bands were detected with Brilliant Blue colloidal stain (**Figure 3.8A**). The whole gel was submitted to the University of Leicester proteomics service where the indicated mitotic GFP-hSUN1 band and equivalent regions of the other lanes were excised and digested with trypsin or Asp-N. Two digestive enzymes were applied to increase the overall coverage of the protein for MS analysis. The bands cut from the GFP-hSUN1 asynchronous and mitotic lanes were confirmed as hSUN1, and was not present in the GFP asynchronous lane, as expected. Combined protein coverage of 84% was achieved, as can be seen in **Figure 3.8B**. Of the 18 serine and threonine residues not covered, 12 are located in the N-terminus and could also contain potential phosphorylation sites.

Phosphorylated peptides can sometimes be masked by equivalent non-phosphorylated peptides so steps were taken to phospho-enrich digested samples using metal immobilised metal affinity chromatography (IMAC). Digested peptides were incubated with an [Fe(III)] chelate matrix. The matrix provided high capacity affinity binding for peptides with phosphate groups i.e. phosphorylated peptides. Other non-phosphorylated peptides were discarded upon washing the bead matrix after which

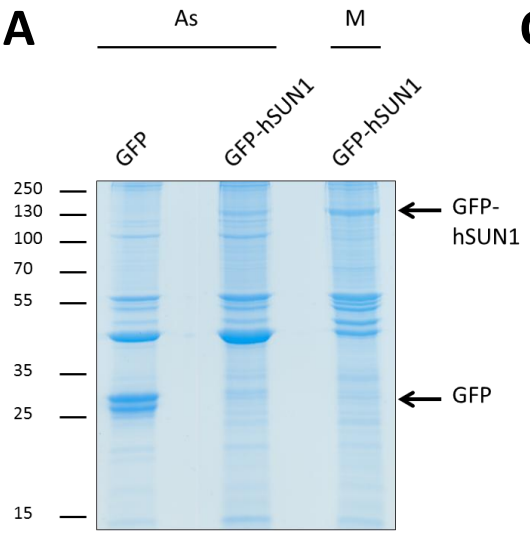

C

Peptide sequence	Phosphorylated residue
KLDPVFD[**pS**]PRM	S48
RRPPVLDE[**pS**]WIRE	S138
RHLDAHTAAHSQ[**pS**]PRL	S333

B **84% hSUN1 protein coverage with trypsin and Asp-N**

2 DFSRLHMYS PPQCVPENTG YTYALSSSYS SDALDFETEH KLDPVFD**S**PR
51 MSRRSLRLAT TACTLGDGEA VGADSGTSSA VSLKNRAART TKQRRSTNKS
101 AFSINHVSRQ VTSSGVSYGG TVSLQDAVTR RPPVLDE**S**WI REQTTVDHFW
151 GLDDDGDLKG GNKAAIQGNG DVGAAAATAH NGFSCSNCSM LSERKDVLTA
201 HPAAPGPVSR VYSRDRNQKC GASFYVNRIL WLARYTASSF SSFLVQLFQV
251 VLMKLSYESE NYKLKTHESK DCESESYKSK SHESKAHASY YGRMNVREVL
301 REDGHLSVNG EALCDDCKGK RHLDAHTAAH SQ**S**PRLPGRA GTLWHIWACA
351 GYFLLQILRR IGAVGQAVSR TAWSALWLAV VAPGKAASGV FWWLGIGWYQ
401 FVTLISWLNV FLLTRCLRNI CKFLVLLIPL FLLLAGLSLR GQGNFFSFLP
451 VLNWASMHRT QRVDDPQDVF KPTTSRLKQP LQGDSEAFPW HWMSGVEQQV
501 ASLSGQCHHH GENLRELTTL LQKLQARVDQ MEGGAAGPSA SVRDAVGQPP
551 RETDFMAFHQ EHEVRMSHLE DILGKLREKS EAIQKELEQT KQK**T**ISAVGE
601 QLLPTVEHLQ LELDQLKSEL SSWRHVKTGC ETVDAVQERV DVQVR**E**MVKL
651 LFSEDQQGGS LEQLLQRFSS QFVSKGDLQT MLRDLQLQIL RNVTHHVSVT
701 KQLPTSEAVV SAVSEAGASG ITEAQARAIV NSALKLYSQD K**T**GMVDFALE
751 SGGGSILSTR CSETYETK**T**A LMSLFGIPLW YFSQSPRVVI QPDIYPGNCW
801 AFKGSQGYLV VRLSMMIHPA AFTLEHIPKT LSPTGNISSA PKDFAVYGLE
851 NEYQEEGQLL GQFTYDQDGE SLQMFQALKR PDDTAFQIVE LRIFSNWGHP
901 EYTCLYRFRV HGEPVK

Figure 3.8. hSUN1 is phosphorylated *in vivo* at three main sites in the N-terminus.

(A) Cultured asynchronous (As) HeLa cells were transiently transfected on a large-scale with either pEGFP C1 or pLEICS21 GFP-hSUN1. Half of the cells expressing hSUN1-GFP were asynchronous, the other half were mitotically arrested (M). Soluble lysates were processed using the GFP-Trap® method and the final GFP-Trap® samples were resolved by SDS-PAGE. The suspected GFP-hSUN1 bands from the asynchronous and mitotic lane were excised from the gel as well as the corresponding region of the negative control GFP lane. Molecular weights (kDa) are indicated. Samples were trypsin or Asp-N digested, phospho-peptide enriched using IMAC and then analysed by LC-MS/MS. **(B)** hSUN1 protein sequence showing in blue the 84% protein coverage achieved for MS analysis by combined tryspin and Asp-N generated peptides. Identified phosphorylation sites are highlighted in red and the transmembrane domain is underlined. **(C)** Derived MS data was analysed using Mascot v2.2.04 software. Data are summarised as a list of the three phosphorylated peptides found in mitotic samples only and the specified phosphorylated residues.

phosphorylated peptides were eluted in the presence of 400 mM ammonium hydroxide. These samples were analysed by LC-MS/MS and three peptides were identified as being phosphorylated in the mitotic sample: S48, S138 and S333 (**Figure 3.8C**). No phosphorylated peptides were retrieved from the GFP or GFP-hSUN1 asynchronous phospho-enriched samples. Evidence for the determination of a single phosphorylation site in each of the three phosphorylated peptides derived from phospho-peptide enriched mitotic GFP-hSUN1 is discussed below.

The process of LC-MS/MS or tandem MS consists of initially separating digested peptides by high pressure liquid chromatography (HPLC), followed by three key stages. Firstly, the sample is ionised to cations by removal of an electron, secondly, the ions are sorted according to their mass-to-charge ratio (m/z) and finally, separated ions are measured according to abundance to form a mass spectra. For tandem MS, samples are further fragmented and compared to established protein databases for protein identification (Wysocki *et al.*, 2005).

For the peptide LDPVFDSPR, the serine corresponding to S48 of hSUN1, was established as the phosphorylated residue. The amino acids and their position in this peptide were determined through subtraction of the m/z ratios of ions peptide fragments against each other as each amino acid has a unique mass (Da) (Wysocki *et al.*, 2005). **Figure 3.9A** shows the fragmentation table with m/z ratios of y and b ions for the given peptide sequence aligned vertically in the centre. Y ions represent cleavage of CO-NH bonds at the C-terminus of the amino acid while the b ions represent cleavage at the N-terminus (**Figure 3.9B**). +2H, -NH3 and -H20 are modifications of the y and b ions. All masses were theoretically calculated and LC-

A

B	B ions	B +2H	B -NH3	B +H20	AA	Y ions	Y+2H	Y -NH3	Y +H20	Y
1	114.1				L	1125.5	563.3	1108.5	1107.5	9
2	229.1			211.1	D	1012.4	506.7	995.4	994.4	8
3	326.2			308.2	P	897.4	449.2	880.4	879.4	7
4	425.2			407.2	V	800.3	400.7	783.3	782.3	6
5	572.3			554.3	F	701.3		684.2	683.3	5
6	687.3	344.2		669.3	D	554.2		537.2	536.2	4
7	854.3	427.7		836.3	S+80	439.2		422.1	421.2	3
8	951.4	476.2		933.4	P	272.2		255.1		2
9	1125.5	563.3	1108.5	1107.5	R	175.1		158.1		1

B

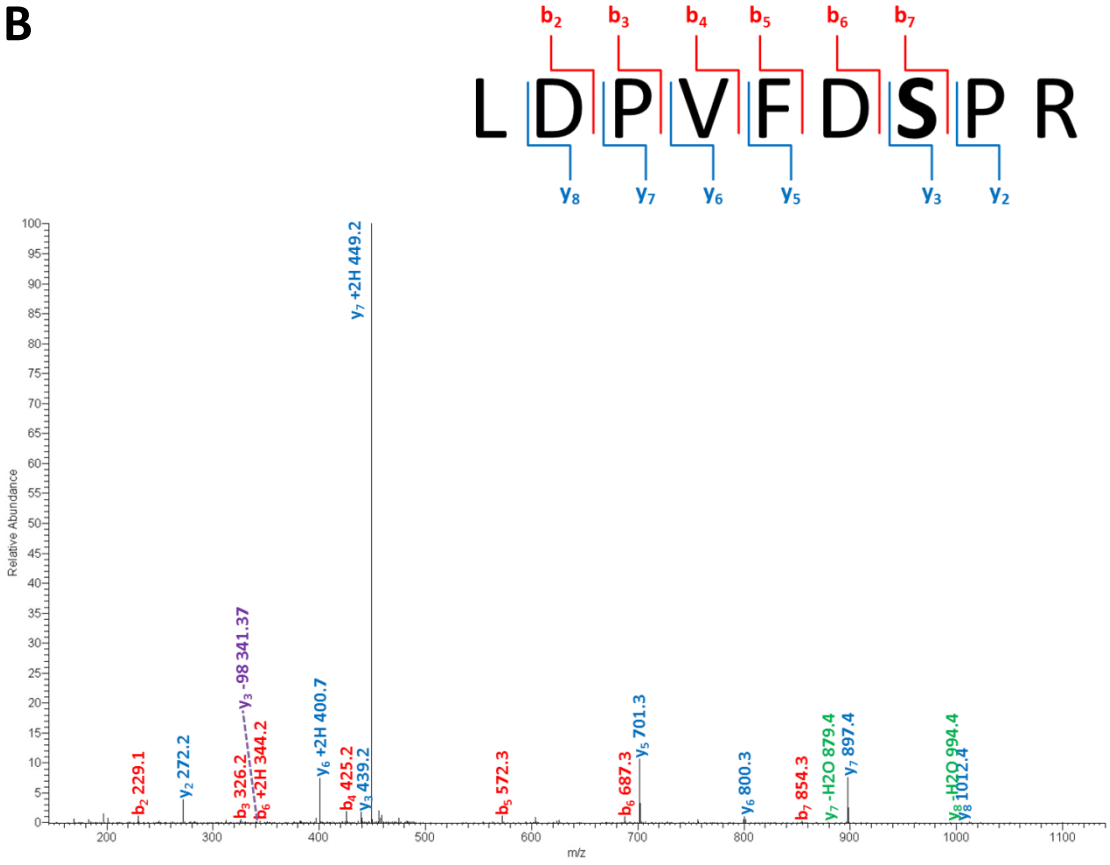

Figure 3.9. IP-MS evidence for phosphorylation on S48.

(A) Mass-to-charge ratio (m/z) of y and b ions in the peptide sequence LDPVFDSPR shown aligned vertically in the centre. Y ions represent cleavage of CO-NH bond at the C-terminus and read right to left whereas b ions represent cleavage of the same bond at the N-terminus and read left to right. All masses have been calculated, values highlighted in red (b ions), blue (y ions) and green (modified ions) are confirmed masses. The serine is annotated at S+80 due to addition of a cation phosphate mass 79+1. **(B)** Peptide sequence LDPVFDSPR labelled with confirmed y and b ions signifying cleavage of CO-NH binds at C and N termini, respectively. Amino acids and order of peptide were determined through m/z subtraction of ions peptide fragments against each other as each amino acid has a specific mass (Da). The mass spectrum shows the m/z of each fragmented ion and their relative abundance where the most abundant ion is set at 100. Confirmed y, b and modified ion peaks stated in the fragmentation table have been labelled. Peaks labelled y_3-98 signify loss of a H_3PO_4 group which in turn indicates loss of a phosphate group from that particular ion fragment.

MS/MS analysis experimentally confirmed those masses. S48 (S+80 in **Figure 3.9A**) was the only residue capable of phosphorylation in this peptide. The +80 refers to the molecular weight of the added phosphate group and the estimated m/z values for this residue were confirmed in both y and b ions (**Figure 3.9A**).

The mass spectrum shows the m/z ratio of each fragmented ion and their relative abundance where the most abundant ion was set at 100 (**Figure 3.9B**). LC-MS/MS experimentally confirmed y, b and modified m/z ratios stated in the fragmentation table have been labelled on the mass spectrum (**Figure 3.9B**). Fragmentation of y_3 and b_7 ions confirmed that the serine at that position was phosphorylated. Phosphate groups are known to disassociate from the residue but can be located in the spectrum denoted as -98, which is a loss of H_3PO_4. Y_3-98 can be seen in **Figure 3.9B** indicating S48 was phosphorylation in this fragmented ion peptide.

The second peptide showing evidence of a phosphorylated site was RPPVLDESWIR. The amino acids and their sequence in this peptide were again confirmed by subtraction of fragmented ions against each other and were shown to contain a single phosphorylation site. The S+80 annotation of fragmented y_4 and b_8 ions for the serine residue, which again was the only potential phosphorylation site in the peptide, together with the data in the mass spectrum showing $y_{4,\ 5,\ 6,\ 7,\ 8,\ 9,\ 10}$-98 and $b_{8,\ 9,\ 10}$-98, signified phosphorylation of the serine residue in this peptide (**Figure 3.10A** and **Figure 3.10B**). The amino acid was equivalent to position 138 in the hSUN1 sequence.

Unlike the previous peptide sequences, the third peptide, HLDAHTAHHSQSPR, contained multiple potential phosphorylation sites. Data from **Figure 3.11A** revealed

A

B	B ions	B +2H	B -NH3	B +H20	AA	Y ions	Y+2H	Y -NH3	Y +H20	Y
1	157.1	79.1	140.1		R	1447.7	724.4	1430.7	1429.7	11
2	254.2	127.6	237.1		P	1291.6	646.3	1274.6	1273.6	10
3	351.2	176.1	334.2		P	1194.6	597.8	1177.5	1176.5	9
4	450.3	225.6	433.3		V	1097.5	549.3	1080.5	1079.5	8
5	563.4	282.2	546.3		L	998.4	499.7	981.4	980.4	7
6	678.4	339.7	661.4	660.4	D	885.4	443.2	868.3	867.3	6
7	807.4	404.2	790.4	789.4	E	770.3		753.3	752.3	5
8	974.4	487.7	957.4	956.4	S+80	641.3		624.3	623.3	4
9	1160.5	580.8	1143.5	1142.5	W	474.3		457.3		3
10	1273.6	637.3	1256.6	1255.6	I	288.2		271.2		2
11	1447.7	724.4	1430.7	1429.7	R	175.1		158.1		1

B

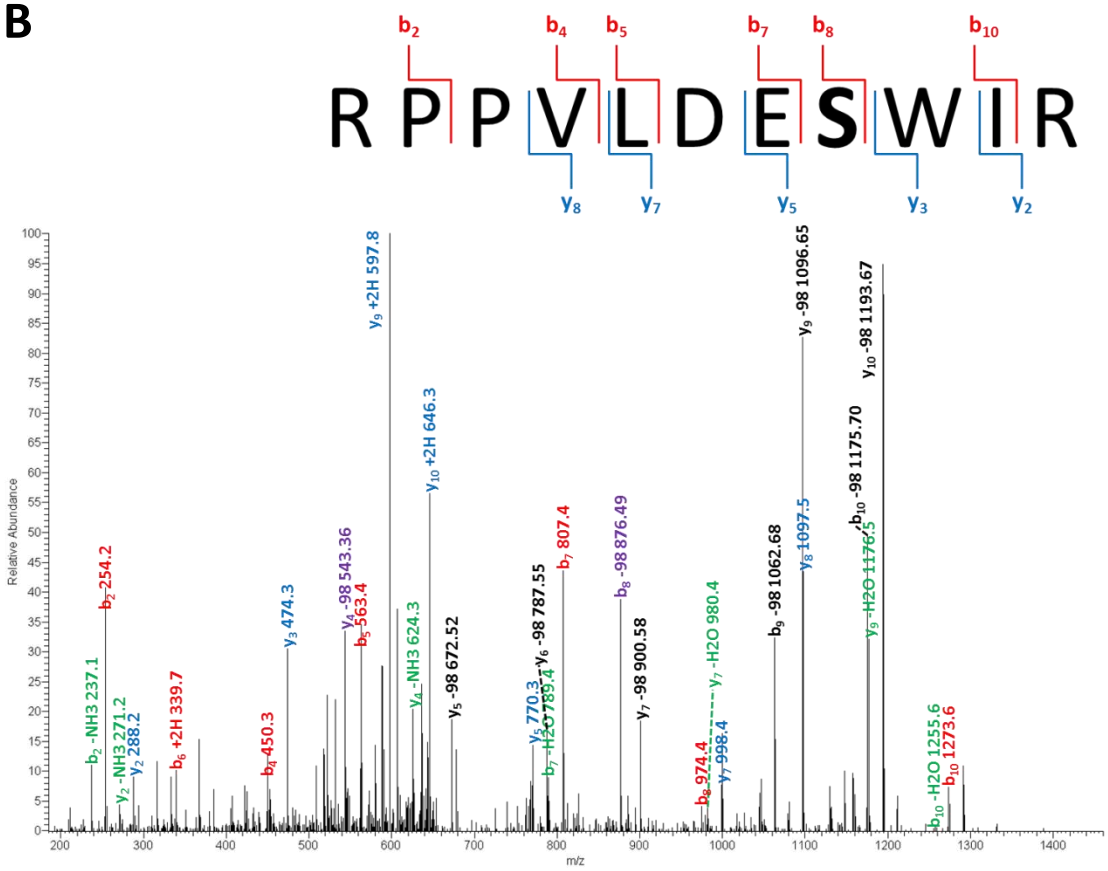

Figure 3.10. IP-MS evidence for phosphorylation on S138.

(A) Mass-to-charge ratio (m/z) of y and b ions in the peptide sequence RPPVLDESWIR shown aligned vertically in the centre. Y ions represent cleavage of CO-NH bond at the C-terminus and read right to left whereas b ions represent cleavage of the same bond at the N-terminus and read left to right. All masses have been calculated, values highlighted in red (b ions), blue (y ions) and green (modified ions) are confirmed masses. The serine is annotated at S+80 due to addition of a cation phosphate mass 79+1. **(B)** Peptide sequence RPPVLDESWIR labelled with confirmed y and b ions signifying cleavage of CO-NH binds at C and N termini, respectively. Amino acids and order of peptide were determined through m/z subtraction of ions peptide fragments against each other as each amino acid has a specific mass (Da). The mass spectrum shows the m/z of each fragmented ion and their relative abundance where the most abundant ion is set at 100. Confirmed y, b and modified ion peaks stated in the fragmentation table have been labelled. Peaks labelled $y_{4,\ 5,\ 6,\ 7,\ 8,\ 9,\ 10}$-98 and $b_{8,\ 9,\ 10}$-98 signify loss of a H_3PO_4 group which in turn indicates loss of a phosphate group from that particular ion fragment.

A

B	B ions	B +2H	B -NH3	B +H20	AA	Y ions	Y +2H	Y -NH3	Y +H20	Y
1	138.1	69.5			H	1607.7	804.4	1590.7	1589.7	14
2	251.2	126.1			L	1470.6	735.8	1453.6	1452.6	13
3	366.2	183.6		348.2	D	1357.6	697.3	1340.5	1339.6	12
4	437.2	219.1		419.2	A	1242.5	621.8	1225.5	1224.5	11
5	574.3	287.6		556.3	H	1171.5	586.3	1154.5	1153.5	10
6	675.3	338.2		657.3	T	1034.4	517.7	1017.4	1016.4	9
7	746.4	373.7		728.3	A	933.4	467.2	916.4	915.4	8
8	817.4	409.2		799.4	A	862.4	431.7	845.3	844.3	7
9	954.5	477.7		936.4	H	791.3	396.2	774.3	773.3	6
10	1041.5	521.1		1023.5	S	654.3		637.2	636.3	5
11	1169.5	585.3	1152.5	1151.5	Q	567.2		550.2	549.2	4
12	1336.5	668.8	1319.5	1318.5	S+80	439.2		422.1	421.2	3
13	1433.6	717.3	1416.6	1415.6	P	272.2		255.1		2
14	1607.7	804.4	1590.7	1589.7	R	175.1		158.1		1

B

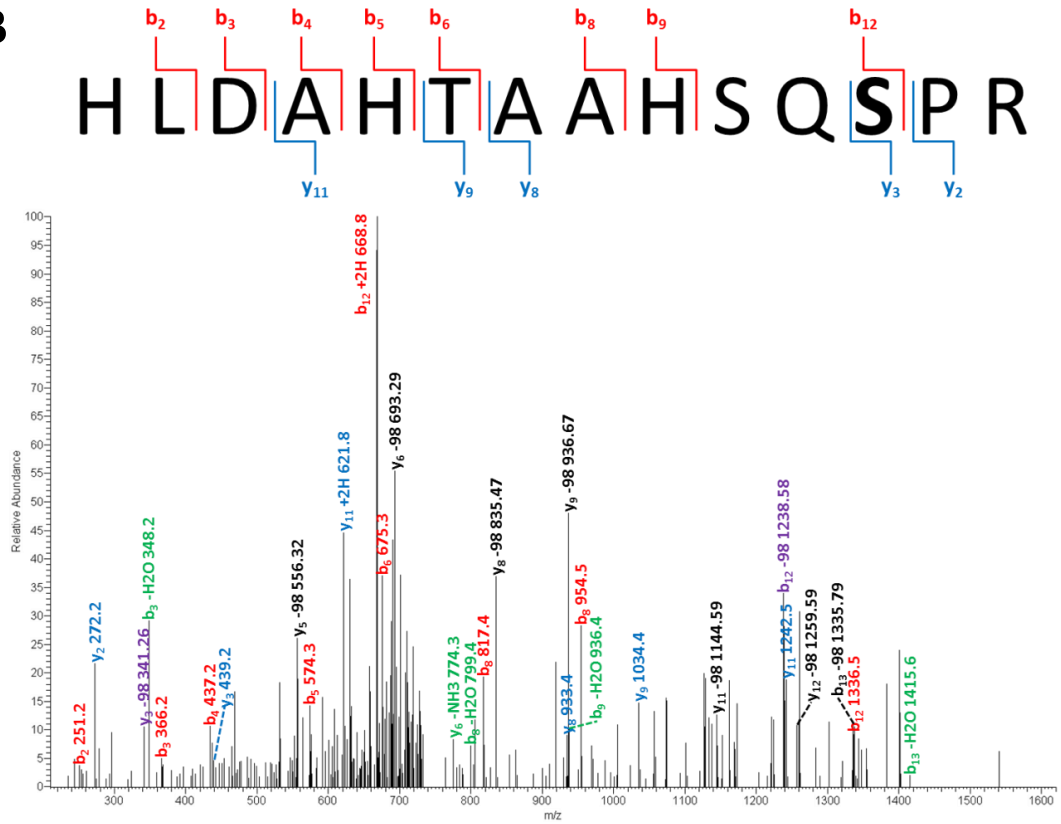

Figure 3.11. IP-MS evidence for phosphorylation on S333.

(A) Mass-to-charge ratio (m/z) of y and b ions in the peptide sequence HLDAHTAAHSQSPR shown aligned vertically in the centre. Y ions represent cleavage of CO-NH bond at the C-terminus and read right to left whereas b ions represent cleavage of the same bond at the N-terminus and read left to right. All masses have been calculated, values highlighted in red (b ions), blue (y ions) and green (modified ions) are confirmed masses. The serine is annotated at S+80 due to addition of a cation phosphate mass 79+1. **(B)** Peptide sequence HLDAHTAAHSQSPR labelled with confirmed y and b ions signifying cleavage of CO-NH binds at C and N termini, respectively. Amino acids and order of peptide were determined through m/z subtraction of ions peptide fragments against each other as each amino acid has a specific mass (Da). The mass spectrum shows the m/z of each fragmented ion and their relative abundance where the most abundant ion is set at 100. Confirmed y, b and modified ion peaks stated in the fragmentation table have been labelled. Peaks labelled $y_{3, 5, 6, 8, 9, 11, 12}$-98 and $b_{12, 13}$-98 signify loss of a H_3PO_4 group which in turn indicates loss of a phosphate group from that particular ion fragment.

that from the single threonine and two serine residues that were been capable of being phosphorylated, only one was annotated with the label S+80 implying that this peptide was not multi-phosphorylated. From the peptide sequence showing the confirmed fragmented ions shown in **Figure 3.11B**, the following peaks were produced in the mass spectrum: $y_{3, 5, 6, 8, 9, 11, 12}$-98 and $b_{12, 13}$-98. These peaks showed that within those fragments there was a phosphorylated serine or threonine but only the fragmented peptide from b_{12} produced a peak designated b_{12}-98 (**Figure 3.11B**). This peptide contained only one of the three possible phosphorylation sites, this residue is S333 in the hSUN1 sequence.

The presence of S48 and S138 confirmed the predictions made in the UniProtKB proteomic database and data from Olsen *et al.* (2006) and Dephoure *et al.* (2008). Unfortunately the S52 predicted phosphorylation site was not confirmed due to insufficient protein coverage.

Multiple species sequence alignment of S48, S138 and S333 revealed that both S48 and S138 were situated in highly conserved regions, whereas S333 was the only serine of all the species aligned that had a proline at the +1 position (**Figure 3.12A**) possibly suggesting S333 is a phosphorylation site specific to the human form of SUN1.

The CDK1 full consensus sequence is [pS/pT]-P-X-[K/R] where p refers to the phosphorylated serine or threonine and X represents any amino acid (Holt *et al.*, 2009). As a minimal sequence of [pS/pT]-P is also sufficient, the proline at the +1 site is a strong preference in the CDK1 consensus sequence (Holt *et al.*, 2009). Both the S48 and S333 residues fit the minimal consensus sequence (**Figure 3.12**).

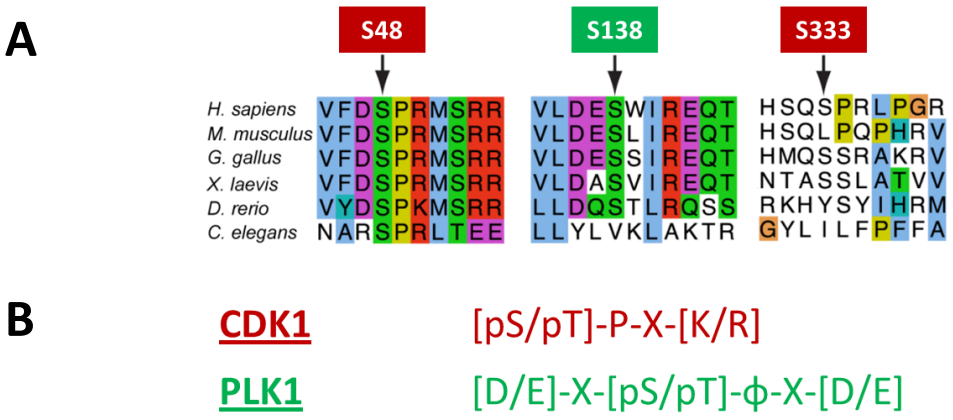

Figure 3.12. Conservation of identified phosphorylation sites and the surrounding sequence.

(A) Sequence alignment of SUN1 (and UNC-84 from *C.elegans*) across six species highlighting the sequence surrounding residues S48, S138 and S333. **(B)** Consensus sequences for CDK1 and PLK1 where p refers to the phosphorylated residue, X can be any amino acid and ϕ denotes a hydrophobic residue.

The full PLK1 consensus sequence is [D/E]-X-[pS/pT]-ϕ-X-[D/E] (**Figure 3.8D**) where ϕ denotes a hydrophobic residue is required for PLK1 phosphorylation but the minimum sequence contains only [D/E]-X-[pS/pT]-ϕ (Nakajima *et al.*, 2003). S138 fits the PLK1 consensus sequence (**Figure 3.12**) and confirms suggestions made by Dephoure *et al.* (2008) linking the hSUN1 S138 site to PLK1 phosphorylation.

3.2.8 *In vitro* identification of three mitotic kinases phosphorylating hSUN1 residues at its N-terminus

Having identified three hSUN1 phosphorylation sites *in vivo*, subsequent experiments were designed to identify the kinases responsible for phosphorylation of each site. CDK1, PLK1 and Aurora A are mitotic kinases required for mitotic entry and progression through to the SAC. Of the three sites identified, two appear to be CDK1 sites while the other resembles a PLK1 site. As mentioned previously, residue S52 was another potential phosphorylation site predicted by the UniProtKB proteomic database, but this was not found *in vivo*. The sequence surrounding S52 is SPRM[S*]RRS, where [S*] represent the potential S52 phosphorylation site. The site appears to fit loosely into an Aurora A kinase consensus sequence [R/K/N]-R-X-[pS/T]-ϕ(not P) and therefore Aurora A was tested as a candidate mitotic kinase. These three mitotic kinases were chosen to be used in *in vitro* kinase assays, to confirm the phosphorylation sites identified *in vivo* and to determine which kinase(s) were responsible for phosphorylation of each of the three sites.

Bacterially expressed MBP-tagged hSUN1 deletion constructs 1-217, 1-362 and 456-916 were used as substrates for the *in vitro* kinase assay, where MBP protein alone acted as a negative control. Truncated hSUN1 fragments were used as full-length MBP-

hSUN1 was toxic to bacterial growth. Constructs 1-217 and 1-362 encompass the N-terminus, which contains the lamin A/C binding site and, for the latter construct, the emerin and nesprin binding sites (**Figure 3.13A**). The 456-916 construct represents the lumenal C-terminus and contains the two coiled-coil domains along with the SUN-domain (**Figure 3.13A**). There is a stretch of 94 amino acids (363-455) that are not covered by these fragments, which harbours the hydrophobic regions and transmembrane domain (**Figure 3.13A**) (Haque *et al.*, 2006). This region is unlikely to contain phosphorylation sites.

Culture volumes were adjusted for each deletion construct to allow equivalent protein expression. It is important to note that MBP hSUN1 1-362 expression was poor and, to achieve equivalent protein expression with the other constructs, a significantly larger culture volume was used for bacteria expression. MBP and MBP-hSUN1 deletion constructs were purified from bacterial lysates by binding to amylose resin. They were then incubated in a kinase buffer containing ATP, as was casein which was used as a positive control. This was supplemented with 100 ng of purified CDK1, PLK1 or Aurora A and 1 µCi of [^{32}P]-γ-ATP and samples were incubated at 30^{o}C for 30 min. SDS-PAGE and Coomassie staining of the gels showed relative protein expression. Dried gels were analysed by autoradiography and bands were then excised, placed in scintillation fluid and levels of radioactivity were measured using a scintillation counter. The lower panels of **Figure 3.13B** show the casein and MBP fusion protein expression on Coomassie gels for samples treated with CDK1, PLK1 or Aurora A.

The extent of phosphorylation by each kinase was measured from scintillation counts for each MBP fusion protein relevant to the casein positive control and normalised

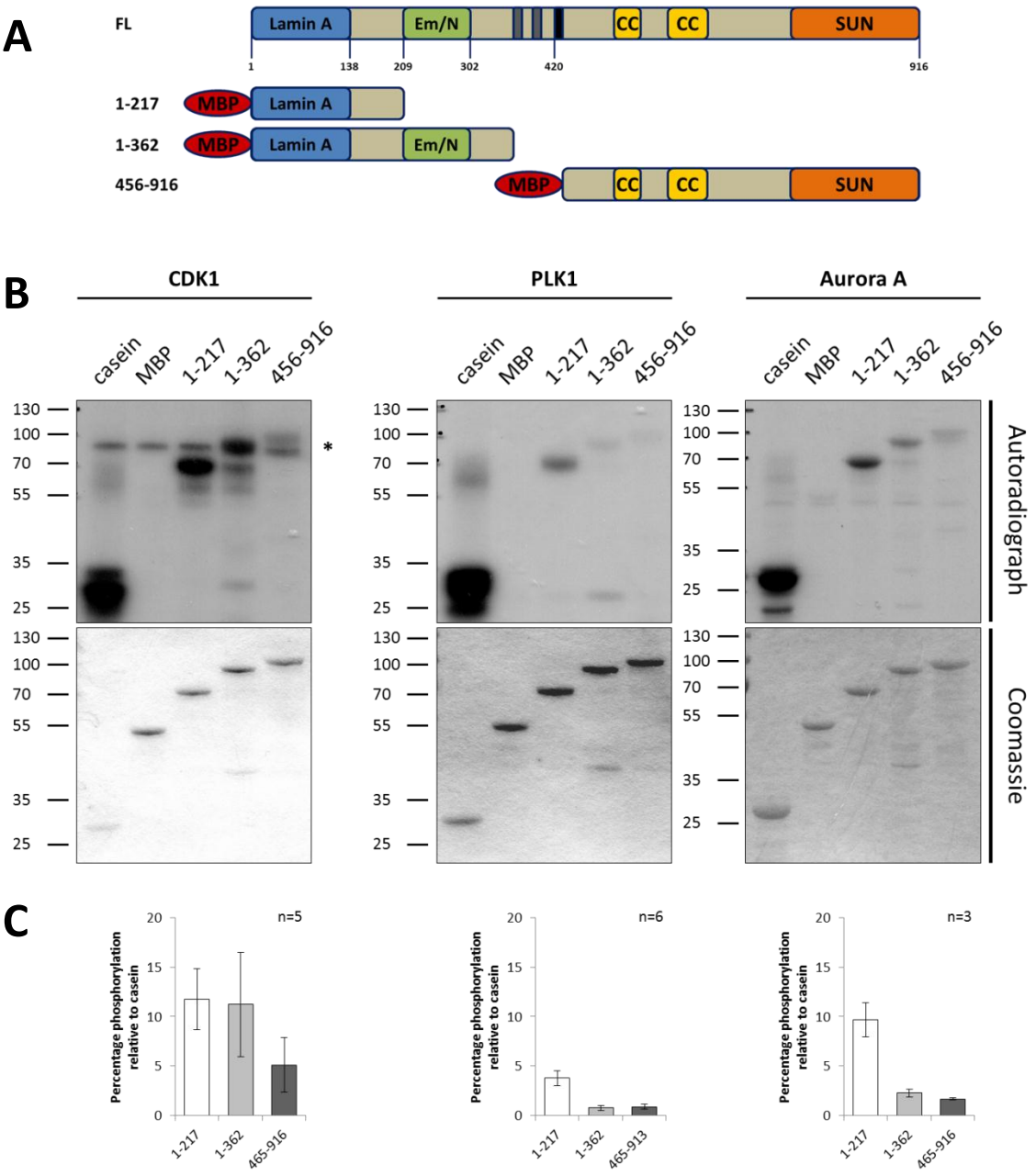

Figure 3.13. hSUN1 is phosphorylated by CDK1, PLK1 and Aurora A *in vitro* at the N-terminus.

(A) Schematic representation of MBP-tagged hSUN1 deletion constructs used in *in vitro* kinase assays. **(B)** *In vitro* kinase assay where MBP-tagged hSUN1 deletion constructs bound to amylose resin were incubated at 30°C for 30 min in kinase buffer containing 100 ng of purified CDK1, PLK1 or Aurora A kinase and supplemented with [^{32}P]-γ-ATP. Casein and MBP were used as positive and negative controls respectively. Molecular weights (kDa) are indicated. * denotes CDK1 auto-phosphorylation. Samples were resolved by SDS-PAGE, Coomassie stained and the dried gels were analysed by autoradiography. **(C)** Percentage phosphorylation of each MBP fusion protein was calculated relative to casein from scintillation counts after background subtraction and normalisation of total protein. Data represented as histograms for each mitotic kinase.

against total protein level (**Figure 3.13B**). MBP-hSUN1 1-217 appeared to have incorporated the [^{32}P]-methionine radiolabel for each of the three kinases tested suggesting that phosphorylation sites for all three kinases may be present within this domain. However, hSUN1 1-362 phosphorylation by PLK1 and Aurora A was much weaker than that of hSUN1 1-217 (**Figure 3.13B** and **Figure 3.13C**). This is surprising as the 1-362 construct overlaps the same region as 1-217 and so would be expected to be phosphorylated to the same extent or even more strongly, due to its additional 145 amino acids, including S333. A possible explanation relates back to the earlier point of MBP-hSUN1 1-362 protein expression not being as efficient as the other fusion proteins. This fragment seems to be unstable and possibly the truncation is disrupting the overall protein structure. The abberant folding of this protein may be hindering access of kinases to phosphorylate sites. There appears to be very little or no incorporation of the radiolabel in the 456-916 fragment, as expected, since the C-terminus resides in the PNS where it is inaccessible to mitotic kinases (**Figure 3.13B** and **Figure 3.13C**). These findings suggest that *in vitro*, CDK1, PLK1, and Aurora A are able to phosphorylate hSUN1 at its N-terminus.

3.2.9 *In vitro* confirmation of hSUN1 phosphorylation sites and the responsible kinases

Cross-referencing of the consensus sequences of CDK1, PLK1 and Aurora A with the *in vivo* phosphorylation sites previously indicated that there were two potential CDK1 sites and one PLK1 and Aurora A site. To establish whether CDK1, PLK1 and Aurora A phosphorylate these sites on hSUN1, the same *in vitro* methods were applied where MBP-tagged hSUN1 deletion fragments 1-217, 1-362 and 456-916 were bacterially

expressed and immobilised on amylose resin. They were then incubated in kinase buffer containing ATP and 100 ng of purified CDK1, PLK1 or Aurora A, but lacking the [^{32}P]-methionine radio-label. To ensure sufficient phosphorylation of the residues by the kinases, the sample incubation time at 30^{o}C was extended to 4 h. Proteins were resolved by SDS-PAGE and detected using Brilliant Blue colloidal stain (**Figure 3.14A**). The gel was sent to the University of Leicester PNACL proteomics facility where the bands indicated by an asterisk in **Figure 3.14A** were excised from the gel and trypsin digested ready for LC-MS/MS analysis. Data received from MS was analysed using MASCOT v2.2.04 and the phospho-peptides for each kinase and each deletion fragment are outlined in **Figure 3.14B**.

Analysis of CDK1-phosphorylated peptides revealed several phosphorylation sites, most of which appeared to be non-specific as they were not found in the *in vivo* analysis and did not correlate to the CDK1 consensus sequence. Importantly, residues S48 and S333 were phosphorylated on peptides derived from 1-217 and/or 1-362 fragments. **Figure 3.13** previously showed that phosphorylation was concentrated at the N-terminus. Analysis of MS data for the 456-916 C-terminal fragment revealed ten CDK1 phosphorylation sites. As this portion of the protein normally resides within the PNS, these sites most likely represent non-specific phosphorylation.

S138 was confirmed as a PLK1 phosphorylation site as phosphorylated peptides were recovered from both 1-217 and 1-362 fragments. T144 and T145 were also phosphorylated and fit the minimal PLK1 consequence. MASCOT was unable to distinguish which of the two threonine residues was phosphorylated due to their close proximity to each other. However, as they were not seen *in vivo*, these sites may not

A

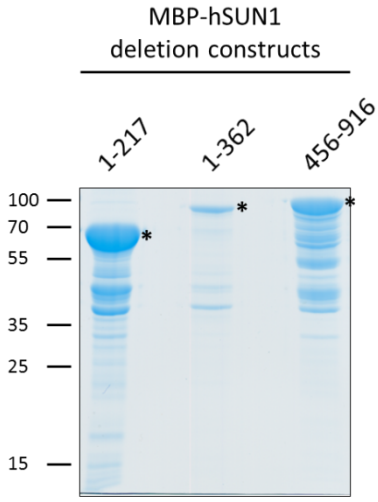

B

Mitotic kinase	Protein coverage	MBP-hSUN1 construct	Peptide sequence	Phosphorylated residue
CDK1	84%	1-217	KLDPVFD[**pS**]PRM	S48
			RLHMYSPPQCVPENTGYTYALSSSYSSD ALDFETEHKLDPVFD[**pS**]PRM	S48
			RLATTACTLGDGEAVGAD[**pS**]G[**pT**] [**pS**][**pS**]AV[**pS**]LKN	S75, T77, S78, S79, S82
		1-362	KLDPVFD[**pS**]PRM	S48
			RLATTACTLGDGEAVGAD[**pS**]G[**pT**] [**pS**][**pS**]AV[**pS**]LKN	S75, T77, S78, S79, S82
			RHLDAH[**pT**]AAH[**pS**]Q[**pS**]PRL	T327, S331, S333
		456-916	RVDDPQDVFKP[**pT**][**pT**][**pS**]RL	T473, T474, S475
			RNVTHHV[**pS**]V[**pT**]KQ	S698, T700
			K[**pT**]GMVDFALE[**pS**]GGG[**pS**]IL[**pS**] [**pT**]RC	T742, S751, S755, S758, T759
			K[**pT**]L[**pS**]P[**pT**]GNI[**pS**]SAPKD	T830 , S832, T834, S838
PLK1	74%	1-217	RRPPVLDE[**pS**]WIRE	S138
			REQ[**pT**][**pT**]VDHFWGLDDDGDLKG	T144, T145
		1-362	RRPPVLDE[**pS**]WIRE	S138
			REQ[**pT**][**pT**]VDHFWGLDDDGDLKG	T144, T145
		456-916	RVDQMEGGAAGP[**pS**]A[**pS**]VRD	S539, S541
			KL[**pY**][**pS**]QDK[**pT**]GMVDFALESGGGS ILSTRC	Y737, S738, T742
			KTL[**pS**]P[**pT**]GNI[**pS**][**pS**]APKD	S832, T834, S838, S839
Aurora A	88%	1-217	**NO PHOSPHORYLATED PEPTIDES DETECTED**	
		1-362	KSAF[**pS**]INHVSRQ	S103
			KCGA[**pS**]F[**pY**]VNRI	S223, Y225
			REVLREDGHL[**pS**]VNGEALCDDCKG	S307
		456-916	RNVTHHV[**pS**]V[**pT**]KQ	S698, T700
			K[**pT**]L[**pS**]P[**pT**]GNI[**pS**][**pS**]APKD	T830, S832, T834, S838, S839

Figure 3.14. *In vitro* confirmation of phophorylation sites.

(A) *In vitro* kinase assay where MBP-tagged hSUN1 deletion constructs bound to amylose resin were incubated at 30°C for 4 h in kinase buffer containing 100 ng of purified CDK1, PLK1 or Aurora A kinase. Samples were resolved by SDS-PAGE and Coomassie stained. Bands marked * were excised from the gel, trypsin and Asp-N digested and then LC-MS/MS analysed. Molecular weights (kDa) are indicated. **(B)** Derived MS data were analysed using Mascot v2.2.04 software. Data are summarised as a list of phosphorylated peptides obtained for each mitotic kinase. Protein coverage is based on the total protein taking into account 10% of the protein not included (residues 363-455). N.B Where there is more than one phosphorylation site highlighted in the sequence, multi copies of the peptide were retrieved, each with a single phosphorylation site. For sequence REQ[pT][pT]VDHFWGLDDDGDLKG, MASCOT was unable to distinguish a single phosphorylation site.

be genuine and therefore were disregarded. Like CDK1, PLK1 phosphorylated several sites in the C-terminal fragment of hSUN1 which were again likely to be due to non-specific phosphorylation. This is supported by the fact that there was also one phosphorylated tyrosine, which is surprising as PLK1 is a serine/threonine kinase.

No Aurora A phosphorylated residues were detected in the 1-217 fragment which was strange as S103 was phosphorylated in the 1-362 hSUN1 fragment. Of the four phosphorylated sites, none met the criteria of the consensus site and one was a tyrosine residue. Moreover, there were no phosphorylation sites for Aurora A identified in the MS analysis but [^{32}P]-methionine was incorporated into the N-terminal fusion proteins (**Figure 3.13B**). Presumably the phosphorylation site is within the 16% of non-covered sequence. Previous coverage of hSUN1 with trypsin alone failed to produce peptides containing the S52 residue which, according to the UniProtKB database, is a potential phosphorylation site. Unfortunately despite the increase in protein coverage, this particular residue was still not retrieved.

In summary, these experiments show that hSUN1 is phosphorylated at the N-terminus both *in vitro* and *in vivo* at S48, S138 and S333. Furthermore, the *in vitro* data indicated that CDK1 is responsible for phosphorylation of S48 and S333 whilst PLK1 phosphorylates S138. An Aurora A site may lie within the sequence not covered in the MS analysis.

3.2.10 SUN1 is phosphorylated *in vivo* by the mitotic kinases CDK1 and PLK1

To confirm that CDK1 and PLK1 contribute to mitotic hSUN1 phosphorylation *in vivo*, specific kinase inhibitors were used and their ability to prevent the mitotic hSUN1

band-shift was assessed. Mitotically arrested HeLa cells were treated with inhibitors of CDK1 (Roscovitine), PLK1 (BI 2536), Aurora A (MLN 8054) and MEK (UO126) 4 h prior to harvesting. The latter inhibitor was used as a negative control. MG132, a proteasome inhibitor, was also added simultaneously to prevent protein degradation and exit from mitosis. Samples were resolved by SDS-PAGE and immuno-blotted with anti-hSUN1 Atlas, anti-cyclin B1 and anti-β-actin antibodies.

Mitotic cells treated with roscovitine showed a significant reduction in the band-shift compared to the untreated sample (**Figure 3.15**), indicating that CDK1 does phosphorylate SUN1 *in vivo* and contributes to the mitotic hSUN1 band-shift. Treatment with BI2536 reduced the mobility shift, although to a lesser extent than observed with roscovitine. Thus, PLK1 also contributes to hSUN1 phosphorylation in mitosis. Both drugs in combination showed a greater overall loss of the band-shift but the hSUN1 band did not return to the asynchronous state suggesting that other mitotic kinases are involved or that other post-translational modifications are occurring. In contrast, the Aurora A inhibitor appeared to have no effect on the band-shift, supporting findings for the lack of Aurora A phosphorylation sites identified by MS. The MEK inhibitor, used in a negative control capacity, also did not induce a loss of the band-shift. Blotting for cyclin B1 confirmed that the samples were still in mitosis.

To conclude, CDK1 and PLK1 play a role in hSUN1 mitotic phosphorylation but are not the sole cause for the band-shift in mitotic samples.

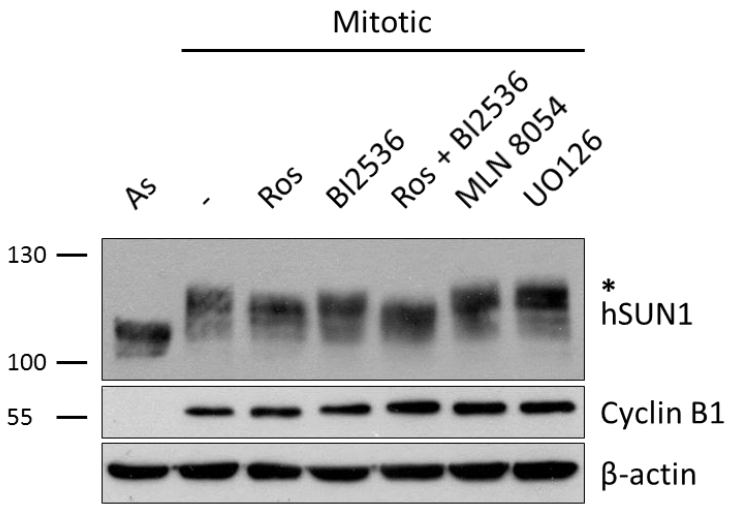

Figure 3.15. CDK1 and PLK1 contribute to the hSUN1 mobility shift in mitosis.

HeLa cells growing asynchronously (As) were mitotically arrested and treated with MG132 (10 µM) and kinase inhibitors Roscovitine (Ros) (100 µM), BI2536 (100 nM), MLN 8054 (1 µM) or UO126 (10 µM), as indicated, 4 h prior to harvesting. Samples were collected by cell-scraping (As) or by mechanical shake-off, soluble lysates resolved by SDS-PAGE and immuno-blotted with anti-hSUN1 Atlas, anti-cyclin B1 and anti-β-actin antibodies. * represents the mobility shift seen for hSUN1. Molecular weights (kDa) are indicated.

3.2.12 Phospho-deficient mutants expression and localisation to the NE

To investigate the importance of S48, S138 and S333 residues in hSUN1 mitotic phosphorylation, phospho-deficient myc-tagged mutants were made (**Figure 3.16**). Serine residues were mutated to alanine to generate phospho-deficient mutants incapable of phosphorylation. Three single phospho-deficient mutants, each corresponding to one of the three identified mitotic sites, were made as well as a double phospho-deficient mutant (2A) targeting the two CDK1 (S48 and S333) sites and a triple phospho-deficient mutant (3A) encompassing all three sites (**Figure 3.16**).

Expression of phospho-deficient mutants was assessed by transiently transfecting 1 µg of each pLEICS20 myc-hSUN1 mutant into asynchronously growing HeLa cells and analysing total cell extracts by western blot (**Figure 3.17A**). Immuno-blotting with anti-c-myc and anti-β-actin antibodies revealed that all the mutants were expressed at equivalent levels to wild-type hSUN1 (**Figure 3.17A**).

Indirect immunofluorescence microscopy was also performed. Cells were co-stained with anti-c-myc, anti-lamin A/C antibodies (as a marker of the NE) and DAPI to stain the DNA. The phospho-deficient mutants all localised to the NE, as expected since these mutants should behave like the wild-type protein in interphase cells, as phosphorylation only occurs during mitosis.

To assess how much of the mitotic hSUN1 band-shift could be attributed to each phosphorylation site, the electrophoretic mobility of the phospho-deficient mutants in mitotic lysates was observed. HeLa cells were transiently transfected with single, double (2A) and triple (3A) myc-tagged phospho-deficient mutants and mitotically-

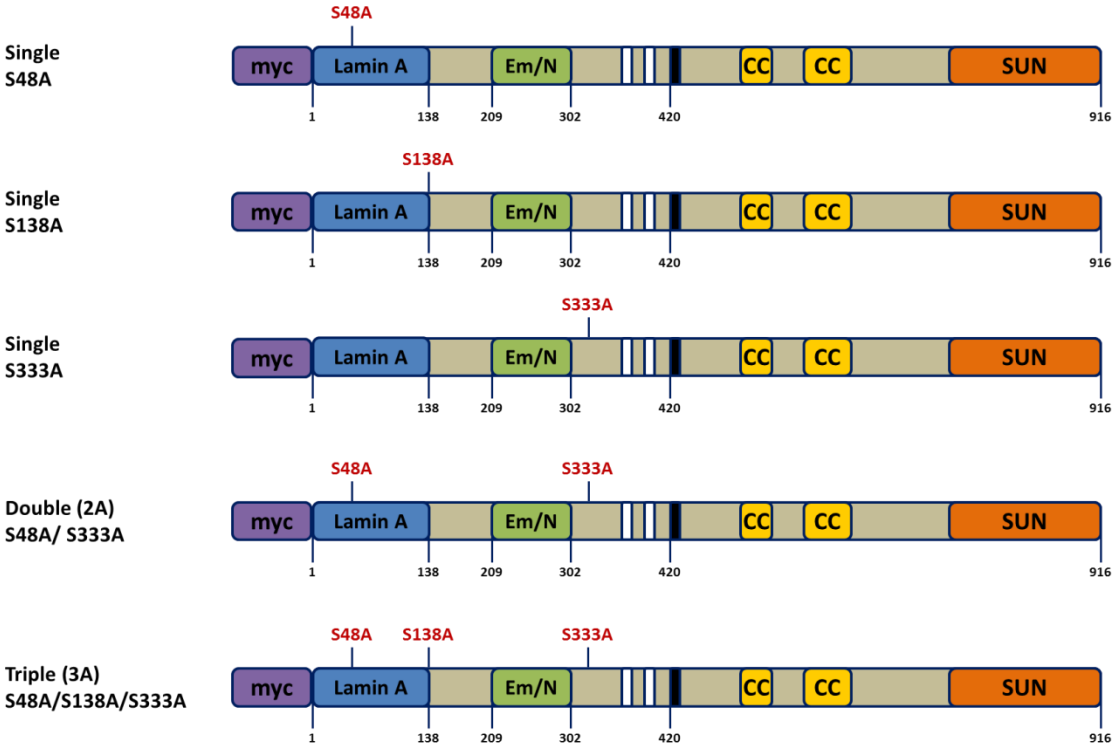

Figure 3.16. Schematic representation of single, double and triple phospho-deficient mutants.

Serine to alanine substitutions at each of the identified hSUN1 mitotic phosphorylation sites were introduced. Myc-tagged single phospho-deficient mutants corresponding one of the three hSUN1 mitotic phosphorylation sites as well as double phospho-deficient mutants targeting the two CDK1 phosphorylation sites and a triple phospho-deficient mutant encompassing all three sites were made. The position of the mutations in the myc-tagged hSUN1 protein sequence are indicated.

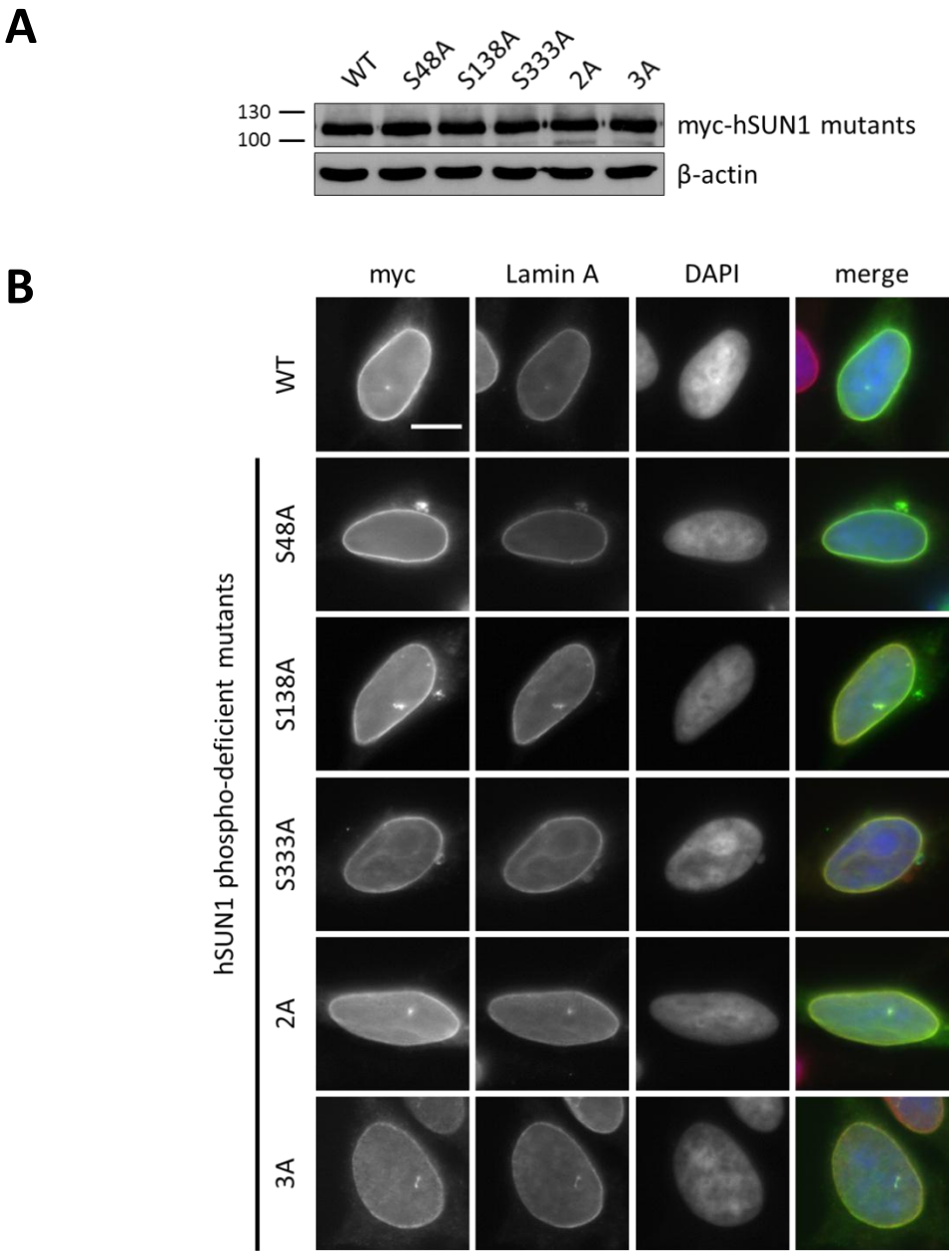

Figure 3.17. hSUN1 phospho-deficient mutant expression and subcellular localisation.

(A) Total cell lysates from asynchronous HeLa cells transiently transfected with pLEICS20 myc-tagged wild-type (WT) hSUN1 or phospho-deficient mutants (S>A), as outlined in previous figure, were resolved by SDS-PAGE and immuno-blotted with anti-c-myc and anti-β-actin antibodies. 2A is the double phospho-deficient mutant targeting the two CDK1 sites, S48 and S333, while 3A is the triple phospho-deficient mutant encompassing all three hSUN1 mitotic phosphorylation sites. Molecular weights (kDa) are indicated. **(B)** HeLa cells seeded onto coverslips were transiently transfected with pLEICS20 myc-hSUN1 phospho-deficient mutants and fixed in methanol 24-h post transfection. Cells were co-stained with anti-c-myc, anti-lamin A/C antibodies and DAPI. Scale bar 10 µm.

arrested according to the pre-arrest mitotic synchronisation protocol. Soluble lysates were resolved by SDS-PAGE and immuno-blotted with anti-c-myc, anti-cyclin B1 and anti-β-actin antibodies. All three single mutants showed a slight loss in band-shift, especially the hSUN1 S48A and S333A mutants, highlighting the importance of the CDK1 sites (**Figure 3.18**). The double (2A) and triple (3A) mutants showed even more pronounced effects, the triple phospho-deficient mutant almost entirely losing its band-shift (**Figure 3.18**). These findings confirm that all three of the serines identified by MS contribute to hSUN1 phosphorylation *in vivo* and to the mitotic band-shift. However, it is possible that there are further undiscovered phosphorylation sites.

3.2.13 Generation and validation of a hSUN1 S48 phospho-specific antibody

After assessing the findings so far, it was decided that a phospho-specific antibody to S48 would be a useful tool to investigating the potential role of phosphorylated hSUN1. The reasoning behind choosing this residue over the other two was that, not only were the CDK1 sites producing more pronounced effects in the band-shift and other assays (see **Chapter 5**), but that S48 in particular resided in a highly conserved region and so it may be more central to mitotic regulation of hSUN1.

The phospho-peptide LDPVFD[pS]PRMSRR was used as an antigen to raise a phospho-specific antibody in two rabbits. Phospho-specific antibody was affinity purified, using a non-modified peptide to remove antibodies that also recognise the non-phosphorylated form.

Initial validation of the S48 phospho-specific hSUN1 antibody (hSUN1 pS48) involved assessing the specificity of the antibody towards phosphorylated hSUN1 in *in vitro*

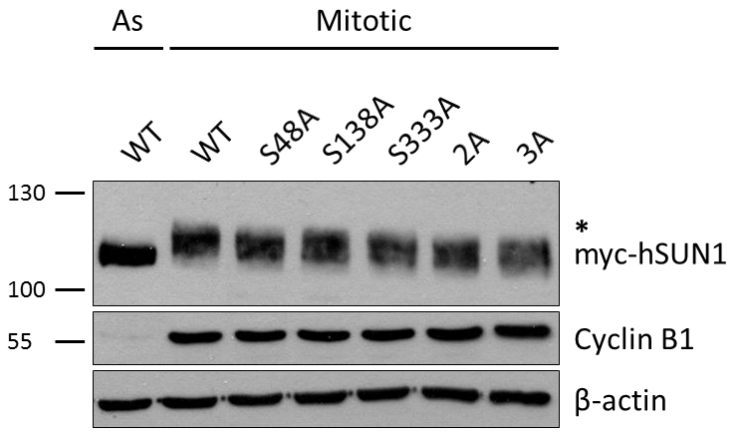

Figure 3.18. S48, S138 and S333 all contribute to the hSUN1 mobility shift at mitosis.

HeLa cells growing asynchronously (As) were transiently transfected with pLEICS20 myc-hSUN1 phospho-deficient mutants and mitotically arrested. Samples were collected by cell-scraping or by mechanical shake-off. Soluble lysates were resolved by SDS-PAGE and immuno-blotted with anti-c-myc, anti-cyclin B1 and anti-β-actin antibodies. * represents the mobility shift seen for myc-hSUN1. Molecular weights (kDa) are indicated.

kinases assays. Bacterially expressed MBP and MBP hSUN1 1-217 wild-type (WT) and S48A were bound to amylose resin. Bound fusion proteins and casein positive control were incubated in kinase buffer containing ATP and 1 µCi of [^{32}P]-γ-ATP, with or without 100 ng of purified CDK1. Samples were incubated at 30^{o}C for 30 min, resolved by SDS-PAGE, Coomassie stained and the gels were analysed by autoradiography (**Figure 3.19**). The autoradiograph shows that casein and hSUN1 1-217 WT were only phosphorylated in the presence of CDK1 and that MBP and the hSUN1 1-217 S48A mutant were not phosphorylated. The same experiment was performed in parallel in the absence of the [^{32}P]-γ-ATP radiolabel and was incubated for 4 h rather than 30 min. Western blot analysis of these samples with the anti-hSUN1 pS48 antibody revealed that only phosphorylated hSUN1 was detected by the antibody (**Figure 3.19, bottom panel**). No bands were detected in samples lacking CDK1 or when S48 was mutated to prevent phosphorylation (**Figure 3.19, bottom panel**). These data confirm that, at least *in vitro*, the pS48 antibody is specific for the phosphorylated form of S48.

3.2.14 Confirmation of hSUN1 pS48 phospho-specific antibody specificity *in vivo*

To test hSUN1 pS48 antibody specificity *in vivo*, HeLa cells were mitotically arrested. Soluble lysates were subjected to pre-clearing with protein A-sepharose beads and immunoprecipitated using 2 µg of anti-hSUN1 2383 antibody. Soluble lysates and IPs were immuno-blotted with anti-hSUN1 Atlas and anti-hSUN1 pS48 antibodies (**Figure 3.20A**). The characteristic endogenous hSUN1 band-shift was present in the mitotic lysate and IP upon detection with the hSUN1 Atlas antibody. The hSUN1 pS48 antibody did not detect anything in the asynchronous lysate or IP lane as expected but two bands were seen between 100-130 kDa in the mitotic lysate lane but not the IP lane,

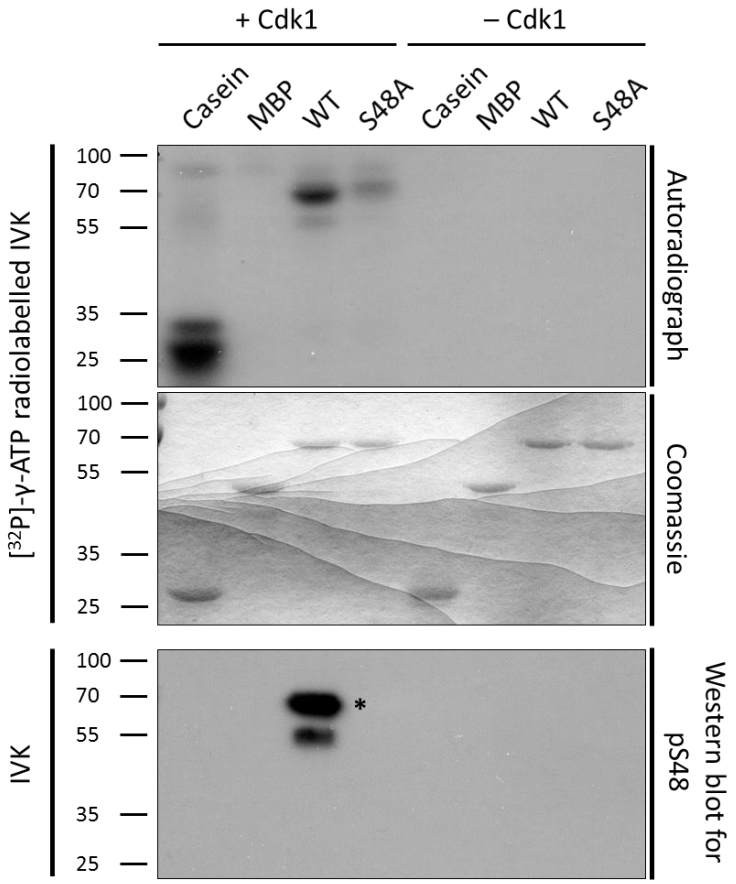

Figure 3.19. *In vitro* validation of pS48 antibody.

(Top, middle) *in vitro* kinase assay where MBP-tagged hSUN1 1-217 WT and S48A bound to amylose resin were incubated at 30°C for 30 min in [^{32}P]-γ-ATP-supplemented kinase buffer containing or not containing 100 ng of purified CDK1. Samples were resolved by SDS-PAGE, Coomassie stained and dried gels were analysed by autoradiography. (Bottom) in parallel, the same experiment was carried out lacking [^{32}P]-γ-ATP and was incubated at 30°C for 4 h. Samples were resolved by SDS-PAGE and immuno-blotted with anti-pS48 antibody. Casein and MBP were used as positive and negative controls respectively. Molecular weights (kDa) are indicated. * refers to band of interest.

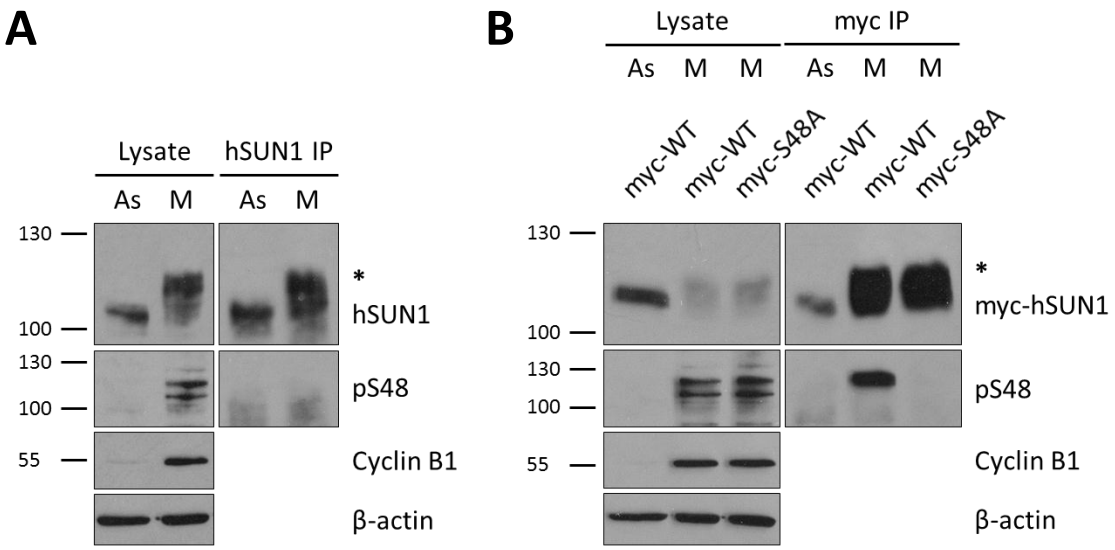

Figure 3.20. *In vivo* validation of pS48 antibody.

(A) Asynchronous (As) cultured HeLa cells were mitotically arrested (M) and collected by either cell scraping or mechanical shake-off, respectively. Soluble lysates were subjected to IP with with 2 µg of anti-hSUN1 2383 antibody. Lysates and IP samples were resolved by SDS-PAGE and immuno-blotted with anti-hSUN1 Atlas, anti-pS48, anti-cyclin B1 and anti-β-actin antibodies. **(B)** A parallel experiment was carried out where HeLa cells were transiently transfected with pLEICS20 myc-WT or -S48A 10 h prior to synchronising cells. Soluble lysates were subjected to IP with 2 µg of anti-c-myc antibody. Lysates and IP samples were resolved by SDS-PAGE and immuno-blotted with anti-c-myc, anti-pS48, anti-cyclin B1 and anti-β-actin antibodies. * represents the mobility shift seen for (myc-)hSUN1. Molecular weights (kDa) are indicated.

which could correspond to phosphorylated forms of hSUN1. However, it is not clear why these bands were not present also in the IP lane. It has to be considered that this phospho-specific antibody was raised against a CDK1 phosphorylation site with proline at the +1 position and could be detecting other CDK1 substrates.

To overcome potential antibody sensitivity or specificity issues, a similar experiment was carried out where cells were instead transiently transfected with pLEICS20 myc-hSUN1 WT or pLEICS20 myc-hSUN1 S48A 10 h prior to synchronisation, immunoprecipitated with anti-c-myc antibody and probed with anti-c-myc and anti-hSUN1 pS48 antibodies. The myc-hSUN1 mobility shift was present in lysate and IP samples. Samples were confirmed as being mitotic by probing for cyclin B1 and were equally loaded as can be seen from the β-actin blot (**Figure 3.20B**). In the lysate samples, the hSUN1 pS48 double band pattern that was observed in the endogenous hSUN1 IP was also present here. However, myc-IP of mitotic myc-hSUN1 WT showed a single prominent band (**Figure 3.20B**). This band was not seen in asynchronous myc-hSUN1 WT or mitotic myc-hSUN1 S48A. This indicates that the S48 phospho-antibody requires a high level of phosphorylated hSUN1 protein expression for detection. Moreover, results show that the antibody is specific for S48 *in vivo* as it was not seen in the mitotic myc-hSUN1 S48A IP lane.

To establish whether the two bands between 100-130 kDa observed using the pS48 antibody in IP samples were connected to the phosphorylated hSUN1, asynchronously growing HeLa cells were transiently transfected with two different siRNA oligos targeted for hSUN1. Cells were then mitotically arrested and soluble lysates were resolved by SDS-PAGE and immuno-blotted. Probing with anti-hSUN1 Atlas antibody

confirmed the band-shift in the mitotic sample (**Figure 3.21**). The shifted-band was lost following siRNA treatment, confirming knockdown of hSUN1. However, the pS48 antibody still detected the two bands at 100 and 130 kDa in siRNA-treated samples indicating that these bands are not related to hSUN1. These findings show that this antibody is able to detect phosphorylated S48 on hSUN1 but in order to do so, requires high protein levels expressed through transient transfection.

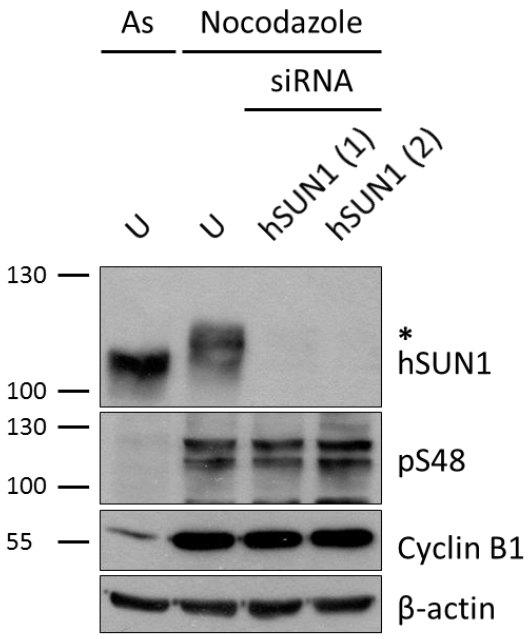

Figure 3.21. Bands detected by hSUN1 pS48 antibody in mitotic lysates are not phosphorylated hSUN1.

HeLa cells were transfected with two different siRNAs against hSUN1. Protein extracts were prepared 48 h after transfection and immuno-blotted with anti-hSUN1 Atlas, anti-hSUN1 pS48, anti-cyclin B1 and anti-β-actin antibodies. U denotes untransfected samples. * represents the mobility shift seen for (myc-)hSUN1. Molecular weights (kDa) are indicated.

3.3 Discussion

The onset of mitosis radically changes the architecture of the NE. Depolymerisation of the nuclear lamina, dissociation of the lamins from the integral proteins as well as INM protein detachment from their micro-networks and disassembly of the NPCs are required to allow NEBD, chromosome segregation and cell division to occur (Gerace & Blobel, 1980; Foisner & Gerace, 1993; Heald & Mckeon, 1990; Luscher *et al.*, 1991; Peter *et al.*, 1990; Laurell *et al.*, 2011). A post-translational modification known to initiate these events is phosphorylation.

Findings in this chapter have shown that hSUN1 does indeed undergo phosphorylation at mitosis and that the three sites identified are located in the N-terminus governed by two prominent mitotic kinases, CDK1 and PLK1.

3.3.1 Preliminary evidence of SUN1 phosphorylation

Initial experiments using *in vitro* translated protein and mitotic factor-rich *Xenopus* egg extracts failed to show any significant change in electrophoretic mobility with mSUN1; this was also true for *in vivo* cell synchronisation experiments in mouse NIH 3T3 cell lines (**Figure 3.1** and **Figure 3.2**). As hSUN1 was predicted and subsequently proven to be phosphorylated, it is very unlikely that mSUN1 does not undergo similar phosphorylation as the two sequences share 66.8% homology (UniProtKB sequence alignment) and more importantly the consensus phosphorylation sites at S48 and S138 are conserved (**Figure 3.12A**). Thus, the absence of a band-shift for mSUN2 is likely to be due to differences in the exact amino acid composition such that phosphorylation does not affect protein electrophoretic mobility.

The SUN1 orthologue mSUN2 exhibited a slight band-shift *in vitro.* The *in vitro* translated protein was a splice variant lack exon 5 which corresponded to amino acids 154-185 in the N-terminus (**Figure 3.1**). The 30 amino acid stretch may have contained phosphorylation sites that could have further contributed to the band-shift. However, this finding was not replicated *in vivo.* In fact, mitotic mSUN2 appears to show slightly reduced protein expression (**Figure 3.2**) implying that if mSUN2 is phosphorylated, this may target the protein for proteolytic degradation.

Similar studies on INM proteins LAP1, LAP2 and p54 show a change in electrophoretic mobility of these proteins upon phosphorylation *in vivo* and *in vitro* (Foisner & Gerace, 1993; Bailer *et al.*, 1991) supporting the idea that a band-shift can indicate possible substrate phosphorylation. Despite these arguments for potential phosphorylation and its purpose in the mouse sequences, the project focused on human sequences as the band-shift results were more convincing.

In vivo experiments using the pre-arrest mitotic synchronisation protocol showed that hSUN1 underwent a mobility shift at mitosis (**Figure 3.2**, **Figure 3.3** and **Figure 3.4**). This shift was not seen at any other point in the cell-cycle for hSUN1 and so was concluded to be mitosis specific. λ ppase treatment of soluble HeLa lysates confirmed that the band-shift was due to phosphorylation (**Figure 3.5**). Unfortunately, as an asynchronous sample was not run alongside the mitotically arrested samples, it is difficult to say whether the whole band-shift is entirely due to phosphorylation or just in part. The phosphorylation time-frame was also determined to be from 30 min post G2 and persisting for 1 h, which coincides with the timing of mitosis (**Figure 3.6**). The band-shift was then lost, presumably due to hSUN1 regulation through phosphatases

at the end of mitosis. Results obtained for hSUN2 were, in contrast, rather inconsistent and because of these inconsistencies, hSUN2 phosphorylation was not pursued any further.

3.3.2 Identification of hSUN1 phosphorylation sites

As the preliminary experiments showed hSUN1 was mitotically phosphorylated, steps were taken to determine the phosphorylation sites. The conventional method for detection of phosphorylation sites has been through use of tandem MS. An IP-MS approach was taken to identify hSUN1 phosphorylation sites.

Initially, I had intended on immunoprecipitating endogenous hSUN1 avoiding artefacts or non-specific binding that may have been brought about through overexpression of exogenous protein. Unfortunately as SUN1 is a low abundance protein and highly insoluble, extracting enough protein for IP and MS identification proved difficult. So much so, that MS analysis of a band thought to be hSUN1, was actually α-actinin and, western blots of the same samples showed most protein remained in the insoluble fraction (**Figure 3.7B**). The realisation that enough protein was not being solubilised and that more abundant proteins could be masking hSUN1 identification by MS lead to optimisation of the large-scale IP-MS of exogenous hSUN1.

GFP-Trap® was favoured over traditional IP because of its high efficiency to capture GFP-tagged proteins and the protocol was more time efficient, therefore the risk of protein degradation was reduced. As the GFP-Trap® system does not use whole antibodies, there was no antibody heavy chain located around the 50 kDa mark. This was not an issue for this particular experiment but there was an opportunity to use the

same gel to identify potential binding partners in asynchronous and mitotic lysates (see **Chapter 4**). The heavy chain seen in IP experiments may have masked some potential interactions and so GFP-Trap® was further optimised for the large-scale GFP-hSUN1 IP.

To digest the hSUN1 protein into as many peptides covering the maximal hSUN1 sequences, hence determining hSUN1 phosphorylation sites, two digestive enzymes, trypsin and Asp-N were used. Together they gave protein coverage of 84% (**Figure 3.8B**). Phospho-peptide enrichment of samples and MS analysis showed that hSUN1 was phosphorylated at S48, S138 and S333 in mitotic extracts only. These sites were also confirmed by *in vitro* kinase assays coupled with MS but was accompanied by a great deal of non-specific phosphorylation (**Figure 3.14B**). Peptides retrieved for the C-terminal MBP-tagged fragment hSUN1 456-916 revealed serine, threonine and tyrosine phosphorylation sites. However, these sites are unlikely to be true phosphorylation sites because the C-terminus is sequestered in the PNS hence inaccessible to mitotic kinases.

These results support the UniProtKB database S48 phospho-serine prediction but evidence for the S52 phospho-serine was not found *in vivo* or *in vitro*. It is still possible that S52 is a hSUN1 phosphorylation site. Detection of the S138 phosphorylation site was consistent with findings from the large-scale global phospho-proteomic study by Dephoure *et al*. (2008).

All three sites are in the N-terminus of hSUN1 located in the nucleoplasm. S48 and S138 are highly conserved across species and reside in the lamin A/C binding region

(Figure **3.16**). In contrast, the S333 is not within a known binding region and appears to be species specific (**Figure 3.12A**).

3.3.3 Identification of mitotic kinases responsible for hSUN1 phosphorylation

IP-MS data identified S48, S138 and S333 as mitotic hSUN1 phosphorylation sites. Comparison of the protein sequence in these regions to mitotic kinase consensus sequences, suggested that S48 and S333 were potential CDK1 phosphorylation sites whilst S138 was more likely a PLK1 phosphorylation site (**Figure 3.12**).

To confirm phosphorylation sites *in vitro* but more importantly to determine mitotic kinases responsible for hSUN1 phosphorylation, a series of *in vitro* kinase assays were performed. MBP-tagged truncated hSUN1 constructs collectively covered 90% of the hSUN1 sequences but missed residues 363-455. This region contains three hydrophobic regions, the C-terminal region being the true transmembrane domain, hence analysis of this region was unlikely to have yielded any phosphorylation sites. The purified MBP-fusion proteins were used as substrates for candidate kinases CDK1, PLK1 and Aurora A. These particular kinases were chosen because of their established roles in mitotic entry and progression.

Protein expression of hSUN1 fragment 1-362 was extremely low in comparison to the others and results suggest that it did not behave as expected. A possible explanation for this could be that this truncated protein was unable to fold correctly or that it was toxic to the *E.coli* strain it was grown in. In turn, this may have masked certain residues or hindered access to phosphorylation sites for the kinases. Quantification of the data reflected this issue as 1-217 and 1-362 deletion fragments should have behaved in a

similar manner as 1-362 includes the entire 1-217 sequence plus an additional 145 amino acids (**Figure 3.13C**). CDK1 phosphorylation of N-terminal constructs was similar whereas phosphorylation of 1-362 by PLK1 or Aurora A was significantly weaker than that of 1-217, which implied that 1-362 phosphorylation was impaired (**Figure 3.13C**). This supports the presence of two CDK1 sites and one PLK1 site but is inconsistent with data showing a lack of Aurora A sites (**Figure 3.14B**).

MS analysis of *in vitro* kinase assays confirmed that CDK1 was responsible for S48 and S333 phosphorylation and that S138 is a PLK1 phosphorylation site. Amongst all the non-specific phosphorylated residues that failed to match the minimum criteria of the consensus sequences, another potential PLK1 site was uncovered. MS could not distinguish which site was phosphorylated between T144 and T145 due to their close proximity (**Figure 3.14B**). They both matched the consensus sequence with a degree of flexibly but were not recovered *in vivo*, indicating that these were not genuine sites.

CDK1 is known to be the master mitotic kinase and has been shown to phosphorylate multiple mitotic substrates (Heald & Mckeon, 1990; Luscher *et al.*, 1991; Peter *et al.*, 1990; Laurell *et al.*, 2011; Courvalin *et al.*, 1992; Bailer *et al.*, 1991; Gajewski *et al.*, 2004) and has dominated the field in terms of kinases that disassemble the NE. However, investigations into NPC disassembly show evidence for Nup98 phosphorylation by PLK1 and NIMA-related kinases in addition to CDK1 (Laurell *et al.*, 2011).

3.3.4 Characterisation of the phospho-deficient mutants

Various myc-tagged hSUN1 phospho-deficient mutants were generated, as outlined in **Figure 3.16** to determine the contribution of each phosphorylation site to the mitotic hSUN1 band-shift. The results indicated that all three sites contribute to the band-shift and that together, they account for most of the observed band-shift. This does not rule out the possibility that there are other hSUN1 mitotic phosphorylation sites as the whole hSUN1 sequence was not covered by IP-MS analysis, but these three sites alone are enough to account for the majority of the mobility shift.

3.3.5 Validation of hSUN1 S48 phospho-specific antibody

The decision to make a phospho-antibody was so that it could be used as a tool to investigate the phenotype of hSUN1 S48 phosphorylation. Ideally it would have been beneficial to create all three phospho-specific antibodies but this was not feasible and hSUN1 pS48 was chosen as this residue appeared to be the major contributor to functional effects seen in **Chapter 5**.

Validation of the antibody shows that it is capable of detecting hSUN1 *in vitro* and *in vivo* (**Figure 3.19** and **Figure 3.20**) but requires high protein expression to overcome the low sensitivity of the hSUN1 pS48 antibody. The problem with a phospho-specific antibody directed at a CDK1 site is that the [pS/pT]-P motif is common to several substrates in mitosis as CDK1 is the master kinase in mitosis (Baumann, 2010) and therefore non-specific detection of other proteins maybe masking hSUN1 identification. Hence, experiments with this antibody also require IP of exogenous hSUN1 for its use in subsequent assays.

3.3.6 Possible disassembly of hSUN1 networks through mitotic phosphorylation

Together my data show that three phosphorylation sites reside within the N-terminus of the hSUN1 protein and are phosphorylated by CDK1 and PLK1. Furthermore, Aurora A may phosphorylate an additional site. It is also interesting to note that the N-terminus is where the lamin A/C, nesprin and emerin binding sites are located suggesting that phosphorylated hSUN1 may dissociate its known binding partners.

For over 30 years the notion that phosphorylation of lamin, INM and NPC proteins is linked to NE disassembly has been supported greatly and continues to be so. Lamina disassembly as a pre-requisite to NEBD has been shown by a range of methods from comparison of isoelectric points between interphase and mitotic cells, analysis of lamin solubility by subcellular fractionation to phospho-amino acid analysis, phospho-tryptic peptide mapping, *in vitro Xenopus* larvae studies (Gerace & Blobel, 1980; Heald & Mckeon, 1990; Peter *et al.*, 1990).

The importance of mapping specific phosphorylation sites is becoming more and more apparent as a clue to determine how protein networks are disassembled. Specific site mapping of lamin A/C shows that phosphorylation of two particular sites outside the α-helical rod-domain are important for depolymerising the lamin A/C network. (Heald & Mckeon, 1990).

MS analysis coupled with phospho-peptide enrichment has become the latest strategy to determine such sites (Laurell *et al.*, 2011; Hirano *et al.*, 2005; Hirano *et al.*, 2009; Glavy *et al.*, 2007; Gajewski *et al.*, 2004).(Hirano *et al.*, 2009; Glavy *et al.*, 2007; Gajewski *et al.*, 2004)

LAP2 interacts with lamin B1 in interphase but mitotic phosphorylation of LAP2 disrupts this interaction and binding to chromatin (Foisner & Gerace, 1993). However, it was over 10 years later that the loss of chromatin-binding could be attributed to a CDK1 phosphorylation site at S423 (Gajewski *et al.*, 2004). Hyperphosphorylated of up to 13 sites on the nucleoporin Nup98 at the onset of mitosis causes it to dissociate from the NPC, thereby increasing the permeability of the NE (Laurell *et al.*, 2011). Site-specific phosphorylation of Nup96, Nup107, Nup133 and Nup160, which are components of the Nup107-160 subcomplex, results in the dissociation of the subcomplex away from other proteins (Glavy *et al.*, 2007). Emerin LC-MS/MS analysis mapped five phosphorylation sites, one in particular S175 was important in regulating the dissociation of emerin from BAF, a DNA bridging protein (Hirano *et al.*, 2005).

These are just a few examples showing how the NE structure is remodelled during mitosis and suggests that SUN1 phosphorylation may contribute to the dynamic changes of the NE in mitosis.

CHAPTER 4
Identification of potential hSUN1 binding partners

Chapter 4 Identification of potential hSUN1 binding partners

4.1 Introduction

Mammalian SUN1 and SUN2 interact with many proteins at both their N-termini and C-termini. It is well documented that the C-terminal SUN-domain of these proteins binds the conserved C-terminal KASH-domain of nesprin isoforms that are positioned on the ONM. Nesprins, in turn, bind actin, microtubule and intermediate filament networks (Crisp *et al.*, 2006; Haque *et al.*, 2010; Wilhelmsen *et al.*, 2005; Roux *et al.*, 2009; Starr & Han, 2002; Padmakumar *et al.*, 2005; Haque *et al.*, 2006; Postel *et al.*, 2011). The extreme N-termini of SUN1 and SUN2 are bound to lamin A/C, a nuclear lamina component (Haque *et al.*, 2006) and there is evidence for SUN1 binding to chromatin (Chi *et al.*, 2007; Lu *et al.*, 2008). These various protein-protein interactions form a bridge across the PNS where the core SUN-KASH interaction is termed the LINC complex (**Figure 1.7B** and **Figure 1.9**).

In addition, SUN1 and SUN2 are capable of N-terminal binding with smaller nesprin isoforms of the INM such as nesprins-1α and nesprin-2α and another integral membrane protein known as emerin (Haque *et al.*, 2010). SUN proteins, lamin A/C, small nesprin isoforms and emerin form a network of connections with each at the NE (Haque *et al.*, 2010).

While we understand the functional relevance behind the C-terminal lumenal interactions, little is known about the purpose of the nucleoplasmic SUN, nesprin and emerin interactions. They are likely to be important for mechanical resistance to strain and/or mechanotransduction.

SUN1 and SUN2 also oligomerise to form homodimer and tetramer arrangements as well as heterodimers with SUN2 via the coiled-coil domains (Lu *et al.*, 2008). More recently structural analysis of SUN2 shows that a trimer formation of SUN proteins forms binding sites for three nesprin KASH-domains (Sosa *et al.*, 2012).

SUN1 and SUN2 have common binding partners suggesting a degree of redundancy but emerging evidence shows that SUN1 and SUN2 do have distinct functions. As well as interacting with the nuclear lamina and proteins on the ONM, SUN1 but not SUN2 also associates with some NPC components in interphase and mitosis (Liu *et al.*, 2007; Talamas & Hetzer, 2011; Lu *et al.*, 2008). SUN1-specific functions in association with NPC components include, ensuring a uniform distribution of NPCs across the NE together with transmembrane bound nucleoporin POM121 in interphase (Talamas & Hetzer, 2011) and in NPC assembly in late mitosis with Nup153 (Liu *et al.*, 2007).

SUN1 has also been shown to bind to chromatin (Chi *et al.*, 2007; Lu *et al.*, 2008) and research into the mitotic role of SUN1 has shown that in HeLa cells SUN1 chaperones hALP to mitotic chromosomes where SUN1 binds chromatin via a region in its N-terminus and hALP acetylation causes chromosome decondensation (Chi *et al.*, 2007). There is also evidence that SUN1 and SUN2 contribute to telomere anchorage at the nuclear periphery in meiosis (Ding *et al.*, 2007; Schmitt *et al.*, 2007), the functional importance is evident as SUN1 knockout mice are infertile.

Despite all the known interactions, studies from *Lmna*$^{-/-}$ MEFs show that lamin A/C is not required for mammalian SUN1 to localise at the INM (Crisp *et al.*, 2006; Haque *et al.*, 2006). Neither emerin nor nesprins are responsible for SUN1 anchorage as they are

both mislocalised in *Lmna*$^{-/-}$ MEFs (Sullivan *et al.*, 1999; Libotte *et al.*, 2005; Zhang *et al.*, 2005). This suggests that there are likely to be additional binding partners mediating SUN1 retention at the INM. In contrast, in *Lmna*$^{-/-}$ MEFs, SUN2 mislocalises to the ER and, surprisingly, re-introducing lamin A back into cells failed to recruit SUN2 to the NE (Crisp *et al.*, 2006).

It is clear that SUN1 binding partners, their purpose and function have not been fully characterised. The aim of this chapter is to identify further hSUN1 binding proteins. Two approaches have been adopted, a candidate approach and a non-bias global proteomic MS approach.

4.2 Results

4.2.1 Identification of NET5/SAMP1 as a candidate binding partner for SUN1

NET5 was one of 80 NE components identified from a large-scale subtractive proteomics study carried out on enriched NE fractions obtained from rat liver (Schirmer *et al.*, 2003). NET5 is involved in the repositioning of chromosome 5 (E.Schirmer, personal communication) and was chosen as a candidate for hSUN1 interaction based on functions reported in its yeast and human orthologues.

The yeast homologue of NET5, Ima1 is an integral membrane protein of the INM and contributes to coupling of the SPB to DNA by binding heterochromatin and tethering centromeric DNA to Sad1-Kms2, the yeast LINC complex. In addition, it supports the nucleus against the microtubule-generated forces (King *et al.*, 2008).

The human orthologue of Ima1, SAMP1, resides at the INM in interphase. It is composed of 392 amino acids with a molecular weight of 43 kDa. SAMP1 contains five transmembrane domains and is orientated so its C-terminus is in the nucleoplasm and the N-terminus in the PNS (Buch *et al.*, 2009) (**Figure 4.1A**). The protein sequence harbours four CXXC motifs suggesting the presence of two zinc fingers with the potential to bind DNA (Buch *et al.*, 2009). In interphase SAMP1 is involved in coupling the centrosome to the NE demonstrating that, like SUN1, it is functionally connected to the cytoskeleton (Buch *et al.*, 2009). It was thought that SAMP1 may be coupling the centrosome to the nucleus in association with LINC complex components i.e. SUN1/SUN2.

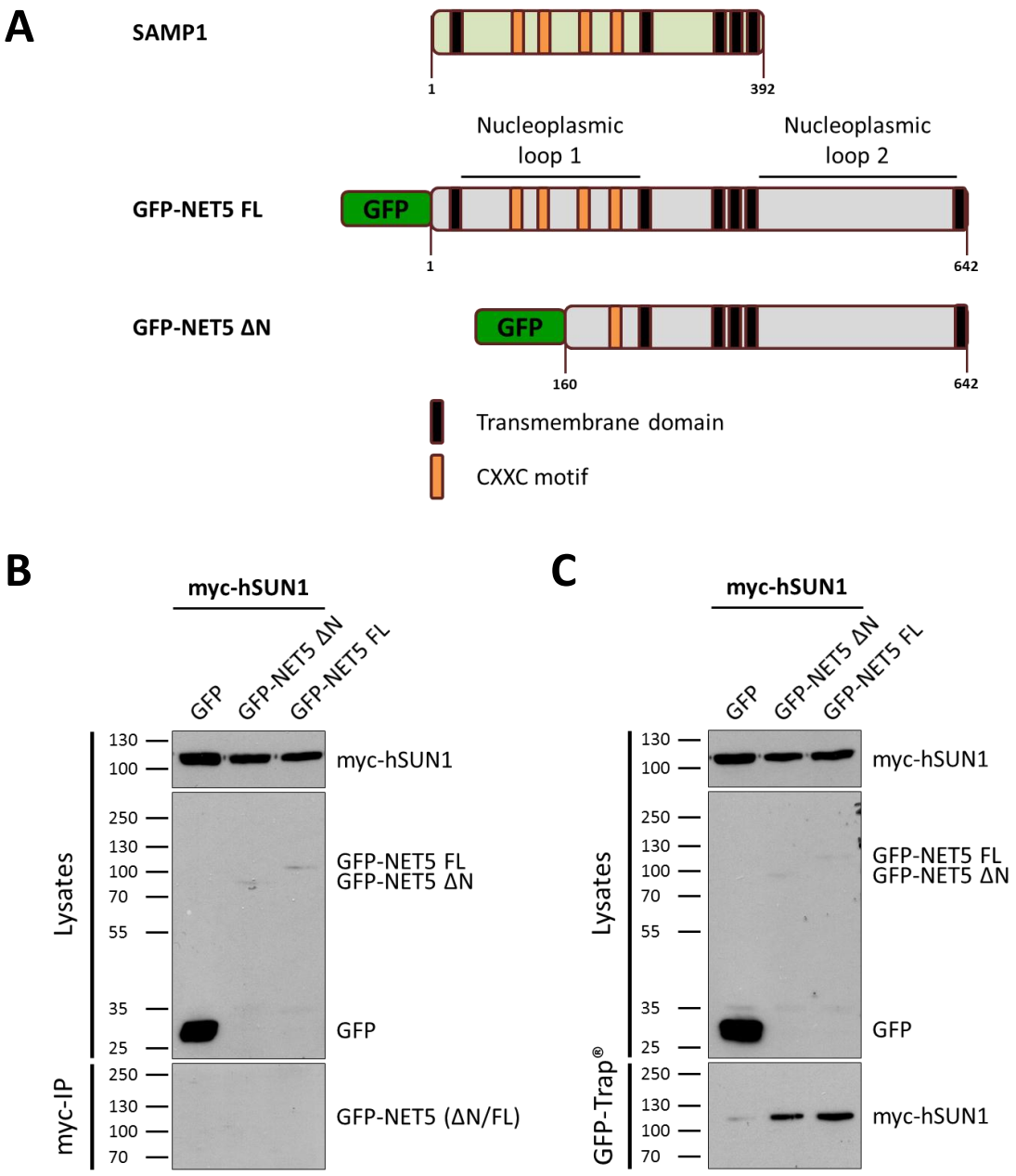

Figure 4.1. hSUN1 interacts with NET5.

(A) Schematic representation of the human SAMP1, rat GFP-NET5 FL and ΔN constructs. The rat GFP-NET5 ΔN is a partial cDNA lacking the N-terminus. Black segments represent transmembrane domains while orange segments denote regions containing the CXXC motif. The presence of up to four CXXC sequences suggests a possible zinc finger domain. **(B** and **C)** HeLa cells were transiently co-transfected with pEGFP C1/pEGFP NET5 FL/pEGFP NET5 ΔN and pLEICS20 myc-hSUN1. Soluble lysates were either **(B)** subjected to co-IP with 2 µg of anti-c-myc antibody or **(C)** processed using the GFP-Trap® protocol. Soluble lysate fractions and the final IP/GFP-Trap® samples were resolved by SDS-PAGE and immuno-blotted with anti-c-myc and anti-GFP antibodies. Molecular weights (kDa) are indicated.

4.2.1.1 NET5 interacts with SUN1

At the time of investigation, no antibodies were available for NET5 or SAMP1. The published SAMP1 isoform (Buch *et al.*, 2009) is only a partial sequence in comparison to rNET5 and I wanted to use full-length protein therefore, NET5 GFP-tagged constructs were obtained from Dr Eric Schirmer (University of Edinburgh). Two DNA plasmid constructs were kindly sent to the laboratory to study the possible interaction with the hSUN1, the full-length rat orthologue (pEGFP NET5 FL) and a partial cDNA lacking the N-terminus (pEGFP NET5 ΔN) (**Figure 4.1A**).

To test the possible interaction between hSUN1 and NET5, HeLa cells were co-transfected with pLEICS20 myc-hSUN1 and either pEGFP NET5 FL or pEGFP NET5 ΔN. Soluble lysates were then subjected to IP using anti-myc antibody. Initial lysates and IP samples were resolved by SDS-PAGE and immuno-blotted with anti-c-myc and anti-GFP antibodies. Expression of myc-hSUN1 was high, as seen previously with this construct, in contrast to the NET5 constructs which were extremely poorly expressed (**Figure 4.1B**). The IP failed to show any sign of an interaction between the two proteins (**Figure 4.1B**).

Before dismissing the interaction, the reciprocal IP was carried out where, GFP-Trap® was implemented to pull-down NET5 and co-immunoprecipitating myc-hSUN1 detected with anti-myc antibody. Again expression levels of the myc- and GFP-tagged proteins in the lysate fractions reflected results from **Figure 4.1B** but the IP blot showed that hSUN1 does interact with both the short and long isoforms of NET5 but not GFP alone (**Figure 4.1C**). In addition to demonstrating an interaction between

hSUN1 and NET5 this result also maps the SUN1 binding site to residues 160-642 of the full-length isoform of NET5.

4.2.2 IP-MS approach to identify novel SUN1 binding partners

An IP-MS approach has many advantages over the candidate approach as it requires no prior knowledge of protein function and therefore, no bias is introduced. Furthermore, the sensitivity of MS identification of proteins can produce a library of potential interacting proteins. However, difficulties can be encountered with non-specific binding, whether that is to the bead matrix, the tag attached to the protein of interest or non-specific interactions with overexpressed protein. In addition, subtle interactions can be masked by the presence of abundant proteins, so strategies have to be developed to overcome such issues.

My strategy for identifying new hSUN1 binding partners was based on a large-scale GFP-Trap®. GFP-tagged hSUN1 would be overexpressed in asynchronously growing HeLa cells for visible detection on a Coomassie stained gel. GFP-hSUN1 would then be purified with its co-immunoprecipitating binding partners by the GFP-Trap® protocol. GFP-Trap® samples would be resolved by SDS-PAGE and stained to highlight protein bands. Confirmation of the presence of GFP-hSUN1 by MS would then be followed by identification of potential binding partners. An additional mitotic sample, also transiently transfected with GFP-hSUN1, would be processed alongside the asynchronous sample to observe whether protein interactions had been lost or gained in mitosis. This would also replicate experiments conducted and described in **section 5.2**. HeLa cells transfected with GFP empty vector only and processed in asynchronous conditions was to be used as a negative control.

Cultured asynchronous HeLa cells were transiently transfected on a large-scale with either pEGFP C1 or pLEICS21 GFP-hSUN1. Half of the cells expressing GFP-hSUN1 were asynchronous and the other half were mitotically arrested as described in **section 2.4.10**. The GFP fusion proteins were purified from soluble lysates using the GFP-Trap® method and both lysate input fractions and the final GFP-Trap® samples were resolved by SDS-PAGE. The gel was stained with Brilliant Blue Colloidal G stain (**Figure 4.2**). The suspected GFP-hSUN1 bands from the asynchronous and mitotic lanes were excised from the gel, as was the corresponding band in the negative control GFP lane, for confirmation of hSUN1 identity (slices corresponding to bands 1, 2 and 3 in **Figure 4.2**). The remaining gel was sectioned as indicated in **Figure 4.2** and analysed by MS to identify possible binding partners. Gel slices were submitted rather than the whole gel lane to reduce the complexity of proteins analysed and reduce masking effects.

Results from MS were analysed using Scaffold3 software where parameters were set to a minimum of three peptides to confirm presence of each identified protein and a 95% statistical confidence that those peptides belonged to that protein. Proteins found in the GFP (async) negative control were cross-referenced with the other two samples and were subtracted from the list of possible binding partners. The remaining proteins were sorted into those that bound hSUN1 in both asynchronous and mitotic conditions and those that bound in only one condition. IP-MS for hSUN1 was carried out only twice because of the large costs incurred by MS and the fact that any potential interaction with hSUN1 would be confirmed later by co-IP. The complete set of raw data can be found in **Appendix E**. **Table 4.1** outlines selected proteins of interest that have been grouped into various catergories.

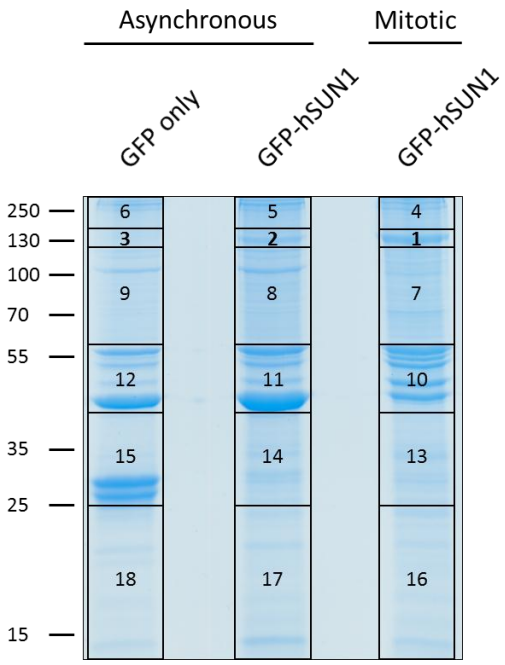

Figure 4.2. Coomassie gel sectioning for LC-MS/MS to identify novel binding partners.

Cultured asynchronous HeLa cells were transiently transfected on a large-scale with either pEGFP C1 or pLEICS21 GFP-hSUN1. Half of the cells expressing GFP-hSUN1 were asynchronous and the other half were mitotically arrested. Soluble lysates were processed using the GFP-Trap® method. Lysate fractions and the final GFP-Trap® samples were resolved by SDS-PAGE. The suspected GFP-hSUN1 bands from the asynchronous and mitotic lanes were excised from the gel as well as the corresponding band in the negative control GFP lane (bands 1, 2 and 3) for confirmation of hSUN1 identity. The remaining gel was sectioned as indicated and trypsin digested then analysed by LC-MS/MS to identify possible binding partners. Molecular weights (kDa) are indicated.

Table 4.1. A select list of potential hSUN1 binding partners derived from IP-MS analysis.

A list of 33 proteins from the 348 potential hSUN1 binding partners categorised according to subcellular localisation or function. Their presence in asynchronous or mitotic IP conditions and their presence between experimental repeats are indicated.

Protein category	Protein name	UniProtKB accession number	Presence detected			
			Repeat 1		Repeat 2	
			Async	Mitotic	Async	Mitotic
NE components	Nurim	Q8IXM6	+	+	+	+
	Nesprin-1	Q8NF91	-	+	+	+
	Emerin	P50402	+	-	+	+
	Nup155	O75694	-	+	+	+
	Lamin B1	P20700	-	+	+	+
	Transmembrane protein 43	Q9BTV4	+	-	Not detected	
	Nesprin-2	Q8WXH0	Not detected		+	+
	Lamin-associated protein β/γ (LAP2 β/γ)	P42167	Not detected		+	+
	Nup358/Ran binding protein 2 (RanBP2)	P49792	Not detected		-	+
	Lamin B2	Q03252	Not detected		+	-
Nucleo-cytoplasmic transport	Importin α2	P52292	+	-	-	+
	Importin β1	Q14974	+	+	+	+
	Exportin 2	P55060	-	+	-	+
	Importin 7	O95373	Not detected		-	+
	Exportin T	O43592	Not detected		-	+
	RanGTPase activating protein 1 (RanGAP1)	P46060	Not detected		-	+
Kinases and phosphatases	Cyclin-dependent kinase 1 (CDK1)	P06493	Not detected		-	+
	Cyclin B1	P14635	Not detected		-	+
	Aurora A	O14965	Not detected		-	+
	BUB3	O43684	Not detected		+	+
	Casein kinase 1α	P48729	-	+	Not detected	
	Cyclin-dependent kinase 6 (CDK6)	Q00534	Not detected		-	+
	Protein phosphatase 2A (PP2A)	P63151	Not detected		-	+
Chromatin-associated	Histone H1.2	P16403	+	-	+	+
	Histone H2A.1	O75367	+	-	Not detected	
	Retinoblastoma binding protein 4 (RBBP4)	Q09028	+	+	Not detected	
	Heterochromatin protein 1γ (HP1γ)	Q13185	Not detected		-	+
	Histone deacetylase 10 (HDAC 10)	Q969S8	Not detected		-	+
	Histone acetyltransferase 1 (HAT1)	O14929	Not detected		-	+
Mitotic protein	Regulator of chromosome condensation 2 (RCC2)	Q9P258	+	+	+	+
	Kinesin family member 20A (KIF20A)	O95235	Not detected		-	+
Motor protein	Dynein heavy chain	Q14204	-	+	+	+
Transcriptional regulator	Four and a half LIM domain protein 2 (FHL2)	Q14192	-	+	+	+

The first experimental repeat identified a total of 314 proteins whereas the second experimental repeat uncovered 582 proteins. Each complete data set was analysed by initially subtracting proteins reteived form the asynchronous GFP negative control sample from the asynchronous and mitotic GFP-hSUN1 samples. The remaining 348 potential binding partners were categorised into strong and weak hSUN1 candidates, as shown in **Appendix F**. Those proteins regarded as strong potential binding partners (highlighted in blue in **Table 4.1**) were present in both experimental repeats and absent from both negative controls. Weak candidates were either, present in both experimental repeats but absent from one negative control, or were present in one experimental repeat and absent from its negative control.

The aim of this chapter was to identify direct interactors of the nucleoplasmic domain of hSUN1. Amongst the 348 potential hSUN1 binding proteins detected, a large number of what were considered contaminant or indirectly bound proteins were found, such as proteins of the cytoskeleton, ribosome, microsome, mitochondria, proteosome, heat-shock proteins, plasma membrane and ER (**Appendix F**). These proteins were eliminated from the list of proteins of interest as they were either located in an area thought to be irelevant to the NE or have been noted to be potential non-specific binders (Schirmer *et al.*, 2003; Trinkle-Mulcahy *et al.*, 2008). The remaining proteins that were considered as potential true SUN1 interactors, were selected due to their appropriate subcellular location and/or function (**Table 4.1**).

Analysis of the MS data showed that known interacting binding partners lamin A/C, emerin and giant nesprin isoforms were co-immunoprecipitated with hSUN1. However, peptides for emerin and nesprin-2 giant were found in one of the negative

GFP control samples, demoting them to weak candidates. The NE components section in **Table 4.1** accounts for 10 of the 33 proteins of interest. Novel potential NE binding partners include, B-type lamins, three known integral membrane proteins of the INM and two nucleoporins, one of which is involved in nucleo-cytoplamsic transport.

Other proteins of interest were grouped under four headings, nucleo-cytoplasmic transport proteins, kinases and phosphatases, chromatin-associated proteins and mitotic proteins. Two exceptions were dynein heavy chain and FHL2 which were catergorised under motor protein and transcriptional regulator, respectively.

4.3 Discussion

In order to identify novel hSUN1 binding partners, two strategies were adopted, a candidate approach and an IP-MS approach. The candidate approach was based on prior knowledge in the field and a possible interaction was investigated by co-IP. The IP-MS approach was an unbiased way of globally assessing hSUN1 interactions without the need for previous knowledge of the proteins. Both methods were successful in identifying binding partners.

4.3.1 hSUN1 binds NET5

GFP-NET5 FL and ΔN constructs were kindly given to us by Dr Eric Schirmer for the purpose of testing the possibility of an interaction with hSUN1. At the time of testing the initial interaction, the endogenous hSUN1 IP was not sufficiently optimised and so exogenously expressed myc-hSUN1 was used instead. After co-expressing myc-hSUN1 and GFP-NET5, the hSUN1-NET5 interaction was demonstrated using the GFP-Trap® method. Failure to establish the connection in the myc-IP was probably due to the fact that the myc-hSUN1 construct was highly expressed in comparison to the low expression of the GFP-NET5 constructs. Therefore, immunoprecipitating hSUN1 to detect co-precipitating NET5 would be difficult in these circumstances. The reciprocal IP (GFP Trap®) revealed the interaction, as the low expressing GFP-NET5 constructs were concentrated on the beads and so it was easier to detect the co-immunoprecipitating highly expressed myc-hSUN1.

NET5 was originally identified as a NE membrane protein from a large-scale MS proteomic study (Schirmer *et al.*, 2003) and has shown to play a role in positioning of chromosome 5 (E.Schirmer, personal communication). Since then research has been

conducted with its human orthologue SAMP1 in establishing its localisation at the INM (Buch *et al.*, 2009), as well as deciphering its functions as a key protein in centrosome anchorage to the nucleus (Buch *et al.*, 2009). Recent studies show that SAMP1 has three alternative spliced isoforms, SAMP1A, 1B and 1C (Borrego-Pinto *et al.*, 2012), SAMP1A corresponding to the C-terminally truncated form studied by Buch *et al.* (2009) and SAMP1C corresponding to NET5 (**Figure 4.3**).

To date, an interaction between hSUN1 and any of the SAMP1 isoforms has not been published, only that SAMP1 appears to colocalise with hSUN1 shown by overlaying co-stained indirect immunofluorescence (Gudise *et al.*, 2011). Early research on SAMP1 from the Hallberg laboratory used the SAMP1A variant (Buch *et al.*, 2009; Gudise *et al.*, 2011). SAMP1A lacks the C-terminal sequence present in both SAMP1B and 1C. NET5 FL is the equivalent of SAMP1C and my results, showing that NET5 ΔN maintains interaction with SUN1, suggest that the C-terminus of SAMP1C contains the SUN1 binding site, as depicted in **Figure 4.3**. However, experimental confirmation would be required. This may also explain why an interaction between SAMP1A and hSUN1 was not detected earlier (E.Hallberg, personal communication), since the C-terminus is absent from this isoforms of SAMP1.

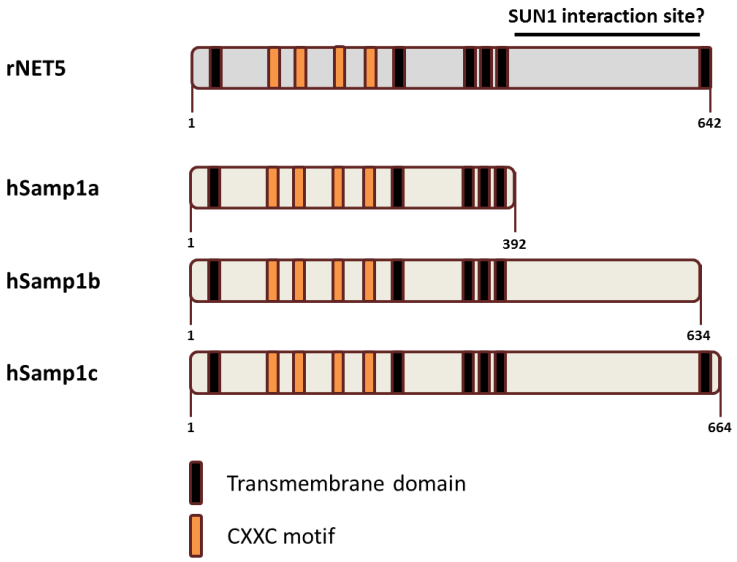

Figure 4.3. Schematic representation of rat NET5 in comparison with human SAMP1 isoforms.

There are three human SAMP1 splice variants, SAMP1A, 1B, and 1C. It is not currently known whether the rat NET5 orthologue has splice variants. SAMP1A does not bind SUN1 and lacks the C-terminal sequence that SAMP1B and 1C. NET5 is most like SAMP1C and data shows NET5 and hSUN1 bind. The suggested binding site has been labelled as shown. NET5, SAMP1B and 1C have two nucleoplasmic loops. All isoforms have four CXXC motifs suggesting the presence of potential zinc fingers.

Deletion constructs of NET5 are available from the Schirmer laboratory for the two nucleoplasmic loops (37-209 and 375-636). It would be interesting to map the hSUN1 interaction site and I would expect only NET5 loop 2 (375-636) to bind hSUN1. Also, mapping the NET5 interaction site on hSUN1 with N-terminal hSUN1 deletion constructs would be of interest. It maybe that the binding site lies in a region distinct from the identified mitotic phosphorylation sites, possibly explaining why the interaction is still maintained in mitosis, as explained in **Chapter 5**.

Interestingly, SAMP1C has been shown to interact with SUN2 and is a component of TAN lines (Borrego-Pinto *et al.*, 2012) (**section 1.2.4.1**). TAN lines are required for centrosome orientation and nuclear movement prior to cell migration as well as cellular migration (Luxton *et al.*, 2011). SAMP1C also interacts with lamin A/C, which anchors this particular LINC complex and allows efficient movement of the nucleus (Borrego-Pinto *et al.*, 2012; Gudise *et al.*, 2011). Thus, a major role of the NET5/SAMP1-SUN1 interaction could be in stabilising the LINC complex and promoting nuclear-cytoskeletal coupling.

Together, these findings add NET5/SAMP1 to the growing list of LINC complex-associated proteins and furthermore, identify NET5/SAMP1 as another candidate for involvement in the muscular nuclear envelopathy EDMD.

4.3.2 IP-MS identifies multiple novel SUN1 binding partners

Ideally determination of potential hSUN1 interacting partners should have utilised endogenous rather than exogenous protein, to avoid false positives due to hSUN1 overexpression. SUN1 is found in the ER when overexpressed and could explain the

presence of ER proteins found by MS analysis (Haque *et al.*, 2006). Initial optimisation of the IP-MS method was based on immunoprecipitating endogenous hSUN1 from HeLa cells using one of two hSUN1 antibodies. However, attempts to solubilise enough hSUN1 protein from cells proved difficult as protein expression was evident by western blot analysis but levels were insufficient for detection by Coomassie staining (**Figure 3.7**). A decision was therefore made to perform large-scale IP of exogenous GFP-hSUN1 to overcome expression issues. Optimisation of the large-scale IP is explained in **Chapter 3**.

Data received from MS analysis showed that hSUN1 had the potential to bind a range of proteins. The full list of proteins can be found in **Appendix E** and **Appendix F**. The first and second experimental repeats identified a total of 314 and 582 proteins, respectively, of which 348 were shown to be potential hSUN1 binding partners determined by criteria outline previously. At first glance, the two data sets show the biological variance that can occur from conducting these types of experiments. Other difficulties encountered were the fact that abundant proteins such as cytoskeletal proteins tended to mask the low expressing proteins and therefore mask possible interacting partners. One strategy employed to ease this effect was to divide the protein lane to be analysed into segments (**Figure 4.2**), each corresponding to a single sample, and run these separately on the mass spectrometer.

Use of overexpressed GFP-hSUN1 raised other problems, such as the potential for non-specific protein-protein interactions. A GFP sample purified from asynchronous cells was therefore run alongside the GFP-hSUN1 sample as a negative control. This was to ensure that any non-specific binding to the GFP moiety could be subtracted when

analysing result from the hSUN1 sample. Unfortunately, this was not as straight forward as expected as the data shows that some proteins experimentally proven to bind hSUN1, such as lamin A/C and emerin, were detected in the negative control. A possible explanation for this could be that lamin A/C and emerin are known to precipitate non-specifically i.e. they are 'sticky' proteins. Hence data could not be taken at 'face-value' and so were regarded as a starting point for further analysis.

Tagged proteins have been shown to bind non-specifically most likely through transient interactions (Trinkle-Mulcahy *et al.*, 2008). Research looking into characterising non-specific binding partners of GFP in IP and GFP-Trap® summarised data and found a list of proteins that frequently co-IP with GFP matrices non-specifically (Trinkle-Mulcahy *et al.*, 2008). These included various cytoskeletal and heat-shock proteins. In light of this research, considerations were made when analysing the two data sets. Ideally there should have been a third experimental repeat but MS analysis was extremely costly and my time was limited. Furthermore, possible binding partners would inevitably have had to be confirmed experimentally by co-IP and western blots.

It is perhaps not surprising that direct comparisons between asynchronous and mitotic samples were not achievable. For example, data outlined in **Chapter 5** shows loss of hSUN1 binding with lamin A/C and emerin in mitosis yet peptides from these proteins were still detectable in the mitotic MS sample. Overall, the experimental procedure was not quantitative and in hindsight could have been designed to be so. LC-MS/MS is not quantitative and, rather like yeast-2-hybrid, it provides a starting point for further analysis. An alternative method is SILAC. It is a quantitative proteomic approach that

can be coupled with MS. It is based on incorporation of an amino acid residue labelled with stable isotopic elements, for example, carbon 13 or nitrogen 15 into cell cultures. Two cell populations are grown in parallel in the same media but one contains the labelled form of the particular amino acid, and is referred to as the 'heavy' form. The labelled amino acid is incorporated into newly synthesised proteins and eventually replaces the naturally occurring form over many cell divisions. SILAC can be used to measure relative interactions in light and heavy cell populations. However, this method is very expensive to run but, is effective and reproducible.

The majority of proteins identified in the GFP negative control lane were regarded as non-specific binders and were subtracted from the hSUN1 asynchronous and mitotic. The remaining 348 proteins were grouped by the criteria outlined previously into strong and weak candidates for interaction with hSUN1. Strong candidates are highlighted in blue in **Table 4.1**. A large proportion of these proteins were cytoskeletal, ribosomal, microsomal, mitochondrial, proteosomal, heat-shock proteins, plasma membrane proteins and ER proteins. These proteins were not included in the list of proteins of interest as they were regarded as being located in regions irrelevant to the NE or were potential non-specific binders (Schirmer *et al.*, 2003; Trinkle-Mulcahy *et al.*, 2008). The 33 proteins in **Table 4.1** were chosen based on subcellular localisation or function and are discussed below.

4.3.2.1 Nuclear envelope components

4.3.2.1.1 Nuclear lamina

Lamin A/C was co-immunoprecipitated with hSUN1, as shown by the MS data, but it was also seen in the GFP asynchronous sample. MS detection is a sensitive method and

lamin A/C peptides were found in both neagtive control samples and therefore, these were eliminated from the final data sets, despite them being known SUN1 binding partners (Crisp *et al.*, 2006; Haque *et al.*, 2006). Lamin A/C are well known as 'sticky' proteins that are common contaminants in co-IPs because of their coiled-coil domains, which could explain their presence in the negative control samples. This highlights the limitations of the the technique and suggest that potential hSUN1 interactors could be missed. The hSUN1 interaction with lamin A/C has been established for some time and its purpose is to connect the LINC complex to the nuclear interior as well as to stabilise hSUN1 at the NE (Crisp *et al.*, 2006; Haque *et al.*, 2006).

Lamin B1 and lamin B2 peptides were detected in the hSUN1 co-IP. There is limited evidence showing that SUN1 binds lamin B1, but it appears to have a higher binding affinity for lamin A (Crisp *et al.*, 2006). Aside from its role as a component of the nuclear lamina, lamin B also has functions in spindle assembly (Tsai *et al.*, 2006). Lamin B has shown to be a structural component of the spindle matrix, a static network that secures spindle assembly factors (SAFs), aiding assembly and cushioning against forces exerted by the microtubules (Tsai *et al.*, 2006). To assemble the lamin B spindle matrix in mitosis, RanGTP is required to displace importin-α and importin-β from lamin B hence becoming more accessible for matrix assembly (Tsai *et al.*, 2006), and interestingly, Ran-associated proteins were also isolated by IP-MS. It is possible that hSUN1 interaction with lamin B in mitosis is of more relevance than in interphase and that hSUN1 may be part of the spindle matrix possibly acting, like lamin B, as a structural component or SAF. This can only be determined by quantitative measurements of relative binding in mitotic and asynchronous cells. In support of this,

SAMP1A also colocalises to the mitotic spindle and I have shown that long isoforms of this protein interact with hSUN1. It would be interesting to determine whether long isoforms of SAMP1 also localise to the mitotic spindle.

4.3.2.1.2 NE membrane proteins

Known hSUN1 binding partners emerin, nesprin-1 giant and nesprin-2 giant were identified by IP-MS hSUN1, yet smaller nesprin isoforms were not isolated. This may be because HeLa cells do not express those particular isoforms.

Nurim peptides were retrieved in both experimental repeats and were absent from the negative control. Nurim is a multi-spanning INM protein and, unlike other INM proteins, it lacks a large hydrophilic N-terminus required for anchorage by the nuclear lamina or other INM proteins, yet it remains tightly bound to the nucleus (Rolls *et al.*, 1999; Hofemeister & O'Hare, 2005). It does not bind to NPCs, nor is it targeted to the INM through lamina interaction (Hofemeister & O'Hare, 2005). Moreover, in conditions that completely extracted lamins, nurim only partially solubilises from the nucleus (Hofemeister & O'Hare, 2005). This suggests that nurim is retained at the INM through an alternative mechanism possibly through interactions involving its transmembrane domains. hSUN1 remains at the INM in the absence of lamin A/C, emerin and nesprins, therefore it is possible that either hSUN1 is directly anchored through the same unknown mechanism that retains nurim at the INM or that nurim anchors hSUN1 to the INM. This could be tested by observing hSUN1 localisation by immunofluorescence microscopy in cells depleted of nurim.

Transmembrane domain protein 43 (TMEM43)/LUMA was identified as a potential hSUN1 interacting protein. This INM protein was first identified by a proteomic based approach (Dreger *et al.*, 2001) and contains a large hydrophilic domain and four transmembrane domains which are required for its targeting to the NE as well as for homo-oligomerisation (Bengtsson & Otto, 2008). LUMA has a few known binding partners including A-type and B-type lamins, emerin and SUN2 (Bengtsson & Otto, 2008; Liang *et al.*, 2011). Lamin A/C interaction is required for its retention at the INM (Bengtsson & Otto, 2008). It was reported that there was no interaction between LUMA and SUN1 (Liang *et al.*, 2011) which conflicts with data found in this experiment. Further confirmation through co-IP experiments with full-length hSUN1 would confirm this. The protein is encoded by the gene *TMEM43* and a missense mutation in this gene leads to ARVC and other mutations in *TMEM43* are thought to contribute to the pathological mechanism of EDMD (Liang *et al.*, 2011; Merner *et al.*, 2008). With this in mind, and the fact that other mutant LINC complex components such as emerin, nesprins, SUN proteins and lamin A/C play roles in the pathogenicity of EDMD, it suggests that LUMA may contribute to anchorage of the LINC complex at the NE.

Lamina-associated protein 2β/γ (LAP2) was another INM protein to be identified as a SUN1 interactor from the IP-MS data. LAP2 is alternatively spliced to give rise to 6 proteins, of which LAP2 β, γ, δ and ε are membrane bound proteins (Foisner, 2003). LAP2, in particular the β isoform, binds lamin B and DNA (Foisner & Gerace, 1993). Binding of these proteins to the nuclear lamina is thought to maintain the structural integrity of the NE and also play a role in chromatin organisation in interphase. Like SUN1, LAP2 is phosphorylated during mitosis , which prevents binding of LAP2 to lamin

B and mitotic chromosomes but, in late anaphase, LAP2 is able to bind mitotic chromosomes again which indicates a role in NE assembly (Furukawa *et al.*, 1997). It could be speculated that SUN1 may be in complex with LAP2 to co-ordinate such events, especially considering the role of SUN1 in decondensation of mitotic chromosomes (Chi *et al.*, 2007) and NPC assembly (Liu *et al.*, 2007).

4.3.2.1.3 Nuclear pore complex proteins

SUN1 clusters around NPC proteins and is considered an important factor for uniform spatial NPC distribution in the NE (Liu *et al.*, 2007; Lu *et al.*, 2008). This requires both N- and C-termini of SUN1 and elimination or overexpression of SUN1 can cause NPC clustering (Liu *et al.*, 2007). Surprisingly, SUN2 is found at distinct foci devoid of NPCs (Liu *et al.*, 2007). SUN1 is also involved in initiating interphase NPC assembly by transiently interacting with the NPC protein POM121 (Talamas & Hetzer, 2011). The emergence of two NPC proteins from the data was therefore not surprising.

Interestingly, Nup155 is recruited to chromatin for the reformation and fusion of the NE at the end of mitosis (Franz *et al.*, 2005) and when in complex with Nup160 and POM121, contributes to NPC formation and anchorage of the NPC to the membrane (Mitchell *et al.*, 2010). The N-terminal β-propeller anchors the protein to the NPC while the C-terminal α-solenoid region is involved in localising LBR to the INM (Mitchell *et al.*, 2010; Busayavalasa *et al.*, 2012). Nup155 depletion leads to mislocalisation of INM proteins to the cytoplasm and a reduction in the number of NPCs at the NE, thereby altering the NE structure (Mitchell *et al.*, 2010; Busayavalasa *et al.*, 2012). As Nup155 is capable of anchoring INM proteins to the INM, it makes it a good candidate for the protein responsible for hSUN1 retention at the INM. Also, if the hSUN1-Nup155 and

hSUN1-POM121 interactions are both genuine, there is the possibility of hSUN1 being part of a complex involved in NPC assembly and regulation.

Nup358, also known as RanBP2, is a core component of the 100 nm filament extending from the NPC at the cytoplasmic face in interphase (Wu *et al.*, 1995). It is involved in nucleo-cytoplasmic transport but is not vital for this function (Salina *et al.*, 2003). In contrast, in mitosis it is localised to kinetochores and microtubule spindles but throughout the cell cycle it is associated with RanGAP1 (Joseph *et al.*, 2002). RanGAP1 is the GTPase activating protein for RanGTP, which is important in regulation of nucleo-cytoplasmic transport. Nup358/RanBP2 and RanGAP1 were both found in this hSUN1 potential binding partner screen.

Many Nups, including Nup358/RanBP2, relocate from the NPC to the kinetochore in mitosis and Nup358/RanBP2 is also found at spindle microtubules (Joseph *et al.*, 2002). It is essential for kinetochore assembly and sister chromatid segregation because in the absence of Nup358/RanBP2, chromosomes fail to align properly on the mitotic spindle, leading to abnormal segregation of the sister chromatids (Salina *et al.*, 2003). The assembly of other kinetochore components is also altered resulting in malformed kinetochore structure (Salina *et al.*, 2003). Without Nup358/RanBP2, maybe Ran components such as RanGAP1 and RanGTP are not recruited to the kinetochore adding to the perturbed phenotype. MS analysis showed that both Nup358/RanBP2 and RanGAP1 bound hSUN1 in mitotic samples only and suggests roles for SUN1 in mitotic progression through to the SAC.

4.3.2.2 Nucleo-cytoplasmic transport

A range of importins and exportins were pulled down in the IP-MS. Importins and exportins recognise proteins with NLS or NES signals, respectively, and are involved in transporting protein cargos in and out of the nucleus via the NPC and operate by the energy-dependent Ran GTPase nucleo-cytoplasmic transport system (**Figure 1.4**). Their presence along with other components of the RanGTP mechanism for example, RanGAP1 and Nup358/RanBP2 described earlier, suggest that SUN1 is actively transported to the INM by this energy-dependent mechanism or that it has another role in nucleo-cytoplasmic transport. In support of the former idea, SUN2 has a cNLS sequence in its N-terminus which aids targeting of SUN2 to the INM (Turgay *et al.*, 2010).

4.3.2.3 Kinases and phosphatases

As the cell commits to mitosis for the segregation of chromosomes and the production of two daughter cells, the nuclear dynamics of the cell are altered dramatically. This requires mitotic kinase CDK1 and members of the Aurora and PLK families to target a range of substrates and drive progression through mitosis (Nigg, 2001). These events require regulation and once the SAC has deemed the cell fit for mitotic exit, kinases are inactivated and phosphatases steer cell dynamics towards NE reassembly and an interphase cell state (Wurzenberger & Gerlich, 2011).

In the second experimental repeat, a range of kinases and two phosphatases were isolated, which were not seen in the first experiment. Considering that the addition and removal of a phosphate group is a transient event, this could explain the fact that they were only identified in one repeat. As demonstrated in **Chapter 3**, CDK1, together

with its regulatory subunit cyclin B1, mitotically phosphorylates hSUN1 thus, the identification of CDK1 adds further weight to this. PLK1 was another kinase shown to phosphorylate hSUN1 but was not present in the IP-MS data. Surprisingly, Aurora A was also pulled down by hSUN1, despite finding no specific Aurora A phosphorylation sites. Data from *in vitro* kinase assays (**Figure 3.13B**) showed that hSUN1 appears to be phosphorylated at the extreme N-terminal region by Aurora A. This would again indicate that possible Aurora A phosphorylation sites are contained in the sequence not covered by IP-MS analysis and the MS data here supports this idea. Therefore, hSUN1 could still be a substrate for Aurora A kinase.

BUB3 is another mitotic kinase which establishes the stable attachment of kinetochores to microtubules and also inhibits the APC/C when the SAC is operational (Logarinho *et al.*, 2008; Tang *et al.*, 2004). hSUN1 may be a substrate for BUB3 involved in mitotic events promoting or maintaining the SAC.

Casein kinase 1α localises at the centrosomes in interphase and the kinetochore fibres in mitosis and may be involved in chromosome segregation (Brockman *et al.*, 1992). This places casein kinase 1α in close proximity to cytoskeletal networks associated with the LINC complex and further supports a potential role for hSUN1 in mitotic progression.

CDK6 was also identified in this screen. This kinase is not mitosis specific but conversely CDK6, in combination with its regulatory subunit cyclin D, drives the G1 to S transition through phosphorylation thereby inactivating Rb (Meyerson & Harlow, 1994). The presence of this kinase implies that hSUN1 may undergo phosphorylation in

interphase, possibly as part of a signal transduction pathway. Evidence to support this idea comes from data showing that LBR, emerin and lamins are phosphorylated in interphase (Ottaviano & Gerace, 1985; Nikolakaki *et al.*, 1997; Roberts *et al.*, 2006; Tifft *et al.*, 2009). However, we found no evidence of hSUN1 phosphorylation in interphase and CDK6 was detected in the mitotic sample only therefore, this seems unlikely and it could represent a non-specific interactor.

Protein phosphatase 2 (PP2A) was retrieved from the MS data. Protein phosphatase 1 (PP1) was also pulled out by hSUN1 but because of its presence in the GFP negative control it was eliminated from further analysis. Despite finding that many NE components are phosphorylated at the onset of mitosis by various mitotic kinases, there is limited data on the identification of the phosphatases. *In vitro* studies found that PP1 dephosphorylation of emerin and LBR regulates their binding to chromatin upon NE reassembly (Hiraoka *et al.*, 2011). Furthermore, *in vivo* data shows PP1 is required for NE reassembly at the end of mitosis and lamin B dephosphorylation by PP1 is also required to exit mitosis. (Thompson *et al.*, 1997; Tseng & Chen, 2011). Thus, the presence of PP1 and PP2 could play a similar role in dephosphorylating hSUN1 at the end of mitosis to allow reassociation with the nuclear lamina and chromatin.

4.3.2.4 Chromatin-associated proteins

SUN1 co-immunoprecipitated some histone and histone binding/associated proteins. Histones are required for the packaging and ordering of DNA into nucleosomes and are the major component of chromatin. Chromatin also forms direct and indirect interactions with the nuclear lamina and INM proteins (Sullivan *et al.*, 1999; Goldman *et al.*, 2004; Nili *et al.*, 2001; Polioudaki *et al.*, 2001; Mansharamani & Wilson, 2005;

Pyrpasopoulou *et al.*, 1996). The presence of histones suggests that SUN1 may be involved in chromatin organisation at the NE periphery. They could also be the missing anchor for hSUN1 at the INM.

Retinoblastoma binding protein 4 (RBBP4), like hALP, is involved in histone acetylation and chromatin remodelling as well as transcriptional repression and silencing (Chi *et al.*, 2007; Zhang *et al.*, 2000). Heterochromatin protein 1γ (HP1γ) is also involved in transcriptional silencing for heterochromatin structures (Andrulis *et al.*, 1998). This protein mediates the association of heterochromatin with the INM, as it binds LBR (Polioudaki *et al.*, 2001; Ye *et al.*, 1997). Taken together, these proteins could be involved in chromatin organisation in interphase, anchoring heterochromatin at the nuclear periphery as proposed for other NE proteins. *Lmna*$^{-/-}$ mice and fibroblasts from EDMD patients show a loss of peripheral heterochromatin (Sullivan *et al.*, 1999; Zhang *et al.*, 2007). In addition, it may have a role in organisation and dynamics of chromosomes upon mitotic exit, guiding and anchoring heterochromatin to the nuclear periphery through SUN proteins.

Both a histone deacetylase (HDAC 10) and a histone acetyltransferase (HAT1) were present in the mitotic sample alone, indicating a potential mitosis-specific interaction. SUN1 has previously shown to chaperone the acetyltransferase protein hALP to chromatin at the end of mitosis to promote acetylation and decondensation of chromatin (Chi *et al.*, 2007). Therefore, SUN1 may be acting as a chaperone for proteins regulating chromatin through acetylation and deacetylation at the onset and exit of mitosis, respectively.

4.3.2.5 Mitotic proteins

Regulator of chromosome condensation 2 (RCC2), also known as telophase disc-60 (TD-60), was an interesting protein pulled down in the IP-MS screen. It is structurally similar to RCC1 and has numerous roles in mitosis. RCC1 is a guanine nucleotide exchange factor (GEF) for Ran and has a role in nuclear import/export where it maintains a high concentration of RanGTP in the nucleus during interphase. In mitosis RCC1 is involved in regulating the onset of chromosome condensation, the reformation of the NE and the mitosis to G1 transition (Ohtsubo *et al.*, 1987; Zhang & Clarke, 2000; Hetzer *et al.*, 2000). RCC2 is a RacGEF and a component of the chromosomal passenger complex (CPC) which is crucial in regulating the progression from pro-metaphase to metaphase by aligning kinetochores and spindle microtubules correctly and it is also important for the completion of cytokinesis (Yang *et al.*, 2007; Mollinari *et al.*, 2003; Grigera *et al.*, 2012). Possible hSUN1 connections with RCC2 add to the idea that SUN1 could play a role in mitotic progression and NE assembly.

Kinesin family member 20A (KIF20A) is a mitosis-specific plus-end-directed motor protein. It is a substrate for PLK1 and, phosphorylated KIF20A is required for execution of the cleavage furrow and cytokinesis (Neef *et al.*, 2003). A role for hSUN1 in NE reformation for mitotic exit has been favourable from the data but, hSUN1 as part of the LINC complex could possibly aid formation of the actin ring in cytokinesis.

4.3.2.6 Motor proteins

Dynein heavy chain 1 was co-immunoprecipitated from IP-MS samples. It is a minus-end-directed motor protein involved in the motility of vesicles and organelles along microtubules (Morgan, 2006). It is also involved in the formation of the bipolar spindle

(Vaisberg *et al.*, 1993). Its ability to bind microtubules, together with its ATPase activity, generates the force for movement of cargoes along the microtubules. Dynein is involved in retracting the nuclear membranes away from chromosomes after NEBD (Beaudouin *et al.*, 2002; Salina *et al.*, 2002) but it remains elusive as to what it binds on the NE surface. Dynein could dock at the LINC complex to carry out this function.

4.3.2.7 Transcriptional regulator

Four and a half LIM domain protein 2 (FHL2) protein was included in the proteins of interest list as some EDMD patients carry mutations in the related *FHL1* gene, and so the protein could be functionally linked to the LINC complex (Gueneau *et al.*, 2009).

FHL2 is a translational coactivator and acts as a novel molecular transmitter in the Rho signalling pathway. Triggering of the Rho signalling pathway induces translocation of FHL2 to the nucleus to transmit extracellular signals to the nucleus (Ng *et al.*, 2002; Muller *et al.*, 2002). It is probable that FHL2 may transiently bind hSUN1 and that SUN1 may be involved in the same signalling pathway.

In summary, hSUN1 may be involved in a range of novel functions from, chromosome organisation and regulation, mitotic progression as part of the spindle matrix, to roles in late mitosis in NPC and NE reassembly and cytokinesis.

CHAPTER 5
Functional analysis of hSUN1 phosphorylation

Chapter 5 Functional analysis of hSUN1 phosphorylation

5.1 Introduction

In vertebrates, the transition from prophase to prometaphase is defined by NEBD (Foisner, 2003). This involves a series of sequential events reorganising the structure of the NE to allow progression through mitosis. The key events leading up to NEBD are depolymerisation of the nuclear lamina, the dissociation of NE protein interactions and disassembly of NPCs. These changes take place in a timely and orderly fashion, preparing the cell for NEBD.

Immediately before mitosis the nuclear lamina is depolymerised through hyperphosphorylation of all the lamin isoforms, predominantly by serine/threonine mitotic kinase CDK1 (Gerace & Blobel, 1980; Heald & Mckeon, 1990; Luscher *et al.*, 1991; Peter *et al.*, 1990; Ottaviano & Gerace, 1985; Ward & Kirschner, 1990; Kuga *et al.*, 2010). Research has suggested, and some studies have shown, that other kinases act upon lamins and other NE components in mitosis (Luscher *et al.*, 1991; Ward & Kirschner, 1990; Thompson & Fields, 1996). A-type lamins depolymerise in prophase before depolymerisation of B-type lamins in metaphase, suggesting firstly that there are two independent networks rather than one interweaved arrangement and secondly, that B-type lamins have a more prevalent role in mitosis (Georgatos *et al.*, 1997).

Likewise, nucleoporins are phosphorylated for disassembly of the NPC to allow mixing of the nucleoplasmic and cytoplasmic proteins (Laurell *et al.*, 2011; Dultz *et al.*, 2008). In *D.melanogaster* it has been shown that NPC disassembly precedes nuclear lamin

phosphorylation *(Katsani et al., 2008).* Mitosis-specific phosphorylation of gp210, a membrane embedded nucleoporin, dissociates it from the NPC (Onischenko *et al.*, 2007), while phosphorylation of four of the Nup107-160 subcomplex components does not disrupt interactions within the subcomplex but is thought to regulate binding with other Nups in the NPC structure or other interacting proteins (Glavy *et al.*, 2007). A key event in preparation for NEBD is the hyperphosphorylation of Nup98 by CDK1, PLK1 and Nek kinases which results in the increased permeabilisation of the NE (Laurell *et al.*, 2011).

In addition, integral INM proteins LAP1, LAP2, LBR, emerin, MAN1 and p54 are all mitotically phosphorylated, which detaches the INM from the nuclear lamina and chromatin, further weakening the NE in preparation for NEBD and promoting chromatin condensation (Foisner & Gerace, 1993; Pfaller *et al.*, 1991; Courvalin *et al.*, 1992; Hirano *et al.*, 2005; Hirano *et al.*, 2009; Bailer *et al.*, 1991)(Foisner & Gerace, 1993; Courvalin *et al.*, 1992; Hirano *et al.*, 2009).

In interphase, SUN1 is retained at the NE by interactions with other NE and nuclear proteins. This makes it highly insoluble and immobile (Ostlund *et al.*, 2009; Haque *et al.*, 2006; Lu *et al.*, 2008). Chapter 3 established that hSUN1 is phosphorylated at the onset of mitosis at three sites in the N-terminus by CDK1 and PLK1. My hypothesis states that the likely role of hSUN1 phosphorylation is to contribute to the timely disassembly of the nuclear lamina, and also the LINC complex. This is not to say it has no function during mitosis, on the contrary, SUN1 is required for the decondensation of chromosomes on the reforming NE at the end of mitosis (Chi *et al.*, 2007). The aim of this chapter was to determine the role of hSUN1 mitotic phosphorylation and to test

my hypothesis that phosphorylation promotes disassembly of hSUN1-containing NE complexes in mitosis to aid NEBD.

5.2 Results

5.2.1 hSUN1 phospho-mimetic mutants are expressed at equivalent levels to wild-type hSUN1 in U2OS asynchronous cell extracts

In order to look more closely at the hSUN1 phosphorylation sites and their function *in vivo*, myc-tagged mammalian expression vectors containing hSUN1 phospho-mimetic mutants were constructed. S48, S138 and S333 were mutated, converting the serine to an aspartic acid residue, to mimic the negative charge of the phosphorylated serine. hSUN1 phospho-mimetic mutants containing a single mutated site, as well as a double phospho-mimetic mutant (2D) corresponding to the two CDK1 sites (S48 and S333), and a triple phospho-mimetic mutant (3D) were generated, analogous to the phospho-deficient mutants described in **section 3.2.12** (**Figure 5.1A**).

All phospho-mimetic constructs were transiently transfected into U2OS cells. Total cell extracts were resolved by SDS-PAGE and western blots were probed with anti-c-myc and anti-β-actin antibodies (**Figure 5.1B**). As previous experiments had used HeLa cells, the phospho-deficient mutants were also examined in U2OS cells, alongside the phospho-mimetic mutants, to confirm that the cell type was not affecting exogenous protein expression. Protein expression for all phospho-mimetic and phospho-deficient mutants was comparable to wild-type hSUN1, showing that mutation of the phosphorylation sites individually or in combination does not affect protein expression (**Figure 5.1B**). Also, the cell line used has no effect on relative protein expression.

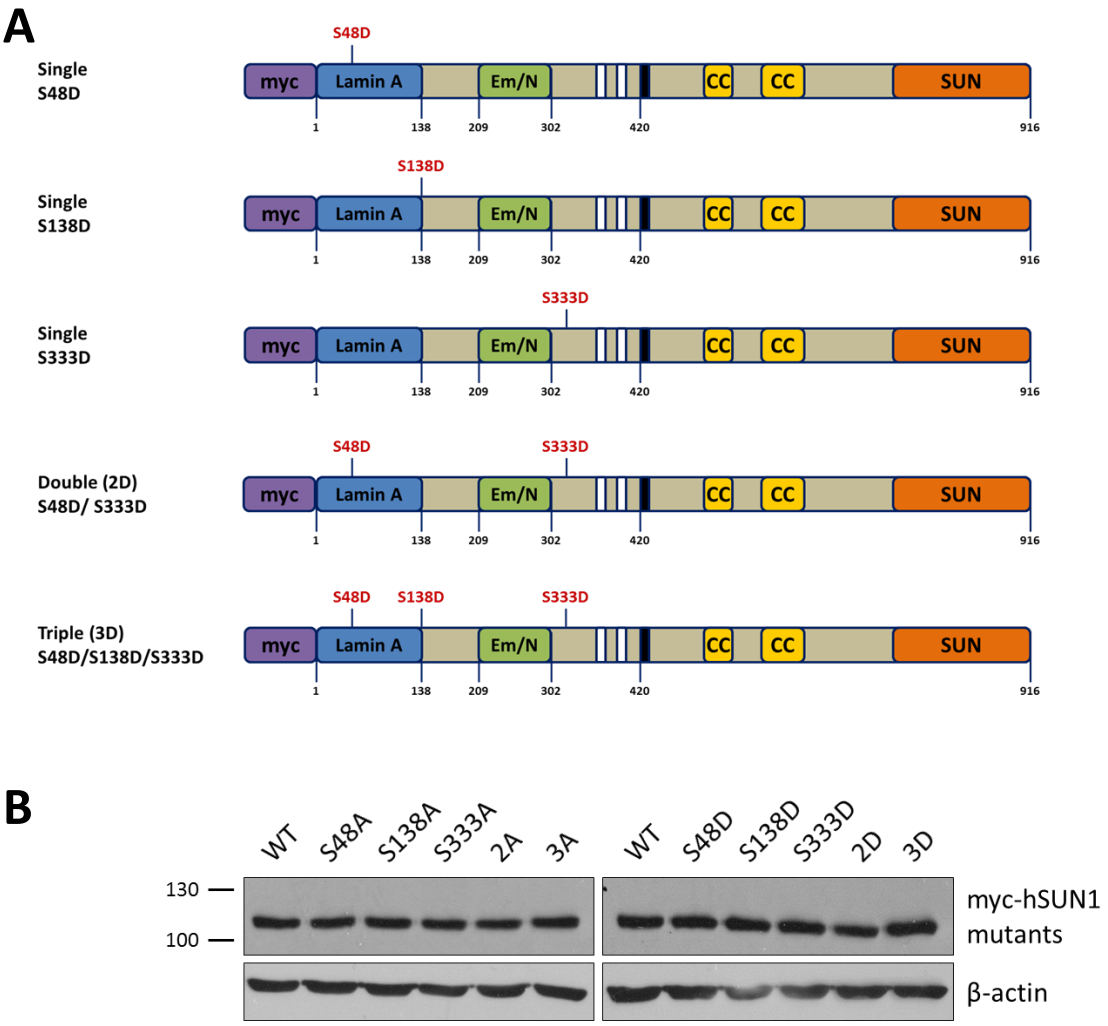

Figure 5.1. Expression of hSUN1 phospho-deficient and phospho-mimetic mutants in U20S cells.

(A) Schematic representation of phospho-mimetic mutants made. Serine to aspartic acid substitutions were made at each of the identified hSUN1 mitotic phosphorylation sites. Myc-tagged single phospho-mimetic mutants corresponding each of the three hSUN1 mitotic phosphorylation sites, as well as double phospho-mimetic mutants targeting the two CDK1 phosphorylation sites (2D) and a triple phospho-mimetic mutant encompassing all three sites (3D) were generated. Positions of mutations in the myc-tagged hSUN1 protein sequence are indicated. **(B)** Total cell lysates from asynchronous U20S cells transiently transfected with pLEICS20 myc-tagged phospho-deficient mutants (S>A) or pLEICS20 myc hSUN1 phospho-mimetic mutants (S>D) were resolved by SDS-PAGE and immuno-blotted with anti-c-myc and anti-β-actin antibodies. Molecular weights (kDa) are indicated.

5.2.2 hSUN1 phospho-mimetic mutants have reduced association with the NE

As hSUN1 is immobilised at the NE through various protein interactions, we predicted that phosphorylation disrupts these interactions. I therefore wanted to determine whether hSUN1 phospho-mimetic mutants were less efficiently retained at the NE than the wild-type protein. Both the hSUN1 phospho-mimetic and phospho-deficient mutants, along with wild-type hSUN1 were each transiently transfected into U2OS cells adhered to coverslips. Twenty-four hours post-transfection, coverslips were fixed in methanol and cells were co-stained with anti-c-myc antibody to visualise the mutants and DAPI to stain the DNA.

All phospho-deficient mutants efficiently localised to the NE, as expected, because the mutants should have behaved like interphase hSUN1 (**Figure 5.2A**), as previously observed in HeLa cells (**Figure 3.17B**). The hSUN1 phospho-mimetic mutants were also localised at the NE but in some cells a proportion was mislocalised to the cytoplasm, presumably the ER. This was particularly evident for the hSUN1 S48D, 2D and 3D mutants, whilst S138D caused a milder mislocalisation and S333D had no obvious effect on hSUN1 localisation to the NE (**Figure 5.2A**).

To confirm these observations and quantify the degree of mislocalisation, fluorescence intensity measurements were performed to calculate the relative fluorescence in the cytoplasm verses the DAPI-stained nucleus. Over 2500 cells were analysed in two independent experiments and analysis confirmed that the ratio of cytoplasmic:nuclear distribution was higher for the hSUN1 phospho-mimetic S48D, 2D and 3D mutants compared to wild-type and phospho-deficient mutants. Moreover, the mislocalisation of hSUN1 S48D, 2D and 3D proved to be highly statistically significant by student t-test

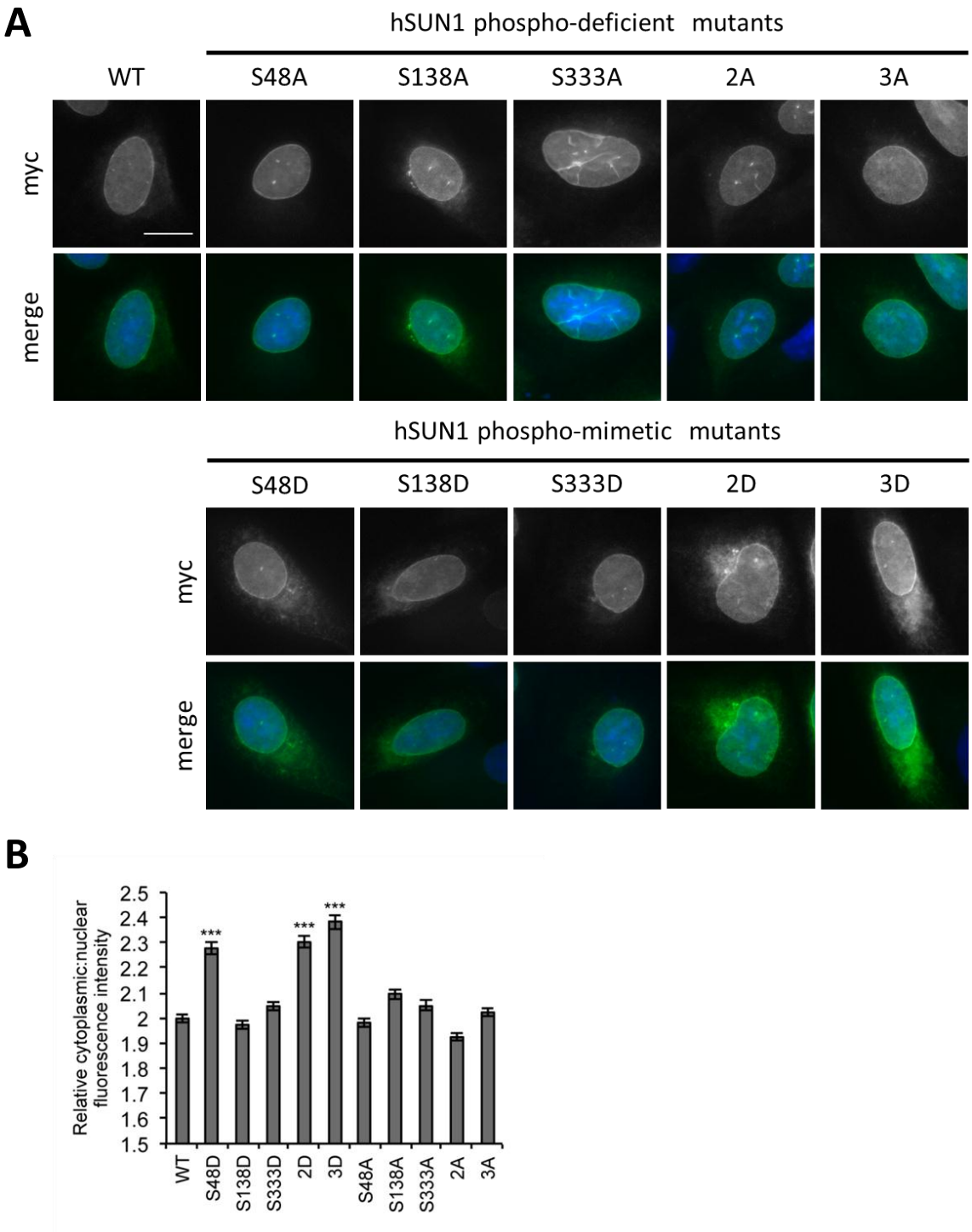

Figure 5.2. hSUN1 phospho-mimetic mutants have reduced association with the NE.

(A) U2OS cells grown on coverslips were transiently transfected with the indicated wild-type (WT), myc-tagged phospho-deficient or phospho-mimetic mutant constructs for 20 h, fixed in methanol and co-stained with anti-c-myc antibody and DAPI. Representative images are shown. Scale bar, 10 µm. **(B)** Quantification of the relative cytoplasmic versus nuclear total fluorescence intensity for the mutants shown in **A**, (n≥2500 from two independent experiments; +/- s.e.m.) *** represents *P* value <0.0001 when compared to WT.

(**Figure 5.2B**). In contrast, hSUN1 S138D and S333D mutants were not significantly mislocalised. This reveals that hSUN1 S48 phosphorylation site is the major contributor to reduced retention at the INM.

5.2.3 hSUN1 phospho-mimetic mutants have increased solubility

hSUN1 is highly insoluble in interphase cells (Haque *et al.*, 2006) but my data indicate that phosphorylated hSUN1 is less efficiently retained at the NE. I next wanted to determine whether, like lamins, phosphorylation changes the solubility of hSUN1. HeLa cells were transiently transfected with pLEICS20 myc-hSUN1 WT, 2D or 3D. Twenty-four hours post-transfection cells were collected by trypsinisation and incubated in low salt (50 mM) or high salt (500 mM) extraction buffers. The insoluble pellet (P) fraction was separated from the soluble supernatant (S) fraction by centrifugation. Total cell extracts, pellet and supernatant fractions were resolved by SDS-PAGE and immuno-blotted with anti-c-myc antibody (**Figure 5.3A**).

Wild-type hSUN1 was highly insoluble under both salt conditions with 9% and 29% soluble in low and high salt concentrations, respectively. As expected, hSUN1 phospho-deficient 3A mutant behaved like the wild-type protein. In contrast, hSUN1 phospho-mimetic 3D mutant showed a two-fold increase in solubility at both high and low salt conditions which was statistically significant, in comparison to wild-type hSUN1 (**Figure 5.3B**). These results indicate that phosphorylation of these three sites leads to increased solubility of mitotic hSUN1.

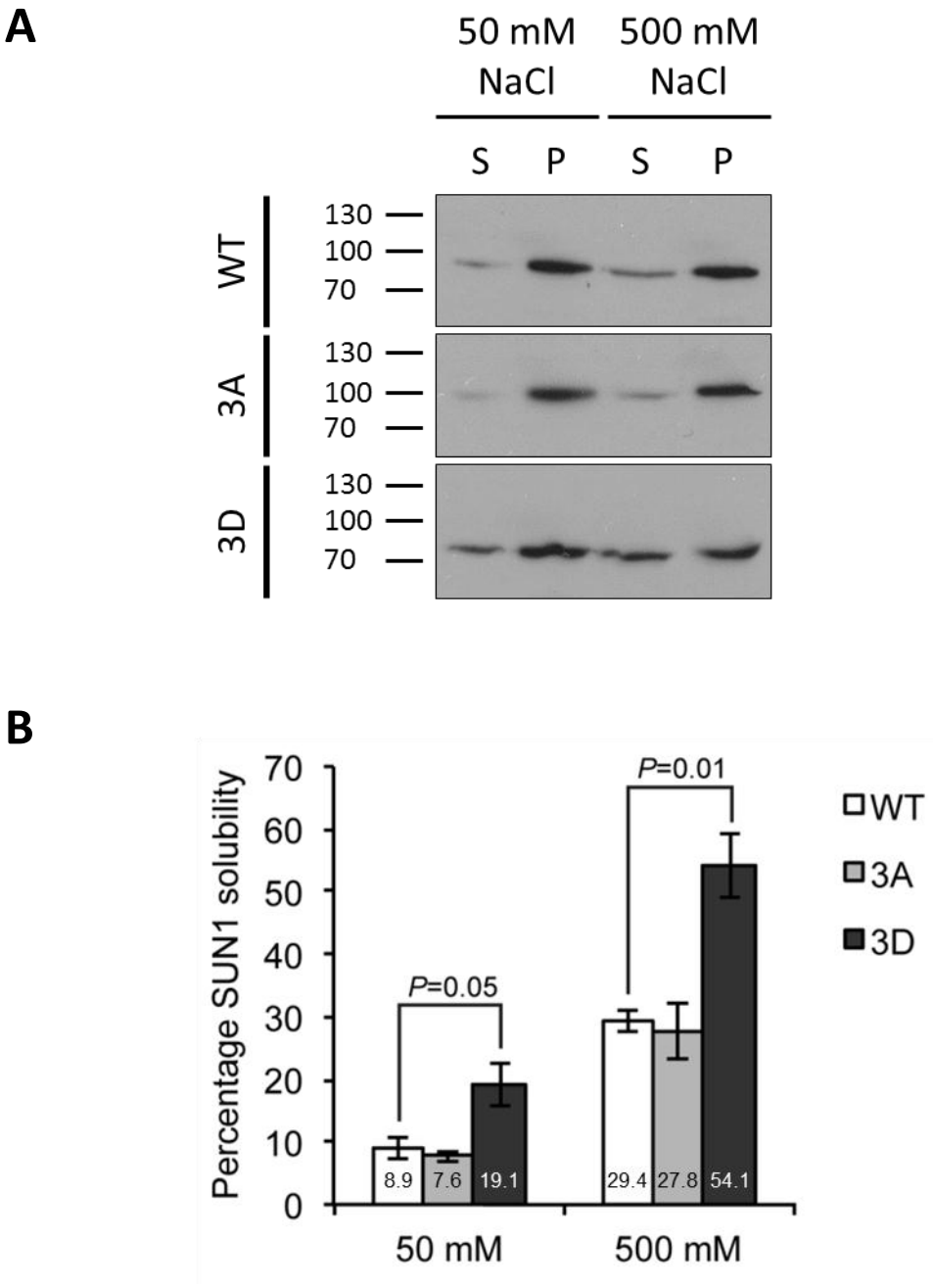

Figure 5.3. The hSUN1 triple phospho-mimetic mutant is more soluble than wild-type hSUN1.

(A) HeLa cells were transiently transfected with hSUN1 wild-type (WT), triple phospho-deficient (3A) or triple phospho-mimetic (3D) mutants and proteins were extracted using buffer containing 50mM or 500mM NaCl. Following centrifugation, supernatants (S) and pellets (P) were immuno-blotted and probed with anti-c-myc antibody to determine protein solubility. **(B)** Densitometric analysis of panel **A**, showing the percentage of protein in the supernatant, representing the soluble fraction. Exact percentage values are indicated (n=3; +/- s.e.m.).

5.2.4 hSUN1 mitotic phosphorylation partially disrupts LINC complex interactions

I have shown that the three mitotic phosphorylation sites of hSUN1 contribute to its reduced association with the NE and increased solubility. These findings suggested that hSUN1 phosphorylation may disrupt interactions that anchor hSUN1 at the NE. With this in mind, I wanted to observe the state of hSUN1 interactions with known binding partners in mitosis. Initially, I examined hSUN1 interactions with emerin and lamin A/C; these proteins are known to interact with the nucleoplasmic N-terminal domain of SUN1. HeLa cells were mitotically arrested and cells were collected by mechanical shake-off. In a parallel plate, HeLa cells were cultured asynchronously and collected by scraping plates. Soluble lysates were subjected to IP with 2 µg of anti-hSUN1 2383 antibody. Soluble lysates and IPs were then resolved by SDS-PAGE and western blots were probed with anti-hSUN1 Atlas, anti-lamin A/C and anti-emerin GM antibodies (**Figure 5.4**).

The hSUN1 blot confirmed that the characteristic hSUN1 band-shift was present in the sample treated with nocodazole only and that hSUN1 was successfully immunoprecipitated from both samples. Probing with anti-lamin A/C and anti-emerin antibodies confirmed previous findings that these proteins interact with hSUN1 in asynchronous cells, but, strikingly, all three proteins were absent from mitotic hSUN1 IP samples (**Figure 5.4**). This indicates that phosphorylated hSUN1 disassociates from its known nucleoplasmic binding partners, lamin A/C and emerin, in mitosis.

Various nesprin isoforms bind hSUN1 at its N- and C-termini (**Figure 1.7B**) and therefore these interactions were also examined in mitotic extracts. Due to the complexity of nesprin isoforms, antibodies that reliably detect specific isoforms are not

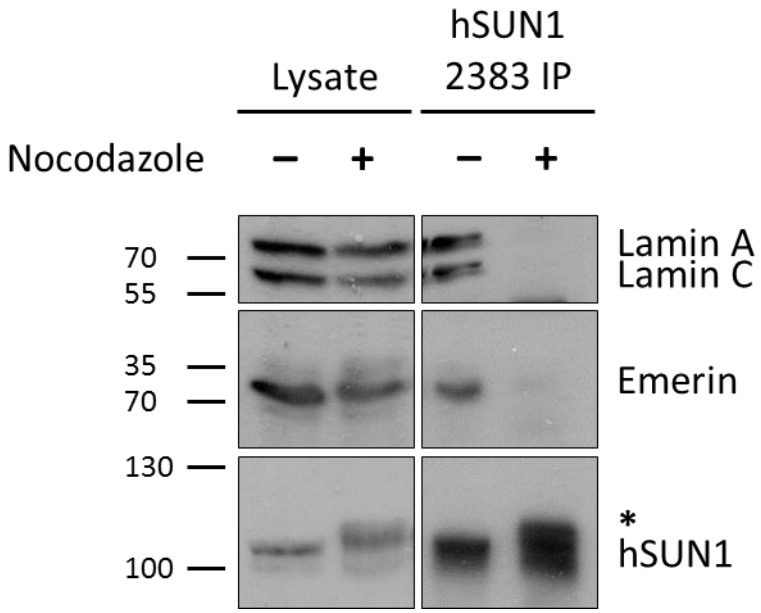

Figure 5.4. hSUN1 loses its interactions with N-terminal binding partners lamin A/C and emerin in mitosis.

Asynchronously growing HeLa cells were mitotically arrested with nocodazole and subjected to co-IP with 2 µg of anti-hSUN1 2383 antibody. Soluble lysate fractions and the final IP sample were resolved by SDS-PAGE and immuno-blotted with anti-lamin A/C, anti-emerin GM and anti-hSUN1 Atlas antibodies. * indicates the hSUN1 band-shift. Molecular weights (kDa) are indicated.

readily available, hence these proteins were expressed exogenously as in previous studies (Haque *et al.*, 2010; Haque *et al.*, 2006) (**Figure 5.5A**).

HeLa cells were transiently transfected with pEGFP nesprin-2α or pEGFP C1, as a negative control, and then nocodazole treated. In parallel plates, HeLa cells were cultured asynchronously. Mitotically arrested cells were collected by mechanical shake-off while non-treated cells were collected by scraping plates. Soluble lysates were subjected to IP with 2µg anti-hSUN1 2383 antibody. Soluble lysates and IPs were resolved by SDS-PAGE and immuno-blotted with anti-hSUN1 Atlas and anti-GFP antibodies (**Figure 5.5B**).

The hSUN1 mobility-shift was evident in both lysate and IP samples. GFP was not present in the IP samples, as expected, as it is not a hSUN1 binding partner. Interestingly, GFP-nesprin-2α was present in both asynchronous and mitotic IP lanes, indicating that nesprin-2α maintains its interaction with hSUN1 in mitosis (**Figure 5.5B**). Nesprin-2α has been shown to interact with both N- and C-termini of SUN1 (Haque *et al.*, 2010; Haque *et al.*, 2006) depending on whether it is located at the ONM or INM.(**Figure 1.7B** and **Figure 5.5**). If positioned at the ONM, the C-terminal KASH-domain of nesprin-2α interacts with the C-terminal SUN-domain of SUN1. If nesprin-2α is at the INM, interactions between nesprin-2α and SUN1 are via their N-termini (Haque *et al.*, 2010).

The experiment performed in **Figure 5.5** did not determine whether nesprin-2α retained its interactions with both termini of hSUN1 during mitosis. To address this question, the same IP procedure was carried out on mitotically arrested HeLa cells

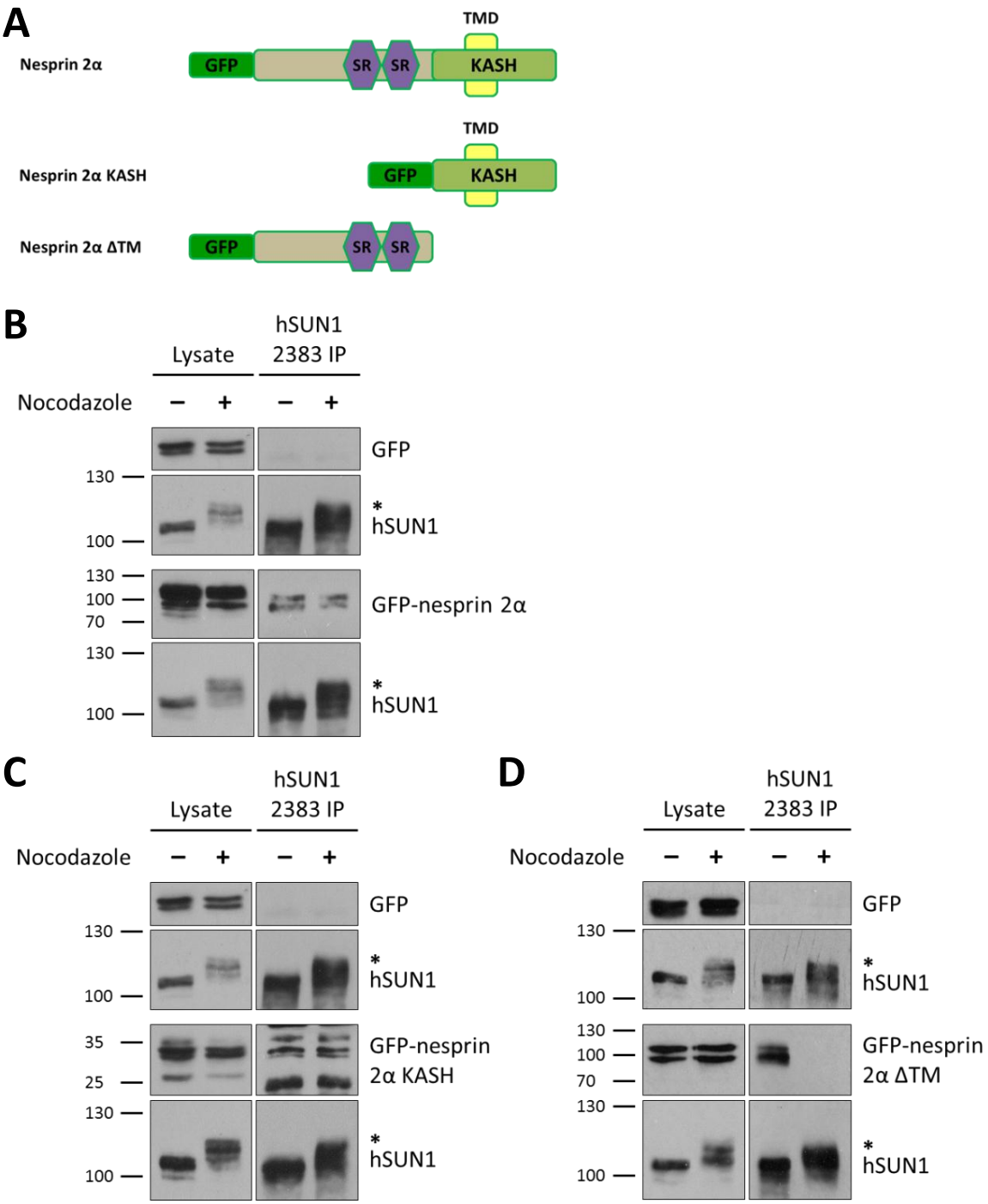

Figure 5.5. hSUN1 loses its interaction with nesprin-2α at its N-terminus but not its C-terminus during mitosis.

(A) Schematic diagram of the nesprin constructs used in this study. The spectrin repeats (SR) and transmembrane domain (TMD) are indicated. **(B)** Asynchronously growing HeLa cells were transiently transfected with pEGFP C1 or pEGFP nesprin-2α and mitotically arrested. Soluble lysates were were subjected to co-IP with 2 µg of anti-hSUN1 2383 antibody. Soluble lysate fractions and the final IP sample were resolved by SDS-PAGE and immuno-blotted with anti-GFP and anti-hSUN1 Atlas antibodies. **(C** and **D)** Asynchronously growing HeLa cells were transiently transfected with pEGFP and either pEGFP nesprin-2α KASH **(C)** or pEGFP nesprin-2α ΔTM **(D)** and processed as described in **B**. Four 10cm culture dished were used per condition. Molecular weights (kDa) are indicated.

transiently transfected with nesprin-2α deletion constructs encoding just the KASH-domain (pEGFP nesprin-2α KASH) or the N-terminus only (pEGFP nesprin-2α ΔTM) (**Figure 5.5A**). After IP with anti-hSUN1 Atlas antibody, the nesprin-2α deletion mutants were detected with anti-GFP antibody as shown in **Figure 5.5C**. Nesprin-2α KASH was present in both asynchronous and mitotic IP lanes indicating that the lumenal SUN domain-KASH domain interaction is maintained during mitosis (**Figure 5.5C**). In contrast, nesprin-2α ΔTM was present in the asynchronous but not the mitotic lane (**Figure 5.5D**). These findings indicate that the LINC complex, formed between the hSUN1 C-terminus and the nesprin-2α KASH-domain, remains intact during mitosis while the interaction between the nucleoplasmic N-termini is lost. This supports the notion that mitotic hSUN1 phosphorylation within its N-terminus disrupts interactions occurring at the nucleoplasmic face of the NE.

5.2.5 hSUN1 novel interaction with NET5 is maintained in mitosis

As described in **section 4.2.1.1**, co-IP experiments established an interaction between SUN1 and NET5/SAMP1C, a novel NE protein. I was therefore interested to determine whether this interaction was disrupted in mitosis. HeLa cells were transiently transfected with pEGFP NET5 FL or pEGFP C1 and then mitotically arrested. Soluble lysates were subjected to IP with 2 µg anti-hSUN1 2383 antibody. Soluble lysates and IPs were resolved by SDS-PAGE and immuno-blotted with anti-hSUN1 Atlas and anti-GFP antibodies (**Figure 5.6**).

Probing of lysates confirmed equal expression of each protein in both asynchronous and mitotic samples. NET5 was co-immunoprecipitated with hSUN1 in the asynchronous lane supporting previous findings with hSUN1 (**Figure 4.1C**). Surprisingly,

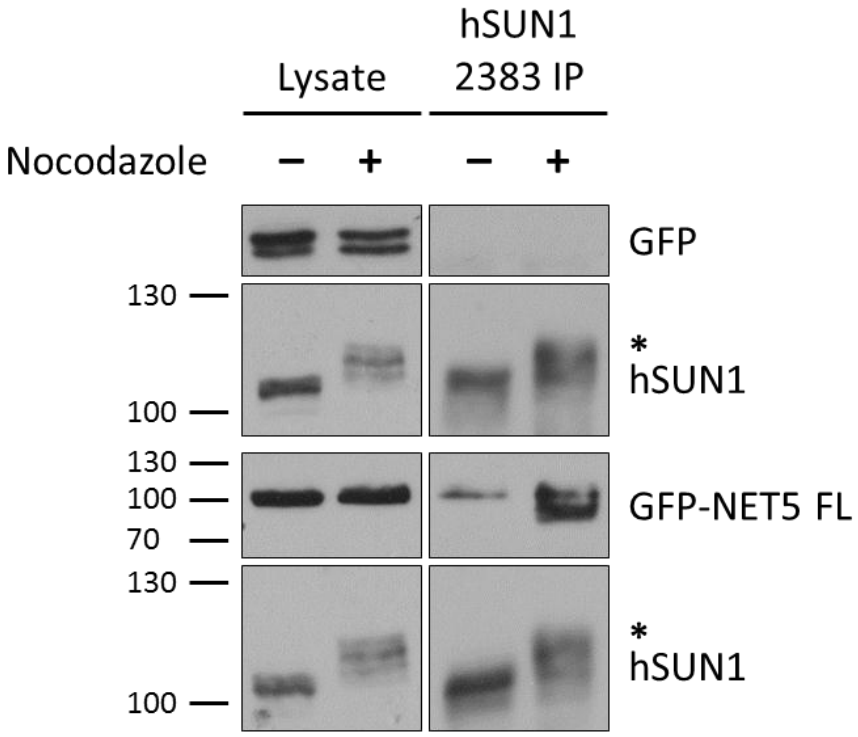

Figure 5.6. hSUN1 maintains its interactions with novel binding partner NET5 in mitosis.

Asynchronously growing HeLa cells were transiently transfected with pEGFP C1 or pEGFP NET5 FL and mitotically arrested. Soluble lysates were subjected to co-IP with 2 µg of anti-hSUN1 2383 antibody. Soluble lysate fractions and the final IP sample were resolved by SDS-PAGE and immuno-blotted with anti-GFP and anti-hSUN1 Atlas antibodies. Molecular weights (kDa) are indicated.

NET5 was also present in the mitotic lane, showing that the interaction is maintained in mitosis. Moreover, the band was more intense and appeared as a doublet, with the second band migrating faster than the band observed in the asynchronous lane (**Figure 5.6**). Therefore, these data show that NET5/SAMP1C-hSUN1 interaction is maintained with higher affinity in mitosis and suggest that NET5 undergoes a post-translational modification in mitosis.

5.2.6 hSUN1 phospho-mimetic mutants maintain interactions with lamin A/C and emerin in asynchronous conditions

The findings so far have shown that hSUN1 loses interaction with lamin A/C, emerin and the N-terminus of nesprin-2α during mitosis. The next step was to investigate the importance of the three identified mitotic hSUN1 phosphorylation sites in regulating these interactions by using hSUN1 phospho-deficient 3A and hSUN1 phospho-mimetic 3D mutants. The phospho-mimetic mutant should mimic mitotic hSUN1 and therefore I expected to see a loss of interaction even in asynchronous cells. The phospho-deficient mutant acted as a control as it behaves like interphase hSUN1. HeLa cells were transiently transfected with pEGFP C1 and pLEICS21 myc-hSUN1 WT, 3A or 3D. Soluble lysates subjected to IP using the GFP-Trap® system. Soluble lysates and GFP-Trap® samples were resolved by SDS-PAGE and immuno-blotted with anti-GFP, anti-lamin A/C and anti-emerin GM antibodies (**Figure 5.7**).

As expected lamin A/C and emerin were co-immunoprecipitated with hSUN1 WT and the hSUN1 phospho-deficient 3A mutant but not GFP alone. However, there was no loss of interaction with the hSUN1 phospho-mimetic 3D mutant. These results suggest that hSUN1 phosphorylation at S48, S138 and S333 does not disrupt binding to lamin

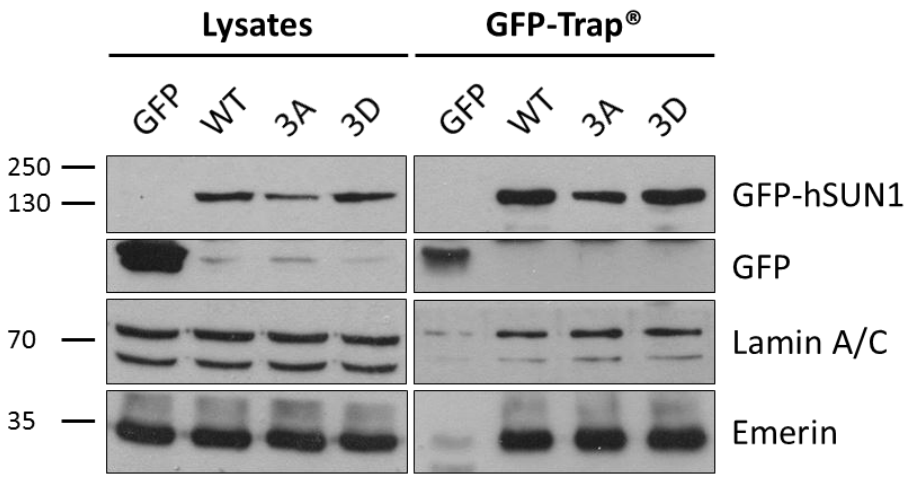

Figure 5.7. hSUN1 triple phospho-mimetic mutant still binds its known N-terminal binding partners lamin A/C and emerin in asynchronous conditions.

HeLa cells were transiently transfected with pEGFP C1 or pLEICS21 GFP-hSUN1 WT, 3A or 3D. Soluble lysates were processed using the GFP-Trap® protocol. Soluble lysate fractions and the final GFP-Trap® sample were resolved by SDS-PAGE and immuno-blotted with anti-GFP, anti-lamin A/C and anti-emerin GM antibodies. Molecular weights (kDa) are indicated.

A/C and emerin (**Figure 5.7**). These results conflict with earlier findings and suggest that phosphorylation of lamin A/C and emerin may also be required for loss of interaction.

5.2.7 hSUN1 triple phospho-mimetic mutant maintains self-interaction in asynchronous conditions

Several studies have shown that SUN proteins are capable of oligomerisation with one study suggesting dimer and tetramer states (Lu *et al.*, 2008). Conversely x-ray crystallography studies reveal that the SUN-domain of SUN2 exists as a trimer (Zhou *et al.*, 2012b; Sosa *et al.*, 2012). As an alternative to the experiments described above in **section 5.2.6**, I wanted to determine whether this self-interaction is disrupted by hSUN1 phosphorylated S48, S138 and S333. HeLa cells were co-transfected with GFP- or myc-tagged hSUN1 constructs or with GFP alone as indicated in **Figure 5.8**. Soluble lysates were subjected to IP with 2 µg anti-c-myc antibody. Soluble lysates and IP samples were resolved by SDS-PAGE and immuno-blotted with anti-c-myc and anti-GFP antibodies.

Myc-tagged proteins expressed evenly in the lysate fractions, unlike the GFP-tagged proteins which were very poorly expressed. This could be due to competition between myc- and GFP-tagged constructs for incorporation and expression in HeLa cells. Unfortunately, GFP-hSUN1 was not detected in any of the IP samples including the positive control (myc-hSUN1 WT and GFP-hSUN1 WT) (**Figure 5.8A**). The reciprocal experiment was therefore carried out using GFP-Trap® to concentrate the GFP-tagged hSUN1 proteins. Soluble lysates and GFP-Trap® samples were resolved by SDS-PAGE

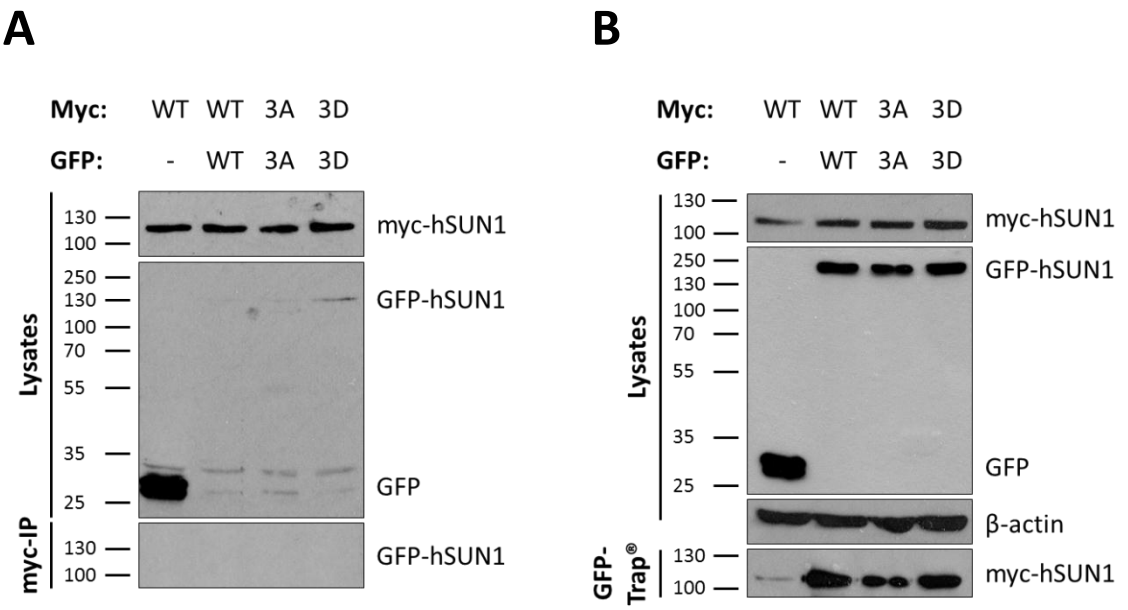

Figure 5.8. hSUN1 triple phospho-mimetic mutant maintains self-interaction in asynchronous conditions.

(A) HeLa cells were transiently co-transfected with myc- or GFP-tagged hSUN1 constructs or with GFP alone (-), as indicated. Soluble lysates were subjected to co-IP with 2 µg of anti-c-myc antibody. Soluble lysate fractions and the final IP sample were resolved by SDS-PAGE and immuno-blotted with anti-c-myc and anti-GFP antibodies. **(B)** Samples were prepared as described in **A** but were processed using the GFP-Trap® protocol. Soluble lysate fractions and the final GFP-Trap® sample were resolved by SDS-PAGE and immuno-blotted with anti-c-myc and anti-GFP antibodies. Molecular weights (kDa) are indicated.

and immuno-blotted with anti-c-myc, anti-GFP and anti-β-actin antibodies (**Figure 5.8B**).

On this occasion, lysates showed good protein expression for both myc- and GFP-tagged hSUN1 WT and mutant proteins. The β-actin blot confirmed equal protein loading. The GFP-Trap® samples showed that wild-type and hSUN1 phospho-deficient 3A mutant were capable of self-interaction, but the hSUN1 phospho-mimetic 3D mutant was equally able to self-interact (**Figure 5.8B**). This result implies that oligomerisation is not disrupted by the three phosphorylation sites. However, other potential phosphorylation sites not covered by the *in vivo* and *in vitro* analysis may well do.

5.3 Discussion

A key event in preparing the cell for NEBD is the global phosphorylation of NE components where mitotic kinases act to depolymerise the nuclear lamina, disassemble the NPCs and disassociate integral membrane proteins from chromatin, the nuclear lamina and from each other. Research in the field has focused on the role of phosphorylation in NEBD but it is unknown whether other post-translational modifications which may also contribute to NEBD.

After establishing that hSUN1 is mitotically phosphorylated, I explored the role of this phosphorylation and found that phosphorylation partially released hSUN1 anchorage from the NE.

5.3.1 Phosphorylated hSUN1 has increased solubility and reduced association with the NE

As a first step in analysing the role of hSUN1 mitotic phosphorylation, I observed the subcellular localisation of hSUN1 phospho-deficient and phospho-mimetic mutants. Whilst all phospho-deficient mutants remained fully localised at the NE, several myc-tagged phospho-mimetic mutants showed a population of hSUN1 in the cytoplasm (**Figure 5.2A**). Quantification of fluorescence intensity showed all mutants containing S48D (i.e. myc-hSUN1 S48D, 2D and 3D) had a statistically significant increase in cytoplasmic hSUN1 staining. In contrast, S138D and S333D did not significant increase cytoplasmic hSUN1 localisation compared to wild-type (**Figure 5.2B**). Thus, phosphorylation of S48 appears to be the major contributor to hSUN1 relocalisation to the cytoplasm. A possible explanation for this relocalisation could be due to loss of anchorage to the INM. This would result in proteins being more mobile and so

diffusing back to the ER via the POM and suggests loss of interactions for retention at the INM. In support of this, LBR was shown to relo(Ellenberg *et al.*, 1997)

calise to the ER prior to NEBD (Ellenberg *et al.*, 1997).

Some protein was still visible at the NE (**Figure 5.2B**) since the ONM is a continuation of the ER so proteins can randomly diffuse to the INM too. SUN1 exists as an oligomer (Lu *et al.*, 2008) and localisation patterns in this experiment suggest oligomerisation was occurring between endogenous and exogenous hSUN1 proteins. It would be interesting to see whether depleting endogenous hSUN1 and transfection of siRNA resistant hSUN1 phospho-mimetic mutants containing S48 were able to deliver a more prominent phenotype.

A similar redistribution of endogenous hSUN1 from the NE to the ER in prophase was not noted by Chi *et al.* (2007), however, this study used a splice variant of hSUN1 lacking exons 7-8 (encoding residues 220-286), whilst studies in this thesis have applied the full-length hSUN1 (residues 1-916) to experiments, hence localisation patterns may differ between isoforms. It would be interesting to follow and observe the hSUN1 full-length isoform through mitosis by fluorescence microscopy.

Phosphorylation of the nuclear lamina (Gerace & Blobel, 1980; Luscher *et al.*, 1991; Peter *et al.*, 1990; Ward & Kirschner, 1990; Kuga *et al.*, 2010) and INM proteins (Bailer *et al.*, 1991) converts them from detergent-resistant to detergent-extractable, hence increasing their solubility. SUN1 is a highly insoluble INM protein when anchored at the NE in interphase (Ostlund *et al.*, 2009; Haque *et al.*, 2006) but little is known about its dynamic nature in mitosis. Low/high salt extraction experiments with the myc-tagged

hSUN1 triple phospho-deficient and phospho-mimetic mutants showed that like myc-hSUN1 WT, myc-hSUN1 3A was mainly in the insoluble pellet fraction with only a 7.6% (low)/27.8% (high) of the protein solubilising to the supernatant (**Figure 5.3**). However, myc-hSUN1 3D had a statistically significant shift from the insoluble pellet fraction to the soluble supernatant fraction (**Figure 5.3B**). Thus, like lamins, phosphorylated hSUN1 is more readily extracted than wild-type (Gerace & Blobel, 1980; Luscher *et al.*, 1991; Peter *et al.*, 1990; Ottaviano & Gerace, 1985; Ward & Kirschner, 1990). Data from the myc-hSUN1 3D mutant showing increased solubility and reduced NE localisation support the notion that phosphorylation of SUN1 dissociates it from its anchoring protein network in preparation for NEBD.

5.3.2 The LINC complex is partially disassembled in mitosis

Data from the solubility experiments suggested that hSUN1 protein interactions in interphase are no longer maintained in mitosis. Lamin A/C, emerin and nesprins are known SUN1 binding partners. Lamin A/C binds at the extreme N-terminus of hSUN1 at residues 1-138 in the nucleoplasm, while the emerin and nucleoplasmic domains of small nesprin isoform binding sites are further downstream between residues 209-302 (Haque *et al.*, 2010) (**Figure 1.7B** and **Figure 1.10**). Whether emerin and nesprin compete for this binding site remains unknown. SUN proteins also bind the KASH-domain of nesprins via its SUN-domain in the PNS (Crisp *et al.*, 2006; Padmakumar *et al.*, 2005; Haque *et al.*, 2006).

A series of co-IP experiments with endogenous hSUN1 showed that mitotic, but not asynchronous, hSUN1 lost binding with its N-terminal binding partners lamin A/C, emerin and small nesprin isoforms (**Figure 5.4** and **Figure 5.5D**). Two of the three

identified hSUN1 mitotic phosphorylation sites, S48 and S138, lie within and at the very end of the lamin A/C binding site, respectively, while S333 does not lie in any mapped binding region (**Figure 5.1A**). It is possible that S48 and S138 directly disrupt the binding site for lamin A/C whilst S333 phosphorylation (or even phosphorylation of all three sites) could change the hSUN1 protein conformation, thereby indirectly disrupting protein interactions.

Interestingly the interaction between the nesprin-2α KASH-domain and hSUN1 SUN-domain was maintained (**Figure 5.5B** and **Figure 5.5C**). This was perhaps anticipated as this interaction occurs in the PNS, which is inaccessible to mitotic kinases and it is unlikely that the conformational changes occurring in the N-terminus would be transmitted to the C-terminus. This highlights that N-terminal hSUN1 interactions are dispensable in mitosis and suggests that the C-terminal SUN-KASH complex interaction may play a role during mitosis. This is supported by the fact that nesprin-1 giant remains associated with the NE in prophase (Zhen *et al.*, 2002).

Experiments with the hSUN1 3D mutant tried to emulate the loss of binding with lamin A/C and emerin seen with the endogenous hSUN1, in order to confirm the involvement of the three identified phosphorylation sites in regulating these interactions. However, co-IPs failed to show a loss of binding (**Figure 5.7**). The endogenous hSUN1 co-IP was carried out using mitotic extracts, while the myc-hSUN1 3D IP was performed in asynchronous conditions. The conflict in experimental findings suggests that phosphorylation of one component of the protein network is insufficient for detachment. It is possible that SUN1, lamin A/C and emerin all need to be phosphorylated to disassemble the protein network. It would be interesting to observe

myc-hSUN1 3A binding in mitotic extracts, where global phosphorylation of the NE has occurred. If the interactions were maintained it would indicate that the three identified phosphorylation sites were responsible for loss of lamin A/C and emerin binding in mitosis, alternatively, if the interactions were lost it would suggest that other unidentified phosphorylation sites are possibly causing the disruptions. Another possible explanation could be that the phospho-mimetic mutant is not causing the same conformational change as seen upon true phosphorylation. Alternative phospho-mimetic mutants could be generated substituting the serines for glutamic acid residues. To date, there has been no data on the loss of protein interactions at the NE with phospho-mimetic mutants. Point mutations in two lamin phosphorylation sites flanking the rod-domain induced nuclear lamina disassembly but these sites were not purposely mutated to mimic phosphorylation (Heald & Mckeon, 1990).

There is the possibility that not all hSUN1 phosphorylation sites have been identified by MS. UniProtKB proposed serine 52 (S52) as a hSUN1 phosphorylation site but this was not detected by IP-MS due to the lack of coverage of this region, furthermore, there may be undiscovered phosphorylation sites in the sequence not covered by MS analysis. To fully identify hSUN1 phosphorylation sites, peptides of sequence not covered previously could be constructed with a cleavable tag and either expressed in a mammalian system or analysed by an *in vitro* kinase assay. Isolated and cleaved peptides would then be presented for MS analysis. Also, presence of endogenous hSUN1 may prevent the effect of the hSUN1 phospho-mimetic mutant and, this could be resolved by depleting endogenous hSUN1 by RNAi. Considering the above, it is

puzzling that hSUN1 3D mislocalises to the cytoplasm (**Figure 5.2**). Maybe mislocalisation would be greater with additional phosphorylated sites mutated.

To try to overcome the difficulties of observing hSUN1 interactions with other proteins that can also be phosphorylated in mitosis, I decided to observe hSUN1 self-interaction. hSUN1 is known to oligomerise via a coiled-coil domain and its C-terminus (Lu *et al.*, 2008), but an N-terminal domain interaction has also been observed (Haque *et al.*, 2006) which could be disrupted by phosphorylation. However, interaction between 3D mutants was not lost (**Figure 5.8B**). This supports previous data showing that the SUN-KASH interaction is maintained (**Figure 5.5C**) and would not be so if SUN1 underwent disassembly. It is likely that the energy expenditure for the cell to breakdown the core LINC complex interaction and unravel the oligomer formation would be too costly for such a short period of time, only to reform once again upon mitotic exit. Again, the presence of endogenous hSUN1 could mask interactions. In hindsight, an N-terminal only construct would have been a better construct to use in this experiment.

In summary, my data have shown that mitotic phosphorylation of endogenous hSUN1 induces partial disassembly of the LINC complex, but have yet to directly link the contribution of hSUN1 S48, S138 and S333 in disassembly of hSUN1 protein networks.

5.3.3 A possible role for the LINC complex during in NE reassembly

The maintenance of the SUN1 oligomer and the core LINC complex interaction during mitosis supports roles for the LINC complex in mitosis. SUN1 has already been shown to aid decondensation of chromosomes upon mitotic exit (Chi *et al.*, 2007), but with its

numerous interactions and splice variants it is likely that SUN1 has more than one role in mitosis. In addition, nesprin-1 giant still associates with the NE in prophase (Zhen *et al.*, 2002).

As established in the **Chapter 4** hSUN1 binds a novel INM protein, NET5/SAMP1C, in interphase. Observation of its mitotic interactions with hSUN1 showed that the hSUN1-NET5 interaction was not only maintained in mitosis but NET5 had a higher affinity for hSUN1 and appeared to be post-translationally modified (**Figure 5.6**). SAMP1, the human homologue of NET5, redistributes to the polar regions of the mitotic spindle in metaphase hence its name (Buch *et al.*, 2009) and suggests it may be part of the elusive spindle matrix. In addition, SAMP1 is recruited in telophase to the reforming NE (Buch *et al.*, 2009). hSUN1 is also found on reforming NE membranes during mitosis but at an earlier stage in anaphase (Chi *et al.*, 2007). There is the possibility that hSUN1 may form the initial interaction with chromatin bringing the ER tubules closer to the chromatin followed by the spreading of the ER surface on chromatin. This may bring SAMP1 in close proximity to chromatin for chromosome positioning (E.Schirmer, personal communication).

Exploration of the functional role of mitotic phosphorylated SUN1 in this chapter has scratched the surface on the potential role of SUN1 in mitosis. It would be interesting to observe the hSUN1 phospho-deficient and phospho-mimetic mutants during mitosis and see whether they have an effect on timing of NEBD or NE reassembly or whether they disrupt spindle architecture. Data has shown that hSUN1 displays characteristic of an INM protein preparing for NEBD with its more dynamic nature and loss of certain protein networks.

CHAPTER 6
Discussion

Chapter 6 Discussion

6.1 SUN protein and mitotic regulation

During interphase the integrity and rigidity of the NE is maintained through its array of protein-protein interactions between the nuclear lamina, the integral proteins of the INM and chromatin (Foisner, 2003). Further stabilisation of the NE is achieved through components of the LINC complex, SUN-domain and KASH-domain proteins, which form a molecular chain from the nuclear interior to all three cytoskeletal networks (Razafsky & Hodzic, 2009).

However, at the onset of open mitosis, architectural changes in the NE are necessary for mitotic entry. It has been established for over 30 years that nuclear lamina disassembly is required for NEBD to occur (Gerace & Blobel, 1980). Nuclear lamina disassembly is regarded as a driving force weakening the NE to allow microtubule-dependent mechanisms to induce NEBD (Gerace & Blobel, 1980; Luscher *et al.*, 1991; Peter *et al.*, 1990; Beaudouin *et al.*, 2002; Salina *et al.*, 2002). Nuclear lamina depolymerisation is initiated through phosphorylation of lamins A, B and C which changes the conformation of the proteins and leads to disruption of the higher ordered structure of the nuclear lamina (Gerace & Blobel, 1980; Heald & Mckeon, 1990; Luscher *et al.*, 1991; Peter *et al.*, 1990; Ottaviano & Gerace, 1985; Ward & Kirschner, 1990; Kuga *et al.*, 2010; Georgatos *et al.*, 1997; Thompson & Fields, 1996). Furthermore the identification of the lamin phospho-specific sites provides insights into how these modifications disassemble the nuclear lamina (Heald & Mckeon, 1990; Kuga *et al.*, 2010).

Research initially focused on the lamin phosphorylation and its role in NEBD but has now extended to the other NE domains, the NPC and the integral membrane proteins. A range of Nups are phosphorylated at the onset of mitosis to partially disassemble the NPC and increase the permeability of the NE (Laurell *et al.*, 2011; Glavy *et al.*, 2007; Onischenko *et al.*, 2007). Integral membrane proteins of the INM LBR, LAP2, emerin and MAN1 contain phosphorylation sites which help detach their direct/indirect associations with chromosomes in mitosis (Ye *et al.*, 1997; Foisner & Gerace, 1993; Hirano *et al.*, 2005; Hirano *et al.*, 2009). However, it is unclear as to what happens to their other protein-protein interactions at the NE, including proteins such as the SUN and KASH-domain families.

These observations posed the question as to whether NE specific SUN proteins were also phosphorylated in mitosis. To date, no detailed research has been conducted in cell-cycle dependent regulation of SUN proteins, only that global phospho-proteomic studies have identified SUN1 and SUN2 phosphorylated residues and the proteomic database UniProtKB has predicted possible phospho-serines based on sequence similarity with other phospho-proteins (Dephoure *et al.*, 2008; Olsen *et al.*, 2006; Gronborg *et al.*, 2002; Mayya *et al.*, 2009) (UniProtKB accession numbers SUN1 O94901 SUN2 Q9UH99). One function for SUN protein phosphorylation has been demonstrated with the *C.elegans* homologue matefin whereby phosphorylation on serine 12 by PLK2 promotes homolog pairing in meiotic cells (Labella *et al.*, 2011). At the start of this research I hypothesised that SUN protein phosphorylation at mitosis would induce complete disassembly of the LINC complex weakening the NE and aiding NEBD and my findings have confirmed this hypothesis.

6.1.1 Human SUN1 is phosphorylated at the onset of mitosis

My preliminary studies of hSUN1 demonstrated that this protein is specifically phosphorylated at the onset of mitosis, accounting for the band-shift observed in nocodazole-arrested cells. This is consistent with the fact that other INM proteins are also phosphorylated as they enter mitosis (Foisner & Gerace, 1993; Courvalin *et al.*, 1992; Hirano *et al.*, 2005; Hirano *et al.*, 2009; Bailer *et al.*, 1991; Nikolakaki *et al.*, 1997).

hSUN1 phosphorylation sites were identified at serines 48, 138 and 333. All three identified sites reside in the N-terminus of hSUN1, exposed to the nucleoplasm and this is where many of SUN1 protein interactions occur (Haque *et al.*, 2010; Haque *et al.*, 2006). Moreover, two of the sites (S48 and S138) were located in the lamin A/C binding site, which highlighted early on in the research a possible mechanism in disruption of SUN1 interaction with lamin A/C. However, the purpose of hSUN1 phosphorylation was unknown at this stage.

Analysis of the three phosphorylation sites, showed that two (S48 and S333) were positioned in CDK1 consensus sites. Subsequent studies confirmed that CDK1 indeed phosphorylated these sites and that CDK1 phosphorylation partially contributed to the SUN1 band-shift. In contrast, S138 was found to be phosphorylated y PLK1. Research in the field to date has not implicated PLK1 as a mitotic kinase for INM proteins but has shown that it phosphorylates NPC components (Laurell *et al.*, 2011). A possible explanation for why two mitotic kinases are acting upon the same substrate could be because one of them is a priming kinase. CDK1 has the ability to prime substrates by phosphorylating the target protein in order to guide other kinases to that location for

subsequent phosphorylation (Salaun *et al.*, 2008). It would therefore be interesting to determine whether CDK1 acts as a priming kinase for PLK1.

Another mitotic kinase, Aurora A was implicated in hSUN1 phosphorylation. *In vitro* kinases assays showed that Aurora A phosphorylated the hSUN1 N-terminus to the same degree as CDK1 and it was identified as a potential binding partner for mitotic hSUN1. Despite this, no phosphorylation sites were identified *in vivo*. This could be partially due to the incomplete coverage of the protein sequence by MS analysis and, indeed, a predicted Aurora A phosphorylation site does lie at S52, which was not covered in the MS analysis.

In summary, my data strongly suggest that hSUN1 phosphorylation contributes to global phosphorylation of the NE at the onset of mitosis. This may be required to change the protein conformation, weakening the protein interaction networks thereby making the NE more malleable for NE tearing. However, this may not be a comprehensive view of mitotic hSUN1 phosphorylation and there maybe additional phosphorylation sites and kinases for hSUN1.

6.1.2 Possible hSUN2 degradation at the onset of mitosis

Proteomic investigations into global protein phosphorylation in mitosis predicted the presence of multi-phosphorylation sites for hSUN2 (Olsen *et al.*, 2006; Gronborg *et al.*, 2002; Mayya *et al.*, 2009). However, preliminary studies into hSUN2 potential phosphorylation produced conflicting results, making it hard to decipher what was happening to hSUN2 in mitosis. Some of the data suggested that there was a loss in the protein expression in mitosis but this was not always reproducible.

If this was the case then it may be plausible that hSUN2 phosphorylation is a means of targeting the protein for proteosomal degradation. This seems unlikely though as mitosis is such a brief phase in the human cell cycle, approximately 1 hour (Morgan, 2006), so to degrade a protein in mitosis only to transcribe and translate it for use in G1 would appear to be a waste of energy. Hodzic *et al.* (2004) showed that their antibody generated against SUN2 detected three bands with molecular weights of 65, 75 and 85 kDa. It is possible that the 65 and 85 kDa bands are non-specific cross-reacting proteins but if these are true isoforms they may display different protein expression levels during the cell cycle.

6.1.3 Mitotic phosphorylation of SUN1 dissociates the LINC complex away from the nuclear lamina

SUN1 phosphorylation did not appear to result in proteosomal degradation, due to its abundance in mitotic extracts. My studies revealed that mitotic phosphorylation of SUN1 disrupted interactions at the N-terminus with, not only lamin A/C, but also with emerin and INM-localised isoforms of nesprin-2. In contrast, interaction with the nesprin-2 KASH-domain was maintained in mitosis indicating that the core components of the LINC complex remain intact. In addition, the IP-MS data for GFP-hSUN1 showed that nesprin-1 giant was present in both asynchronous and mitotic samples. Further support for these findings comes from immunofluorescence staining for nesprin-2 giant (NUANCE) showing that it remains at NE in prophase and only disperses into the cytoplasm at prometaphase (Zhen *et al.*, 2002). This suggests that nesprins are still associated with SUN proteins during mitosis.

The three identified phosphorylation sites S48, S138 and S333 are all located in the N-terminus, where lamin A/C, emerin and nucleoplasmic nesprins binding sites has been mapped to SUN1. S48 lies within the lamin A/C binding region while S138 is at the edge of the lamin A/C binding site. In contrast, S333 does not lie within any of the mapped binding sites. Mitotic phosphorylation of hSUN1 induces a conformational change in hSUN1 which disrupts lamin A/C, emerin and nucleoplasmic nesprins N-terminal interactions.

hSUN1 mitotic phosphorylation does not transmit conformational change from the N-terminus to the C-terminus, nor does it pass through the transmembrane domain. In mitosis the cell energy expenditure is quite high and so it is plausible to think that cell inputs energy for disruption of certain interactions. As the binding affinities of SUN1 with its various interaction partners have not been determined, it is hard to say whether or not the decision to provide cellular energy for disrupting protein-protein interactions is based on a threshold value. An alternative theory is that because the SUN-KASH interaction is in the PNS isolates it from modifying factors so the inability of the LINC complex to disassembly could be due to restricted access. Retaining the LINC complex in mitosis, suggests it may play a role during mitosis possibly to maintain the lumenal spacing of the NE/ER (Crisp *et al.*, 2006) or in NE reassembly as discussed in **section 7.2.3**.

Whilst I was able to demonstrate loss of hSUN1 interaction at the INM in mitotic cells, unfortunately, the recombinant hSUN1 3D phospho-mimetic mutant did not exhibit the same loss of interactions. One possible explanation for this is that these three phosphorylation sites are not the major contributors to the loss of hSUN1 interactions

in mitosis. The potential Aurora A site at S52 could also contribute to disruption of these interactions and should be investigated in future studies. However, this does not tally with the fact that the hSUN1 3D mutant failed to fully localise at the NE and has significantly increased solubility compared to wild-type hSUN1, both of which suggest that the hSUN1 3D mutant does have defects in its anchorage at the INM. These findings highlighted a few potential issues with the experimental design. Firstly, the experiment could have been conducted under mitotic conditions as phosphorylation of emerin and lamin A/C may also be required for disassembly. In support of this, mitotically phosphorylated LAP1 still binds to assembled lamins in semi-*in vitro* conditions (Foisner & Gerace, 1993). However, placing the phospho-mimetic mutant in mitotic conditions may phosphorylate other possible sites on SUN1 that have not been identified in this research, therefore any loss of binding cannot be solely attributed to the three identified phosphorylation sites.

One possible solution could be to implement an *in vitro* pull-down experiment where bacterially expressed MBP-hSUN1 3D phospho-mimetic mutant immobilised on amylose resin is incubated with mitotic extracts from HeLa cells, the latter containing phosphorylated lamin A/C and emerin. Therefore, the ability of the hSUN1 phospho-mimetic mutant to pull down lamin A/C and emerin would depend on the three identified phosphorylation sites alone.

Secondly, phospho-mimetic mutants can be created by the substitution of the serine or threonine with aspartic acid or glutamic acid. All the phospho-mimetic mutant constructs for this research contained aspartic acid substitutions since the R group of serine was considered to be more similar to aspartic acid than to glutamic acid.

However, glutamic acid phospho-mimetic mutants may have induced a stronger disassociation and so perhaps both aspartic acid and glutamic acid mutants should have been tested.

Considering all my data characterising hSUN1 phosphorylation and its protein interactions in mitosis, I propose the following model, illustrated in **Figure 6.1**. During interphase, the LINC complex connects the cytoskeleton to the nuclear interior, which involves the SUN proteins tethering the nesprins to the NE via their KASH-domain while simultaneously interacting with lamin A/C and chromatin to anchor the complex at the NE. The LINC complex is further stabilised by additional interactions with other residents of the INM such as emerin and nucleoplasmic nesprins. At the onset of mitosis, hSUN1 is phosphorylated at multiple sites in its N-terminus. This induces conformational changes in the nucleoplasmic domain, disrupting interactions with binding partners lamin A/C and emerin. The LINC complex remains intact possibly for roles during mitosis or for maintenance of the ER lumenal spacing. Hence, mitotic phosphorylation of hSUN1 dissociates LINC complex away from the nuclear lamina and chromatin.

6.2 Identification of potential SUN1 binding partners

Two independent proteomic studies focusing on identification of components of the NE indicated the presence of approximately 80 proteins at the NE, yet only a few have been characterised to date (Dreger *et al.*, 2001; Schirmer *et al.*, 2003). This highlights the infancy of research in the NE field.

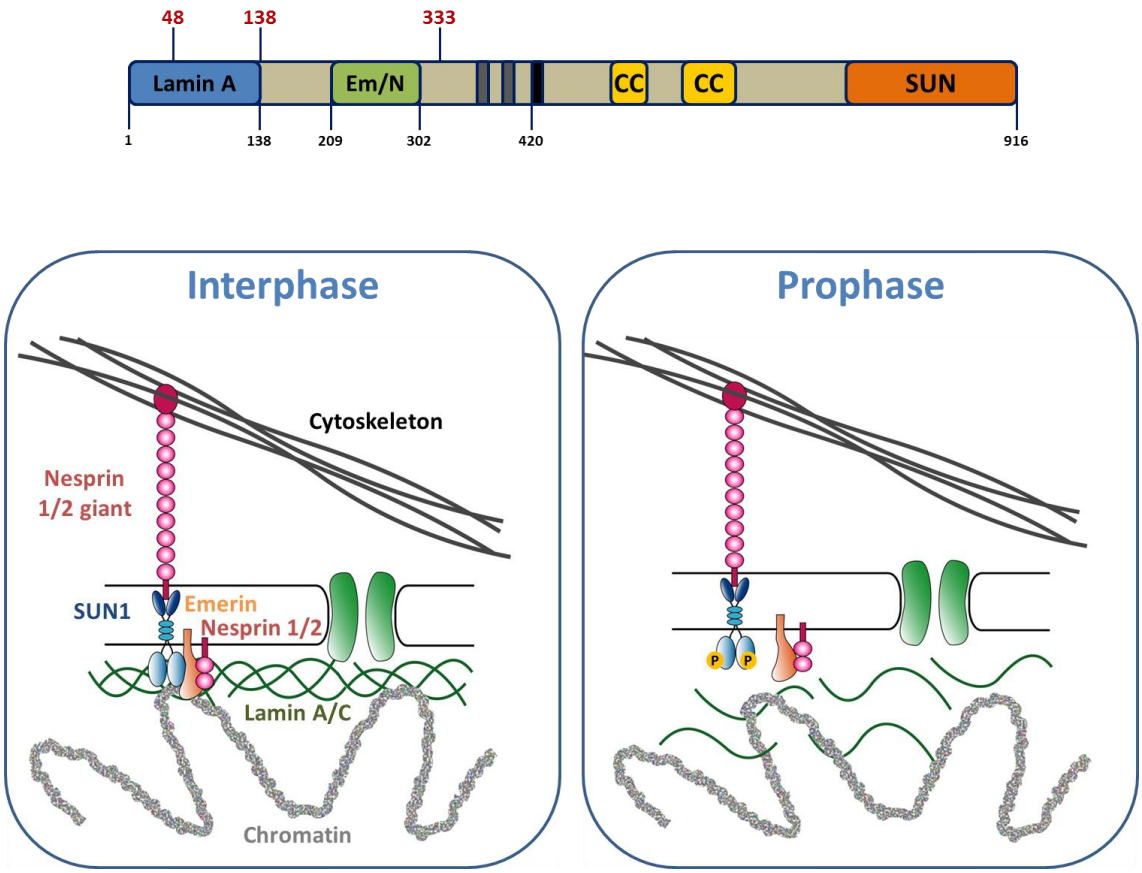

Figure 6.1. Mitotic phosphorylation of hSUN1 induces LINC complex dissociation away from the nuclear lamina.

(A) Schematic representation of hSUN1 protein domains indicating the lamin A/C, emerin and nucleoplasmic nesprin N-terminal binding regions. The identified mitotic hSUN1 phosphorylation sites are also indicated. **(B)** Model proposing that, in interphase, SUN1 binds nesprins via its C-terminal SUN-domain forming a protein bridge over the PNS, otherwise known as the LINC complex. At its N-terminus, SUN1 interactions with lamin A/C, emerin, nucleoplasmic nesprins and SUN2 (not shown for clarity) stabilise the LINC complex thereby connecting the cytoskeleton to the nuclear interior. At the onset of mitosis, N-terminal phosphorylation of SUN1 causes conformation changes in its protein structure releasing its N-terminal binding partners but keeping the LINC complex intact, hence the LINC complex dissociates away from the nuclear lamina in preparation for NEBD.

A great deal of research has been conducted on SUN proteins across species and isoforms and much of the work is still on-going. SUN1 and SUN2 have been established as major components of the LINC complex which is highly conserved across species (Razafsky & Hodzic, 2009). In addition, both SUN proteins also bind A-type lamins, emerin and nucleoplasmic nesprin isoforms (Crisp *et al.*, 2006; Haque *et al.*, 2010; Haque *et al.*, 2006). However, SUN protein networks have not been completely defined at the NE, for instance, unlike SUN2, SUN1 remains at the INM in the absence of A-type lamins hence other unknown interacting partners must be anchoring SUN1 at the INM (Crisp *et al.*, 2006).

Upon commencing my research, I postulated that SUN1 had many more interacting partners than were known at that time and that SUN1 was a component of multiple protein complexes in addition to the LINC complex. It was also reasonable to assume that cell cycle events may regulate binding of protein partners.

6.2.1 NET5/SAMP1C, a confirmed SUN1 binding partner

Data in this thesis demonstrated an interaction between hSUN1 and NET5, the rat orthologue of human SAMP1C and yeast Ima1. Prior to this revelation, characterisation of SAMP1 showed that it is an integral membrane protein localised to the INM and is required to anchor centrosomes near the nuclei. In mitosis, SAMP1 was found at the polar regions of microtubule spindles, hence its name (Buch *et al.*, 2009). In addition, the *S.pombe* Ima1 orthologue facilitates coupling of SPB (and cytoplasmic microtubules) to nuclear heterochromatin via the yeast LINC complex (King *et al.*, 2008).

Further studies have since shown that SAMP1 has three isoforms, SAMP1A, B and C, with similar N-terminal sequences but varying C-terminal regions (Borrego-Pinto *et al.*, 2012). SAMP1A is the isoform initially characterised by Buch *et al.* (2009) and Gudise *et al.* (2011) and has now been shown to bind emerin, SUN2, and lamin A/C implying it has a functional association with the LINC complex. Furthermore lamin A/C is required for its retention at the INM and likewise SAMP1A is required for the NE localisation of emerin (Gudise *et al.*, 2011).

In addition to SUN2 and nesprin-2 giant, SAMP1 has now been shown to be a component of TAN lines that couple nuclei to actin cables during fibroblast migration (Borrego-Pinto *et al.*, 2012). Surprisingly, SUN1 does not localise to TAN lines but it is required for nuclear movement (Luxton *et al.*, 2011) thus, this interaction could also contribute to nuclear movement.

hSUN1 was still bound to NET5 in mitosis, moreover, NET5 appeared to be modified in mitosis and have a higher affinity with hSUN1. The increased association of the proteins could be due to post-translational modifications i.e. NET5 phosphorylation could increase its binding association with SUN1, furthermore, this suggests a role for the SAMP1/SUN1 complex during mitosis.

SAMP1A is associated with spindle microtubules during mitosis, this suggests that it has a significant function associated with the mitotic spindle (Buch *et al.*, 2009). The maintenance of the NET5/SAMP1C-SUN1 interaction in mitosis implies that SUN1 has a role at the mitotic spindle too.

Researchers have speculated about the existence of a spindle matrix for decades. The spindle matrix is postulated to serve as a static scaffold anchoring SAFs as well as aiding mitotic spindle assembly and cushioning against the forces generated by the spindle microtubules. However, the molecular composition of the spindle matrix remains to be determined (Tsai *et al.*, 2006; Zheng & Tsai, 2006). The LINC complex transmits microtubule- and actin-generated force from the cytoskeleton to the nucleus. In doing so, it protects the nucleus from mechanical stress and ensures cellular rigidity (Maniotis *et al.*, 1997; Stewart-Hutchinson *et al.*, 2008; Houben *et al.*, 2007). Therefore, it seems logical that the LINC complex, in association with SAMP1C, may be protecting the cell in mitosis from spindle microtubule-generated force possibly as components of the spindle matrix.

6.2.2 Further potential hSUN1 interactions at the nuclear envelope

Data from the IP-MS experiment recovered 348 potential hSUN1 interacting partners and, of those, 10 were components of the NE. Integral membrane proteins LUMA and LAP2β/γ and nucleoporin Nup155 bound in asynchronous samples, suggesting that SUN1 may be involved in more protein networks than previously anticipated. Binding additional INM proteins may be required for LINC complex stabilisation at the INM. SUN1 is known to associate with the NPC (Liu *et al.*, 2007; Talamas & Hetzer, 2011) and data here shows yet another possible connection with the NPC. Expansion of the hSUN1 protein network also increases the number of candidate proteins involved in EDMD especially NET5/SAMP1. The presence of lamin B1 and B2 in the data shows that SUN1 could possible bind both A-type and B-type lamins, the latter supported by

co-IP studies showing weak interactions between SUN1 and lamin B1 (Crisp *et al.*, 2006).

The IP-MS data presented nurim as a strong candidate for a hSUN1 interacting protein. The INM protein nurim is highly immobilie and insoluble at the NE, more so than components of the nuclear lamina (Rolls *et al.*, 1999). Its anchorage does not reply on lamins but by a unique unknown mechanism (Rolls *et al.*, 1999). It is quite distinct from other INM proteins as its N-terminus is only 4-5 amino acids in comparison to the large nucleoplasmic domains harboured by SUN1, SUN2, LBR, emerin and LAP2 (Foisner, 2003; Crisp *et al.*, 2006; Ye & Worman, 1994; Manilal *et al.*, 1996; Rolls *et al.*, 1999; Hodzic *et al.*, 2004; Haque *et al.*, 2006). Its function remains elusive but the IP-MS data in this thesis show that nurim was present in both the asynchronous and mitotic samples, suggesting a possible role with hSUN1 during mitosis. Also, because nurim does not rely on the nuclear lamina for its retention, it could be the protein responsible for anchorage of hSUN1 at the INM. IP experiments to establish a connection between the proteins would need to be conducted first, and depending on the outcome, hSUN1 localisation could then be observed in nurim depleted cells. Nurim is extremely insoluble and suitable solubilisation strategies would need to optimised prior to experimentation.

Alternatively, chromatin could be the missing link anchoring hSUN1 at the NE. Some studies have already shown that SUN1 interacts with chromatin-associated protein (Chi *et al.*, 2007; Lu *et al.*, 2008). Moreover, Mps3, the *S.cerevisiae* SUN protein orthologue requires histone H.2AZ for targeting to the INM (Gardner *et al.*, 2011). Analysis of the IP-MS data retrieved a range of chromatin-associated proteins, for

example, histone H1.2, histone-binding protein RBBP4 and core histone macro-H2A.1, supporting the theory that SUN1 is tethered at the INM by chromatin. Again, these interactions must firstly be confirmed by direct co-IP. hSUN1 deletion constructs could be used to map the binding site and to determine whether this interaction is responsible for the NE localisation of hSUN1.

6.2.3 A role for the LINC complex in nuclear envelope reassembly

Data in this thesis has suggested a possible role for hSUN1 during mitosis. The maintenance of the LINC complex, NET5/SAMP1C and potential interactions with proteins found in the mitotic sample only, such as RCC2, RanGTPase, RanBP2, dynein, kinesin-like protein KIF20A, and a range of importins/exportins supports this idea.

Chi *et al.* (2007) showed that, in late mitosis, hSUN1 chaperones hALP to segregated chromosomes to induce histone acetylation and chromosome decondensation. Insights into SUN1 behaviour in mitosis show that hSUN1 is located on the reassembling NE at the lateral margins of newly segregated chromosomes from late anaphase to early telophase (Liu *et al.*, 2007; Chi *et al.*, 2007). NPCs are also found in this distinct region and previous studies have shown that SUN1, but not SUN2, is associated with various components of the NPC (Liu *et al.*, 2007; Talamas & Hetzer, 2011). This localisation pattern differs from SUN2, as SUN2 concentrates in the longitudinal region of the telophase chromatin mass which is devoid of NPCs (Liu *et al.*, 2007). Surprisingly SUN1 and SUN2 behave in a similar manner to LBR and emerin, respectively, with regards to where the proteins are found on the reforming NE (Liu *et al.*, 2007; Chi *et al.*, 2007; Tseng & Chen, 2011; Haraguchi *et al.*, 2000).

LBR has a role in NE reassembly, recruiting ER membranes to the chromatin mass in early telophase (Tseng & Chen, 2011; Anderson *et al.*, 2009; Pyrpasopoulou *et al.*, 1996; Wilson & Newport, 1988; Collas *et al.*, 1996; Haraguchi *et al.*, 2008). SUN1 has been previously shown at the reforming NE (Liu *et al.*, 2007; Chi *et al.*, 2007) but I postulate that, in addition to this, that SUN1 recruits NPCs to chromatin through its association with NPC components such as POM121 and possibly Nup358/RanBP2 and Nup155.

For research to progress further with regards to NE reassembly it would be interesting to observe the wild-type, phospho-mimetic and phospho-deficient hSUN1 mutants by live-cell imaging to assess their change in behaviour during mitosis. It would be important to establish how soon after the SAC SUN1 re-associates with chromatin and whether the interaction is regulated by the phosphorylation sites identified in this thesis, in other words, whether the phospho-mimetic and phospho-deficient mutants delay or accelerate NE reassembly. In addition, it would be useful to establish timings or sequential patterns for various INM proteins and nucleoporins associating with the newly forming NE, in particular, LBR, emerin, SUN2, nurim and transmembrane nucleoporins pom121, Ndc1 and gp210. Furthermore, parallel experiments with cells depleted of SUN1 could be conducted to track NPC localisation at the reforming NE.

CHAPTER 7
Bibliography

Chapter 7 BIBLIOGRAPHY

Alberts, B., 2002. *Molecular biology of the cell.* 4th ed. New York: Garland Science.

Anderson, D.J. & Hetzer, M.W., 2008. Reshaping of the endoplasmic reticulum limits the rate for nuclear envelope formation. *The Journal of Cell Biology.* **182,** 911-924.

Anderson, D.J. & Hetzer, M.W., 2007. Nuclear envelope formation by chromatin-mediated reorganization of the endoplasmic reticulum. *Nature Cell Biology.* **9,** 1160-1166.

Anderson, D.J., Vargas, J.D., Hsiao, J.P., Hetzer, M.W., 2009. Recruitment of functionally distinct membrane proteins to chromatin mediates nuclear envelope formation in vivo. *Journal of Cell Biology.* **186,** 183-191.

Andres, V. & Gonzalez, J.M., 2009. Role of A-type lamins in signaling, transcription, and chromatin organization. *Journal of Cell Biology.* **187,** 945-957.

Andrulis, E.D., Neiman, A.M., Zappulla, D.C., Sternglanz, R., 1998. Perinuclear localization of chromatin facilitates transcriptional silencing. *Nature.* **394,** 592-595.

Antoniacci, L.M., Kenna, M.A., Skibbens, R.V., 2007. The nuclear envelope and spindle pole body-associated Mps3 protein bind telomere regulators and function in telomere clustering. *Cell Cycle (Georgetown, Tex.).* **6,** 75-79.

Apel, E.D., Lewis, R.M., Grady, R.M., Sanes, J.R., 2000. Syne-1, a dystrophin- and Klarsicht-related protein associated with synaptic nuclei at the neuromuscular junction. *The Journal of Biological Chemistry.* **275,** 31986-31995.

Bailer, S.M., Eppenberger, H.M., Griffiths, G., Nigg, E.A., 1991. Characterization of a 54-Kd Protein of the Inner Nuclear-Membrane - Evidence for Cell Cycle-Dependent Interaction with the Nuclear Lamina. *Journal of Cell Biology.* **114,** 389-400.

Barr, F.A., Elliott, P.R., Gruneberg, U., 2011. Protein phosphatases and the regulation of mitosis. *Journal of Cell Science.* **124,** 2323-2334.

Baumann, K., 2010. CELL CYCLE Activities of a mitotic master. *Nature Reviews Molecular Cell Biology.* **11,** 389-389.

Beaudouin, J., Gerlich, D., Daigle, N., Eils, R., Ellenberg, J., 2002. Nuclear envelope breakdown proceeds by microtubule-induced tearing of the lamina. *Cell.* **108,** 83-96.

Bengtsson, L. & Otto, H., 2008. LUMA interacts with emerin and influences its distribution at the inner nuclear membrane. *Journal of Cell Science.* **121,** 536-548.

Bengtsson, L. & Wilson, K.L., 2004. Multiple and surprising new functions for emerin, a nuclear membrane protein. *Current Opinion in Cell Biology.* **16,** 73-79.

Berger, R., Theodor, L., Shoham, J., Gokkel, E., Brok-Simoni, F., Avraham, K.B., Copeland, N.G., Jenkins, N.A., Rechavi, G., Simon, A.J., 1996. The characterization and localization of the mouse thymopoietin/lamina-associated polypeptide 2 gene and its alternatively spliced products. *Genome Research.* **6,** 361-370.

Bione, S., Maestrini, E., Rivella, S., Mancini, M., Regis, S., Romeo, G., Toniolo, D., 1994. Identification of a novel X-linked gene responsible for Emery-Dreifuss muscular dystrophy. *Nature Genetics.* **8,** 323-327.

Bonner, W.M., 1975. Protein migration into nuclei. I. Frog oocyte nuclei in vivo accumulate microinjected histones, allow entry to small proteins, and exclude large proteins. *The Journal of Cell Biology.* **64,** 421-430.

Borrego-Pinto, J., Jegou, T., Osorio, D.S., Aurade, F., Gorjanacz, M., Koch, B., Mattaj, I.W., Gomes, E.R., 2012. Samp1 is a component of TAN lines and is required for nuclear movement. *Journal of Cell Science.* **125,** 1099-1105.

Bostock, C.J., Prescott, D.M., Kirkpatrick, J.B., 1971. An evaluation of the double thymidine block for synchronizing mammalian cells at the G1-S border. *Experimental Cell Research.* **68,** 163-168.

Brockman, J.L., Gross, S.D., Sussman, M.R., Anderson, R.A., 1992. Cell cycle-dependent localization of casein kinase I to mitotic spindles. *Proceedings of the National Academy of Sciences of the United States of America.* **89,** 9454-9458.

Broers, J.L.V., Peeters, E.A.G., Kuijpers, H.J.H., Endert, J., Bouten, C.V.C., Oomens, C.W.J., Baaijens, F.P.T., Ramaekers, F.C.S., 2004. Decreased mechanical stiffness in LMNA-/- cells is caused by defective nucleo-cytoskeletal integrity: implications for the development of laminopathies. *Human Molecular Genetics.* **13,** 2567-2580.

Broers, J.L.V., Ramaekers, F.C.S., Bonne, G., Ben Yaou, R., Hutchison, C.J., 2006. Nuclear lamins: Laminopathies and their role in premature ageing. *Physiological Reviews.* **86,** 967-1008.

Buch, C., Lindberg, R., Figueroa, R., Gudise, S., Onischenko, E., Hallberg, E., 2009. An integral protein of the inner nuclear membrane localizes to the mitotic spindle in mammalian cells. *Journal of Cell Science.* **122,** 2100-2107.

Bupp, J.M., Martin, A.E., Stensrud, E.S., Jaspersen, S.L., 2007. Telomere anchoring at the nuclear periphery requires the budding yeast Sad1-UNC-84 domain protein Mps3. *Journal of Cell Biology.* **179,** 845-854.

Burke, B. & Ellenberg, J., 2002. Remodelling the walls of the nucleus. *Nature Reviews.Molecular Cell Biology.* **3,** 487-497.

Burke, B. & Stewart, C.L., 2006. The laminopathies: the functional architecture of the nucleus and its contribution to disease. *Annual Review of Genomics and Human Genetics.* **7,** 369-405.

Burke, B. & Stewart, C.L., 2002. Life at the edge: The nuclear envelope and human disease. *Nature Reviews Molecular Cell Biology.* **3,** 575-585.

Burke, B., 2012. It Takes KASH to Hitch to the SUN. *Cell.* **149,** 961-3.

Burke, B. & Roux, K.J., 2009. Nuclei Take a Position: Managing Nuclear Location. *Developmental Cell.* **17,** 587-597.

Busayavalasa, K., Chen, X., Farrants, A.K., Wagner, N., Sabri, N., 2012. The Nup155-mediated Organization of Inner Nuclear Membrane Proteins is Independent of Nup155 Anchoring to the Metazoan Nuclear Pore Complex. *Journal of Cell Science.*

Capell, B.C. & Collins, F.S., 2006. Human laminopathies: nuclei gone genetically awry. *Nature Reviews Genetics.* **7,** 940-952.

Chaouch, M., Allal, Y., De Sandre-Giovannoli, A., Vallat, J.M., Amer-el-Khedoud, A., Kassouri, N., Chaouch, A., Sindou, P., Hammadouche, T., Tazir, M., Levy, N., Grid, D., 2003. The phenotypic manifestations of autosomal recessive axonal Charcot-Marie-Tooth due to a mutation in Lamin A/C gene. *Neuromuscular Disorders : NMD.* **13,** 60-67.

Chen, C.Y., Chi, Y.H., Mutalif, R.A., Starost, M.F., Myers, T.G., Anderson, S.A., Stewart, C.L., Jeang, K.T., 2012. Accumulation of the inner nuclear envelope protein Sun1 is pathogenic in progeric and dystrophic laminopathies. *Cell.* **149,** 565-577.

Chestukhin, A., Pfeffer, C., Milligan, S., DeCaprio, J.A., Pellman, D., 2003. Processing, localization, and requirement of human separase for normal anaphase progression. *Proceedings of the National Academy of Sciences of the United States of America.* **100,** 4574-4579.

Chi, Y., Haller, K., Peloponese, J., Jr., Jeang, K., 2007. Histone acetyltransferase hALP and nuclear membrane protein hsSUN1 function in de-condensation of mitotic chromosomes. *Journal of Biological Chemistry.* **282,** 27447-27458.

Chikashige, Y., Tsutsumi, C., Yamane, M., Okamasa, K., Haraguchi, T., Hiraoka, Y., 2006. Meiotic proteins bqt1 and bqt2 tether telomeres to form the bouquet arrangement of chromosomes. *Cell.* **125,** 59-69.

Clarke, P.R. & Zhang, C., 2004. Spatial and temporal control of nuclear envelope assembly by Ran GTPase. *Symposia of the Society for Experimental Biology.* **(56),** 193-204.

Collas, P., Courvalin, J.C., Poccia, D., 1996. Targeting of membranes to sea urchin sperm chromatin is mediated by a lamin B receptor-like integral membrane protein. *The Journal of Cell Biology.* **135,** 1715-1725.

Conrad, M.N., Lee, C., Wilkerson, J.L., Dresser, M.E., 2007. MPS3 mediates meiotic bouquet formation in Saccharomyces cerevisiae. *Proceedings of the National Academy of Sciences of the United States of America.* **104,** 8863-8868.

Courvalin, J.C., Segil, N., Blobel, G., Worman, H.J., 1992. The Lamin-B Receptor of the Inner Nuclear-Membrane Undergoes Mitosis-Specific Phosphorylation and is a Substrate for P34cdc2-Type Protein-Kinase. *Journal of Biological Chemistry.* **267,** 19035-19038.

Crasta, K., Lim, H.H., Zhang, T., Nirantar, S., Surana, U., 2008. Consorting kinases, end of destruction and birth of a spindle. *Cell Cycle (Georgetown, Tex.).* **7,** 2960-2966.

Crisp, M., Liu, Q., Roux, K., Rattner, J.B., Shanahan, C., Burke, B., Stahl, P.D., Hodzic, D., 2006. Coupling of the nucleus and cytoplasm: role of the LINC complex. *Journal of Cell Biology.* **172,** 41-53.

Croft, J.A., Bridger, J.M., Boyle, S., Perry, P., Teague, P., Bickmore, W.A., 1999. Differences in the localization and morphology of chromosomes in the human nucleus. *The Journal of Cell Biology.* **145,** 1119-1131.

Cronshaw, J.M., Krutchinsky, A.N., Zhang, W., Chait, B.T., Matunis, M.J., 2002. Proteomic analysis of the mammalian nuclear pore complex. *The Journal of Cell Biology.* **158,** 915-927.

D'Angelo, M.A., Anderson, D.J., Richard, E., Hetzer, M.W., 2006. Nuclear pores form de novo from both sides of the nuclear envelope. *Science (New York, N.Y.).* **312,** 440-443.

D'Angelo, M.A. & Hetzer, M.W., 2008. Structure, dynamics and function of nuclear pore complexes. *Trends in Cell Biology.* **18,** 456-466.

De Sandre-Giovannoli, A., Bernard, R., Cau, P., Navarro, C., Amiel, J., Boccaccio, I., Lyonnet, S., Stewart, C.L., Munnich, A., Le Merrer, M., Levy, N., 2003. Lamin a truncation in Hutchinson-Gilford progeria. *Science (New York, N.Y.).* **300,** 2055.

De Sandre-Giovannoli, A., Chaouch, M., Kozlov, S., Vallat, J.M., Tazir, M., Kassouri, N., Szepetowski, P., Hammadouche, T., Vandenberghe, A., Stewart, C.L., Grid, D., Levy, N., 2002. Homozygous defects in LMNA, encoding lamin A/C nuclear-envelope proteins, cause autosomal recessive axonal neuropathy in human (Charcot-Marie-Tooth disorder type 2) and mouse. *American Journal of Human Genetics.* **70,** 726-736.

Dechat, T., Adam, S.A., Goldman, R.D., 2009. Nuclear lamins and chromatin: when structure meets function. *Advances in Enzyme Regulation.* **49,** 157-166.

Dechat, T., Pfleghaar, K., Sengupta, K., Shimi, T., Shumaker, D.K., Solimando, L., Goldman, R.D., 2008. Nuclear lamins: major factors in the structural organization and function of the nucleus and chromatin. *Genes & Development.* **22,** 832-853.

Dechat, T., Shimi, T., Adam, S.A., Rusinol, A.E., Andres, D.A., Spielmann, H.P., Sinensky, M.S., Goldman, R.D., 2007. Alterations in mitosis and cell cycle progression caused by a mutant lamin A known to accelerate human aging. *Proceedings of the National Academy of Sciences of the United States of America.* **104,** 4955-4960.

Dechat, T., Vlcek, S., Foisner, R., 2000. Review: lamina-associated polypeptide 2 isoforms and related proteins in cell cycle-dependent nuclear structure dynamics. *Journal of Structural Biology.* **129,** 335-345.

Dephoure, N., Zhou, C., Villen, J., Beausoleil, S.A., Bakalarski, C.E., Elledge, S.J., Gygi, S.P., 2008. A quantitative atlas of mitotic phosphorylation. *Proceedings of the National Academy of Sciences of the United States of America.* **105,** 10762-10767.

Desai, A., Murray, A., Mitchison, T.J., Walczak, C.E., 1999. The use of Xenopus egg extracts to study mitotic spindle assembly and function in vitro. *Methods in Cell Biology, Vol 61.* **61,** 385-412.

Dhe-Paganon, S., Werner, E.D., Chi, Y.I., Shoelson, S.E., 2002. Structure of the globular tail of nuclear lamin. *The Journal of Biological Chemistry.* **277,** 17381-17384.

Ding, R., West, R.R., Morphew, D.M., Oakley, B.R., McIntosh, J.R., 1997. The spindle pole body of Schizosaccharomyces pombe enters and leaves the nuclear envelope as the cell cycle proceeds. *Molecular Biology of the Cell.* **8,** 1461-1479.

Ding, X., Xu, R., Yu, J., Xu, T., Zhuang, Y., Han, M., 2007. SUN1 is required for telomere attachment to nuclear envelope and gametogenesis in mice. *Developmental Cell.* **12,** 863-872.

Doree, M. & Galas, S., 1994. The cyclin-dependent protein kinases and the control of cell division. *FASEB Journal : Official Publication of the Federation of American Societies for Experimental Biology.* **8,** 1114-1121.

Dreger, M., Bengtsson, L., Schoneberg, T., Otto, H., Hucho, F., 2001. Nuclear envelope proteomics: novel integral membrane proteins of the inner nuclear membrane. *Proceedings of the National Academy of Sciences of the United States of America.* **98,** 11943-11948.

Drummond, S., Ferrigno, P., Lyon, C., Murphy, J., Goldberg, M., Allen, T., Smythe, C., Hutchison, C.J., 1999. Temporal differences in the appearance of NEP-B78 and an LBR-like protein during Xenopus nuclear envelope reassembly reflect the ordered recruitment of functionally discrete vesicle types. *The Journal of Cell Biology.* **144,** 225-240.

Dultz, E., Zanin, E., Wurzenberger, C., Braun, M., Rabut, G., Sironi, L., Ellenberg, J., 2008. Systematic kinetic analysis of mitotic dis- and reassembly of the nuclear pore in living cells. *Journal of Cell Biology.* **180,** 857-865.

Dunnigan, M.G., Cochrane, M.A., Kelly, A., Scott, J.W., 1974. Familial lipoatrophic diabetes with dominant transmission. A new syndrome. *The Quarterly Journal of Medicine.* **43,** 33-48.

Ellenberg, J., Siggia, E.D., Moreira, J.E., Smith, C.L., Presley, J.F., Worman, H.J., Lippincott-Schwartz, J., 1997. Nuclear membrane dynamics and reassembly in living cells: targeting of an inner nuclear membrane protein in interphase and mitosis. *Journal of Cell Biology.* **138,** 1193-1206.

Ellis, D.J., Jenkins, H., Whitfield, W.G., Hutchison, C.J., 1997. GST-lamin fusion proteins act as dominant negative mutants in Xenopus egg extract and reveal the function of the lamina in DNA replication. *Journal of Cell Science.* **110 (Pt 20),** 2507-2518.

Emery, A.E.H., 1989. Emery-Dreifuss Syndrome. *Journal of Medical Genetics.* **26,** 637-641.

Eriksson, M., Brown, W.T., Gordon, L.B., Glynn, M.W., Singer, J., Scott, L., Erdos, M.R., Robbins, C.M., Moses, T.Y., Berglund, P., Dutra, A., Pak, E., Durkin, S., Csoka, A.B., Boehnke, M., Glover, T.W., Collins, F.S., 2003. Recurrent de novo point mutations in lamin A cause Hutchinson-Gilford progeria syndrome. *Nature.* **423,** 293-298.

Fahrenkrog, B. & Aebi, U., 2003. The nuclear pore complex: nucleocytoplasmic transport and beyond. *Nature Reviews.Molecular Cell Biology.* **4,** 757-766.

Fang, G., Yu, H., Kirschner, M.W., 1998. Direct binding of CDC20 protein family members activates the anaphase-promoting complex in mitosis and G1. *Molecular Cell.* **2,** 163-171.

Ferrari, S., 2006. Protein kinases controlling the onset of mitosis. *Cellular and Molecular Life Sciences.* **63,** 781-795.

Fischer, J.A., Acosta, S., Kenny, A., Cater, C., Robinson, C., Hook, J., 2004. Drosophila klarsicht has distinct subcellular localization domains for nuclear envelope and microtubule localization in the eye. *Genetics.* **168,** 1385-1393.

Fischer-Vize, J.A. & Mosley, K.L., 1994. Marbles mutants: uncoupling cell determination and nuclear migration in the developing Drosophila eye. *Development (Cambridge, England).* **120,** 2609-2618.

Fisher, D.Z., Chaudhary, N., Blobel, G., 1986. cDNA sequencing of nuclear lamins A and C reveals primary and secondary structural homology to intermediate filament proteins. *Proceedings of the National Academy of Sciences of the United States of America.* **83,** 6450-6454.

Foisner, R., 2003. Cell cycle dynamics of the nuclear envelope. *TheScientificWorldJournal.* **3,** 1-20.

Foisner, R. & Gerace, L., 1993. Integral Membrane-Proteins of the Nuclear-Envelope Interact with Lamins and Chromosomes, and Binding is Modulated by Mitotic Phosphorylation. *Cell.* **73,** 1267-1279.

Franz, C., Askjaer, P., Antonin, W., Iglesias, C.L., Haselmann, U., Schelder, M., de Marco, A., Wilm, M., Antony, C., Mattaj, I.W., 2005. Nup155 regulates nuclear envelope and nuclear pore complex formation in nematodes and vertebrates. *The EMBO Journal.* **24,** 3519-3531.

Fridkin, A., Mills, E., Margalit, A., Neufeld, E., Lee, K.K., Feinstein, N., Cohen, M., Wilson, K.L., Gruenbaum, Y., 2004. Matefin, a Caenorhabditis elegans germ line-specific SUN-domain nuclear membrane protein, is essential for early embryonic and germ cell development. *Proceedings of the National Academy of Sciences of the United States of America.* **101,** 6987-6992.

Fridolfsson, H.N., Ly, N., Meyerzon, M., Starr, D.A., 2010. UNC-83 coordinates kinesin-1 and dynein activities at the nuclear envelope during nuclear migration. *Developmental Biology.* **338,** 237-250.

Fridolfsson, H.N. & Starr, D.A., 2010. Kinesin-1 and dynein at the nuclear envelope mediate the bidirectional migrations of nuclei. *The Journal of Cell Biology.* **191,** 115-128.

Fried, H. & Kutay, U., 2003. Nucleocytoplasmic transport: taking an inventory. *Cellular and Molecular Life Sciences : CMLS.* **60,** 1659-1688.

Frohnert, C., Schweizer, S., Hoyer-Fender, S., 2011. SPAG4L/SPAG4L-2 are testis-specific SUN domain proteins restricted to the apical nuclear envelope of round spermatids facing the acrosome. *Molecular Human Reproduction.* **17,** 207-218.

Furukawa, K., Glass, C., Kondo, T., 1997. Characterization of the chromatin binding activity of lamina-associated polypeptide (LAP) 2. *Biochemical and Biophysical Research Communications.* **238,** 240-246.

Furukawa, K. & Hotta, Y., 1993. cDNA cloning of a germ cell specific lamin B3 from mouse spermatocytes and analysis of its function by ectopic expression in somatic cells. *The EMBO Journal.* **12,** 97-106.

Furukawa, K., Inagaki, H., Hotta, Y., 1994. Identification and cloning of an mRNA coding for a germ cell-specific A-type lamin in mice. *Experimental Cell Research.* **212,** 426-430.

Gajewski, A., Csaszar, E., Foisner, R., 2004. A phosphorylation cluster in the chromatin-binding region regulates chromosome association of LAP2 alpha. *Journal of Biological Chemistry.* **279,** 35813-35821.

Galy, V., Antonin, W., Jaedicke, A., Sachse, M., Santarella, R., Haselmann, U., Mattaj, I., 2008. A role for gp210 in mitotic nuclear-envelope breakdown. *Journal of Cell Science.* **121,** 317-328.

Gardner, J.M., Smoyer, C.J., Stensrud, E.S., Alexander, R., Gogol, M., Wiegraebe, W., Jaspersen, S.L., 2011. Targeting of the SUN protein Mps3 to the inner nuclear membrane by the histone variant H2A.Z. *Journal of Cell Biology.* **193,** 489-507.

Georgatos, S.D., Pyrpasopoulou, A., Theodoropoulos, P.A., 1997. Nuclear envelope breakdown in mammalian cells involves stepwise lamina disassembly and microtubule-driven deformation of the nuclear membrane. *Journal of Cell Science.* **110,** 2129-2140.

Gerace, L. & Blobel, G., 1980. Nuclear-Envelope Lamina is Reversibly Depolymerized during Mitosis. *Cell.* **19,** 277-287.

Gerace, L. & Burke, B., 1988. Functional-Organization of the Nuclear-Envelope. *Annual Review of Cell Biology.* **4,** 335-374.

Gerace, L., Ottaviano, Y., Kondor-Koch, C., 1982. Identification of a major polypeptide of the nuclear pore complex. *The Journal of Cell Biology.* **95,** 826-837.

Ghosh, S., Gardner, J.M., Smoyer, C.J., Friederichs, J.M., Unruh, J.R., Slaughter, B.D., Alexander, R., Chisholm, R.D., Lee, K.K., Workman, J.L., Jaspersen, S.L., 2012. Acetylation of the SUN protein Mps3 by Eco1 regulates its function in nuclear organization. *Molecular Biology of the Cell.* **23,** 2546-2559.

Glavy, J.S., Krutchinsky, A.N., Cristea, I.M., Berke, I.C., Boehmer, T., Blobel, G., Chait, B.T., 2007. Cell-cycle-dependent phosphorylation of the nuclear pore Nup107-160 subcomplex. *Proceedings of the National Academy of Sciences of the United States of America.* **104,** 3811-3816.

Glotzer, M., Murray, A.W., Kirschner, M.W., 1991. Cyclin is degraded by the ubiquitin pathway. *Nature.* **349,** 132-138.

Gob, E., Meyer-Natus, E., Benavente, R., Alsheimer, M., 2011. Expression of individual mammalian Sun1 isoforms depends on the cell type. *Communicative & Integrative Biology.* **4,** 440-442.

Goldman, R.D., Gruenbaum, Y., Moir, R.D., Shumaker, D.K., Spann, T.P., 2002. Nuclear lamins: building blocks of nuclear architecture. *Genes & Development.* **16,** 533-547.

Goldman, R.D., Shumaker, D.K., Erdos, M.R., Eriksson, M., Goldman, A.E., Gordon, L.B., Gruenbaum, Y., Khuon, S., Mendez, M., Varga, R., Collins, F.S., 2004. Accumulation of mutant lamin A causes progressive changes in nuclear architecture in Hutchinson-Gilford progeria syndrome. *Proceedings of the National Academy of Sciences of the United States of America.* **101,** 8963-8968.

Gomes, E., Jani, S., Gundersen, G., 2005. Nuclear movement regulated by Cdc42, MRCK, myosin and actin flow establishes MTOC polarization in migrating cells. *Cell Structure and Function.* **30,** 60-60.

Graumann, K., Runions, J., Evans, D.E., 2010. Characterization of SUN-domain proteins at the higher plant nuclear envelope. *The Plant Journal : For Cell and Molecular Biology.* **61,** 134-144.

Greber, U.F., Senior, A., Gerace, L., 1990. A major glycoprotein of the nuclear pore complex is a membrane-spanning polypeptide with a large lumenal domain and a small cytoplasmic tail. *The EMBO Journal.* **9,** 1495-1502.

Grigera, P.R., Ma, L., Borgman, C.A., Pinto, A.F., Sherman, N.E., Parsons, J.T., Fox, J.W., 2012. Mass spectrometric analysis identifies a cortactin-RCC2/TD60 interaction in mitotic cells. *Journal of Proteomics.* **75,** 2153-2159.

Gronborg, M., Kristiansen, T.Z., Stensballe, A., Andersen, J.S., Ohara, O., Mann, M., Jensen, O.N., Pandey, A., 2002. A mass spectrometry-based proteomic approach for identification of serine/threonine-phosphorylated proteins by enrichment with phospho-specific antibodies - Identification of a novel protein, Frigg, as a protein kinase A substrate. *Molecular & Cellular Proteomics.* **1,** 517-527.

Gruenbaum, Y., Margalit, A., Goldman, R.D., Shumaker, D.K., Wilson, K.L., 2005. The nuclear lamina comes of age. *Nature Reviews Molecular Cell Biology.* **6,** 21-31.

Gudise, S., Figueroa, R.A., Lindberg, R., Larsson, V., Hallberg, E., 2011. Samp1 is functionally associated with the LINC complex and A-type lamina networks. *Journal of Cell Science.* **124,** 2077-2085.

Gueneau, L., Bertrand, A.T., Jais, J.P., Salih, M.A., Stojkovic, T., Wehnert, M., Hoeltzenbein, M., Spuler, S., Saitoh, S., Verschueren, A., Tranchant, C., Beuvin, M., Lacene, E., Romero, N.B., Heath, S., Zelenika, D., Voit, T., Eymard, B., Ben Yaou, R., Bonne, G., 2009. Mutations of the FHL1 gene cause Emery-Dreifuss muscular dystrophy. *American Journal of Human Genetics.* **85,** 338-353.

Guettinger, S., Laurell, E., Kutay, U., 2009. Orchestrating nuclear envelope disassembly and reassembly during mitosis. *Nature Reviews Molecular Cell Biology.* **10,** 178-191.

Guo, Y., Jangi, S., Welte, M.A., 2005. Organelle-specific control of intracellular transport: distinctly targeted isoforms of the regulator Klar. *Molecular Biology of the Cell.* **16,** 1406-1416.

Hagan, I. & Yanagida, M., 1995. The product of the spindle formation gene sad1+ associates with the fission yeast spindle pole body and is essential for viability. *The Journal of Cell Biology.* **129,** 1033-1047.

Hagting, A., Den Elzen, N., Vodermaier, H.C., Waizenegger, I.C., Peters, J.M., Pines, J., 2002. Human securin proteolysis is controlled by the spindle checkpoint and reveals when the APC/C switches from activation by Cdc20 to Cdh1. *The Journal of Cell Biology.* **157,** 1125-1137.

Hallberg, E., Wozniak, R.W., Blobel, G., 1993. An integral membrane protein of the pore membrane domain of the nuclear envelope contains a nucleoporin-like region. *The Journal of Cell Biology.* **122,** 513-521.

Hames, R.S., Wattam, S.L., Yamano, H., Bacchieri, R., Fry, A.M., 2001. APC/C-mediated destruction of the centrosomal kinase Nek2A occurs in early mitosis and depends upon a cyclin A-type D-box. *Embo Journal.* **20,** 7117-7127.

Hanks, S.K., 2003. Genomic analysis of the eukaryotic protein kinase superfamily: a perspective. *Genome Biology.* **4,** 111.

Haque, F., Lloyd, D.J., Smallwood, D.T., Dent, C.L., Shanahan, C.M., Fry, A.M., Trembath, R.C., Shackleton, S., 2006. SUN1 interacts with nuclear lamin A and cytoplasmic nesprins to provide a physical connection between the nuclear lamina and the cytoskeleton. *Molecular & Cellular Biology.* **26,** 3738-3751.

Haque, F., Mazzeo, D., Patel, J.T., Smallwood, D.T., Ellis, J.A., Shanahan, C.M., Shackleton, S., 2010. Mammalian SUN Protein Interaction Networks at the Inner Nuclear Membrane and Their Role in Laminopathy Disease Processes. *Journal of Biological Chemistry.* **285,** 3487-3498.

Haraguchi, T., Koujin, T., Hayakawa, T., Kaneda, T., Tsutsumi, C., Imamoto, N., Akazawa, C., Sukegawa, J., Yoneda, Y., Hiraoka, Y., 2000. Live fluorescence imaging reveals early recruitment of emerin, LBR, RanBP2, and Nup153 to reforming functional nuclear envelopes. *Journal of Cell Science.* **113,** 779-794.

Haraguchi, T., Kojidani, T., Koujin, T., Shimi, T., Osakada, H., Mori, C., Yamamoto, A., Hiraoka, Y., 2008. Live cell imaging and electron microscopy reveal dynamic processes of BAF-directed nuclear envelope assembly. *Journal of Cell Science.* **121,** 2540-2554.

Harris, C.A., Andryuk, P.J., Cline, S.W., Mathew, S., Siekierka, J.J., Goldstein, G., 1995. Structure and mapping of the human thymopoietin (TMPO) gene and relationship of human TMPO beta to rat lamin-associated polypeptide 2. *Genomics.* **28,** 198-205.

Hasan, S., Guttinger, S., Muhlhausser, P., Anderegg, F., Burgler, S., Kutay, U., 2006. Nuclear envelope localization of human UNC84A does not require nuclear lamins. *FEBS Letters.* **580,** 1263-1268.

Heald, R. & Mckeon, F., 1990. Mutations of Phosphorylation Sites in Lamin-a that Prevent Nuclear Lamina Disassembly in Mitosis. *Cell.* **61,** 579-589.

Hedgecock, E.M. & Thomson, J.N., 1982. A gene required for nuclear and mitochondrial attachment in the nematode Caenorhabditis elegans. *Cell.* **30,** 321-330.

Hetzer, M., Bilbao-Cortes, D., Walther, T.C., Gruss, O.J., Mattaj, I.W., 2000. GTP hydrolysis by Ran is required for nuclear envelope assembly. *Molecular Cell.* **5,** 1013-1024.

Hirano, T., 2000. Chromosome cohesion, condensation, and separation. *Annual Review of Biochemistry.* **69,** 115-144.

Hirano, Y., Iwase, Y., Ishii, K., Kumeta, M., Horigome, T., Takeyasu, K., 2009. Cell cycle-dependent phosphorylation of MAN1. *Biochemistry.* **48,** 1636-1643.

Hirano, Y., Segawa, M., Ouchi, F.S., Yamakawa, Y., Furukawa, K., Takeyasu, K., Horigome, T., 2005. Dissociation of emerin from barrier-to-autointegration factor is regulated through mitotic phosphorylation of emerin in a Xenopus egg cell-free system. *Journal of Biological Chemistry.* **280,** 39925-39933.

Hiraoka, Y. & Dernburg, A.F., 2009. The SUN Rises on Meiotic Chromosome Dynamics. *Developmental Cell.* **17,** 598-605.

Hiraoka, Y., Maekawa, H., Asakawa, H., Chikashige, Y., Kojidani, T., Osakada, H., Matsuda, A., Haraguchi, T., 2011. Inner nuclear membrane protein Ima1 is dispensable for intranuclear positioning of centromeres. *Genes to Cells.* **16,** 1000-1011.

Hodzic, D.M., Yeater, D.B., Bengtsson, L., Otto, H., Stahl, P.D., 2004. Sun2 is a novel mammalian inner nuclear membrane protein. *Journal of Biological Chemistry.* **279,** 25805-25812.

Hofemeister, H. & O'Hare, P., 2005. Analysis of the localization and topology of nurim, a polytopic protein tightly associated with the inner nuclear membrane. *Journal of Biological Chemistry.* **280,** 2512-2521.

Hoffmann, K., Dreger, C.K., Olins, A.L., Olins, D.E., Shultz, L.D., Lucke, B., Karl, H., Kaps, R., Muller, D., Vaya, A., Aznar, J., Ware, R.E., Sotelo Cruz, N., Lindner, T.H., Herrmann, H., Reis, A., Sperling, K., 2002. Mutations in the gene encoding the lamin B receptor produce an altered nuclear morphology in granulocytes (Pelger-Huet anomaly). *Nature Genetics.* **31,** 410-414.

Hoger, T.H., Krohne, G., Franke, W.W., 1988. Amino acid sequence and molecular characterization of murine lamin B as deduced from cDNA clones. *European Journal of Cell Biology.* **47,** 283-290.

Hoger, T.H., Zatloukal, K., Waizenegger, I., Krohne, G., 1990. Characterization of a second highly conserved B-type lamin present in cells previously thought to contain only a single B-type lamin. *Chromosoma.* **99,** 379-390.

Holmer, L., Pezhman, A., Worman, H.J., 1998. The human lamin B receptor/sterol reductase multigene family. *Genomics.* **54,** 469-476.

Holmer, L. & Worman, H.J., 2001. Inner nuclear membrane proteins: functions and targeting. *Cellular and Molecular Life Sciences : CMLS.* **58,** 1741-1747.

Holt, I., Ostlund, C., Stewart, C.L., Man, N., Worman, H.J., Morris, G.E., 2003. Effect of pathogenic mis-sense mutations in lamin A on its interaction with emerin in vivo. *Journal of Cell Science.* **116,** 3027-3035.

Holt, L.J., Tuch, B.B., Villen, J., Johnson, A.D., Gygi, S.P., Morgan, D.O., 2009. Global Analysis of Cdk1 Substrate Phosphorylation Sites Provides Insights into Evolution. *Science.* **325,** 1682-1686.

Horvitz, H.R. & Sulston, J.E., 1980. Isolation and genetic characterization of cell-lineage mutants of the nematode Caenorhabditis elegans. *Genetics.* **96,** 435-454.

Houben, F., Ramaekers, F.C.S., Snoeckx, L.H.E.H., Broers, J.L.V., 2007. Role of nuclear lamina-cytoskeleton interactions in the maintenance of cellular strength. *Biochimica Et Biophysica Acta-Molecular Cell Research.* **1773,** 675-686.

Imai, S., Nishibayashi, S., Takao, K., Tomifuji, M., Fujino, T., Hasegawa, M., Takano, T., 1997. Dissociation of Oct-1 from the nuclear peripheral structure induces the cellular aging-associated collagenase gene expression. *Molecular Biology of the Cell.* **8,** 2407-2419.

Ito, H., Koyama, Y., Takano, M., Ishii, K., Maeno, M., Furukawa, K., Horigome, T., 2007. Nuclear envelope precursor vesicle targeting to chromatin is stimulated by protein phosphatase 1 in Xenopus egg extracts. *Experimental Cell Research.* **313,** 1897-1910.

Jenkins, H., Holman, T., Lyon, C., Lane, B., Stick, R., Hutchison, C., 1993. Nuclei that lack a lamina accumulate karyophilic proteins and assemble a nuclear matrix. *Journal of Cell Science.* **106 (Pt 1),** 275-285.

Johnson, D.G. & Walker, C.L., 1999. Cyclins and cell cycle checkpoints. *Annual Review of Pharmacology and Toxicology.* **39,** 295-312.

Joseph, J., Tan, S.H., Karpova, T.S., McNally, J.G., Dasso, M., 2002. SUMO-1 targets RanGAP1 to kinetochores and mitotic spindles. *The Journal of Cell Biology.* **156,** 595-602.

Katsani, K.R., Karess, R.E., Dostatni, N., Doye, V., 2008. In vivo dynamics of Drosophila nuclear envelope components. *Molecular Biology of the Cell.* **19,** 3652-3666.

Kennedy, B.K., Barbie, D.A., Classon, M., Dyson, N., Harlow, E., 2000. Nuclear organization of DNA replication in primary mammalian cells. *Genes & Development.* **14,** 2855-2868.

Kennedy, C., Sebire, K., de Kretser, D.M., O'Bryan, M.K., 2004. Human sperm associated antigen 4 (SPAG4) is a potential cancer marker. *Cell and Tissue Research.* **315,** 279-283.

Ketema, M., Wilhelmsen, K., Kuikman, I., Janssen, H., Hodzic, D., Sonnenberg, A., 2007. Requirements for the localization of nesprin-3 at the nuclear envelope and its interaction with plectin. *Journal of Cell Science.* **120,** 3384-3394.

King, M.C., Lusk, C.P., Blobel, G., 2006. Karyopherin-mediated import of integral inner nuclear membrane proteins. *Nature.* **442,** 1003-1007.

King, M.C., Drivas, T.G., Blobel, G., 2008. A network of nuclear envelope membrane proteins linking centromeres to microtubules. *Cell.* **134,** 427-438.

Korfali, N., Wilkie, G.S., Swanson, S.K., Srsen, V., Batrakou, D.G., Fairley, E.A., Malik, P., Zuleger, N., Goncharevich, A., de Las Heras, J., Kelly, D.A., Kerr, A.R., Florens, L., Schirmer, E.C., 2010. The leukocyte nuclear envelope proteome varies with cell activation and contains novel transmembrane proteins that affect genome architecture. *Molecular & Cellular Proteomics : MCP.* **9,** 2571-2585.

Kracklauer, M.P., Banks, S.M.L., Xie, X., Wu, Y., Fischer, J.A., 2007. Drosophila klaroid encodes a SUN domain protein required for Klarsicht localization to the nuclear envelope and nuclear migration in the eye. *Fly.* **1,** 75-85.

Kracklauer, M.P., Wiora, H.M., Deery, W.J., Chen, X., Bolival, B.,Jr., Romanowicz, D., Simonette, R.A., Fuller, M.T., Fischer, J.A., Beckingham, K.M., 2010. The Drosophila SUN protein Spag4 cooperates with the coiled-coil protein Yuri Gagarin to maintain association of the basal body and spermatid nucleus. *Journal of Cell Science.* **123,** 2763-2772.

Krimm, I., Ostlund, C., Gilquin, B., Couprie, J., Hossenlopp, P., Mornon, J.P., Bonne, G., Courvalin, J.C., Worman, H.J., Zinn-Justin, S., 2002. The Ig-like structure of the C-terminal domain of lamin A/C, mutated in muscular dystrophies, cardiomyopathy, and partial lipodystrophy. *Structure (London, England : 1993).* **10,** 811-823.

Kuga, T., Nozaki, N., Matsushita, K., Nomura, F., Tomonaga, T., 2010. Phosphorylation statuses at different residues of lamin B2, B1, and A/C dynamically and independently change throughout the cell cycle. *Experimental Cell Research.* **316,** 2301-2312.

Labella, S., Woglar, A., Jantsch, V., Zetka, M., 2011. Polo Kinases Establish Links between Meiotic Chromosomes and Cytoskeletal Forces Essential for Homo log Pairing. *Developmental Cell.* **21,** 948-958.

Lammerding, J., Hsiao, J., Schulze, P.C., Kozlov, S., Stewart, C.L., Lee, R.T., 2005. Abnormal nuclear shape and impaired mechanotransduction in emerin-deficient cells. *Journal of Cell Biology.* **170,** 781-791.

Lange, A., Mills, R.E., Lange, C.J., Stewart, M., Devine, S.E., Corbett, A.H., 2007. Classical nuclear localization signals: definition, function, and interaction with importin alpha. *The Journal of Biological Chemistry.* **282,** 5101-5105.

Laurell, E., Beck, K., Krupina, K., Theerthagiri, G., Bodenmiller, B., Horvath, P., Aebersold, R., Antonin, W., Kutay, U., 2011. Phosphorylation of Nup98 by Multiple Kinases Is Crucial for NPC Disassembly during Mitotic Entry. *Cell.* **144,** 539-550.

Lee, K.K., Starr, D., Cohen, M., Liu, J., Han, M., Wilson, K.L., Gruenbaum, Y., 2002. Lamin-dependent localization of UNC-84, a protein required for nuclear migration in Caenorhabditis elegans. *Molecular Biology of the Cell.* **13,** 892-901.

Li, H., Liu, X.S., Yang, X., Song, B., Wang, Y., Liu, X., 2010. Polo-like kinase 1 phosphorylation of p150(Glued) facilitates nuclear envelope breakdown during prophase. *Proceedings of the National Academy of Sciences of the United States of America.* **107,** 14633-14638.

Liang, W.C., Mitsuhashi, H., Keduka, E., Nonaka, I., Noguchi, S., Nishino, I., Hayashi, Y.K., 2011. TMEM43 mutations in Emery-Dreifuss muscular dystrophy-related myopathy. *Annals of Neurology.* **69,** 1005-1013.

Libotte, T., Zaim, H., Abraham, S., Padmakumar, V.C., Schneider, M., Lu, W.S., Munck, M., Hutchison, C., Wehnert, M., Fahrenkrog, B., Sauder, U., Aebi, U., Noegel, A.A., Karakesisoglou, L., 2005. Lamin A/C-dependent localization of Nesprin-2, a giant scaffolder at the nuclear envelope. *Molecular Biology of the Cell.* **16,** 3411-3424.

Lin, F. & Worman, H.J., 1995. Structural Organization of the Human Gene (Lmnb1) Encoding Nuclear Lamin B1. *Genomics.* **27,** 230-236.

Lin, F. & Worman, H.J., 1993. Structural Organization of the Human Gene Encoding Nuclear Lamin-a and Nuclear Lamin-C. *Journal of Biological Chemistry.* **268,** 16321-16326.

Lindqvist, A., Rodriguez-Bravo, V., Medema, R.H., 2009. The decision to enter mitosis: feedback and redundancy in the mitotic entry network. *The Journal of Cell Biology.* **185,** 193-202.

Liu, Q., Hirohashi, Y., Du, X., Greene, M.I., Wang, Q., 2010. Nek2 targets the mitotic checkpoint proteins Mad2 and Cdc20: a mechanism for aneuploidy in cancer. *Experimental and Molecular Pathology.* **88,** 225-233.

Liu, Q., Pante, N., Misteli, T., Elsagga, M., Crisp, M., Hodzic, D., Burke, B., Roux, K.J., 2007. Functional association of Sun1 with nuclear pore complexes. *Journal of Cell Biology.* **178,** 785-798.

Lloyd, D.J., Trembath, R.C., Shackleton, S., 2002. A novel interaction between lamin A and SREBP1: implications for partial lipodystrophy and other laminopathies. *Human Molecular Genetics.* **11,** 769-777.

Logarinho, E., Resende, T., Torres, C., Bousbaa, H., 2008. The human spindle assembly checkpoint protein Bub3 is required for the establishment of efficient kinetochore-microtubule attachments. *Molecular Biology of the Cell.* **19,** 1798-1813.

Lombardi, M.L., Jaalouk, D.E., Shanahan, C.M., Burke, B., Roux, K.J., Lammerding, J., 2011. The Interaction between Nesprins and Sun Proteins at the Nuclear Envelope Is Critical for Force Transmission between the Nucleus and Cytoskeleton. *Journal of Biological Chemistry.* **286,** 26743-26753.

Lu, W.S., Gotzmann, J., Sironi, L., Jaeger, V.M., Schneider, M., Luke, Y., Uhlen, M., Szigyarto, C.A.K., Brachner, A., Ellenberg, J., Foisner, R., Noegel, A.A., Karakesisoglou, I., 2008. Sun1 forms immobile macromolecular assemblies at the nuclear envelope. *Biochimica Et Biophysica Acta-Molecular Cell Research.* **1783,** 2415-2426.

Lu, X., Shi, Y., Lu, Q., Ma, Y., Luo, J., Wang, Q., Ji, J., Jiang, Q., Zhang, C., 2010. Requirement for Lamin B Receptor and Its Regulation by Importin beta and Phosphorylation in Nuclear Envelope Assembly during Mitotic Exit. *Journal of Biological Chemistry.* **285,** 33281-33293.

Luo, J. & Liu, X., 2012. Polo-like kinase 1, on the rise from cell cycle regulation to prostate cancer development. *Protein & Cell.* **3,** 182-197.

Luscher, B., Brizuela, L., Beach, D., Eisenman, R.N., 1991. A Role for the P34cdc2 Kinase and Phosphatases in the Regulation of Phosphorylation and Disassembly of Lamin-B2 during the Cell-Cycle. *Embo Journal.* **10,** 865-875.

Lusk, C.P., Blobel, G., King, M.C., 2007. Highway to the inner nuclear membrane: rules for the road. *Nature Reviews.Molecular Cell Biology.* **8,** 414-420.

Luxton, G.W., Gomes, E.R., Folker, E.S., Worman, H.J., Gundersen, G.G., 2011. TAN lines: a novel nuclear envelope structure involved in nuclear positioning. *Nucleus (Austin, Tex.).* **2,** 173-181.

Machiels, B.M., Zorenc, A.H., Endert, J.M., Kuijpers, H.J., van Eys, G.J., Ramaekers, F.C., Broers, J.L., 1996. An alternative splicing product of the lamin A/C gene lacks exon 10. *The Journal of Biological Chemistry.* **271,** 9249-9253.

Malik, P., Korfali, N., Srsen, V., Lazou, V., Batrakou, D.G., Zuleger, N., Kavanagh, D.M., Wilkie, G.S., Goldberg, M.W., Schirmer, E.C., 2010. Cell-specific and lamin-dependent targeting of novel transmembrane proteins in the nuclear envelope. *Cellular and Molecular Life Sciences : CMLS.* **67,** 1353-1369.

Malone, C.J., Fixsen, W.D., Horvitz, H.R., Han, M., 1999. UNC-84 localizes to the nuclear envelope and is required for nuclear migration and anchoring during C-elegans development. *Development.* **126,** 3171-3181.

Malone, C.J., Misner, L., Le Bot, N., Tsai, M.C., Campbell, J.M., Ahringer, J., White, J.G., 2003. The C. elegans hook protein, ZYG-12, mediates the essential attachment between the centrosome and nucleus. *Cell.* **115,** 825-836.

Malumbres, M. & Barbacid, M., 2005. Mammalian cyclin-dependent kinases. *Trends in Biochemical Sciences.* **30,** 630-641.

Mancini, M.A., Shan, B., Nickerson, J.A., Penman, S., Lee, W.H., 1994. The Retinoblastoma Gene-Product is a Cell Cycle-Dependent, Nuclear Matrix-Associated Protein. *Proceedings of the National Academy of Sciences of the United States of America.* **91,** 418-422.

Manilal, S., Man, N.T., Sewry, C.A., Morris, G.E., 1996. The Emery-Dreifuss muscular dystrophy protein, emerin, is a nuclear membrane protein. *Human Molecular Genetics.* **5,** 801-808.

Maniotis, A.J., Chen, C.S., Ingber, D.E., 1997. Demonstration of mechanical connections between integrins cytoskeletal filaments, and nucleoplasm that stabilize nuclear structure. *Proceedings of the National Academy of Sciences of the United States of America.* **94,** 849-854.

Mansharamani, M. & Wilson, K.L., 2005. Direct binding of nuclear membrane protein MAN1 to emerin in vitro and two modes of binding to barrier-to-autointegration factor. *The Journal of Biological Chemistry.* **280,** 13863-13870.

Margalit, A., Vlcek, S., Gruenbaum, Y., Foisner, R., 2005. Breaking and making of the nuclear envelope. *Journal of Cellular Biochemistry.* **95,** 454-465.

Martins, S.B., Eide, T., Steen, R.L., Jahnsen, T., Skalhegg, B.S., Collas, P., 2000. HA95 is a protein of the chromatin and nuclear matrix regulating nuclear envelope dynamics. *Journal of Cell Science.* **113 Pt 21,** 3703-3713.

Mayya, V., Lundgren, D.H., Hwang, S., Rezaul, K., Wu, L., Eng, J.K., Rodionov, V., Han, D.K., 2009. Quantitative Phosphoproteomic Analysis of T Cell Receptor Signaling Reveals System-Wide Modulation of Protein-Protein Interactions. *Science Signaling.* **2,** A37-A52.

McGee, M.D., Rillo, R., Anderson, A.S., Starr, D.A., 2006. UNC-83 is a KASH protein required for nuclear migration and is recruited to the outer nuclear membrane by a physical interaction with the SUN protein UNC-84. *Molecular Biology of the Cell.* **17,** 1790-1801.

Mcgee, M.D., Stagljar, I., Starr, D.A., 2009. KDP-1 is a nuclear envelope KASH protein required for cell-cycle progression. *Journal of Cell Science.* **122,** 2895-2905.

Meier, J. & Georgatos, S.D., 1994. Type B lamins remain associated with the integral nuclear envelope protein p58 during mitosis: implications for nuclear reassembly. *The EMBO Journal.* **13,** 1888-1898.

Mekhail, K. & Moazed, D., 2010. The nuclear envelope in genome organization, expression and stability. *Nature Reviews Molecular Cell Biology.* **11,** 317-328.

Mellad, J.A., Warren, D.T., Shanahan, C.M., 2011. Nesprins LINC the nucleus and cytoskeleton. *Current Opinion in Cell Biology.* **23,** 47-54.

Merner, N.D., Hodgkinson, K.A., Haywood, A.F., Connors, S., French, V.M., Drenckhahn, J.D., Kupprion, C., Ramadanova, K., Thierfelder, L., McKenna, W., Gallagher, B., Morris-Larkin, L., Bassett, A.S., Parfrey, P.S., Young, T.L., 2008. Arrhythmogenic right ventricular cardiomyopathy type 5 is a fully penetrant, lethal arrhythmic disorder caused by a missense mutation in the TMEM43 gene. *American Journal of Human Genetics.* **82,** 809-821.

Meyerson, M. & Harlow, E., 1994. Identification of G1 kinase activity for cdk6, a novel cyclin D partner. *Molecular and Cellular Biology.* **14,** 2077-2086.

Meyerzon, M., Fridolfsson, H.N., Ly, N., McNally, F.J., Starr, D.A., 2009. UNC-83 is a nuclear-specific cargo adaptor for kinesin-1-mediated nuclear migration. *Development.* **136,** 2725-2733.

Minn, I.L., Rolls, M.M., Hanna-Rose, W., Malone, C.J., 2009. SUN-1 and ZYG-12, Mediators of Centrosome-Nucleus Attachment, Are a Functional SUN/KASH Pair in Caenorhabditis elegans. *Molecular Biology of the Cell.* **20,** 4586-4595.

Mislow, J.M., Kim, M.S., Davis, D.B., McNally, E.M., 2002a. Myne-1, a spectrin repeat transmembrane protein of the myocyte inner nuclear membrane, interacts with lamin A/C. *Journal of Cell Science.* **115,** 61-70.

Mislow, J.M.K., Holaska, J.M., Kim, M.S., Lee, K.K., Segura-Totten, M., Wilson, K.L., McNally, E.M., 2002b. Nesprin-1 alpha self-associates and binds directly to emerin and lamin A in vitro. *FEBS Letters.* **525,** 135-140.

Mitchell, J.M., Mansfeld, J., Capitanio, J., Kutay, U., Wozniak, R.W., 2010. Pom121 links two essential subcomplexes of the nuclear pore complex core to the membrane. *Journal of Cell Biology.* **191,** 505-521.

Moir, R.D., Montag-Lowy, M., Goldman, R.D., 1994. Dynamic properties of nuclear lamins: lamin B is associated with sites of DNA replication. *The Journal of Cell Biology.* **125,** 1201-1212.

Mollinari, C., Reynaud, C., Martineau-Thuillier, S., Monier, S., Kieffer, S., Garin, J., Andreassen, P.R., Boulet, A., Goud, B., Kleman, J.P., Margolis, R.L., 2003. The mammalian passenger protein TD-60 is an RCC1 family member with an essential role in prometaphase to metaphase progression. *Developmental Cell.* **5,** 295-307.

Morgan, D.O., 1997. Cyclin-dependent kinases: engines, clocks, and microprocessors. *Annual Review of Cell and Developmental Biology.* **13,** 261-291.

Morgan, D.O., 1995. Principles of CDK regulation. *Nature.* **374,** 131-134.

Morgan, D.O., 2006. *The cell cycle : principles of control.* London: New Science Press.

Mosley-Bishop, K.L., Li, Q., Patterson, L., Fischer, J.A., 1999. Molecular analysis of the klarsicht gene and its role in nuclear migration within differentiating cells of the Drosophila eye. *Current Biology : CB.* **9,** 1211-1220.

Muller, J.M., Metzger, E., Greschik, H., Bosserhoff, A.K., Mercep, L., Buettner, R., Schule, R., 2002. The transcriptional coactivator FHL2 transmits Rho signals from the cell membrane into the nucleus. *The EMBO Journal.* **21,** 736-748.

Murphy, S.P., Simmons, C.R., Bass, H.W., 2010. Structure and expression of the maize (Zea mays L.) SUN-domain protein gene family: evidence for the existence of two divergent classes of SUN proteins in plants. *Bmc Plant Biology.* **10,** 269.

Nakajima, H., Toyoshima-Morimoto, F., Taniguchi, E., Nishida, E., 2003. Identification of a consensus motif for Plk (Polo-like kinase) phosphorylation reveals Myt1 as a Plk1 substrate. *Journal of Biological Chemistry.* **278,** 25277-25280.

Neef, R., Preisinger, C., Sutcliffe, J., Kopajtich, R., Nigg, E.A., Mayer, T.U., Barr, F.A., 2003. Phosphorylation of mitotic kinesin-like protein 2 by polo-like kinase 1 is required for cytokinesis. *The Journal of Cell Biology.* **162,** 863-875.

Newport, J.W., Wilson, K.L., Dunphy, W.G., 1990. A lamin-independent pathway for nuclear envelope assembly. *The Journal of Cell Biology.* **111,** 2247-2259.

Ng, E.K., Chan, K.K., Wong, C.H., Tsui, S.K., Ngai, S.M., Lee, S.M., Kotaka, M., Lee, C.Y., Waye, M.M., Fung, K.P., 2002. Interaction of the heart-specific LIM domain protein, FHL2, with DNA-binding nuclear protein, hNP220. *Journal of Cellular Biochemistry.* **84,** 556-566.

Nigg, E.A., 2001. Mitotic kinases as regulators of cell division and its checkpoints. *Nature Reviews.Molecular Cell Biology.* **2,** 21-32.

Nikolakaki, E., Meier, J., Simos, G., Georgatos, S.D., Giannakouros, T., 1997. Mitotic phosphorylation of the lamin B receptor by a serine/arginine kinase and p34(cdc2). *Journal of Biological Chemistry.* **272,** 6208-6213.

Nili, E., Cojocaru, G.S., Kalma, Y., Ginsberg, D., Copeland, N.G., Gilbert, D.J., Jenkins, N.A., Berger, R., Shaklai, S., Amariglio, N., Brok-Simoni, F., Simon, A.J., Rechavi, G., 2001. Nuclear membrane protein LAP2beta mediates transcriptional repression alone and together with its binding partner GCL (germ-cell-less). *Journal of Cell Science.* **114,** 3297-3307.

Ohba, T., Schirmer, E.C., Nishimoto, T., Gerace, L., 2004. Energy- and temperature-dependent transport of integral proteins to the inner nuclear membrane via the nuclear pore. *The Journal of Cell Biology.* **167,** 1051-1062.

Ohtsubo, M., Kai, R., Furuno, N., Sekiguchi, T., Sekiguchi, M., Hayashida, H., Kuma, K., Miyata, T., Fukushige, S., Murotsu, T., 1987. Isolation and characterization of the active

cDNA of the human cell cycle gene (RCC1) involved in the regulation of onset of chromosome condensation. *Genes & Development.* **1,** 585-593.

Olins, A.L., Hoang, T.V., Zwerger, M., Herrmann, H., Zentgraf, H., Noegel, A.A., Karakesisoglou, I., Hodzic, D., Olins, D.E., 2009. The LINC-less granulocyte nucleus. *European Journal of Cell Biology.* **88,** 203-214.

Olsen, J.V., Blagoev, B., Gnad, F., Macek, B., Kumar, C., Mortensen, P., Mann, M., 2006. Global, in vivo, and site-specific phosphorylation dynamics in signaling networks. *Cell.* **127,** 635-648.

Onischenko, E.A., Crafoord, E., Hallberg, E., 2007. Phosphomimetic mutation of the mitotically phosphorylated serine 1880 compromises the interaction of the transmembrane nucleoporin gp210 with the nuclear pore complex. *Experimental Cell Research.* **313,** 2744-2751.

Ostlund, C., Bonne, G., Schwartz, K., Worman, H.J., 2001. Properties of lamin A mutants found in Emery-Dreifuss muscular dystrophy, cardiomyopathy and Dunnigan-type partial lipodystrophy. *Journal of Cell Science.* **114,** 4435-4445.

Ostlund, C., Folker, E.S., Choi, J.C., Gomes, E.R., Gundersen, G.G., Worman, H.J., 2009. Dynamics and molecular interactions of linker of nucleoskeleton and cytoskeleton (LINC) complex proteins. *Journal of Cell Science.* **122,** 4099-4108.

Ottaviano, Y. & Gerace, L., 1985. Phosphorylation of the nuclear lamins during interphase and mitosis. *The Journal of Biological Chemistry.* **260,** 624-632.

Ozaki, T., Saijo, M., Murakami, K., Enomoto, H., Taya, Y., Sakiyama, S., 1994. Complex formation between lamin A and the retinoblastoma gene product: identification of the domain on lamin A required for its interaction. *Oncogene.* **9,** 2649-2653.

Ozawa, R., Hayashi, Y.K., Ogawa, M., Kurokawa, R., Matsumoto, H., Noguchi, S., Nonaka, I., Nishino, I., 2006. Emerin-lacking mice show minimal motor and cardiac dysfunctions with nuclear-associated vacuoles. *The American Journal of Pathology.* **168,** 907-917.

Padmakumar, V.C., Abraham, S., Braune, S., Noegel, A.A., Tunggal, B., Korenbaum, E., Karakesisoglou, I., 2004. Enaptin, a giant actin-binding protein, is an element of the nuclear membrane and the actin cytoskeleton. *European Journal of Cell Biology.* **83,** 65-65.

Padmakumar, V.C., Libotte, T., Lu, W., Zaim, H., Abraham, S., Noegel, A.A., Gotzmann, J., Foisner, R., Karakesisoglou, I., 2005. The inner nuclear membrane protein Sun1 mediates the anchorage of Nesprin-2 to the nuclear envelope. *Journal of Cell Science.* **118,** 3419-3430.

Pagano, M., Pepperkok, R., Verde, F., Ansorge, W., Draetta, G., 1992. Cyclin A is required at two points in the human cell cycle. *The EMBO Journal.* **11,** 961-971.

Paine, P.L., Moore, L.C., Horowitz, S.B., 1975. Nuclear envelope permeability. *Nature.* **254,** 109-114.

Patterson, K., Molofsky, A.B., Robinson, C., Acosta, S., Cater, C., Fischer, J.A., 2004. The functions of Klarsicht and nuclear lamin in developmentally regulated nuclear migrations of photoreceptor cells in the Drosophila eye. *Molecular Biology of the Cell.* **15,** 600-610.

Penkner, A.M., Fridkin, A., Gloggnitzer, J., Baudrimont, A., Machacek, T., Woglar, A., Csaszar, E., Pasierbek, P., Ammerer, G., Gruenbaum, Y., Jantsch, V., 2009. Meiotic Chromosome Homology Search Involves Modifications of the Nuclear Envelope Protein Matefin/SUN-1. *Cell.* **139,** 920-933.

Penkner, A., Tang, L., Novatchkova, M., Ladurner, M., Fridkin, A., Gruenbaum, Y., Schweizer, D., Loidl, J., Jantsch, V., 2007. The nuclear envelope protein matefin/SUN-1 is required for homologous pairing in C-elegans meiosis. *Developmental Cell.* **12,** 873-885.

Peter, M., Nakagawa, J., Doree, M., Labbe, J.C., Nigg, E.A., 1990. Invitro Disassembly of the Nuclear Lamina and M-Phase Specific Phosphorylation of Lamins by Cdc2 Kinase. *Cell.* **61,** 591-602.

Peter, M. & Nigg, E.A., 1991. Ectopic expression of an A-type lamin does not interfere with differentiation of lamin A-negative embryonal carcinoma cells. *Journal of Cell Science.* **100 (Pt 3),** 589-598.

Pfaller, R., Smythe, C., Newport, J.W., 1991. Assembly Disassembly of the Nuclear-Envelope Membrane - Cell-Cycle Dependent Binding of Nuclear-Membrane Vesicles to Chromatin Invitro. *Cell.* **65,** 209-217.

Pines, J., 2011. Cubism and the cell cycle: the many faces of the APC/C (vol 12, pg 427, 2011). *Nature Reviews Molecular Cell Biology.* **12,** .

Polioudaki, H., Kourmouli, N., Drosou, V., Bakou, A., Theodoropoulos, P.A., Singh, P.B., Giannakouros, T., Georgatos, S.D., 2001. Histones H3/H4 form a tight complex with the inner nuclear membrane protein LBR and heterochromatin protein 1. *EMBO Reports.* **2,** 920-925.

Postel, R., Ketema, M., Kuikman, I., de Pereda, J.M., Sonnenberg, A., 2011. Nesprin-3 augments peripheral nuclear localization of intermediate filaments in zebrafish. *Journal of Cell Science.* **124,** 755-764.

Pyrpasopoulou, A., Meier, J., Maison, C., Simos, G., Georgatos, S.D., 1996. The lamin B receptor (LBR) provides essential chromatin docking sites at the nuclear envelope. *The EMBO Journal.* **15,** 7108-7119.

Qian, J., Lesage, B., Beullens, M., Van Eynde, A., Bollen, M., 2011. PP1/Repo-man dephosphorylates mitotic histone H3 at T3 and regulates chromosomal aurora B targeting. *Current Biology : CB.* **21,** 766-773.

Rajgor, D., Mellad, J.A., Autore, F., Zhang, Q., Shanahan, C.M., 2012. Multiple novel nesprin-1 and nesprin-2 variants act as versatile tissue-specific intracellular scaffolds. *PloS One.* **7,** e40098.

Randles, K.N., Lam, L.T., Sewry, C.A., Puckelwartz, M., Furling, D., Wehnert, M., McNally, E.M., Morris, G.E., 2010. Nesprins, But Not Sun Proteins, Switch Isoforms at the Nuclear Envelope During Muscle Development. *Developmental Dynamics.* **239,** 998-1009.

Rao, H.B.D.P., Shinohara, M., Shinohara, A., 2011. Mps3 SUN domain is important for chromosome motion and juxtaposition of homologous chromosomes during meiosis. *Genes to Cells.* **16,** 1081-1096.

Razafsky, D. & Hodzic, D., 2009. Bringing KASH under the SUN: the many faces of nucleo-cytoskeletal connections. *Journal of Cell Biology.* **186,** 461-472.

Reinsch, S. & Gonczy, P., 1998. Mechanisms of nuclear positioning - Commentary. *Journal of Cell Science.* **111,** 2283-2295.

Rieder, C.L. & Salmon, E.D., 1998. The vertebrate cell kinetochore and its roles during mitosis. *Trends in Cell Biology.* **8,** 310-318.

Rivero, F., Kuspa, A., Brokamp, R., Matzner, M., Noegel, A.A., 1998. Interaptin, an actin-binding protein of the alpha-actinin superfamily in Dictyostelium discoideum, is developmentally and cAMP-regulated and associates with intracellular membrane compartments. *The Journal of Cell Biology.* **142,** 735-750.

Roberts, R.C., Sutherland-Smith, A.J., Wheeler, M.A., Jensen, O.N., Emerson, L.J., Spiliotis, I.I., Tate, C.G., Kendrick-Jones, J., Ellis, J.A., 2006. The Emery-Dreifuss muscular dystrophy associated-protein emerin is phosphorylated on serine 49 by protein kinase A. *Febs Journal.* **273,** 4562-4575.

Rolls, M.M., Stein, P.A., Taylor, S.S., Ha, E., McKeon, F., Rapoport, T.A., 1999. A visual screen of a GFP-fusion library identifies a new type of nuclear envelope membrane protein. *Journal of Cell Biology.* **146,** 29-43.

Rosenberg-Hasson, Y., Renert-Pasca, M., Volk, T., 1996. A Drosophila dystrophin-related protein, MSP-300, is required for embryonic muscle morphogenesis. *Mechanisms of Development.* **60,** 83-94.

Rothbauer, U., Zolghadr, K., Muyldermans, S., Schepers, A., Cardoso, M.C., Leonhardt, H., 2008. A versatile nanotrap for biochemical and functional studies with fluorescent fusion proteins. *Molecular & Cellular Proteomics.* **7,** 282-289.

Roux, K.J., Crisp, M.L., Liu, Q., Kim, D., Kozlov, S., Stewart, C.L., Burke, B., 2009. Nesprin 4 is an outer nuclear membrane protein that can induce kinesin-mediated cell polarization. *Proceedings of the National Academy of Sciences of the United States of America.* **106,** 2194-2199.

Rusinol, A.E. & Sinensky, M.S., 2006. Farnesylated lamins, progeroid syndromes and farnesyl transferase inhibitors. *Journal of Cell Science.* **119,** 3265-3272.

Salaun, P., Rannou, Y., Prigent, C., 2008. Cdk1, Plks, Auroras, and Neks: the mitotic bodyguards. *Advances in Experimental Medicine and Biology.* **617,** 41-56.

Salina, D., Bodoor, K., Eckley, D.M., Schroer, T.A., Rattner, J.B., Burke, B., 2002. Cytoplasmic dynein as a facilitator of nuclear envelope breakdown. *Cell.* **108,** 97-107.

Salina, D., Enarson, P., Rattner, J.B., Burke, B., 2003. Nup358 integrates nuclear envelope breakdown with kinetochore assembly. *Journal of Cell Biology.* **162,** 991-1001.

Salpingidou, G., Smertenko, A., Hausmanowa-Petrucewicz, I., Hussey, P.J., Hutchison, C.J., 2007. A novel role for the nuclear membrane protein emerin in association of the centrosome to the outer nuclear membrane. *Journal of Cell Biology.* **178,** 897-904.

Sarkar, P.K. & Shinton, R.A., 2001. Hutchinson-Guilford progeria syndrome. *Postgraduate Medical Journal.* **77,** 312-317.

Sasagawa, S., Yamamoto, A., Ichimura, T., Omata, S., Horigome, T., 1999. In vitro nuclear assembly with affinity-purified nuclear envelope precursor vesicle fractions, PV1 and PV2. *European Journal of Cell Biology.* **78,** 593-600.

Sato, A., Isaac, B., Phillips, C.M., Rillo, R., Carlton, P.M., Wynne, D.J., Kasad, R.A., Dernburg, A.F., 2009. Cytoskeletal Forces Span the Nuclear Envelope to Coordinate Meiotic Chromosome Pairing and Synapsis. *Cell.* **139,** 907-919.

Schirmer, E.C., Florens, L., Guan, T.L., Yates, J.R., Gerace, L., 2003. Nuclear membrane proteins with potential disease links found by subtractive proteomics. *Science.* **301,** 1380-1382.

Schirmer, E.C. & Gerace, L., 2005. The nuclear membrane proteome: extending the envelope. *Trends in Biochemical Sciences.* **30,** 551-558.

Schirmer, E.C., Guan, T., Gerace, L., 2001. Involvement of the lamin rod domain in heterotypic lamin interactions important for nuclear organization. *The Journal of Cell Biology.* **153,** 479-489.

Schmitt, J., Benavente, R., Hodzic, D., Hoog, C., Stewarts, C.L., Alsheimer, M., 2007. Transmembrane protein Sun2 is involved in tethering mammalian meiotic telomeres to the nuclear envelope. *Proceedings of the National Academy of Sciences of the United States of America.* **104,** 7426-7431.

Schober, H., Ferreira, H., Kalck, R., Gehlen, L.R., Gasser, S.M., 2009. Yeast telomerase and the SUN domain protein Mps3 anchor telomeres and repress subtelomeric recombination. *Genes & Development.* **23,** 928-938.

Schulz, I., Baumann, O., Samereier, M., Zoglmeier, C., Graef, R., 2009. Dictyostelium Sun1 is a dynamic membrane protein of both nuclear membranes and required for centrosomal association with clustered centromeres. *European Journal of Cell Biology.* **88,** 621-638.

Segura-Totten, M. & Wilson, K.L., 2004. BAF: roles in chromatin, nuclear structure and retrovirus integration. *Trends in Cell Biology.* **14,** 261-266.

Shackleton, S., Lloyd, D.J., Jackson, S.N., Evans, R., Niermeijer, M.F., Singh, B.M., Schmidt, H., Brabant, G., Kumar, S., Durrington, P.N., Gregory, S., O'Rahilly, S., Trembath, R.C., 2000. LMNA, encoding lamin A/C, is mutated in partial lipodystrophy. *Nature Genetics.* **24,** 153-156.

Shao, X.P., Tarnasky, H.A., Lee, J.P., Oko, R., van der Hoorn, F.A., 1999. Spag4, a novel sperm protein, binds outer dense-fiber protein Odf1 and localizes to microtubules of manchette and axoneme. *Developmental Biology.* **211,** 109-123.

Shimada, N., Inouye, K., Sawai, S., Kawata, T., 2010. SunB, a novel Sad1 and UNC-84 domain-containing protein required for development of Dictyostelium discoideum. *Development Growth & Differentiation.* **52,** 577-590.

Shumaker, D.K., Kuczmarski, E.R., Goldman, R.D., 2003. The nucleoskeleton: lamins and actin are major players in essential nuclear functions. *Current Opinion in Cell Biology.* **15,** 358-366.

Smith, S. & Blobel, G., 1993. The first membrane spanning region of the lamin B receptor is sufficient for sorting to the inner nuclear membrane. *The Journal of Cell Biology.* **120,** 631-637.

Sosa, B.A., Rothballer, A., Kutay, U., Schwartz, T.U., 2012. LINC Complexes Form by Binding of Three KASH Peptides to Domain Interfaces of Trimeric SUN Proteins. *Cell.* **149,** 1035-47.

Soullam, B. & Worman, H.J., 1995. Signals and structural features involved in integral membrane protein targeting to the inner nuclear membrane. *The Journal of Cell Biology.* **130,** 15-27.

Soullam, B. & Worman, H.J., 1993. The amino-terminal domain of the lamin B receptor is a nuclear envelope targeting signal. *The Journal of Cell Biology.* **120,** 1093-1100.

Spann, T.P., Goldman, A.E., Wang, C., Huang, S., Goldman, R.D., 2002. Alteration of nuclear lamin organization inhibits RNA polymerase II-dependent transcription. *The Journal of Cell Biology.* **156,** 603-608.

Spann, T.P., Moir, R.D., Goldman, A.E., Stick, R., Goldman, R.D., 1997. Disruption of nuclear lamin organization alters the distribution of replication factors and inhibits DNA synthesis. *The Journal of Cell Biology.* **136,** 1201-1212.

Starr, D.A. & Han, M., 2002. Role of ANC-1 in tethering nuclei to the actin cytoskeleton. *Science.* **298,** 406-409.

Starr, D.A., Hermann, G.J., Malone, C.J., Fixsen, W., Priess, J.R., Horvitz, H.R., Han, M., 2001. Unc-83 Encodes a Novel Component of the Nuclear Envelope and is Essential for Proper Nuclear Migration. *Development (Cambridge, England).* **128,** 5039-5050.

Starr, D.A., 2011. KASH and SUN proteins. *Current Biology.* **21,** R414-R415.

Stavru, F., Hulsmann, B.B., Spang, A., Hartmann, E., Cordes, V.C., Gorlich, D., 2006. NDC1: a crucial membrane-integral nucleoporin of metazoan nuclear pore complexes. *The Journal of Cell Biology.* **173,** 509-519.

Stemmann, O., Zou, H., Gerber, S.A., Gygi, S.P., Kirschner, M.W., 2001. Dual inhibition of sister chromatid separation at metaphase. *Cell.* **107,** 715-726.

Stewart-Hutchinson, P.J., Hale, C.M., Wirtz, D., Hodzic, D., 2008. Structural requirements for the assembly of LINC complexes and their function in cellular mechanical stiffness. *Experimental Cell Research.* **314,** 1892-1905.

Stuurman, N., Heins, S., Aebi, U., 1998. Nuclear lamins: their structure, assembly, and interactions. *Journal of Structural Biology.* **122,** 42-66.

Sullivan, T., Escalante-Alcalde, D., Bhatt, H., Anver, M., Bhat, N., Nagashima, K., Stewart, C.L., Burke, B., 1999. Loss of A-type lamin expression compromises nuclear envelope integrity leading to muscular dystrophy. *Journal of Cell Biology.* **147,** 913-920.

Sulston, J.E. & Horvitz, H.R., 1981. Abnormal cell lineages in mutants of the nematode Caenorhabditis elegans. *Developmental Biology.* **82,** 41-55.

Sumara, I., Vorlaufer, E., Stukenberg, P.T., Kelm, O., Redemann, N., Nigg, E.A., Peters, J.M., 2002. The dissociation of cohesin from chromosomes in prophase is regulated by Polo-like kinase. *Molecular Cell.* **9,** 515-525.

Takano, M., Koyama, Y., Ito, H., Hoshino, S., Onogi, H., Hagiwara, M., Furukawa, K., Horigome, T., 2004. Regulation of binding of lamin B receptor to chromatin by SR protein kinase and cdc2 kinase in Xenopus egg extracts. *The Journal of Biological Chemistry.* **279,** 13265-13271.

Talamas, J.A. & Hetzer, M.W., 2011. POM121 and Sun1 play a role in early steps of interphase NPC assembly. *The Journal of Cell Biology.* **194,** 27-37.

Tang, Z., Shu, H., Oncel, D., Chen, S., Yu, H., 2004. Phosphorylation of Cdc20 by Bub1 provides a catalytic mechanism for APC/C inhibition by the spindle checkpoint. *Molecular Cell.* **16,** 387-397.

Technau, M. & Roth, S., 2008. The Drosophila KASH domain proteins Msp-300 and Klarsicht and the SUN domain protein klaroid have no essential function during oogenesis. *Fly.* **2,** 82-91.

Thompson, L.J., Bollen, M., Fields, A.P., 1997. Identification of protein phosphatase 1 as a mitotic lamin phosphatase. *Journal of Biological Chemistry.* **272,** 29693-29697.

Thompson, L.J. & Fields, A.P., 1996. beta(II) protein kinase C is required for the G(2)/M phase transition of cell cycle. *Journal of Biological Chemistry.* **271,** 15045-15053.

Tifft, K.E., Bradbury, K.A., Wilson, K.L., 2009. Tyrosine phosphorylation of nuclear-membrane protein emerin by Src, Abl and other kinases. *Journal of Cell Science.* **122,** 3780-3790.

Tran, E.J. & Wente, S.R., 2006. Dynamic nuclear pore complexes: life on the edge. *Cell.* **125,** 1041-1053.

Trinkle-Mulcahy, L., Andersen, J., Lam, Y.W., Moorhead, G., Mann, M., Lamond, A.I., 2006. Repo-Man recruits PP1 gamma to chromatin and is essential for cell viability. *The Journal of Cell Biology.* **172,** 679-692.

Trinkle-Mulcahy, L., Boulon, S., Lam, Y.W., Urcia, R., Boisvert, F.M., Vandermoere, F., Morrice, N.A., Swift, S., Rothbauer, U., Leonhardt, H., Lamond, A., 2008. Identifying specific protein interaction partners using quantitative mass spectrometry and bead proteomes. *The Journal of Cell Biology.* **183,** 223-239.

Tsai, M.Y., Wang, S., Heidinger, J.M., Shumaker, D.K., Adam, S.A., Goldman, R.D., Zheng, Y., 2006. A mitotic lamin B matrix induced by RanGTP required for spindle assembly. *Science (New York, N.Y.).* **311,** 1887-1893.

Tseng, L. & Chen, R., 2011. Temporal control of nuclear envelope assembly by phosphorylation of lamin B receptor. *Molecular Biology of the Cell.* **22,** 3306-3317.

Turgay, Y., Ungricht, R., Rothballer, A., Kiss, A., Csucs, G., Horvath, P., Kutay, U., 2010. A classical NLS and the SUN domain contribute to the targeting of SUN2 to the inner nuclear membrane. *Embo Journal.* **29,** 2262-2275.

Tzur, Y.B., Wilson, K.L., Gruenbaum, Y., 2006. SUN-domain proteins: 'Velcro' that links the nucleoskeleton to the cytoskeleton. *Nature Reviews Molecular Cell Biology.* **7,** 782-788.

Uhlmann, F., Lottspeich, F., Nasmyth, K., 1999. Sister-chromatid separation at anaphase onset is promoted by cleavage of the cohesin subunit Scc1. *Nature.* **400,** 37-42.

Vagnarelli, P., Hudson, D.F., Ribeiro, S.A., Trinkle-Mulcahy, L., Spence, J.M., Lai, F., Farr, C.J., Lamond, A.I., Earnshaw, W.C., 2006. Condensin and Repo-Man-PP1 co-operate in the regulation of chromosome architecture during mitosis. *Nature Cell Biology.* **8,** 1133-1142.

Vaisberg, E.A., Koonce, M.P., McIntosh, J.R., 1993. Cytoplasmic dynein plays a role in mammalian mitotic spindle formation. *The Journal of Cell Biology.* **123,** 849-858.

Vaughan, O.A., Alvarez-Reyes, M., Bridger, J.M., Broers, J.L.V., Ramaekers, F.C.S., Wehnert, M., Morris, G.E., Whitfield, W.G.F., Hutchison, C.J., 2001. Both emerin and lamin C depend on lamin A for localization at the nuclear envelope. *Journal of Cell Science.* **114,** 2577-2590.

Vigers, G.P.A. & Lohka, M.J., 1991. A Distinct Vesicle Population Targets Membranes and Pore Complexes to the Nuclear-Envelope in Xenopus Eggs. *Journal of Cell Biology.* **112,** 545-556.

Vigouroux, C., Magre, J., Vantyghem, M.C., Bourut, C., Lascols, O., Shackleton, S., Lloyd, D.J., Guerci, B., Padova, G., Valensi, P., Grimaldi, A., Piquemal, R., Touraine, P., Trembath, R.C., Capeau, J., 2000. Lamin A/C gene: sex-determined expression of mutations in Dunnigan-type familial partial lipodystrophy and absence of coding mutations in congenital and acquired generalized lipoatrophy. *Diabetes.* **49,** 1958-1962.

Visintin, R., Craig, K., Hwang, E.S., Prinz, S., Tyers, M., Amon, A., 1998. The phosphatase Cdc14 triggers mitotic exit by reversal of Cdk-dependent phosphorylation. *Molecular Cell.* **2,** 709-718.

Voeltz, G.K., Rolls, M.M., Rapoport, T.A., 2002. Structural organization of the endoplasmic reticulum. *EMBO Reports.* **3,** 944-950.

Volk, T., 1992. A new member of the spectrin superfamily may participate in the formation of embryonic muscle attachments in Drosophila. *Development (Cambridge, England).* **116,** 721-730.

Ward, G.E. & Kirschner, M.W., 1990. Identification of cell cycle-regulated phosphorylation sites on nuclear lamin C. *Cell.* **61,** 561-577.

Waterham, H.R., Koster, J., Mooyer, P., Noort Gv, G., Kelley, R.I., Wilcox, W.R., Wanders, R.J., Hennekam, R.C., Oosterwijk, J.C., 2003. Autosomal recessive HEM/Greenberg skeletal dysplasia is caused by 3 beta-hydroxysterol delta 14-reductase deficiency due to mutations in the lamin B receptor gene. *American Journal of Human Genetics.* **72,** 1013-1017.

Wen, W., Meinkoth, J.L., Tsien, R.Y., Taylor, S.S., 1995. Identification of a signal for rapid export of proteins from the nucleus. *Cell.* **82,** 463-473.

Wheeler, M.A., Davies, J.D., Zhanq, Q., Emerson, L.J., Hunt, J., Shanahan, C.M., Ellis, J.A., 2007. Distinct functional domains in nesprin-1 alpha and nesprin-2 beta bind directly to emerin and both interactions are disrupted in X-linked Emery-Dreifuss muscular dystrophy. *Experimental Cell Research.* **313,** 2845-2857.

Wiche, G., 1998. Role of plectin in cytoskeleton organization and dynamics. *Journal of Cell Science.* **111 (Pt 17),** 2477-2486.

Wilhelmsen, K., Litjens, S.H., Kuikman, I., Tshimbalanga, N., Janssen, H., van den Bout, I., Raymond, K., Sonnenberg, A., 2005. Nesprin-3, a novel outer nuclear membrane protein, associates with the cytoskeletal linker protein plectin. *Journal of Cell Biology.* **171,** 799-810.

Wilkie, G.S., Korfali, N., Swanson, S.K., Malik, P., Srsen, V., Batrakou, D.G., de las Heras, J., Zuleger, N., Kerr, A.R., Florens, L., Schirmer, E.C., 2011. Several novel nuclear envelope transmembrane proteins identified in skeletal muscle have cytoskeletal associations. *Molecular & Cellular Proteomics : MCP.* **10,** M110.003129.

Wilson, K.L. & Newport, J., 1988. A trypsin-sensitive receptor on membrane vesicles is required for nuclear envelope formation in vitro. *The Journal of Cell Biology.* **107,** 57-68.

Worman, H.J. & Bonne, G., 2007. "Laminopathies": A wide spectrum of human diseases. *Experimental Cell Research.* **313,** 2121-2133.

Worman, H.J., Evans, C.D., Blobel, G., 1990. The lamin B receptor of the nuclear envelope inner membrane: a polytopic protein with eight potential transmembrane domains. *The Journal of Cell Biology.* **111,** 1535-1542.

Worman, H.J., Yuan, J., Blobel, G., Georgatos, S.D., 1988. A lamin B receptor in the nuclear envelope. *Proceedings of the National Academy of Sciences of the United States of America.* **85,** 8531-8534.

Wu, J., Matunis, M.J., Kraemer, D., Blobel, G., Coutavas, E., 1995. Nup358, a cytoplasmically exposed nucleoporin with peptide repeats, Ran-GTP binding sites, zinc fingers, a cyclophilin A homologous domain, and a leucine-rich region. *The Journal of Biological Chemistry.* **270,** 14209-14213.

Wu, W., Lin, F., Worman, H.J., 2002. Intracellular trafficking of MAN1, an integral protein of the nuclear envelope inner membrane. *Journal of Cell Science.* **115,** 1361-1371.

Wurzenberger, C. & Gerlich, D.W., 2011. Phosphatases: providing safe passage through mitotic exit. *Nature Reviews.Molecular Cell Biology.* **12,** 469-482.

Wysocki, V.H., Resing, K.A., Zhang, Q., Cheng, G., 2005. Mass spectrometry of peptides and proteins. *Methods (San Diego, Calif.).* **35,** 211-222.

Xie, X. & Fischer, J.A., 2008. On the roles of the Drosophila KASH domain proteins Msp-300 and Klarsicht. *Fly.* **2,** 74-81.

Xiong, H., Rivero, F., Euteneuer, U., Mondal, S., Mana-Capelli, S., Larochelle, D., Vogel, A., Gassen, B., Noegel, A.A., 2008. Dictyostelium Sun-1 connects the centrosome to chromatin and ensures genome stability. *Traffic.* **9,** 708-724.

Yang, F., Camp, D.G.,2nd, Gritsenko, M.A., Luo, Q., Kelly, R.T., Clauss, T.R., Brinkley, W.R., Smith, R.D., Stenoien, D.L., 2007. Identification of a novel mitotic phosphorylation motif associated with protein localization to the mitotic apparatus. *Journal of Cell Science.* **120,** 4060-4070.

Yang, L., Guan, T., Gerace, L., 1997. Lamin-binding fragment of LAP2 inhibits increase in nuclear volume during the cell cycle and progression into S phase. *The Journal of Cell Biology.* **139,** 1077-1087.

Ye, Q., Callebaut, I., Pezhman, A., Courvalin, J.C., Worman, H.J., 1997. Domain-specific interactions of human HP1-type chromodomain proteins and inner nuclear membrane protein LBR. *The Journal of Biological Chemistry.* **272,** 14983-14989.

Ye, Q. & Worman, H.J., 1996. Interaction between an integral protein of the nuclear envelope inner membrane and human chromodomain proteins homologous to Drosophila HP1. *The Journal of Biological Chemistry.* **271,** 14653-14656.

Ye, Q. & Worman, H.J., 1994. Primary structure analysis and lamin B and DNA binding of human LBR, an integral protein of the nuclear envelope inner membrane. *The Journal of Biological Chemistry.* **269,** 11306-11311.

Zhang, C. & Clarke, P.R., 2000. Chromatin-independent nuclear envelope assembly induced by Ran GTPase in Xenopus egg extracts. *Science (New York, N.Y.).* **288,** 1429-1432.

Zhang, Q., Bethmann, C., Worth, N.F., Davies, J.D., Wasner, C., Feuer, A., Ragnauth, C.D., Yi, Q., Mellad, J.A., Warren, D.T., Wheeler, M.A., Ellis, J.A., Skepper, J.N., Vorgerd, M., Schlotter-Weigel, B., Weissberg, P.L., Roberts, R.G., Wehnert, M., Shanahan, C.M., 2007. Nesprin-1 and -2 are involved in the pathogenesis of Emery Dreifuss muscular dystrophy and are critical for nuclear envelope integrity. *Human Molecular Genetics.* **16,** 2816-2833.

Zhang, Q., Ragnauth, C., Greener, M.J., Shanahan, C.M., Roberts, R.G., 2002. The nesprins are giant actin-binding proteins, orthologous to Drosophila melanogaster muscle protein MSP-300. *Genomics.* **80,** 473-481.

Zhang, Q., Ragnauth, C.D., Skepper, J.N., Worth, N.F., Warren, D.T., Roberts, R.G., Weissberg, P.L., Ellis, J.A., Shanahan, C.M., 2005. Nesprin-2 is a multi-isomeric protein that binds lamin and emerin at the nuclear envelope and forms a subcellular network in skeletal muscle. *Journal of Cell Science.* **118,** 673-687.

Zhang, Q., Skepper, J.N., Yang, F., Davies, J.D., Hegyi, L., Roberts, R.G., Weissberg, P.L., Ellis, J.A., Shanahan, C.M., 2001. Nesprins: a novel family of spectrin-repeat-containing proteins that localize to the nuclear membrane in multiple tissues. *Journal of Cell Science.* **114,** 4485-4498.

Zhang, Q., Vo, N., Goodman, R.H., 2000. Histone binding protein RbAp48 interacts with a complex of CREB binding protein and phosphorylated CREB. *Molecular and Cellular Biology.* **20,** 4970-4978.

Zhang, X., Xu, R., Zhu, B., Yang, X., Ding, X., Duan, S., Xu, T., Zhuang, Y., Han, M., 2007. Syne-1 and Syne-2 play crucial roles in myonuclear anchorage and motor neuron innervation. *Development (Cambridge, England).* **134,** 901-908.

Zhen, Y.Y., Libotte, T., Munck, M., Noegel, A.A., Korenbaum, E., 2002. NUANCE, a giant protein connecting the nucleus and actin cytoskeleton. *Journal of Cell Science.* **115,** 3207-3222.

Zheng, Y. & Tsai, M.Y., 2006. The mitotic spindle matrix: a fibro-membranous lamin connection. *Cell Cycle (Georgetown, Tex.).* **5,** 2345-2347.

Zhou, K., Rolls, M.M., Hall, D.H., Malone, C.J., Hanna-Rose, W., 2009. A ZYG-12-dynein interaction at the nuclear envelope defines cytoskeletal architecture in the C. elegans gonad. *The Journal of Cell Biology.* **186,** 229-241.

Zhou, X., Graumann, K., Evans, D.E., Meier, I., 2012a. Novel plant SUN-KASH bridges are involved in RanGAP anchoring and nuclear shape determination. *Journal of Cell Biology.* **196,** 203-211.

Zhou, Z., Du, X., Cai, Z., Song, X., Zhang, H., Mizuno, T., Suzuki, E., Yee, M.R., Berezov, A., Murali, R., Wu, S., Karger, B.L., Greene, M.I., Wang, Q., 2012b. Structure of Sad1-UNC84 Homology (SUN) Domain Defines Features of Molecular Bridge in Nuclear Envelope. *Journal of Biological Chemistry.* **287,** 5317-5326.

Zou, H., McGarry, T.J., Bernal, T., Kirschner, M.W., 1999. Identification of a vertebrate sister-chromatid separation inhibitor involved in transformation and tumorigenesis. *Science (New York, N.Y.).* **285,** 418-422.

Appendix

APPENDIX

Appendix A: Vector maps for pLEICS10 (MBP), pLEICS20 (MYC), pLEICS21 (GFP).

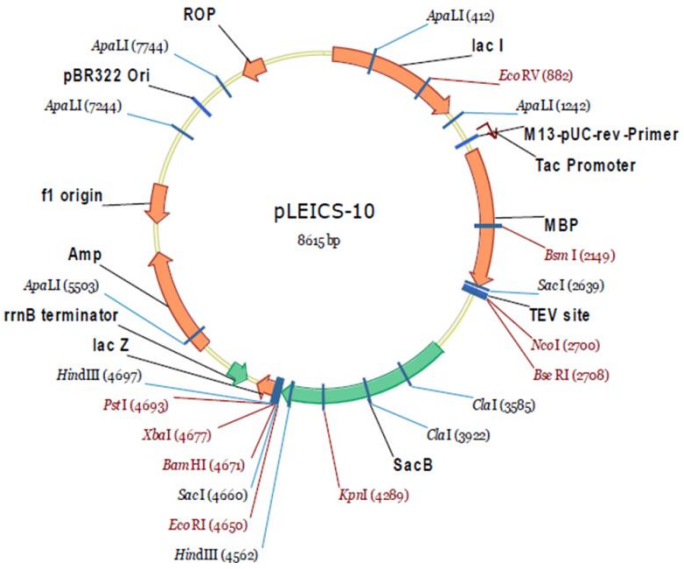

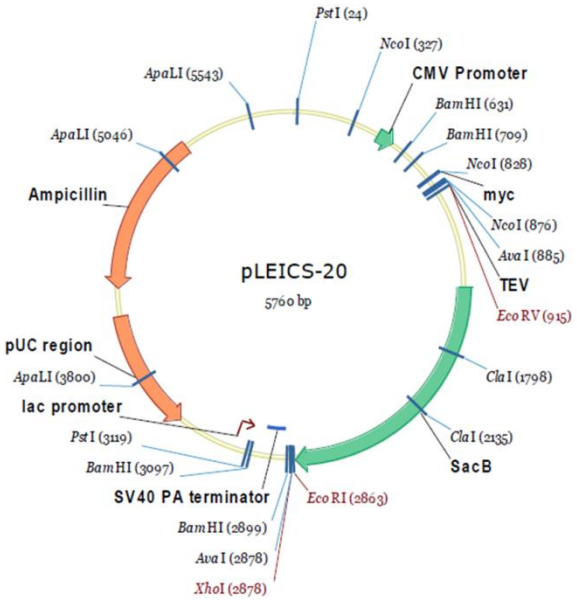

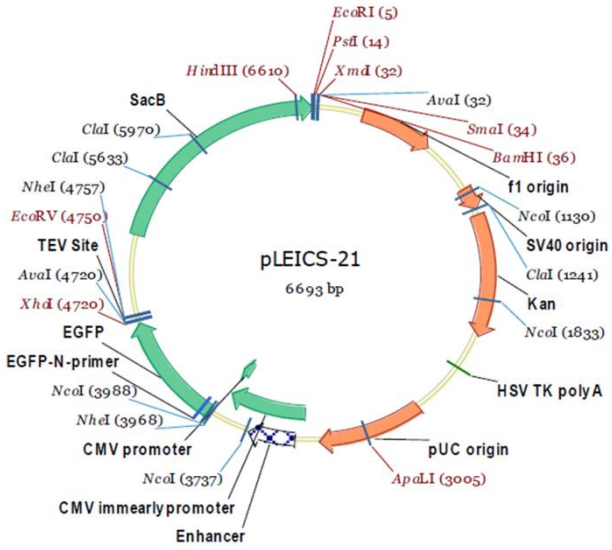

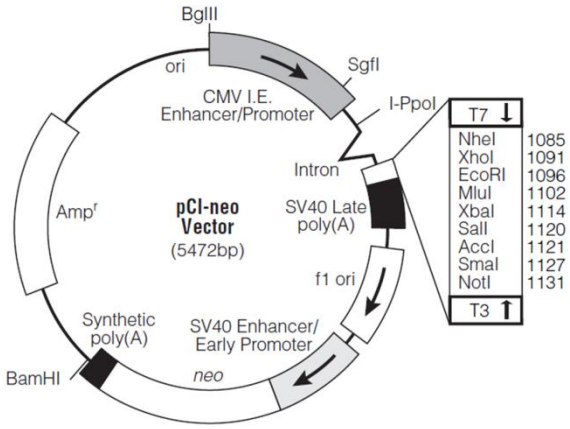
BglII
ori
SgfI
CMV I.E.
Enhancer/Promoter
I-PpoI
T7
NheI 1085
XhoI 1091
EcoRI 1096
MluI 1102
XbaI 1114
SalI 1120
AccI 1121
SmaI 1127
NotI 1131
T3
Intron
Amp^r
pCI-neo
Vector
(5472bp)
SV40 Late
poly(A)
f1 ori
Synthetic
poly(A)
SV40 Enhancer/
Early Promoter
BamHI
neo

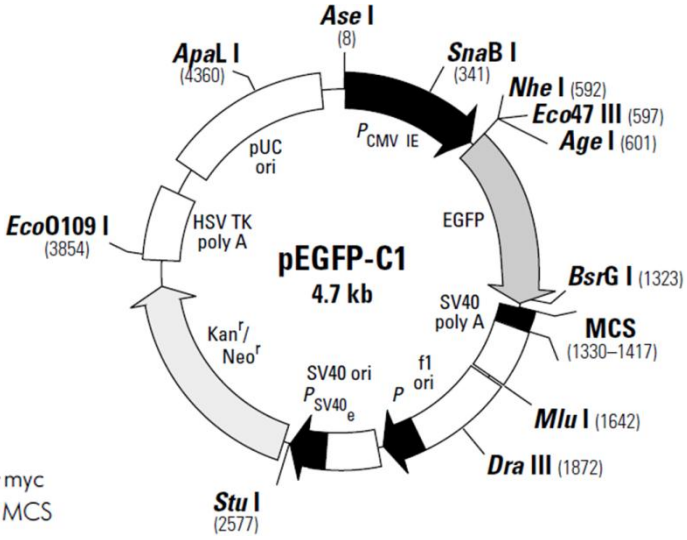
Ase I
(8)
ApaL I
(4360)
SnaB I
(341)
Nhe I (592)
Eco47 III (597)
Age I (601)
pUC
ori
P CMV IE
EGFP
Eco0109 I
(3854)
HSV TK
poly A
pEGFP-C1
4.7 kb
BsrG I (1323)
SV40
poly A
MCS
(1330–1417)
Kan^r/
Neo^r
SV40 ori
P SV40 e
f1
ori
P
Mlu I (1642)
Dra III (1872)
Stu I
(2577)

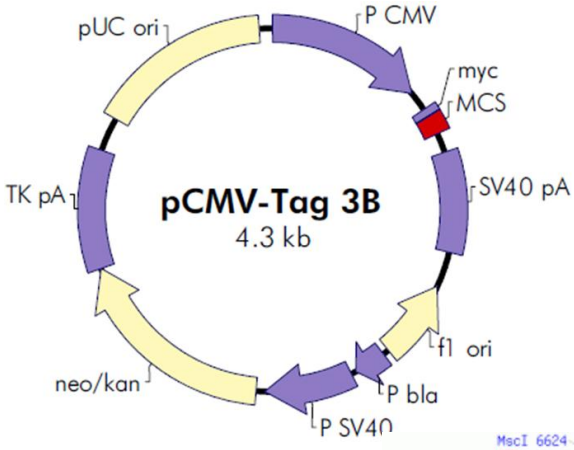
pUC ori
P CMV
myc
MCS
TK pA
pCMV-Tag 3B
4.3 kb
SV40 pA
f1 ori
neo/kan
P bla
P SV40

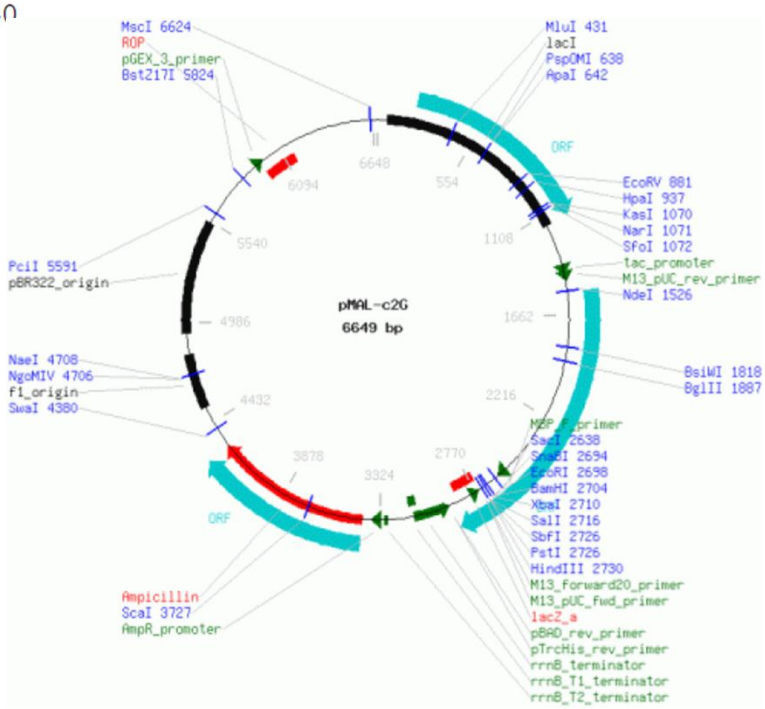
MscI 6624
ROP
pGEX_3_primer
BstZ17I 5824
MluI 431
lacI
PspOMI 638
ApaI 642
ORF
6648
554
6094
EcoRV 881
HpaI 937
KasI 1070
NarI 1071
SfoI 1072
1108
5540
tac_promoter
M13_pUC_rev_primer
NdeI 1526
PciI 5591
pBR322_origin
pMAL-c2G
6649 bp
4986
1662
BsiWI 1818
BglII 1887
NaeI 4708
NgoMIV 4706
f1_origin
SwaI 4380
4432
2216
MBP_primer
SacI 2638
SmaI 2694
EcoRI 2698
BamHI 2704
XbaI 2710
SalI 2716
SbfI 2726
PstI 2726
HindIII 2730
M13_forward20_primer
M13_pUC_fwd_primer
lacZ_a
pBAD_rev_primer
pTrcHis_rev_primer
rrnB_terminator
rrnB_T1_terminator
rrnB_T2_terminator
3878
3324
2770
ORF
Ampicillin
ScaI 3727
AmpR_promoter

Appendix B: List of constructs produced by PROTEX at the University of Leicester by mutagenesis and cloning techniques.

Primers and template are shown along with the final construct.

Construct name	Template	PCR 1		PCR 2
pLEICS20 hSUN1 S48A myc	pLEICS20 hSUN1 WT myc	hSUN1 RecA-F hSUN1 S48A-R	hSUN1 S48A-F hSUN1 RecA-R	hSUN1 RecA-F hSUN1 RecA-R
pLEICS20 hSUN1 S48D myc	pLEICS20 hSUN1 WT myc	hSUN1 RecA-F hSUN1 S48D-R	hSUN1 S48D-F hSUN1 RecA-R	hSUN1 RecA-F hSUN1 RecA-R
pLEICS20 hSUN1 S52A myc	pLEICS20 hSUN1 WT myc	hSUN1 RecA-F hSUN1 S52A-R	hSUN1 S52A-F hSUN1 RecA-R	hSUN1 RecA-F hSUN1 RecA-R
pLEICS20 hSUN1 S52D myc	pLEICS20 hSUN1 WT myc	hSUN1 RecA-F hSUN1 S52D-R	hSUN1 S52D-F hSUN1 RecA-R	hSUN1 RecA-F hSUN1 RecA-R
pLEICS20 hSUN1 S138A myc	pLEICS20 hSUN1 WT myc	hSUN1 RecA-F hSUN1 S138A-R	hSUN1 S138A-F hSUN1 RecA-R	hSUN1 RecA-F hSUN1 RecA-R
pLEICS20 hSUN1 S138D myc	pLEICS20 hSUN1 WT myc	hSUN1 RecA-F hSUN1 S138D-R	hSUN1 S138D-F hSUN1 RecA-R	hSUN1 RecA-F hSUN1 RecA-R
pLEICS20 hSUN1 T144A myc	pLEICS20 hSUN1 WT myc	hSUN1 RecA-F hSUN1 T144A-R	hSUN1 T144A-F hSUN1 RecA-R	hSUN1 RecA-F hSUN1 RecA-R
pLEICS20 hSUN1 T144D myc	pLEICS20 hSUN1 WT myc	hSUN1 RecA-F hSUN1 T144D-R	hSUN1 T144D-F hSUN1 RecA-R	hSUN1 RecA-F hSUN1 RecA-R
pLEICS20 hSUN1 T144E myc	pLEICS20 hSUN1 WT myc	hSUN1 RecA-F hSUN1 T144E-R	hSUN1 T144E-F hSUN1 RecA-R	hSUN1 RecA-F hSUN1 RecA-R
pLEICS20 hSUN1 S333A myc	pLEICS20 hSUN1 WT myc	hSUN1 RecA-F hSUN1 S333A-R	hSUN1 S333A-F hSUN1 RecA-R	hSUN1 RecA-F hSUN1 RecA-R
pLEICS20 hSUN1 S333D myc	pLEICS20 hSUN1 WT myc	hSUN1 RecA-F hSUN1 S333D-R	hSUN1 S333D-F hSUN1 RecA-R	hSUN1 RecA-F hSUN1 RecA-R
pLEICS20 hSUN1 S48A/S138A myc	pLEICS20 hSUN1 S48A myc	hSUN1 RecA-F hSUN1 S138A-R	hSUN1 S138A-F hSUN1 RecA-R	hSUN1 RecA-F hSUN1 RecA-R
pLEICS20 hSUN1 S48D/S138D myc	pLEICS20 hSUN1 S138D myc	hSUN1 RecA-F hSUN1 S48D-R	hSUN1 S48D-F hSUN1 RecA-R	hSUN1 RecA-F hSUN1 RecA-R
pLEICS20 hSUN1 S48A/S333A myc	pLEICS20 hSUN1 S48A myc	hSUN1 RecA-F hSUN1 S333A-R	hSUN1 S333A-F hSUN1 RecA-R	hSUN1 RecA-F hSUN1 RecA-R
pLEICS10 hSUN1 S138A/T144A myc	pLEICS20 hSUN1 S138A myc	hSUN1 RecA-F hSUN1 T144A-R	hSUN1 T144A-F hSUN1 RecA-R	hSUN1 RecA-F hSUN1 RecA-R
pLEICS20 hSUN1 S48A/S138A/S333A myc	pLEICS20 hSUN1 S48A/S138A myc	hSUN1 RecA-F hSUN1 S333A-R	hSUN1 S333A-F hSUN1 RecA-R	hSUN1 RecA-F hSUN1 RecA-R
pLEICS20 hSUN1 S48D/S138D/S333D myc	pLEICS20 hSUN1 S48D/S138D myc	hSUN1 RecA-F hSUN1 S333D-R	hSUN1 S333D-F hSUN1 RecA-R	hSUN1 RecA-F hSUN1 RecA-R
pLEICS20 hSUN1 S48D/S333D GFP	pLEICS20 hSUN1 S333D myc	hSUN1 RecE-F hSUN1 S48D-R	hSUN1 S48D-F hSUN1 RecE-R	hSUN1 RecE-F hSUN1 RecE-R

Appendix C: List of constructs made by PROTEX at the University of Leicester by direct cloning techniques.

Primers and template are shown along with the final construct.

Vector and plasmid	Template	Forward primer	Reverse primer
pLEICS20 hSUN1 WT myc	pCMV3B hSUN1 (1-916) Bgl	hSUN1 RecA-F	hSUN1 RecA-R
pLEICS21 hSUN1 WT GFP	pLEICS20 hSUN1 WT myc	hSUN1 RecE-F	hSUN1 RecE-R
pLEICS21 hSUN1 S48A GFP	pLEICS20 hSUN1 S48A myc	hSUN1 RecE-F	hSUN1 RecE-R
pLEICS21 hSUN1 S48D GFP	pLEICS20 hSUN1 S48D myc	hSUN1 RecE-F	hSUN1 RecE-R
pLEICS21 hSUN1 S138A GFP	pLEICS20 hSUN1 S138A myc	hSUN1 RecE-F	hSUN1 RecE-R
pLEICS21 hSUN1 S138D GFP	pLEICS20 hSUN1 S138D myc	hSUN1 RecE-F	hSUN1 RecE-R
pLEICS21 hSUN1 T144E GFP	pLEICS20 hSUN1 T144E myc	hSUN1 RecE-F	hSUN1 RecE-R
pLEICS21 hSUN1 S333A GFP	pLEICS20 hSUN1 S333A myc	hSUN1 RecE-F	hSUN1 RecE-R
pLEICS21 hSUN1 S333D GFP	pLEICS20 hSUN1 S333D myc	hSUN1 RecE-F	hSUN1 RecE-R
pLEICS21 hSUN1 S48A/S333A GFP	pLEICS20 hSUN1 S48A/S333A myc	hSUN1 RecE-F	hSUN1 RecE-R
pLEICS20 hSUN1 S48D/S333D myc	pLEICS21 hSUN1 S48D/S333D GFP	hSUN1 RecA-F	hSUN1 RecA-R
pLEICS21 hSUN1 S48A/S138A/S333A GFP	pLEICS20 hSUN1 S48A/S138A/S333A myc	hSUN1 RecE-F	hSUN1 RecE-R
pLEICS21 hSUN1 S48D/S138D/S333D GFP	pLEICS20 hSUN1 S48D/S138D/S333D myc	hSUN1 RecE-F	hSUN1 RecE-R
pLEICS10 hSUN1 WT 1-217 MBP	pLEICS20 hSUN1 WT myc	hSUN1 RecA-F	hSUN1 RecA-R 1-217
pLEICS10 hSUN1 WT 1-362 MBP	pLEICS20 hSUN1 WT myc	hSUN1 RecA-F	hSUN1 RecA-R 1-362
pLEICS10 hSUN1 WT 455-916 MBP	pMAL hSUN1 455-916	hSUN1 RecA-F	hSUN1 RecA-R
pLEICS10 hSUN1 S48A 1-217 MBP	pLEICS20 hSUN1 S48A myc	hSUN1 RecA-F	hSUN1 RecA-R 1-217
pLEICS10 hSUN1 S48A 1-362 MBP	pLEICS20 hSUN1 S48A myc	hSUN1 RecA-F	hSUN1 RecA-R 1-362
pLEICS10 hSUN1 S48D 1-362 MBP	pLEICS20 hSUN1 S48D myc	hSUN1 RecA-F	hSUN1 RecA-R 1-362
pLEICS10 hSUN1 S52A 1-362 MBP	pLEICS20 hSUN1 S52A myc	hSUN1 RecA-F	hSUN1 RecA-R 1-362
pLEICS10 hSUN1 S52D 1-362 MBP	pLEICS20 hSUN1 S52D myc	hSUN1 RecA-F	hSUN1 RecA-R 1-362
pLEICS10 hSUN1 S138A 1-217 MBP	pLEICS20 hSUN1 S138A myc	hSUN1 RecA-F	hSUN1 RecA-R 1-217
pLEICS10 hSUN1 S138A 1-362 MBP	pLEICS20 hSUN1 S138A myc	hSUN1 RecA-F	hSUN1 RecA-R 1-362
pLEICS10 hSUN1 S138D 1-362 MBP	pLEICS20 hSUN1 S138D myc	hSUN1 RecA-F	hSUN1 RecA-R 1-362
pLEICS10 hSUN1 T144A 1-217 MBP	pLEICS20 hSUN1 T144A myc	hSUN1 RecA-F	hSUN1 RecA-R 1-217
pLEICS10 hSUN1 T144E 1-362 MBP	pLEICS20 hSUN1 T144E myc	hSUN1 RecA-F	hSUN1 RecA-R 1-362
pLEICS10 hSUN1 S333A 1-362 MBP	pLEICS20 hSUN1 S333A myc	hSUN1 RecA-F	hSUN1 RecA-R 1-362
pLEICS10 hSUN1 S333D 1-362 MBP	pLEICS20 hSUN1 S333D myc	hSUN1 RecA-F	hSUN1 RecA-R 1-362
pLEICS10 hSUN1 1-362 S48A/S333A MBP	pLEICS20 hSUN1 S48A/S333A myc	hSUN1 RecA-F	hSUN1 RecA-R 1-362
pLEICS10 hSUN1	pLEICS10 hSUN1 S138A/T144A	hSUN1 RecA-F	hSUN1 RecA-R 1-

S138A/T144A 1-217 MBP		myc		217
pLEICS10 S48A/S138A/S333A MBP	**hSUN1 1-362**	pLEICS20 hSUN1 S48A/S138A/S333A myc	hSUN1 RecA-F	hSUN1 RecA-R 1-362
pLEICS10 S48D/S138D/S333D MBP	**hSUN1 1-362**	pLEICS20 hSUN1 S48D/S138D/S333D myc	hSUN1 RecA-F	hSUN1 RecA-R 1-362
pLEICS10 GFP 3NLS GFP		Annealing pair of oligos ready to clone into vector. No PCR required		

Appendix D: hSUN1 DNA and protein sequence.

```
atggatttttctcggcttcacatgtacagtcctccccagtgtgtgccggagaacacgggc
 M  D  F  S  R  L  H  M  Y  S  P  P  Q  C  V  P  E  N  T  G
tacacgtatgcgctcagttccagctattcttcagatgctctggattttgagacagagcac
 Y  T  Y  A  L  S  S  S  Y  S  S  D  A  L  D  F  E  T  E  H
aaattggaccctgtatttgattctccacggatgtcccgccgtagtttgcgcctggccacg
 K  L  D  P  V  F  D  S  P  R  M  S  R  R  S  L  R  L  A  T
acagcatgcaccctgggggatggtgaggctgtgggtgccgacagcggcaccagcagcgct
 T  A  C  T  L  G  D  G  E  A  V  G  A  D  S  G  T  S  S  A
gtctccctgaagaaccgagcggccagaacaacaaaacagcgcagaagcacaaacaaatca
 V  S  L  K  N  R  A  A  R  T  T  K  Q  R  R  S  T  N  K  S
gcttttagtatcaaccacgtgtcaaggcaggtcacgtcctctggcgtcagctacggcggc
 A  F  S  I  N  H  V  S  R  Q  V  T  S  S  G  V  S  Y  G  G
actgtcagcctgcaggatgctgtgactcgacggcctcctgtattggacgagtcttggatt
 T  V  S  L  Q  D  A  V  T  R  R  P  P  V  L  D  E  S  W  I
cgtgaacagaccacagtggaccacttctggggtcttgatgatgatggtgatcttaaaggt
 R  E  Q  T  T  V  D  H  F  W  G  L  D  D  D  G  D  L  K  G
ggaaataaagctgccattcagggaaacggggatgtgggagccgccgccgccaccgcgcac
 G  N  K  A  A  I  Q  G  N  G  D  V  G  A  A  A  A  T  A  H
aacggcttctcctgcagcaactgcagcatgctgtccgagcgcaaggacgtgctcacggcg
 N  G  F  S  C  S  N  C  S  M  L  S  E  R  K  D  V  L  T  A
caccccgcggcccccgggcccgtgtcgagagtttattctagggacaggaatcaaaaatgc
 H  P  A  A  P  G  P  V  S  R  V  Y  S  R  D  R  N  Q  K  C
ggtgcgtctttctacgtgaataggattttgtggctggccagatacactgcatcatctttt
 G  A  S  F  Y  V  N  R  I  L  W  L  A  R  Y  T  A  S  S  F
tcatcattttagttcaacttttcaagtggttttaatgaagctcagttatgaatcagaa
 S  S  F  L  V  Q  L  F  Q  V  V  L  M  K  L  S  Y  E  S  E
aattacaaattgaaaactcatgaatcaaaagattgtgaatccgaaagctataagtcaaaa
 N  Y  K  L  K  T  H  E  S  K  D  C  E  S  E  S  Y  K  S  K
agccatgaatcaaaagctcatgccagttactatgggagaatgaatgtgagagaggttctc
 S  H  E  S  K  A  H  A  S  Y  Y  G  R  M  N  V  R  E  V  L
agagaggatggccacctcagtgtaaatggggaagcgctgtgcgacgactgtaagggcaag
 R  E  D  G  H  L  S  V  N  G  E  A  L  C  D  D  C  K  G  K
aggcacctcgacgcgcacacagccgcccactcgcagtcgccacggctgcccggtcgggca
 R  H  L  D  A  H  T  A  A  H  S  Q  S  P  R  L  P  G  R  A
gggaccctctggcacatctgggcatgtgcaggttacttcttgctgcagatcttgcgcagg
 G  T  L  W  H  I  W  A  C  A  G  Y  F  L  L  Q  I  L  R  R
atcggagctgtgggccaggctgtgtccaggacggcgtggtcggccctttggctggccgtg
 I  G  A  V  G  Q  A  V  S  R  T  A  W  S  A  L  W  L  A  V
gttgctccagggaaggcagcctctggagtgttctggtggctggggattggatggtaccag
 V  A  P  G  K  A  A  S  G  V  F  W  W  L  G  I  G  W  Y  Q
tttgttactttgatttcttggctgaatgtgtttcttcttaccaggtgccttcgaaacatc
 F  V  T  L  I  S  W  L  N  V  F  L  L  T  R  C  L  R  N  I
tgcaagtttttagtcttgctcatcccactcttccttttactagcaggtctctccttacgg
 C  K  F  L  V  L  L  I  P  L  F  L  L  L  A  G  L  S  L  R
ggccagggcaatttcttttcgttcttgcccgtgttgaactgggcaagcatgcatagaaca
 G  Q  G  N  F  F  S  F  L  P  V  L  N  W  A  S  M  H  R  T
cagcgggtggatgacccccaggacgtgtttaaacccacgacttctcgcctgaagcagcct
 Q  R  V  D  D  P  Q  D  V  F  K  P  T  T  S  R  L  K  Q  P
ctgcagggtgacagtgaggcttttccgtggcattggatgagtggcgtggagcagcaggtg
 L  Q  G  D  S  E  A  F  P  W  H  W  M  S  G  V  E  Q  Q  V
gcctctctgtctggacagtgccaccaccatggtgagaatctccgagagctgaccactttg
 A  S  L  S  G  Q  C  H  H  H  G  E  N  L  R  E  L  T  T  L
ctacagaagctgcaggctcgggtggaccagatggaaggcggcgctgccgggccgtcagct
 L  Q  K  L  Q  A  R  V  D  Q  M  E  G  G  A  A  G  P  S  A
tcggtcagagacgctgtgggacagcccccgagggagactgactttatggcctttcaccaa
 S  V  R  D  A  V  G  Q  P  P  R  E  T  D  F  M  A  F  H  Q
gaacatgaagtgcgtatgtcacacttggaagatattctgggaaaactgagagaaaaatct
 E  H  E  V  R  M  S  H  L  E  D  I  L  G  K  L  R  E  K  S
gaggccatccagaaggaactagaacagaccaagcaaaaaacaatcagtgcggttggtgag
 E  A  I  Q  K  E  L  E  Q  T  K  Q  K  T  I  S  A  V  G  E
```

```
cagctcctgcccacagtcgagcacctccagctggagctggatcagctaaagtcagagctg
 Q   L   L   P   T   V   E   H   L   Q   L   E   L   D   Q   L   K   S   E   L
tccagctggcgacacgtgaagaccggctgtgagacagtggatgccgtacaagaaagagtg
 S   S   W   R   H   V   K   T   G   C   E   T   V   D   A   V   Q   E   R   V
gacgtgcaagtcagagaaatggtgaaactcctgttttccgaagatcagcaaggcggttct
 D   V   Q   V   R   E   M   V   K   L   L   F   S   E   D   Q   Q   G   G   S
ctggaacagctgctgcagaggttctcatcacagtttgtgagcaaaggcgacttgcagacg
 L   E   Q   L   L   Q   R   F   S   S   Q   F   V   S   K   G   D   L   Q   T
atgctgcgagacctgcagctgcagatcctgcggaacgtcacccaccacgtttccgtgacc
 M   L   R   D   L   Q   L   Q   I   L   R   N   V   T   H   H   V   S   V   T
aagcagctcccaacctcagaagccgtggtgtctgctgtgagcgaggcgggggcgtctgga
 K   Q   L   P   T   S   E   A   V   V   S   A   V   S   E   A   G   A   S   G
ataacagaggcgcaagcacgtgccatcgtgaacagcgccttgaagctgtattcccaagat
 I   T   E   A   Q   A   R   A   I   V   N   S   A   L   K   L   Y   S   Q   D
aagaccgggatggtggactttgctctggaatctggtggtggcagcatcttgagtactcgc
 K   T   G   M   V   D   F   A   L   E   S   G   G   G   S   I   L   S   T   R
tgttctgaaacttacgaaaccaaaacggcgctgatgagtctgtttgggatcccgctgtgg
 C   S   E   T   Y   E   T   K   T   A   L   M   S   L   F   G   I   P   L   W
tacttctcgcagtccccgcgcgtggtcatccagcctgacatttaccccggtaactgctgg
 Y   F   S   Q   S   P   R   V   V   I   Q   P   D   I   Y   P   G   N   C   W
gcatttaaaggctcccaggggtacctggtggtgaggctctccatgatgatccacccagcc
 A   F   K   G   S   Q   G   Y   L   V   V   R   L   S   M   M   I   H   P   A
gccttcactctggagcacatccctaagacgctgtcgccaacaggcaacatcagcagcgcc
 A   F   T   L   E   H   I   P   K   T   L   S   P   T   G   N   I   S   S   A
cccaaggacttcgccgtctatggattagaaaatgagtatcaggaagaagggcagcttctg
 P   K   D   F   A   V   Y   G   L   E   N   E   Y   Q   E   E   G   Q   L   L
ggacagttcacgtatgatcaggatggggagtcgctccagatgttccaggccctgaaaaga
 G   Q   F   T   Y   D   Q   D   G   E   S   L   Q   M   F   Q   A   L   K   R
cccgacgacacagctttccaaatagtggaacttcggatttttttctaactggggccatcct
 P   D   D   T   A   F   Q   I   V   E   L   R   I   F   S   N   W   G   H   P
gagtatacctgtctgtatcggttcagagttcatggcgaacctgtcaagtga
 E   Y   T   C   L   Y   R   F   R   V   H   G   E   P   V   K   -
```

Appendix E. Raw data from the large-scale IP-MS experiments to investigate novel hSUN1 binding partners.

R1 UL01008JP, Samples report created on 06/29/2012						
Experiment: R1 UL01008JP						
Scaffold Version: Scaffold_3.1.4.1						
Peptide Thresholds: 95.0% minimum						
Protein Thresholds: 95.0% minimum and 3 peptides minimum						
R1 UL01008JP	**Identified Proteins (314)**	**UniProtKB Accession Number**	**Molecular Weight**	**Number of peptides detected**		
				1. Async	**2. Mitotic**	**3. GFP**
8	SUN domain-containing protein 1 OS=Homo sapiens GN=SUN1 PE=1 SV=3	O94901	90 kDa	65	151	0
14	Tubulin alpha-1C chain OS=Homo sapiens GN=TUBA1C PE=1 SV=1	Q9BQE3	50 kDa	28	0	0
84	Splicing factor, proline- and glutamine-rich OS=Homo sapiens GN=SFPQ PE=1 SV=2	P23246	76 kDa	6	12	0
95	Emerin OS=Homo sapiens GN=EMD PE=1 SV=1	P50402	29 kDa	8	0	0
98	D-3-phosphoglycerate dehydrogenase OS=Homo sapiens GN=PHGDH PE=1 SV=4	O43175	57 kDa	7	13	0
104	60S ribosomal protein L15 OS=Homo sapiens GN=RPL15 PE=1 SV=2	P61313	24 kDa	5	4	0
116	Polyadenylate-binding protein 1 OS=Homo sapiens GN=PABPC1 PE=1 SV=2	P11940	71 kDa	3	7	0
119	40S ribosomal protein S17 OS=Homo sapiens GN=RPS17 PE=1 SV=2	P08708	16 kDa	8	0	0
124	40S ribosomal protein S5 OS=Homo sapiens GN=RPS5 PE=1 SV=4	P46782	23 kDa	5	7	0
127	Importin subunit beta-1 OS=Homo sapiens GN=KPNB1 PE=1 SV=2	Q14974	97 kDa	2	9	0
128	40S ribosomal protein S10 OS=Homo sapiens GN=RPS10 PE=1 SV=1	P46783	19 kDa	3	10	0
131	NADPH--cytochrome P450 reductase OS=Homo sapiens GN=POR PE=1 SV=2	P16435	77 kDa	0	18	0
138	Brain acid soluble protein 1 OS=Homo sapiens GN=BASP1 PE=1 SV=2	P80723	23 kDa	0	18	0
142	60S ribosomal protein L36a OS=Homo sapiens GN=RPL36A PE=1 SV=2	P83881	12 kDa	4	9	0
146	Glyceraldehyde-3-phosphate dehydrogenase OS=Homo sapiens GN=GAPDH PE=1 SV=3	P04406	36 kDa	6	6	0
147	40S ribosomal protein S26 OS=Homo sapiens GN=RPS26 PE=1 SV=3	P62854	13 kDa	0	10	0
149	Protein ERGIC-53 OS=Homo sapiens GN=LMAN1 PE=1 SV=2	P49257	58 kDa	4	7	0
150	Protein RCC2 OS=Homo sapiens GN=RCC2 PE=1 SV=2	Q9P258	56 kDa	5	6	0
151	Glucose-6-phosphate 1-dehydrogenase OS=Homo sapiens GN=G6PD PE=1 SV=4	P11413	59 kDa	7	0	0
155	Vesicle-trafficking protein SEC22b OS=Homo sapiens GN=SEC22B PE=1 SV=3	O75396	25 kDa	3	9	0
160	BAG family molecular chaperone regulator 2 OS=Homo sapiens GN=BAG2 PE=1 SV=1	O95816	24 kDa	4	4	0
161	60S ribosomal protein L5 OS=Homo sapiens GN=RPL5 PE=1 SV=3	P46777	34 kDa	5	4	0
162	60S ribosomal protein L30 OS=Homo sapiens GN=RPL30 PE=1 SV=2	P62888	13 kDa	5	7	0
164	Sorting and assembly machinery component 50 homolog OS=Homo sapiens GN=SAMM50 PE=1 SV=3	Q9Y512	52 kDa	10	0	0
165	Tubulin alpha-1B chain OS=Homo sapiens GN=TUBA1B PE=1 SV=1	P68363	50 kDa	31	0	0
168	60S ribosomal protein L23 OS=Homo sapiens GN=RPL23 PE=1 SV=1	P62829	15 kDa	5	0	0
169	60S ribosomal protein L13a OS=Homo sapiens GN=RPL13A PE=1 SV=2	P40429	24 kDa	2	0	0
170	Tropomyosin alpha-3 chain OS=Homo sapiens GN=TPM3 PE=1 SV=1	P06753	33 kDa	7	0	0
171	NADH-cytochrome b5 reductase 3 OS=Homo sapiens GN=CYB5R3 PE=1 SV=3	P00387	34 kDa	4	4	0
173	Cytoplasmic dynein 1 heavy chain 1 OS=Homo sapiens GN=DYNC1H1 PE=1 SV=5	Q14204	532 kDa	0	10	0
180	Ras-related protein Rab-5C OS=Homo sapiens GN=RAB5C PE=1 SV=2	P51148	23 kDa	2	6	0
181	Transmembrane emp24 domain-containing protein 10 OS=Homo sapiens GN=TMED10 PE=1 SV=2	P49755	25 kDa	3	0	0
182	Folate receptor alpha OS=Homo sapiens GN=FOLR1 PE=1 SV=3	P15328	30 kDa	5	0	0
183	60S ribosomal protein L31 OS=Homo sapiens GN=RPL31 PE=1 SV=1	P62899	14 kDa	2	0	0
184	40S ribosomal protein S11 OS=Homo sapiens GN=RPS11 PE=1 SV=3	P62280	18 kDa	3	0	0
187	Exportin-2 OS=Homo sapiens GN=CSE1L PE=1 SV=3	P55060	110 kDa	0	4	0
188	Inosine-5'-monophosphate dehydrogenase 2 OS=Homo sapiens GN=IMPDH2 PE=1 SV=2	P12268	56 kDa	3	6	0
189	Plasminogen activator inhibitor 1 RNA-binding protein OS=Homo sapiens GN=SERBP1 PE=1 SV=2	Q8NC51	45 kDa	5	0	0
190	Actin-binding LIM protein 1 OS=Homo sapiens GN=ABLIM1 PE=1 SV=3	O14639	88 kDa	3	0	0
191	Sarcoplasmic/endoplasmic reticulum calcium ATPase 2 OS=Homo sapiens GN=ATP2A2 PE=1 SV=1	P16615	115 kDa	0	13	0
192	Non-POU domain-containing octamer-binding protein OS=Homo sapiens GN=NONO PE=1 SV=4	Q15233	54 kDa	0	15	0
194	60S ribosomal protein L10 OS=Homo sapiens GN=RPL10 PE=1 SV=4	P27635	25 kDa	2	0	0
195	60S ribosomal protein L21 OS=Homo sapiens GN=RPL21 PE=1 SV=2	P46778	19 kDa	0	4	0
198	Trans-2,3-enoyl-CoA reductase OS=Homo sapiens GN=TECR PE=1 SV=1	Q9NZ01	36 kDa	5	0	0
199	Casein kinase I isoform alpha OS=Homo sapiens GN=CSNK1A1 PE=1 SV=2	P48729	39 kDa	0	7	0
201	Histone-binding protein RBBP4 OS=Homo sapiens GN=RBBP4 PE=1 SV=3	Q09028	48 kDa	5	4	0
202	Cytoskeleton-associated protein 4 OS=Homo sapiens GN=CKAP4 PE=1 SV=2	Q07065	66 kDa	5	0	0
204	Elongation factor 2 OS=Homo sapiens GN=EEF2 PE=1 SV=4	P13639	95 kDa	0	4	0
205	Ras-related protein Rab-7a OS=Homo sapiens GN=RAB7A PE=1 SV=1	P51149	23 kDa	2	0	0
206	Nuclear pore complex protein Nup155 OS=Homo sapiens GN=NUP155 PE=1 SV=1	O75694	155 kDa	0	7	0
207	Uncharacterized protein C19orf21 OS=Homo sapiens GN=C19orf21 PE=1 SV=1	Q8IVT2	75 kDa	4	0	0
208	60S ribosomal protein L11 OS=Homo sapiens GN=RPL11 PE=1 SV=2	P62913	20 kDa	4	0	0
209	Vesicle-associated membrane protein-associated protein B/C OS=Homo sapiens GN=VAPB PE=1 SV=3	O95292	27 kDa	0	4	0
211	Signal recognition particle receptor subunit beta OS=Homo sapiens GN=SRPRB PE=1 SV=3	Q9Y5M8	30 kDa	3	4	0
212	Nurim OS=Homo sapiens GN=NRM PE=2 SV=1	Q8IXM6	29 kDa	4	6	0
214	Phenylalanyl-tRNA synthetase alpha chain OS=Homo sapiens GN=FARSA PE=1 SV=3	Q9Y285	58 kDa	4	0	0
215	Tropomyosin beta chain OS=Homo sapiens GN=TPM2 PE=1 SV=1	P07951	33 kDa	8	0	0
217	Eukaryotic translation initiation factor 5A-1 OS=Homo sapiens GN=EIF5A PE=1 SV=2	P63241	17 kDa	2	0	0

221	60S ribosomal protein L9 OS=Homo sapiens GN=RPL9 PE=1 SV=1	P32969	22 kDa	3	0	0
222	Mitochondrial import inner membrane translocase subunit TIM50 OS=Homo sapiens GN=TIMM50 PE=1 SV=2	Q3ZCQ8	40 kDa	2	6	0
224	Eukaryotic translation initiation factor 2 subunit 1 OS=Homo sapiens GN=EIF2S1 PE=1 SV=3	P05198	36 kDa	0	6	0
227	Importin subunit alpha-2 OS=Homo sapiens GN=KPNA2 PE=1 SV=1	P52292	58 kDa	2	0	0
229	Cytochrome c oxidase subunit 2 OS=Homo sapiens GN=MT-CO2 PE=1 SV=1	P00403	26 kDa	4	0	0
230	Membrane-associated progesterone receptor component 1 OS=Homo sapiens GN=PGRMC1 PE=1 SV=3	O00264	22 kDa	0	9	0
231	Twinfilin-2 OS=Homo sapiens GN=TWF2 PE=1 SV=2	Q6IBS0	40 kDa	4	0	0
235	60S ribosomal protein L32 OS=Homo sapiens GN=RPL32 PE=1 SV=2	P62910	16 kDa	3	0	0
236	Heterogeneous nuclear ribonucleoprotein A/B OS=Homo sapiens GN=HNRNPAB PE=1 SV=2	Q99729	36 kDa	3	0	0
238	60S ribosomal protein L17 OS=Homo sapiens GN=RPL17 PE=1 SV=3	P18621	21 kDa	2	4	0
239	Aspartyl/asparaginyl beta-hydroxylase OS=Homo sapiens GN=ASPH PE=1 SV=3	Q12797	86 kDa	2	4	0
240	Elongation factor 1-delta OS=Homo sapiens GN=EEF1D PE=1 SV=5	P29692	31 kDa	0	4	0
241	CD44 antigen OS=Homo sapiens GN=CD44 PE=1 SV=2	P16070	82 kDa	0	4	0
242	Large neutral amino acids transporter small subunit 1 OS=Homo sapiens GN=SLC7A5 PE=1 SV=2	Q01650	55 kDa	4	0	0
243	Transmembrane protein 43 OS=Homo sapiens GN=TMEM43 PE=1 SV=1	Q9BTV4	45 kDa	3	0	0
244	Tight junction protein ZO-1 OS=Homo sapiens GN=TJP1 PE=1 SV=3	Q07157	195 kDa	3	0	0
245	Four and a half LIM domains protein 2 OS=Homo sapiens GN=FHL2 PE=1 SV=3	Q14192	32 kDa	0	4	0
247	CDGSH iron-sulfur domain-containing protein 2 OS=Homo sapiens GN=CISD2 PE=1 SV=1	Q8N5K1	15 kDa	0	4	0
250	Inositol 1,4,5-trisphosphate receptor type 3 OS=Homo sapiens GN=ITPR3 PE=1 SV=2	Q14573	304 kDa	5	0	0
253	Actin-related protein 2/3 complex subunit 4 OS=Homo sapiens GN=ARPC4 PE=1 SV=3	P59998	20 kDa	2	0	0
254	Lysophosphatidylcholine acyltransferase 1 OS=Homo sapiens GN=LPCAT1 PE=1 SV=2	Q8NF37	59 kDa	2	0	0
256	Minor histocompatibility antigen H13 OS=Homo sapiens GN=HM13 PE=1 SV=1	Q8TCT9	41 kDa	0	7	0
257	Core histone macro-H2A.1 OS=Homo sapiens GN=H2AFY PE=1 SV=4	O75367	40 kDa	3	0	0
258	Drebrin-like protein OS=Homo sapiens GN=DBNL PE=1 SV=1	Q9UJU6	48 kDa	4	0	0
259	Ras-related protein Rab-2A OS=Homo sapiens GN=RAB2A PE=1 SV=1	P61019	24 kDa	0	4	0
260	Carbonyl reductase [NADPH] 1 OS=Homo sapiens GN=CBR1 PE=1 SV=3	P16152	30 kDa	3	0	0
261	DnaJ homolog subfamily A member 3, mitochondrial OS=Homo sapiens GN=DNAJA3 PE=1 SV=1	Q96EY1	53 kDa	2	0	0
262	Probable ATP-dependent RNA helicase DDX17 OS=Homo sapiens GN=DDX17 PE=1 SV=1	Q92841	72 kDa	6	0	0
264	Metallothionein-2 OS=Homo sapiens GN=MT2A PE=1 SV=1	P02795	6 kDa	0	6	0
266	Heterogeneous nuclear ribonucleoprotein R OS=Homo sapiens GN=HNRNPR PE=1 SV=1	O43390	71 kDa	2	0	0
267	Long-chain-fatty-acid--CoA ligase 3 OS=Homo sapiens GN=ACSL3 PE=1 SV=3	O95573	80 kDa	3	0	0
268	ADP-ribosylation factor 4 OS=Homo sapiens GN=ARF4 PE=1 SV=3	P18085	21 kDa	3	0	0
269	Transketolase OS=Homo sapiens GN=TKT PE=1 SV=3	P29401	68 kDa	3	0	0
270	Beta-1,4-galactosyltransferase 1 OS=Homo sapiens GN=B4GALT1 PE=1 SV=5	P15291	44 kDa	2	0	0
271	Tubulin alpha-4A chain OS=Homo sapiens GN=TUBA4A PE=1 SV=1	P68366	50 kDa	21	0	0
272	Isochorismatase domain-containing protein 2, mitochondrial OS=Homo sapiens GN=ISOC2 PE=1 SV=1	Q96AB3	22 kDa	2	0	0
273	Protein disulfide-isomerase A3 OS=Homo sapiens GN=PDIA3 PE=1 SV=4	P30101	57 kDa	2	0	0
274	Neutral amino acid transporter B(0) OS=Homo sapiens GN=SLC1A5 PE=1 SV=2	Q15758	57 kDa	0	7	0
275	Aminoacyl tRNA synthase complex-interacting multifunctional protein 2 OS=Homo sapiens GN=AIMP2 PE=1 SV=2	Q13155	35 kDa	0	7	0
276	Glutathione reductase, mitochondrial OS=Homo sapiens GN=GSR PE=1 SV=2	P00390	56 kDa	5	0	0
277	T-complex protein 1 subunit beta OS=Homo sapiens GN=CCT2 PE=1 SV=4	P78371	57 kDa	3	0	0
278	LIM and SH3 domain protein 1 OS=Homo sapiens GN=LASP1 PE=1 SV=2	Q14847	30 kDa	0	4	0
279	Bone marrow stromal antigen 2 OS=Homo sapiens GN=BST2 PE=1 SV=1	Q10589	20 kDa	2	0	0
281	ATP-dependent RNA helicase DDX3X OS=Homo sapiens GN=DDX3X PE=1 SV=3	O00571	73 kDa	0	6	0
282	Alkaline phosphatase, tissue-nonspecific isozyme OS=Homo sapiens GN=ALPL PE=1 SV=4	P05186	57 kDa	0	4	0
283	Trifunctional enzyme subunit alpha, mitochondrial OS=Homo sapiens GN=HADHA PE=1 SV=2	P40939	83 kDa	0	4	0
285	Poly(rC)-binding protein 2 OS=Homo sapiens GN=PCBP2 PE=1 SV=1	Q15366	39 kDa	4	0	0
286	Glutathione S-transferase P OS=Homo sapiens GN=GSTP1 PE=1 SV=2	P09211	23 kDa	2	0	0
287	Lamin-B1 OS=Homo sapiens GN=LMNB1 PE=1 SV=2	P20700	66 kDa	0	4	0
289	Thymidine kinase, cytosolic OS=Homo sapiens GN=TK1 PE=1 SV=2	P04183	25 kDa	0	6	0
290	Nesprin-1 OS=Homo sapiens GN=SYNE1 PE=1 SV=3	Q8NF91	1011 kDa	0	6	0
291	Protein FAM162A OS=Homo sapiens GN=FAM162A PE=1 SV=2	Q96A26	17 kDa	0	4	0
293	Myosin phosphatase Rho-interacting protein OS=Homo sapiens GN=MPRIP PE=1 SV=3	Q6WCQ1	117 kDa	0	4	0
294	Prostaglandin E synthase OS=Homo sapiens GN=PTGES PE=1 SV=2	O14684	17 kDa	0	4	0
296	RNA-binding protein 4 OS=Homo sapiens GN=RBM4 PE=1 SV=1	Q9BWF3	40 kDa	3	0	0
297	Translational activator GCN1 OS=Homo sapiens GN=GCN1L1 PE=1 SV=6	Q92616	293 kDa	0	6	0
298	Protein CYR61 OS=Homo sapiens GN=CYR61 PE=1 SV=1	O00622	42 kDa	0	6	0
300	Interleukin enhancer-binding factor 3 OS=Homo sapiens GN=ILF3 PE=1 SV=3	Q12906	95 kDa	2	0	0
301	Tricarboxylate transport protein, mitochondrial OS=Homo sapiens GN=SLC25A1 PE=1 SV=2	P53007	34 kDa	2	0	0
302	Surfeit locus protein 4 OS=Homo sapiens GN=SURF4 PE=1 SV=3	O15260	30 kDa	0	4	0
306	NADH dehydrogenase [ubiquinone] 1 alpha subcomplex subunit 9, mitochondrial OS=Homo sapiens GN=NDUFA9 PE=1 SV=2	Q16795	43 kDa	3	0	0
307	Leucine-rich repeat flightless-interacting protein 2 OS=Homo sapiens GN=LRRFIP2 PE=1 SV=1	Q9Y608	82 kDa	2	0	0
308	Metaxin-1 OS=Homo sapiens GN=MTX1 PE=1 SV=2	Q13505	51 kDa	2	0	0
309	Protein transport protein Sec16A OS=Homo sapiens GN=SEC16A PE=1 SV=3	O15027	234 kDa	0	4	0
310	Sodium/potassium-transporting ATPase subunit alpha-1 OS=Homo sapiens GN=ATP1A1 PE=1 SV=1	P05023	113 kDa	0	6	0
311	Aminoacyl tRNA synthase complex-interacting multifunctional protein 1 OS=Homo sapiens GN=AIMP1 PE=1 SV=2	Q12904	34 kDa	2	0	0
313	Signal peptidase complex subunit 2 OS=Homo sapiens GN=SPCS2 PE=1 SV=3	Q15005	25 kDa	0	4	0

314	ATPase family AAA domain-containing protein 1 OS=Homo sapiens GN=ATAD1 PE=1 SV=1	Q8NBU5	41 kDa	2	0	0
62	Nucleolin OS=Homo sapiens GN=NCL PE=1 SV=3	P19338	77 kDa	8	15	3
67	Nucleophosmin OS=Homo sapiens GN=NPM1 PE=1 SV=2	P06748	33 kDa	7	7	3
112	A-kinase anchor protein 2 OS=Homo sapiens GN=AKAP2 PE=1 SV=3	Q9Y2D5	95 kDa	7	0	3
114	60S ribosomal protein L13 OS=Homo sapiens GN=RPL13 PE=1 SV=4	P26373	24 kDa	6	0	3
126	60S ribosomal protein L14 OS=Homo sapiens GN=RPL14 PE=1 SV=4	P50914	23 kDa	0	6	3
133	60S ribosomal protein L10a OS=Homo sapiens GN=RPL10A PE=1 SV=2	P62906	25 kDa	3	0	3
153	ATPase family AAA domain-containing protein 3A OS=Homo sapiens GN=ATAD3A PE=1 SV=2	Q9NVI7	71 kDa	0	6	3
172	RNA-binding protein 14 OS=Homo sapiens GN=RBM14 PE=1 SV=2	Q96PK6	69 kDa	0	9	3
174	ATP synthase subunit beta, mitochondrial OS=Homo sapiens GN=ATP5B PE=1 SV=3	P06576	57 kDa	3	4	3
175	40S ribosomal protein S7 OS=Homo sapiens GN=RPS7 PE=1 SV=1	P62081	22 kDa	2	0	3
178	60S ribosomal protein L35 OS=Homo sapiens GN=RPL35 PE=1 SV=2	P42766	15 kDa	3	0	3
193	60S ribosomal protein L24 OS=Homo sapiens GN=RPL24 PE=1 SV=1	P83731	18 kDa	4	0	3
213	Nucleoside diphosphate kinase B OS=Homo sapiens GN=NME2 PE=1 SV=1	P22392	17 kDa	4	0	3
232	X-ray repair cross-complementing protein 6 OS=Homo sapiens GN=XRCC6 PE=1 SV=2	P12956	70 kDa	0	0	3
233	Polypeptide N-acetylgalactosaminyltransferase 2 OS=Homo sapiens GN=GALNT2 PE=1 SV=1	Q10471	65 kDa	0	0	3
234	6-phosphogluconolactonase OS=Homo sapiens GN=PGLS PE=1 SV=2	O95336	28 kDa	0	0	3
237	OCIA domain-containing protein 1 OS=Homo sapiens GN=OCIAD1 PE=1 SV=1	Q9NX40	28 kDa	0	0	3
246	GTP-binding nuclear protein Ran OS=Homo sapiens GN=RAN PE=1 SV=3	P62826	24 kDa	3	0	3
255	Fascin OS=Homo sapiens GN=FSCN1 PE=1 SV=3	Q16658	55 kDa	0	0	3
263	ATP synthase subunit d, mitochondrial OS=Homo sapiens GN=ATP5H PE=1 SV=3	O75947	18 kDa	0	0	3
280	Phenylalanyl-tRNA synthetase beta chain OS=Homo sapiens GN=FARSB PE=1 SV=3	Q9NSD9	66 kDa	0	0	3
284	S-methyl-5'-thioadenosine phosphorylase OS=Homo sapiens GN=MTAP PE=1 SV=2	Q13126	31 kDa	0	0	3
288	Interleukin enhancer-binding factor 2 OS=Homo sapiens GN=ILF2 PE=1 SV=2	Q12905	43 kDa	0	0	3
303	UBX domain-containing protein 1 OS=Homo sapiens GN=UBXN1 PE=1 SV=2	Q04323	33 kDa	0	0	3
304	Calcyclin-binding protein OS=Homo sapiens GN=CACYBP PE=1 SV=2	Q9HB71	26 kDa	0	0	3
305	Proteasome activator complex subunit 2 OS=Homo sapiens GN=PSME2 PE=1 SV=4	Q9UL46	27 kDa	0	0	3
312	Heat shock protein 75 kDa, mitochondrial OS=Homo sapiens GN=TRAP1 PE=1 SV=3	Q12931	80 kDa	0	0	3
32	40S ribosomal protein S27a OS=Homo sapiens GN=RPS27A PE=1 SV=1	P62979 (+3)	9 kDa	15	13	4
51	Heterogeneous nuclear ribonucleoprotein M OS=Homo sapiens GN=HNRNPM PE=1 SV=3	P52272	78 kDa	5	22	4
57	Calnexin OS=Homo sapiens GN=CANX PE=1 SV=2	P27824	68 kDa	7	19	4
73	Lamin-A/C OS=Homo sapiens GN=LMNA PE=1 SV=1	P02545	74 kDa	10	10	4
76	Vesicle-associated membrane protein-associated protein A OS=Homo sapiens GN=VAPA PE=1 SV=3	Q9P0L0	28 kDa	7	10	4
82	Leucine-rich repeat-containing protein 59 OS=Homo sapiens GN=LRRC59 PE=1 SV=1	Q96AG4	35 kDa	8	6	4
85	60S ribosomal protein L18 OS=Homo sapiens GN=RPL18 PE=1 SV=2	Q07020	22 kDa	8	10	4
90	40S ribosomal protein S16 OS=Homo sapiens GN=RPS16 PE=1 SV=2	P62249	16 kDa	5	9	4
94	60S ribosomal protein L6 OS=Homo sapiens GN=RPL6 PE=1 SV=3	Q02878	33 kDa	5	13	4
99	40S ribosomal protein S23 OS=Homo sapiens GN=RPS23 PE=1 SV=3	P62266	16 kDa	5	6	4
101	Coronin-1C OS=Homo sapiens GN=CORO1C PE=1 SV=1	Q9ULV4	53 kDa	7	6	4
102	Transferrin receptor protein 1 OS=Homo sapiens GN=TFRC PE=1 SV=2	P02786	85 kDa	0	13	4
103	40S ribosomal protein S9 OS=Homo sapiens GN=RPS9 PE=1 SV=3	P46781	23 kDa	6	0	4
139	40S ribosomal protein S19 OS=Homo sapiens GN=RPS19 PE=1 SV=2	P39019	16 kDa	4	7	4
140	Complement decay-accelerating factor OS=Homo sapiens GN=CD55 PE=1 SV=4	P08174	41 kDa	0	9	4
141	Serine/threonine-protein phosphatase PP1-alpha catalytic subunit OS=Homo sapiens GN=PPP1CA PE=1 SV=1	P62136	38 kDa	4	4	4
154	40S ribosomal protein S20 OS=Homo sapiens GN=RPS20 PE=1 SV=1	P60866	13 kDa	3	6	4
157	Heterogeneous nuclear ribonucleoprotein A3 OS=Homo sapiens GN=HNRNPA3 PE=1 SV=2	P51991	40 kDa	2	0	4
159	Myosin regulatory light chain 12B OS=Homo sapiens GN=MYL12B PE=1 SV=2	O14950 (+1)	20 kDa	5	0	4
163	Ras-related protein Rab-1A OS=Homo sapiens GN=RAB1A PE=1 SV=3	P62820	23 kDa	0	9	4
166	Nestin OS=Homo sapiens GN=NES PE=1 SV=2	P48681	177 kDa	0	4	4
167	Histone H4 OS=Homo sapiens GN=HIST1H4A PE=1 SV=2	P62805	11 kDa	5	0	4
176	60S ribosomal protein L22 OS=Homo sapiens GN=RPL22 PE=1 SV=2	P35268	15 kDa	3	0	4
177	UPF0568 protein C14orf166 OS=Homo sapiens GN=C14orf166 PE=1 SV=1	Q9Y224	28 kDa	0	7	4
185	Complement component 1 Q subcomponent-binding protein, mitochondrial OS=Homo sapiens GN=C1QBP PE=1 SV=1	Q07021	31 kDa	5	0	4
186	Transforming protein RhoA OS=Homo sapiens GN=RHOA PE=1 SV=1	P61586	22 kDa	0	0	4
196	Cytochrome c1, heme protein, mitochondrial OS=Homo sapiens GN=CYC1 PE=1 SV=2	P08574	35 kDa	0	0	4
200	Histone H1.2 OS=Homo sapiens GN=HIST1H1C PE=1 SV=2	P16403	21 kDa	5	0	4
210	Guanine nucleotide-binding protein subunit beta-2-like 1 OS=Homo sapiens GN=GNB2L1 PE=1 SV=3	P63244	35 kDa	3	0	4
218	Very long-chain specific acyl-CoA dehydrogenase, mitochondrial OS=Homo sapiens GN=ACADVL PE=1 SV=1	P49748	70 kDa	0	0	4
219	S-phase kinase-associated protein 1 OS=Homo sapiens GN=SKP1 PE=1 SV=2	P63208	19 kDa	0	0	4
220	CD59 glycoprotein OS=Homo sapiens GN=CD59 PE=1 SV=1	P13987	14 kDa	0	0	4
223	Cellular nucleic acid-binding protein OS=Homo sapiens GN=CNBP PE=1 SV=1	P62633	19 kDa	0	4	4
225	Isoamyl acetate-hydrolyzing esterase 1 homolog OS=Homo sapiens GN=IAH1 PE=1 SV=1	Q2TAA2	28 kDa	0	0	4
248	Hypoxanthine-guanine phosphoribosyltransferase OS=Homo sapiens GN=HPRT1 PE=1 SV=2	P00492	25 kDa	0	0	4
249	Inverted formin-2 OS=Homo sapiens GN=INF2 PE=1 SV=2	Q27J81	136 kDa	0	0	4
251	Methionine-R-sulfoxide reductase B2, mitochondrial OS=Homo sapiens GN=MSRB2 PE=2 SV=2	Q9Y3D2	20 kDa	0	0	4
252	PDZ and LIM domain protein 1 OS=Homo sapiens GN=PDLIM1 PE=1 SV=4	O00151	36 kDa	0	0	4
265	Twinfilin-1 OS=Homo sapiens GN=TWF1 PE=1 SV=3	Q12792	40 kDa	0	0	4
292	Deoxyuridine 5'-triphosphate nucleotidohydrolase, mitochondrial OS=Homo sapiens GN=DUT PE=1 SV=3	P33316	27 kDa	0	0	4
295	Protein-L-isoaspartate(D-aspartate) O-methyltransferase OS=Homo sapiens GN=PCMT1	P22061	25 kDa	0	0	4

	PE=1 SV=3					
65	Supervillin OS=Homo sapiens GN=SVIL PE=1 SV=2	O95425	248 kDa	13	0	5
80	60S acidic ribosomal protein P2 OS=Homo sapiens GN=RPLP2 PE=1 SV=1	P05387	12 kDa	8	9	5
81	Activated RNA polymerase II transcriptional coactivator p15 OS=Homo sapiens GN=SUB1 PE=1 SV=3	P53999	14 kDa	5	15	5
83	Phosphate carrier protein, mitochondrial OS=Homo sapiens GN=SLC25A3 PE=1 SV=2	Q00325	40 kDa	5	6	5
100	40S ribosomal protein S8 OS=Homo sapiens GN=RPS8 PE=1 SV=2	P62241	24 kDa	6	6	5
105	Probable ATP-dependent RNA helicase DDX5 OS=Homo sapiens GN=DDX5 PE=1 SV=1	P17844	69 kDa	5	0	5
106	60S ribosomal protein L18a OS=Homo sapiens GN=RPL18A PE=1 SV=2	Q02543	21 kDa	5	0	5
118	60S ribosomal protein L8 OS=Homo sapiens GN=RPL8 PE=1 SV=2	P62917	28 kDa	5	0	5
122	40S ribosomal protein S13 OS=Homo sapiens GN=RPS13 PE=1 SV=2	P62277	17 kDa	5	0	5
125	40S ribosomal protein S6 OS=Homo sapiens GN=RPS6 PE=1 SV=1	P62753	29 kDa	3	6	5
134	Plastin-3 OS=Homo sapiens GN=PLS3 PE=1 SV=4	P13797	71 kDa	6	0	5
136	Phostensin OS=Homo sapiens GN=KIAA1949 PE=1 SV=1	Q6NYC8	68 kDa	8	0	5
152	Erythrocyte band 7 integral membrane protein OS=Homo sapiens GN=STOM PE=1 SV=3	P27105	32 kDa	2	6	5
158	Cysteine and glycine-rich protein 1 OS=Homo sapiens GN=CSRP1 PE=1 SV=3	P21291	21 kDa	0	6	5
179	40S ribosomal protein S25 OS=Homo sapiens GN=RPS25 PE=1 SV=1	P62851	14 kDa	3	0	5
216	ATP-citrate synthase OS=Homo sapiens GN=ACLY PE=1 SV=3	P53396	121 kDa	0	0	5
226	Junction plakoglobin OS=Homo sapiens GN=JUP PE=1 SV=3	P14923	82 kDa	2	0	5
228	Paralemmin-2 OS=Homo sapiens GN=PALM2 PE=1 SV=3	Q8IXS6	42 kDa	0	0	5
299	Prostaglandin E synthase 2 OS=Homo sapiens GN=PTGES2 PE=1 SV=1	Q9H7Z7	42 kDa	0	0	5
24	LIM domain only protein 7 OS=Homo sapiens GN=LMO7 PE=1 SV=2	Q8WWI1	193 kDa	20	12	6
50	Myosin light polypeptide 6 OS=Homo sapiens GN=MYL6 PE=1 SV=2	P60660	17 kDa	8	16	6
74	60S ribosomal protein L7 OS=Homo sapiens GN=RPL7 PE=1 SV=1	P18124	29 kDa	8	6	6
86	60S ribosomal protein L12 OS=Homo sapiens GN=RPL12 PE=1 SV=1	P30050	18 kDa	6	6	6
108	60S ribosomal protein L26 OS=Homo sapiens GN=RPL26 PE=1 SV=1	P61254	17 kDa	5	0	6
109	CAD protein OS=Homo sapiens GN=CAD PE=1 SV=3	P27708	243 kDa	0	10	6
113	Guanine nucleotide-binding protein G(i) subunit alpha-2 OS=Homo sapiens GN=GNAI2 PE=1 SV=3	P04899	40 kDa	4	6	6
115	ATP synthase subunit O, mitochondrial OS=Homo sapiens GN=ATP5O PE=1 SV=1	P48047	23 kDa	3	0	6
117	60S ribosomal protein L23a OS=Homo sapiens GN=RPL23A PE=1 SV=1	P62750	18 kDa	5	0	6
129	Destrin OS=Homo sapiens GN=DSTN PE=1 SV=3	P60981	19 kDa	4	0	6
143	Programmed cell death protein 6 OS=Homo sapiens GN=PDCD6 PE=1 SV=1	O75340	22 kDa	4	0	6
144	3-hydroxyacyl-CoA dehydrogenase type-2 OS=Homo sapiens GN=HSD17B10 PE=1 SV=3	Q99714	27 kDa	5	0	6
145	Mitochondrial import receptor subunit TOM22 homolog OS=Homo sapiens GN=TOMM22 PE=1 SV=3	Q9NS69	16 kDa	3	0	6
156	Guanine nucleotide-binding protein G(I)/G(S)/G(T) subunit beta-1 OS=Homo sapiens GN=GNB1 PE=1 SV=3	P62873	37 kDa	0	6	6
54	4F2 cell-surface antigen heavy chain OS=Homo sapiens GN=SLC3A2 PE=1 SV=3	P08195	68 kDa	5	15	7
56	60S ribosomal protein L27 OS=Homo sapiens GN=RPL27 PE=1 SV=2	P61353	16 kDa	6	6	7
66	60S ribosomal protein L7a OS=Homo sapiens GN=RPL7A PE=1 SV=2	P62424	30 kDa	5	7	7
69	Dolichyl-diphosphooligosaccharide--protein glycosyltransferase subunit 1 OS=Homo sapiens GN=RPN1 PE=1 SV=1	P04843	69 kDa	6	10	7
72	40S ribosomal protein S14 OS=Homo sapiens GN=RPS14 PE=1 SV=3	P62263	16 kDa	7	10	7
75	Cofilin-1 OS=Homo sapiens GN=CFL1 PE=1 SV=3	P23528	19 kDa	6	7	7
93	Cytochrome c oxidase subunit 4 isoform 1, mitochondrial OS=Homo sapiens GN=COX4I1 PE=1 SV=1	P13073	20 kDa	6	6	7
96	Inositol 1,4,5-trisphosphate receptor type 1 OS=Homo sapiens GN=ITPR1 PE=1 SV=2	Q14643	314 kDa	8	0	7
107	CTP synthase 1 OS=Homo sapiens GN=CTPS PE=1 SV=2	P17812	67 kDa	6	0	7
120	Annexin A1 OS=Homo sapiens GN=ANXA1 PE=1 SV=2	P04083	39 kDa	5	0	7
132	Heterogeneous nuclear ribonucleoprotein K OS=Homo sapiens GN=HNRNPK PE=1 SV=1	P61978	51 kDa	3	0	7
135	Glutathione S-transferase Mu 3 OS=Homo sapiens GN=GSTM3 PE=1 SV=3	P21266	27 kDa	5	0	7
148	Dynamin-like 120 kDa protein, mitochondrial OS=Homo sapiens GN=OPA1 PE=1 SV=3	O60313	112 kDa	5	0	7
197	Peroxiredoxin-2 OS=Homo sapiens GN=PRDX2 PE=1 SV=5	P32119	22 kDa	2	0	7
19	Tubulin beta-2C chain OS=Homo sapiens GN=TUBB2C PE=1 SV=1	P68371	50 kDa	28	16	8
41	40S ribosomal protein S18 OS=Homo sapiens GN=RPS18 PE=1 SV=3	P62269	18 kDa	9	12	8
42	Prohibitin-2 OS=Homo sapiens GN=PHB2 PE=1 SV=2	Q99623	33 kDa	10	16	8
48	Mitochondrial carrier homolog 2 OS=Homo sapiens GN=MTCH2 PE=1 SV=1	Q9Y6C9	33 kDa	13	0	8
55	Desmoplakin OS=Homo sapiens GN=DSP PE=1 SV=3	P15924	332 kDa	8	10	8
71	Heterogeneous nuclear ribonucleoproteins C1/C2 OS=Homo sapiens GN=HNRNPC PE=1 SV=4	P07910	34 kDa	8	7	8
92	14-3-3 protein theta OS=Homo sapiens GN=YWHAQ PE=1 SV=1	P27348	28 kDa	3	4	8
123	Coiled-coil-helix-coiled-coil-helix domain-containing protein 3, mitochondrial OS=Homo sapiens GN=CHCHD3 PE=1 SV=1	Q9NX63	26 kDa	6	0	8
203	Calmodulin OS=Homo sapiens GN=CALM1 PE=1 SV=2	P62158	17 kDa	0	0	8
46	Tropomodulin-3 OS=Homo sapiens GN=TMOD3 PE=1 SV=1	Q9NYL9	40 kDa	9	10	9
58	40S ribosomal protein S2 OS=Homo sapiens GN=RPS2 PE=1 SV=2	P15880	31 kDa	7	0	9
68	F-actin-capping protein subunit alpha-2 OS=Homo sapiens GN=CAPZA2 PE=1 SV=3	P47755	33 kDa	8	0	9
70	60S acidic ribosomal protein P0 OS=Homo sapiens GN=RPLP0 PE=1 SV=1	P05388	34 kDa	7	7	9
78	Sperm-specific antigen 2 OS=Homo sapiens GN=SSFA2 PE=1 SV=3	P28290	138 kDa	8	0	9
87	Mitochondrial import receptor subunit TOM40 homolog OS=Homo sapiens GN=TOMM40 PE=1 SV=1	O96008	38 kDa	8	0	9
88	Clathrin heavy chain 1 OS=Homo sapiens GN=CLTC PE=1 SV=5	Q00610	192 kDa	8	0	9
89	EF-hand domain-containing protein D2 OS=Homo sapiens GN=EFHD2 PE=1 SV=1	Q96C19	27 kDa	8	0	9
110	Crk-like protein OS=Homo sapiens GN=CRKL PE=1 SV=1	P46109	34 kDa	4	0	9
111	Poly(rC)-binding protein 1 OS=Homo sapiens GN=PCBP1 PE=1 SV=2	Q15365	37 kDa	3	0	9
121	Transgelin-2 OS=Homo sapiens GN=TAGLN2 PE=1 SV=3	P37802	22 kDa	5	0	9

137	Src substrate cortactin OS=Homo sapiens GN=CTTN PE=1 SV=2	Q14247	62 kDa	0	0	9
29	DNA-dependent protein kinase catalytic subunit OS=Homo sapiens GN=PRKDC PE=1 SV=3	P78527	469 kDa	8	34	10
45	Heat shock 70 kDa protein 1A/1B OS=Homo sapiens GN=HSPA1A PE=1 SV=5	P08107	70 kDa	16	16	10
59	Heat shock protein HSP 90-beta OS=Homo sapiens GN=HSP90AB1 PE=1 SV=4	P08238	83 kDa	8	9	10
60	40S ribosomal protein S3a OS=Homo sapiens GN=RPS3A PE=1 SV=2	P61247	30 kDa	8	0	10
63	Stress-70 protein, mitochondrial OS=Homo sapiens GN=HSPA9 PE=1 SV=2	P38646	74 kDa	9	4	10
77	Neuroblast differentiation-associated protein AHNAK OS=Homo sapiens GN=AHNAK PE=1 SV=2	Q09666	629 kDa	2	7	10
97	Myosin-Ib OS=Homo sapiens GN=MYO1B PE=1 SV=3	O43795	132 kDa	6	0	10
27	Heterogeneous nuclear ribonucleoprotein A1 OS=Homo sapiens GN=HNRNPA1 PE=1 SV=5	P09651	39 kDa	18	15	11
35	Heat shock protein beta-1 OS=Homo sapiens GN=HSPB1 PE=1 SV=2	P04792	23 kDa	8	20	11
39	Elongation factor 1-alpha 1 OS=Homo sapiens GN=EEF1A1 PE=1 SV=1	P68104 (+1)	50 kDa	13	10	11
44	Heterogeneous nuclear ribonucleoprotein U OS=Homo sapiens GN=HNRNPU PE=1 SV=6	Q00839	91 kDa	9	7	11
49	Heterogeneous nuclear ribonucleoproteins A2/B1 OS=Homo sapiens GN=HNRNPA2B1 PE=1 SV=2	P22626	37 kDa	12	13	11
64	Voltage-dependent anion-selective channel protein 2 OS=Homo sapiens GN=VDAC2 PE=1 SV=2	P45880	32 kDa	12	0	11
26	78 kDa glucose-regulated protein OS=Homo sapiens GN=HSPA5 PE=1 SV=2	P11021	72 kDa	21	19	12
33	Histone H3.1 OS=Homo sapiens GN=HIST1H3A PE=1 SV=2	P68431 (+2)	15 kDa	8	10	12
130	Cysteine and glycine-rich protein 2 OS=Homo sapiens GN=CSRP2 PE=1 SV=3	Q16527	21 kDa	2	0	12
36	Peptidyl-prolyl cis-trans isomerase A OS=Homo sapiens GN=PPIA PE=1 SV=2	P62937	18 kDa	8	15	13
47	Prohibitin OS=Homo sapiens GN=PHB PE=1 SV=1	P35232	30 kDa	8	4	13
34	Epiplakin OS=Homo sapiens GN=EPPK1 PE=1 SV=2	P58107	556 kDa	10	57	14
40	40S ribosomal protein S4, X isoform OS=Homo sapiens GN=RPS4X PE=1 SV=2	P62701	30 kDa	5	13	14
16	Histone H2B type 1-K OS=Homo sapiens GN=HIST1H2BK PE=1 SV=3	O60814	14 kDa	21	20	15
37	Serum albumin OS=Bos taurus GN=ALB PE=1 SV=4	P02769	?	10	0	15
52	Tropomyosin alpha-4 chain OS=Homo sapiens GN=TPM4 PE=1 SV=3	P67936	29 kDa	7	6	15
53	Importin-5 OS=Homo sapiens GN=IPO5 PE=1 SV=4	O00410	124 kDa	4	4	15
22	Caldesmon OS=Homo sapiens GN=CALD1 PE=1 SV=2	Q05682	93 kDa	26	0	17
43	LIM domain and actin-binding protein 1 OS=Homo sapiens GN=LIMA1 PE=1 SV=1	Q9UHB6	85 kDa	7	0	17
61	F-actin-capping protein subunit alpha-1 OS=Homo sapiens GN=CAPZA1 PE=1 SV=3	P52907	33 kDa	11	0	17
79	Voltage-dependent anion-selective channel protein 3 OS=Homo sapiens GN=VDAC3 PE=1 SV=1	Q9Y277	31 kDa	11	0	17
23	40S ribosomal protein S3 OS=Homo sapiens GN=RPS3 PE=1 SV=2	P23396	27 kDa	15	20	18
30	Myosin-Ic OS=Homo sapiens GN=MYO1C PE=1 SV=3	O00159	122 kDa	19	0	18
31	ADP/ATP translocase 2 OS=Homo sapiens GN=SLC25A5 PE=1 SV=6	P05141	33 kDa	10	10	18
38	F-actin-capping protein subunit beta OS=Homo sapiens GN=CAPZB PE=1 SV=4	P47756	31 kDa	11	0	19
28	60 kDa heat shock protein, mitochondrial OS=Homo sapiens GN=HSPD1 PE=1 SV=2	P10809	61 kDa	15	10	20
91	Spectrin beta chain, brain 2 OS=Homo sapiens GN=SPTBN2 PE=1 SV=2	O15020	271 kDa	16	6	20
18	Drebrin OS=Homo sapiens GN=DBN1 PE=1 SV=4	Q16643	71 kDa	23	0	22
25	Mitochondrial inner membrane protein OS=Homo sapiens GN=IMMT PE=1 SV=1	Q16891	84 kDa	18	0	22
12	Heat shock cognate 71 kDa protein OS=Homo sapiens GN=HSPA8 PE=1 SV=1	P11142	71 kDa	25	23	25
17	Peroxiredoxin-1 OS=Homo sapiens GN=PRDX1 PE=1 SV=1	Q06830	22 kDa	18	10	28
20	Annexin A2 OS=Homo sapiens GN=ANXA2 PE=1 SV=2	P07355	39 kDa	16	10	28
13	Voltage-dependent anion-selective channel protein 1 OS=Homo sapiens GN=VDAC1 PE=1 SV=2	P21796	31 kDa	24	16	29
15	Fatty acid synthase OS=Homo sapiens GN=FASN PE=1 SV=3	P49327	273 kDa	9	6	42
11	Filamin-B OS=Homo sapiens GN=FLNB PE=1 SV=2	O75369	278 kDa	40	0	52
10	Band 3 anion transport protein OS=Homo sapiens GN=SLC4A1 PE=1 SV=3	P02730	102 kDa	38	0	54
21	Alpha-actinin-1 OS=Homo sapiens GN=ACTN1 PE=1 SV=2	P12814	103 kDa	58	0	54
9	Myosin-9 OS=Homo sapiens GN=MYH9 PE=1 SV=4	P35579	227 kDa	45	75	60
4	Vimentin OS=Homo sapiens GN=VIM PE=1 SV=4	P08670	54 kDa	111	145	69
7	Alpha-actinin-4 OS=Homo sapiens GN=ACTN4 PE=1 SV=2	O43707	105 kDa	94	4	79
6	Actin, cytoplasmic 2 OS=Homo sapiens GN=ACTG1 PE=1 SV=1	P63261 (+1)	42 kDa	108	16	97
3	Spectrin beta chain, brain 1 OS=Homo sapiens GN=SPTBN1 PE=1 SV=2	Q01082	275 kDa	123	59	138
2	Spectrin alpha chain, brain OS=Homo sapiens GN=SPTAN1 PE=1 SV=3	Q13813	285 kDa	123	70	140
5	Filamin-A OS=Homo sapiens GN=FLNA PE=1 SV=4	P21333	281 kDa	117	12	140
1	Plectin-1 OS=Homo sapiens GN=PLEC1 PE=1 SV=3	Q15149	532 kDa	226	413	285

R2 UL01052JP, Samples report created on 06/29/2012

Experiment: R2 UL01052JP

Scaffold Version: Scaffold_3.1.4.1

Peptide Thresholds: 95.0% minimum

Protein Thresholds: 95.0% minimum and 3 peptides minimum

R2 UL01052JP	Identified Proteins (582)	UniProtKB Accession Number	Molecular Weight	Number of peptides detected		
				1. Async	2. Mitotic	3. GFP
8	SUN domain-containing protein 1 OS=Homo sapiens GN=SUN1 PE=1 SV=3	O94901	90 kDa	100	100	0
27	Nesprin-1 OS=Homo sapiens GN=SYNE1 PE=1 SV=3	Q8NF91	1011 kDa	6	41	0
84	40S ribosomal protein S27a OS=Homo sapiens GN=RPS27A PE=1 SV=1	P62979 (+3)	9 kDa	9	5	0
85	Actin, alpha cardiac muscle 1 OS=Homo sapiens GN=ACTC1 PE=1 SV=1	P68032 (+1)	42 kDa	0	47	0
118	Nesprin-2 OS=Homo sapiens GN=SYNE2 PE=1 SV=3	Q8WXH0	796 kDa	11	7	0
138	Basigin OS=Homo sapiens GN=BSG PE=1 SV=2	P35613	42 kDa	4	10	0
158	Nurim OS=Homo sapiens GN=NRM PE=2 SV=1	Q8IXM6	29 kDa	9	7	0
166	Hsp70-binding protein 1 OS=Homo sapiens GN=HSPBP1 PE=1 SV=1	Q9NZL4	39 kDa	10	6	0
168	Importin-7 OS=Homo sapiens GN=IPO7 PE=1 SV=1	O95373	120 kDa	0	11	0
170	Thrombospondin-1 OS=Homo sapiens GN=THBS1 PE=1 SV=2	P07996	129 kDa	0	16	0
181	Ras-related protein Rab-7a OS=Homo sapiens GN=RAB7A PE=1 SV=1	P51149	23 kDa	4	8	0
184	60S ribosomal protein L18 OS=Homo sapiens GN=RPL18 PE=1 SV=2	Q07020	22 kDa	6	4	0
186	Mitotic checkpoint protein BUB3 OS=Homo sapiens GN=BUB3 PE=1 SV=1	O43684	37 kDa	3	6	0
187	CD44 antigen OS=Homo sapiens GN=CD44 PE=1 SV=2	P16070	82 kDa	0	7	0
200	BAG family molecular chaperone regulator 2 OS=Homo sapiens GN=BAG2 PE=1 SV=1	O95816	24 kDa	10	5	0
201	Trans-2,3-enoyl-CoA reductase OS=Homo sapiens GN=TECR PE=1 SV=1	Q9NZ01	36 kDa	4	0	0
204	60S ribosomal protein L14 OS=Homo sapiens GN=RPL14 PE=1 SV=4	P50914	23 kDa	5	5	0
214	Large neutral amino acids transporter small subunit 1 OS=Homo sapiens GN=SLC7A5 PE=1 SV=2	Q01650	55 kDa	4	7	0
220	Protein arginine N-methyltransferase 1 OS=Homo sapiens GN=PRMT1 PE=1 SV=2	Q99873	42 kDa	0	7	0
231	Proteasome activator complex subunit 1 OS=Homo sapiens GN=PSME1 PE=1 SV=1	Q06323	29 kDa	8	5	0
232	Ribonucleoside-diphosphate reductase large subunit OS=Homo sapiens GN=RRM1 PE=1 SV=1	P23921	90 kDa	3	7	0
233	Transcription intermediary factor 1-beta OS=Homo sapiens GN=TRIM28 PE=1 SV=5	Q13263	89 kDa	3	9	0
234	Microtubule-associated protein 4 OS=Homo sapiens GN=MAP4 PE=1 SV=3	P27816	121 kDa	0	6	0
239	Translational activator GCN1 OS=Homo sapiens GN=GCN1L1 PE=1 SV=6	Q92616	293 kDa	0	11	0
244	Cell division protein kinase 9 OS=Homo sapiens GN=CDK9 PE=1 SV=3	P50750	43 kDa	3	3	0
250	Histone H1.2 OS=Homo sapiens GN=HIST1H1C PE=1 SV=2	P16403	21 kDa	4	4	0
251	Ras-related protein Rab-11B OS=Homo sapiens GN=RAB11B PE=1 SV=4	Q15907	24 kDa	4	4	0
253	Polypyrimidine tract-binding protein 1 OS=Homo sapiens GN=PTBP1 PE=1 SV=1	P26599	57 kDa	0	5	0
255	DnaJ homolog subfamily C member 10 OS=Homo sapiens GN=DNAJC10 PE=1 SV=2	Q8IXB1	91 kDa	0	11	0
261	Heat shock protein 105 kDa OS=Homo sapiens GN=HSPH1 PE=1 SV=1	Q92598	97 kDa	4	6	0
263	Adenosylhomocysteinase OS=Homo sapiens GN=AHCY PE=1 SV=4	P23526	48 kDa	4	4	0
266	U2 small nuclear ribonucleoprotein A' OS=Homo sapiens GN=SNRPA1 PE=1 SV=2	P09661	28 kDa	0	5	0
271	T-complex protein 1 subunit epsilon OS=Homo sapiens GN=CCT5 PE=1 SV=1	P48643	60 kDa	0	5	0
272	Ras-related protein Rab-1A OS=Homo sapiens GN=RAB1A PE=1 SV=3	P62820	23 kDa	6	6	0
273	Plasminogen activator inhibitor 1 RNA-binding protein OS=Homo sapiens GN=SERBP1 PE=1 SV=2	Q8NC51	45 kDa	0	3	0
274	Importin subunit alpha-2 OS=Homo sapiens GN=KPNA2 PE=1 SV=1	P52292	58 kDa	0	6	0
275	Matrin-3 OS=Homo sapiens GN=MATR3 PE=1 SV=2	P43243	95 kDa	4	5	0
278	Palladin OS=Homo sapiens GN=PALLD PE=1 SV=2	Q8WX93	151 kDa	8	4	0
281	LanC-like protein 1 OS=Homo sapiens GN=LANCL1 PE=1 SV=1	O43813	45 kDa	0	4	0
283	26S proteasome non-ATPase regulatory subunit 13 OS=Homo sapiens GN=PSMD13 PE=1 SV=1	Q9UNM6	43 kDa	5	4	0
288	Apoptosis-inducing factor 1, mitochondrial OS=Homo sapiens GN=AIFM1 PE=1 SV=1	O95831	67 kDa	0	5	0
291	Interleukin enhancer-binding factor 2 OS=Homo sapiens GN=ILF2 PE=1 SV=2	Q12905	43 kDa	4	4	0
293	60S ribosomal protein L10a OS=Homo sapiens GN=RPL10A PE=1 SV=2	P62906	25 kDa	4	4	0
294	Membrane-associated progesterone receptor component 1 OS=Homo sapiens GN=PGRMC1 PE=1 SV=3	O00264	22 kDa	6	5	0
295	60S ribosomal protein L5 OS=Homo sapiens GN=RPL5 PE=1 SV=3	P46777	34 kDa	0	6	0
296	Aminoacyl tRNA synthase complex-interacting multifunctional protein 1 OS=Homo sapiens GN=AIMP1 PE=1 SV=2	Q12904	34 kDa	0	6	0
304	Ras-related protein Rab-6A OS=Homo sapiens GN=RAB6A PE=1 SV=3	P20340	24 kDa	0	5	0
307	Carnitine O-palmitoyltransferase 1, liver isoform OS=Homo sapiens GN=CPT1A PE=1 SV=2	P50416	88 kDa	0	5	0
308	Peroxiredoxin-6 OS=Homo sapiens GN=PRDX6 PE=1 SV=3	P30041	25 kDa	0	4	0
309	Zinc finger CCCH-type antiviral protein 1-like OS=Homo sapiens GN=ZC3HAV1L PE=1 SV=2	Q96H79	33 kDa	4	0	0
310	Heterogeneous nuclear ribonucleoprotein G OS=Homo sapiens GN=RBMX PE=1 SV=3	P38159	42 kDa	0	4	0
311	Isoleucyl-tRNA synthetase, cytoplasmic OS=Homo sapiens GN=IARS PE=1 SV=2	P41252	145 kDa	0	4	0
313	Opioid growth factor receptor OS=Homo sapiens GN=OGFR PE=1 SV=3	Q9NZT2	73 kDa	3	4	0
314	Basic leucine zipper and W2 domain-containing protein 2 OS=Homo sapiens GN=BZW2 PE=1 SV=1	Q9Y6E2	48 kDa	0	3	0
317	rRNA 2'-O-methyltransferase fibrillarin OS=Homo sapiens GN=FBL PE=1 SV=2	P22087	34 kDa	0	6	0
318	Developmentally-regulated GTP-binding protein 1 OS=Homo sapiens GN=DRG1 PE=1 SV=1	Q9Y295	41 kDa	0	5	0
319	Protein transport protein Sec61 subunit alpha isoform 1 OS=Homo sapiens GN=SEC61A1 PE=1 SV=2	P61619	52 kDa	0	4	0
320	Guanine nucleotide-binding protein G(s) subunit alpha isoforms short OS=Homo sapiens GN=GNAS PE=1 SV=1	P63092 (+1)	46 kDa	0	5	0
322	Polypeptide N-acetylgalactosaminyltransferase 2 OS=Homo sapiens GN=GALNT2 PE=1 SV=1	Q10471	65 kDa	0	6	0
324	Peroxisomal 2,4-dienoyl-CoA reductase OS=Homo sapiens GN=DECR2 PE=1 SV=1	Q9NUI1	31 kDa	6	0	0

326	Guanine deaminase OS=Homo sapiens GN=GDA PE=1 SV=1	Q9Y2T3	51 kDa	0	3	0
327	Aminopeptidase B OS=Homo sapiens GN=RNPEP PE=1 SV=2	Q9H4A4	73 kDa	0	3	0
329	Cytosolic phospholipase A2 OS=Homo sapiens GN=PLA2G4A PE=1 SV=1	P47712	85 kDa	0	4	0
332	Mitochondrial import inner membrane translocase subunit TIM50 OS=Homo sapiens GN=TIMM50 PE=1 SV=2	Q3ZCQ8	40 kDa	4	0	0
334	Cytochrome b5 type B OS=Homo sapiens GN=CYB5B PE=1 SV=2	O43169	16 kDa	0	4	0
338	Calcyclin-binding protein OS=Homo sapiens GN=CACYBP PE=1 SV=2	Q9HB71	26 kDa	0	3	0
341	Probable glutathione peroxidase 8 OS=Homo sapiens GN=GPX8 PE=1 SV=2	Q8TED1	24 kDa	0	3	0
342	Heterogeneous nuclear ribonucleoprotein A3 OS=Homo sapiens GN=HNRNPA3 PE=1 SV=2	P51991	40 kDa	0	6	0
343	Ras-related protein Rap-1b OS=Homo sapiens GN=RAP1B PE=1 SV=1	P61224	21 kDa	0	5	0
344	Histone deacetylase 10 OS=Homo sapiens GN=HDAC10 PE=1 SV=1	Q969S8	71 kDa	0	3	0
346	Heterogeneous nuclear ribonucleoprotein R OS=Homo sapiens GN=HNRNPR PE=1 SV=1	O43390	71 kDa	0	4	0
348	Heat shock protein HSP 90-alpha OS=Homo sapiens GN=HSP90AA1 PE=1 SV=5	P07900	85 kDa	0	8	0
350	Membrane-associated progesterone receptor component 2 OS=Homo sapiens GN=PGRMC2 PE=1 SV=1	O15173	24 kDa	3	4	0
351	Guanine nucleotide-binding protein G(I)/G(S)/G(T) subunit beta-1 OS=Homo sapiens GN=GNB1 PE=1 SV=3	P62873	37 kDa	6	0	0
355	Ras-related protein Rab-18 OS=Homo sapiens GN=RAB18 PE=1 SV=1	Q9NP72	23 kDa	3	4	0
356	Lamina-associated polypeptide 2, isoforms beta/gamma OS=Homo sapiens GN=TMPO PE=1 SV=2	P42167	51 kDa	3	3	0
358	NADH dehydrogenase [ubiquinone] iron-sulfur protein 3, mitochondrial OS=Homo sapiens GN=NDUFS3 PE=1 SV=1	O75489	30 kDa	5	0	0
359	Protein ERGIC-53 OS=Homo sapiens GN=LMAN1 PE=1 SV=2	P49257	58 kDa	0	4	0
360	Arginyl-tRNA synthetase, cytoplasmic OS=Homo sapiens GN=RARS PE=1 SV=2	P54136	75 kDa	0	4	0
361	Dolichyl-diphosphooligosaccharide--protein glycosyltransferase 48 kDa subunit OS=Homo sapiens GN=DDOST PE=1 SV=4	P39656	51 kDa	0	5	0
362	Methyltransferase-like protein 11A OS=Homo sapiens GN=METTL11A PE=1 SV=3	Q9BV86	25 kDa	4	0	0
363	14-3-3 protein zeta/delta OS=Homo sapiens GN=YWHAZ PE=1 SV=1	P63104	28 kDa	6	0	0
364	Monocarboxylate transporter 4 OS=Homo sapiens GN=SLC16A3 PE=1 SV=1	O15427	49 kDa	0	4	0
365	Tubulin beta-3 chain OS=Homo sapiens GN=TUBB3 PE=1 SV=2	Q13509	50 kDa	0	20	0
366	Ataxin-10 OS=Homo sapiens GN=ATXN10 PE=1 SV=1	Q9UBB4	53 kDa	0	5	0
368	Succinate dehydrogenase [ubiquinone] iron-sulfur subunit, mitochondrial OS=Homo sapiens GN=SDHB PE=1 SV=3	P21912	32 kDa	4	0	0
370	Isoamyl acetate-hydrolyzing esterase 1 homolog OS=Homo sapiens GN=IAH1 PE=1 SV=1	Q2TAA2	28 kDa	4	0	0
371	Growth factor receptor-bound protein 2 OS=Homo sapiens GN=GRB2 PE=1 SV=1	P62993	25 kDa	5	0	0
372	Probable ATP-dependent RNA helicase DDX17 OS=Homo sapiens GN=DDX17 PE=1 SV=1	Q92841	72 kDa	5	6	0
373	Endoplasmic reticulum-Golgi intermediate compartment protein 1 OS=Homo sapiens GN=ERGIC1 PE=1 SV=1	Q969X5	33 kDa	0	4	0
374	26S protease regulatory subunit 8 OS=Homo sapiens GN=PSMC5 PE=1 SV=1	P62195	46 kDa	0	4	0
375	Ras-related protein Ral-A OS=Homo sapiens GN=RALA PE=1 SV=1	P11233	24 kDa	0	5	0
376	Perilipin-3 OS=Homo sapiens GN=PLIN3 PE=1 SV=2	O60664	47 kDa	0	6	0
377	Myristoylated alanine-rich C-kinase substrate OS=Homo sapiens GN=MARCKS PE=1 SV=4	P29966	32 kDa	0	6	0
378	Myosin-Ib OS=Homo sapiens GN=MYO1B PE=1 SV=3	O43795	132 kDa	0	4	0
379	Aminoacyl tRNA synthase complex-interacting multifunctional protein 2 OS=Homo sapiens GN=AIMP2 PE=1 SV=2	Q13155	35 kDa	0	4	0
380	HLA class I histocompatibility antigen, B-55 alpha chain OS=Homo sapiens GN=HLA-B PE=1 SV=1	P30493 (+1)	40 kDa	0	8	0
381	26S protease regulatory subunit 10B OS=Homo sapiens GN=PSMC6 PE=1 SV=1	P62333	44 kDa	3	0	0
382	Ras-related protein Rab-10 OS=Homo sapiens GN=RAB10 PE=1 SV=1	P61026	23 kDa	0	6	0
383	Serine/threonine-protein phosphatase 2A 55 kDa regulatory subunit B alpha isoform OS=Homo sapiens GN=PPP2R2A PE=1 SV=1	P63151	52 kDa	0	6	0
384	Thyroid receptor-interacting protein 13 OS=Homo sapiens GN=TRIP13 PE=1 SV=2	Q15645	49 kDa	0	5	0
385	LIM and SH3 domain protein 1 OS=Homo sapiens GN=LASP1 PE=1 SV=2	Q14847	30 kDa	0	5	0
387	AH receptor-interacting protein OS=Homo sapiens GN=AIP PE=1 SV=2	O00170	38 kDa	0	6	0
388	26S proteasome non-ATPase regulatory subunit 2 OS=Homo sapiens GN=PSMD2 PE=1 SV=3	Q13200	100 kDa	4	0	0
393	Cell division protein kinase 1 OS=Homo sapiens GN=CDK1 PE=1 SV=2	P06493	34 kDa	0	6	0
394	Serine/threonine-protein kinase 6 OS=Homo sapiens GN=AURKA PE=1 SV=2	O14965	46 kDa	0	5	0
395	Aminopeptidase N OS=Homo sapiens GN=ANPEP PE=1 SV=4	P15144	110 kDa	0	6	0
396	Actin-binding protein anillin OS=Homo sapiens GN=ANLN PE=1 SV=2	Q9NQW6	124 kDa	0	5	0
399	ADP-ribosylation factor-like protein 15 OS=Homo sapiens GN=ARL15 PE=1 SV=1	Q9NXU5	23 kDa	3	0	0
400	UDP-N-acetylglucosamine--peptide N-acetylglucosaminyltransferase 110 kDa subunit OS=Homo sapiens GN=OGT PE=1 SV=3	O15294	117 kDa	4	0	0
401	Plasma membrane calcium-transporting ATPase 1 OS=Homo sapiens GN=ATP2B1 PE=1 SV=3	P20020	139 kDa	0	4	0
402	60S ribosomal protein L17 OS=Homo sapiens GN=RPL17 PE=1 SV=3	P18621	21 kDa	0	4	0
405	Thioredoxin-related transmembrane protein 1 OS=Homo sapiens GN=TMX1 PE=1 SV=1	Q9H3N1	32 kDa	0	3	0
406	Ras-related protein Rab-32 OS=Homo sapiens GN=RAB32 PE=1 SV=3	Q13637	25 kDa	0	4	0
407	Epoxide hydrolase 1 OS=Homo sapiens GN=EPHX1 PE=1 SV=1	P07099	53 kDa	0	3	0
411	Proteasome subunit beta type-5 OS=Homo sapiens GN=PSMB5 PE=1 SV=3	P28074	28 kDa	3	4	0
414	Proteasome subunit alpha type-1 OS=Homo sapiens GN=PSMA1 PE=1 SV=1	P25786	30 kDa	0	3	0
415	Extended synaptotagmin-2 OS=Homo sapiens GN=ESYT2 PE=1 SV=1	A0FGR8	102 kDa	3	3	0
416	Proteasome subunit alpha type-5 OS=Homo sapiens GN=PSMA5 PE=1 SV=3	P28066	26 kDa	3	0	0
417	Splicing factor, arginine/serine-rich 7 OS=Homo sapiens GN=SFRS7 PE=1 SV=1	Q16629	27 kDa	0	3	0
418	Glucosidase 2 subunit beta OS=Homo sapiens GN=PRKCSH PE=1 SV=2	P14314	59 kDa	0	4	0
419	Transforming protein RhoA OS=Homo sapiens GN=RHOA PE=1 SV=1	P61586	22 kDa	0	3	0
420	Pyrroline-5-carboxylate reductase 3 OS=Homo sapiens GN=PYCRL PE=1 SV=2	Q53H96	29 kDa	5	0	0
421	Histone acetyltransferase type B catalytic subunit OS=Homo sapiens GN=HAT1 PE=1 SV=1	O14929	50 kDa	0	4	0
422	UPF0568 protein C14orf166 OS=Homo sapiens GN=C14orf166 PE=1 SV=1	Q9Y224	28 kDa	0	4	0
424	Putative pre-mRNA-splicing factor ATP-dependent RNA helicase DHX15 OS=Homo sapiens GN=DHX15 PE=1 SV=2	O43143	91 kDa	0	5	0

426	X-ray repair cross-complementing protein 5 OS=Homo sapiens GN=XRCC5 PE=1 SV=3	P13010	83 kDa	0	3	0
428	ADP-ribosylation factor-like protein 6-interacting protein 6 OS=Homo sapiens GN=ARL6IP6 PE=1 SV=1	Q8N6S5	25 kDa	4	4	0
429	Cytospin-A OS=Homo sapiens GN=CYTSA PE=1 SV=2	Q69YQ0	125 kDa	0	3	0
433	Tubulin beta-6 chain OS=Homo sapiens GN=TUBB6 PE=1 SV=1	Q9BUF5	50 kDa	13	0	0
434	Lamin-B2 OS=Homo sapiens GN=LMNB2 PE=1 SV=3	Q03252	68 kDa	6	0	0
435	Nicalin OS=Homo sapiens GN=NCLN PE=1 SV=2	Q969V3	63 kDa	0	4	0
436	N(2),N(2)-dimethylguanosine tRNA methyltransferase OS=Homo sapiens GN=TRMT1 PE=1 SV=1	Q9NXH9	72 kDa	0	3	0
437	Eukaryotic translation initiation factor 4E OS=Homo sapiens GN=EIF4E PE=1 SV=2	P06730	25 kDa	3	0	0
438	Leukocyte elastase inhibitor OS=Homo sapiens GN=SERPINB1 PE=1 SV=1	P30740	43 kDa	3	0	0
441	Proteasome subunit alpha type-4 OS=Homo sapiens GN=PSMA4 PE=1 SV=1	P25789	29 kDa	3	0	0
442	28S ribosomal protein S22, mitochondrial OS=Homo sapiens GN=MRPS22 PE=1 SV=1	P82650	41 kDa	3	0	0
448	DnaJ homolog subfamily A member 3, mitochondrial OS=Homo sapiens GN=DNAJA3 PE=1 SV=1	Q96EY1	53 kDa	0	3	0
450	Glutathione peroxidase 1 OS=Homo sapiens GN=GPX1 PE=1 SV=3	P07203	22 kDa	4	0	0
452	E3 SUMO-protein ligase RanBP2 OS=Homo sapiens GN=RANBP2 PE=1 SV=2	P49792	358 kDa	0	5	0
453	Heterogeneous nuclear ribonucleoprotein F OS=Homo sapiens GN=HNRNPF PE=1 SV=3	P52597	46 kDa	0	5	0
454	Atlastin-3 OS=Homo sapiens GN=ATL3 PE=1 SV=1	Q6DD88	61 kDa	0	5	0
456	Tyrosine-protein phosphatase non-receptor type 1 OS=Homo sapiens GN=PTPN1 PE=1 SV=1	P18031	50 kDa	0	4	0
457	Signal transducer and activator of transcription 3 OS=Homo sapiens GN=STAT3 PE=1 SV=2	P40763	88 kDa	0	4	0
458	Secretory carrier-associated membrane protein 3 OS=Homo sapiens GN=SCAMP3 PE=1 SV=3	O14828	38 kDa	0	5	0
459	Ras-related C3 botulinum toxin substrate 1 OS=Homo sapiens GN=RAC1 PE=1 SV=1	P63000	21 kDa	3	0	0
460	Adenylate kinase 2, mitochondrial OS=Homo sapiens GN=AK2 PE=1 SV=2	P54819	26 kDa	4	0	0
461	Myeloid differentiation primary response protein MyD88 OS=Homo sapiens GN=MYD88 PE=1 SV=1	Q99836	33 kDa	5	0	0
462	Uncharacterized protein C2orf47, mitochondrial OS=Homo sapiens GN=C2orf47 PE=1 SV=1	Q8WWC4	33 kDa	4	0	0
463	Myosin-X OS=Homo sapiens GN=MYO10 PE=1 SV=3	Q9HD67	237 kDa	0	5	0
464	Heme oxygenase 2 OS=Homo sapiens GN=HMOX2 PE=1 SV=2	P30519	36 kDa	0	4	0
465	Calumenin OS=Homo sapiens GN=CALU PE=1 SV=2	O43852	37 kDa	0	5	0
466	Retinoic acid-induced protein 3 OS=Homo sapiens GN=GPRC5A PE=1 SV=2	Q8NFJ5	40 kDa	0	5	0
467	Protein CYR61 OS=Homo sapiens GN=CYR61 PE=1 SV=1	O00622	42 kDa	0	6	0
468	Protein transport protein Sec16A OS=Homo sapiens GN=SEC16A PE=1 SV=3	O15027	234 kDa	0	6	0
469	G2/mitotic-specific cyclin-B1 OS=Homo sapiens GN=CCNB1 PE=1 SV=1	P14635	48 kDa	0	6	0
471	Enoyl-CoA hydratase, mitochondrial OS=Homo sapiens GN=ECHS1 PE=1 SV=4	P30084	31 kDa	3	0	0
472	Thyroid receptor-interacting protein 6 OS=Homo sapiens GN=TRIP6 PE=1 SV=3	Q15654	50 kDa	3	0	0
473	Cytokine receptor-like factor 1 OS=Homo sapiens GN=CRLF1 PE=1 SV=1	O75462	46 kDa	3	0	0
475	Translin OS=Homo sapiens GN=TSN PE=1 SV=1	Q15631	26 kDa	0	3	0
476	DNA damage-binding protein 1 OS=Homo sapiens GN=DDB1 PE=1 SV=1	Q16531	127 kDa	0	3	0
477	Oxidoreductase HTATIP2 OS=Homo sapiens GN=HTATIP2 PE=1 SV=1	Q9BUP3	27 kDa	0	3	0
478	Exosome complex exonuclease RRP41 OS=Homo sapiens GN=EXOSC4 PE=1 SV=3	Q9NPD3	26 kDa	0	3	0
479	NAD-dependent deacetylase sirtuin-5 OS=Homo sapiens GN=SIRT5 PE=1 SV=2	Q9NXA8	34 kDa	0	3	0
480	Prostaglandin E synthase 2 OS=Homo sapiens GN=PTGES2 PE=1 SV=1	Q9H7Z7	42 kDa	0	3	0
481	Eukaryotic translation initiation factor 3 subunit H OS=Homo sapiens GN=EIF3H PE=1 SV=1	O15372	40 kDa	0	3	0
482	Ribose-phosphate pyrophosphokinase 1 OS=Homo sapiens GN=PRPS1 PE=1 SV=2	P60891	35 kDa	0	3	0
485	Integrin beta-1 OS=Homo sapiens GN=ITGB1 PE=1 SV=2	P05556	88 kDa	0	3	0
486	UBX domain-containing protein 4 OS=Homo sapiens GN=UBXN4 PE=1 SV=2	Q92575	57 kDa	0	3	0
488	28S ribosomal protein S29, mitochondrial OS=Homo sapiens GN=DAP3 PE=1 SV=1	P51398	46 kDa	3	0	0
489	GTP-binding protein SAR1a OS=Homo sapiens GN=SAR1A PE=1 SV=1	Q9NR31	22 kDa	0	3	0
490	Signal recognition particle receptor subunit alpha OS=Homo sapiens GN=SRPR PE=1 SV=2	P08240	70 kDa	0	3	0
491	60S ribosomal protein L24 OS=Homo sapiens GN=RPL24 PE=1 SV=1	P83731	18 kDa	0	4	0
492	ATPase ASNA1 OS=Homo sapiens GN=ASNA1 PE=1 SV=2	O43681	39 kDa	0	3	0
493	Splicing factor, proline- and glutamine-rich OS=Homo sapiens GN=SFPQ PE=1 SV=2	P23246	76 kDa	3	0	0
495	Calponin-3 OS=Homo sapiens GN=CNN3 PE=1 SV=1	Q15417	36 kDa	0	4	0
496	Cob(I)yrinic acid a,c-diamide adenosyltransferase, mitochondrial OS=Homo sapiens GN=MMAB PE=1 SV=1	Q96EY8	27 kDa	3	0	0
497	HCLS1-associated protein X-1 OS=Homo sapiens GN=HAX1 PE=1 SV=2	O00165	32 kDa	3	0	0
498	Cytospin-B OS=Homo sapiens GN=CYTSB PE=1 SV=1	Q5M775	119 kDa	0	3	0
501	L-lactate dehydrogenase B chain OS=Homo sapiens GN=LDHB PE=1 SV=2	P07195	37 kDa	0	4	0
502	Ran GTPase-activating protein 1 OS=Homo sapiens GN=RANGAP1 PE=1 SV=1	P46060	64 kDa	0	3	0
503	Phospholipid scramblase 1 OS=Homo sapiens GN=PLSCR1 PE=1 SV=1	O15162	35 kDa	0	3	0
506	Alpha-internexin OS=Homo sapiens GN=INA PE=1 SV=2	Q16352	55 kDa	5	0	0
507	Tubulin--tyrosine ligase-like protein 12 OS=Homo sapiens GN=TTLL12 PE=1 SV=2	Q14166	74 kDa	3	0	0
508	Interleukin enhancer-binding factor 3 OS=Homo sapiens GN=ILF3 PE=1 SV=3	Q12906	95 kDa	4	0	0
509	PDZ and LIM domain protein 5 OS=Homo sapiens GN=PDLIM5 PE=1 SV=4	Q96HC4	64 kDa	0	5	0
511	Cysteine-rich protein 2 OS=Homo sapiens GN=CRIP2 PE=1 SV=1	P52943	22 kDa	0	4	0
512	Heterogeneous nuclear ribonucleoprotein Q OS=Homo sapiens GN=SYNCRIP PE=1 SV=2	O60506	70 kDa	0	6	0
513	Sequestosome-1 OS=Homo sapiens GN=SQSTM1 PE=1 SV=1	Q13501	48 kDa	0	5	0
515	Cell division protein kinase 6 OS=Homo sapiens GN=CDK6 PE=1 SV=1	Q00534	37 kDa	0	6	0
516	Insulin-like growth factor-binding protein 7 OS=Homo sapiens GN=IGFBP7 PE=1 SV=1	Q16270	29 kDa	0	5	0
518	mRNA export factor OS=Homo sapiens GN=RAE1 PE=1 SV=1	P78406	41 kDa	3	0	0
521	Proteasome assembly chaperone 1 OS=Homo sapiens GN=PSMG1 PE=1 SV=1	O95456	33 kDa	0	3	0
522	E3 ubiquitin-protein ligase HUWE1 OS=Homo sapiens GN=HUWE1 PE=1 SV=3	Q7Z6Z7	482 kDa	0	3	0
523	26S proteasome non-ATPase regulatory subunit 11 OS=Homo sapiens GN=PSMD11 PE=1 SV=3	O00231	47 kDa	0	3	0
524	DNA-directed RNA polymerases I and III subunit RPAC1 OS=Homo sapiens GN=POLR1C PE=1	O15160	39 kDa	0	3	0

	SV=1					
525	Ras-related protein R-Ras OS=Homo sapiens GN=RRAS PE=1 SV=1	P10301	23 kDa	0	3	0
526	Sodium/potassium-transporting ATPase subunit beta-3 OS=Homo sapiens GN=ATP1B3 PE=1 SV=1	P54709	32 kDa	0	3	0
527	Transitional endoplasmic reticulum ATPase OS=Homo sapiens GN=VCP PE=1 SV=4	P55072	89 kDa	3	0	0
528	Inorganic pyrophosphatase 2, mitochondrial OS=Homo sapiens GN=PPA2 PE=1 SV=2	Q9H2U2	38 kDa	0	3	0
529	28S ribosomal protein S23, mitochondrial OS=Homo sapiens GN=MRPS23 PE=1 SV=2	Q9Y3D9	22 kDa	3	0	0
530	X-ray repair cross-complementing protein 6 OS=Homo sapiens GN=XRCC6 PE=1 SV=2	P12956	70 kDa	0	3	0
531	14-3-3 protein gamma OS=Homo sapiens GN=YWHAG PE=1 SV=2	P61981	28 kDa	6	0	0
532	Sepiapterin reductase OS=Homo sapiens GN=SPR PE=1 SV=1	P35270	28 kDa	0	3	0
533	RNA-binding protein Raly OS=Homo sapiens GN=RALY PE=1 SV=1	Q9UKM9	32 kDa	0	3	0
535	Testisin OS=Homo sapiens GN=PRSS21 PE=2 SV=1	Q9Y6M0	35 kDa	3	0	0
536	Spermidine synthase OS=Homo sapiens GN=SRM PE=1 SV=1	P19623	34 kDa	3	0	0
537	Phosphatidylinositol transfer protein beta isoform OS=Homo sapiens GN=PITPNB PE=1 SV=2	P48739	32 kDa	0	4	0
538	Alpha-soluble NSF attachment protein OS=Homo sapiens GN=NAPA PE=1 SV=3	P54920	33 kDa	0	4	0
539	Exportin-T OS=Homo sapiens GN=XPOT PE=1 SV=2	O43592	110 kDa	0	3	0
540	DnaJ homolog subfamily C member 11 OS=Homo sapiens GN=DNAJC11 PE=1 SV=2	Q9NVH1	63 kDa	3	0	0
541	Triple functional domain protein OS=Homo sapiens GN=TRIO PE=1 SV=2	O75962	347 kDa	0	3	0
542	CCR4-NOT transcription complex subunit 1 OS=Homo sapiens GN=CNOT1 PE=1 SV=2	A5YKK6	267 kDa	0	3	0
543	26S proteasome non-ATPase regulatory subunit 5 OS=Homo sapiens GN=PSMD5 PE=1 SV=3	Q16401	56 kDa	0	4	0
544	Syntenin-1 OS=Homo sapiens GN=SDCBP PE=1 SV=1	O00560	32 kDa	0	5	0
545	Connective tissue growth factor OS=Homo sapiens GN=CTGF PE=1 SV=2	P29279	38 kDa	0	5	0
546	Myb-binding protein 1A OS=Homo sapiens GN=MYBBP1A PE=1 SV=2	Q9BQG0	149 kDa	0	5	0
547	Coagulation factor V OS=Homo sapiens GN=F5 PE=1 SV=3	P12259	252 kDa	0	4	0
548	Suppressor of G2 allele of SKP1 homolog OS=Homo sapiens GN=SUGT1 PE=1 SV=3	Q9Y2Z0	41 kDa	3	0	0
549	Thioredoxin-like protein 1 OS=Homo sapiens GN=TXNL1 PE=1 SV=3	O43396	32 kDa	0	4	0
550	Heat shock 70 kDa protein 4 OS=Homo sapiens GN=HSPA4 PE=1 SV=4	P34932	94 kDa	0	3	0
551	Thioredoxin-dependent peroxide reductase, mitochondrial OS=Homo sapiens GN=PRDX3 PE=1 SV=3	P30048	28 kDa	3	0	0
553	Mitochondrial import inner membrane translocase subunit TIM44 OS=Homo sapiens GN=TIMM44 PE=1 SV=2	O43615	51 kDa	0	3	0
554	Calpastatin OS=Homo sapiens GN=CAST PE=1 SV=4	P20810	77 kDa	0	3	0
555	ADP-ribosylation factor GTPase-activating protein 1 OS=Homo sapiens GN=ARFGAP1 PE=1 SV=2	Q8N6T3	45 kDa	0	3	0
556	Coatomer subunit alpha OS=Homo sapiens GN=COPA PE=1 SV=2	P53621	138 kDa	0	3	0
559	Zinc finger ZZ-type and EF-hand domain-containing protein 1 OS=Homo sapiens GN=ZZEF1 PE=1 SV=6	O43149	331 kDa	0	4	0
560	Transforming growth factor beta-1-induced transcript 1 protein OS=Homo sapiens GN=TGFB1I1 PE=1 SV=2	O43294	50 kDa	0	4	0
561	A-kinase anchor protein 12 OS=Homo sapiens GN=AKAP12 PE=1 SV=3	Q02952	191 kDa	0	4	0
562	Proteasome-associated protein ECM29 homolog OS=Homo sapiens GN=ECM29 PE=1 SV=2	Q5VYK3	204 kDa	0	4	0
563	Testin OS=Homo sapiens GN=TES PE=1 SV=1	Q9UGI8	48 kDa	0	4	0
564	Multidrug resistance-associated protein 1 OS=Homo sapiens GN=ABCC1 PE=1 SV=3	P33527	172 kDa	0	4	0
565	CD97 antigen OS=Homo sapiens GN=CD97 PE=1 SV=4	P48960	92 kDa	0	4	0
566	Nexilin OS=Homo sapiens GN=NEXN PE=1 SV=1	Q0ZGT2	81 kDa	3	0	0
567	Transmembrane emp24 domain-containing protein 1 OS=Homo sapiens GN=TMED1 PE=1 SV=1	Q13445	25 kDa	0	4	0
568	NADH dehydrogenase [ubiquinone] 1 alpha subcomplex subunit 9, mitochondrial OS=Homo sapiens GN=NDUFA9 PE=1 SV=2	Q16795	43 kDa	0	4	0
569	Mitochondrial Rho GTPase 2 OS=Homo sapiens GN=RHOT2 PE=1 SV=2	Q8IXI1	68 kDa	3	0	0
570	Tetratricopeptide repeat protein 1 OS=Homo sapiens GN=TTC1 PE=1 SV=1	Q99614	34 kDa	0	4	0
571	Mitochondrial import receptor subunit TOM70 OS=Homo sapiens GN=TOMM70A PE=1 SV=1	O94826	67 kDa	0	3	0
572	DNA topoisomerase 2-alpha OS=Homo sapiens GN=TOP2A PE=1 SV=3	P11388	174 kDa	0	3	0
573	Tubulin gamma-1 chain OS=Homo sapiens GN=TUBG1 PE=1 SV=2	P23258 (+1)	51 kDa	0	3	0
574	Cellular nucleic acid-binding protein OS=Homo sapiens GN=CNBP PE=1 SV=1	P62633	19 kDa	0	3	0
575	EGF-containing fibulin-like extracellular matrix protein 1 OS=Homo sapiens GN=EFEMP1 PE=1 SV=2	Q12805	55 kDa	0	3	0
576	Chromobox protein homolog 3 OS=Homo sapiens GN=CBX3 PE=1 SV=4	Q13185	21 kDa	0	3	0
577	Protein LYRIC OS=Homo sapiens GN=MTDH PE=1 SV=2	Q86UE4	64 kDa	0	3	0
578	Retinol dehydrogenase 11 OS=Homo sapiens GN=RDH11 PE=1 SV=2	Q8TC12	35 kDa	0	3	0
579	39S ribosomal protein L4, mitochondrial OS=Homo sapiens GN=MRPL4 PE=1 SV=1	Q9BYD3	35 kDa	3	0	0
580	Phospholipase A-2-activating protein OS=Homo sapiens GN=PLAA PE=1 SV=2	Q9Y263	87 kDa	0	3	0
581	Endoplasmic reticulum-Golgi intermediate compartment protein 3 OS=Homo sapiens GN=ERGIC3 PE=1 SV=1	Q9Y282	43 kDa	0	3	0
582	Kinesin-like protein KIF20A OS=Homo sapiens GN=KIF20A PE=1 SV=1	O95235	100 kDa	0	3	0
32	Cytoplasmic dynein 1 heavy chain 1 OS=Homo sapiens GN=DYNC1H1 PE=1 SV=5	Q14204	532 kDa	4	30	3
115	60S ribosomal protein L7 OS=Homo sapiens GN=RPL7 PE=1 SV=1	P18124	29 kDa	5	8	3
133	Guanine nucleotide-binding protein G(i) subunit alpha-2 OS=Homo sapiens GN=GNAI2 PE=1 SV=3	P04899	40 kDa	5	7	3
136	Bifunctional aminoacyl-tRNA synthetase OS=Homo sapiens GN=EPRS PE=1 SV=5	P07814	171 kDa	4	10	3
144	60S ribosomal protein L3 OS=Homo sapiens GN=RPL3 PE=1 SV=2	P39023	46 kDa	4	6	3
154	Crk-like protein OS=Homo sapiens GN=CRKL PE=1 SV=1	P46109	34 kDa	10	3	3
174	Alpha-enolase OS=Homo sapiens GN=ENO1 PE=1 SV=2	P06733	47 kDa	9	4	3
182	Inositol 1,4,5-trisphosphate receptor type 1 OS=Homo sapiens GN=ITPR1 PE=1 SV=2	Q14643	314 kDa	4	3	3
197	Four and a half LIM domains protein 2 OS=Homo sapiens GN=FHL2 PE=1 SV=3	Q14192	32 kDa	3	6	3
210	Serine/threonine-protein phosphatase 2A catalytic subunit alpha isoform OS=Homo sapiens GN=PPP2CA PE=1 SV=1	P67775	36 kDa	5	5	3
219	Transmembrane emp24 domain-containing protein 9 OS=Homo sapiens GN=TMED9 PE=1 SV=2	Q9BVK6	27 kDa	0	6	3

240	ATPase family AAA domain-containing protein 3A OS=Homo sapiens GN=ATAD3A PE=1 SV=2	Q9NVI7	71 kDa	3	4	3
241	Cytochrome b-c1 complex subunit 2, mitochondrial OS=Homo sapiens GN=UQCRC2 PE=1 SV=3	P22695	48 kDa	5	3	3
242	Ras-related protein Rab-2A OS=Homo sapiens GN=RAB2A PE=1 SV=1	P61019	24 kDa	4	4	3
249	Pyruvate dehydrogenase E1 component subunit beta, mitochondrial OS=Homo sapiens GN=PDHB PE=1 SV=3	P11177	39 kDa	0	6	3
257	Proteasome activator complex subunit 3 OS=Homo sapiens GN=PSME3 PE=1 SV=1	P61289	30 kDa	0	4	3
258	Glutamate--cysteine ligase regulatory subunit OS=Homo sapiens GN=GCLM PE=1 SV=1	P48507	31 kDa	0	4	3
267	DnaJ homolog subfamily A member 1 OS=Homo sapiens GN=DNAJA1 PE=1 SV=2	P31689	45 kDa	0	4	3
268	Methionyl-tRNA synthetase, cytoplasmic OS=Homo sapiens GN=MARS PE=1 SV=2	P56192	101 kDa	0	7	3
280	ATP synthase subunit d, mitochondrial OS=Homo sapiens GN=ATP5H PE=1 SV=3	O75947	18 kDa	0	3	3
282	RuvB-like 2 OS=Homo sapiens GN=RUVBL2 PE=1 SV=3	Q9Y230	51 kDa	0	4	3
285	Ubiquitin carboxyl-terminal hydrolase 5 OS=Homo sapiens GN=USP5 PE=1 SV=2	P45974	96 kDa	5	0	3
286	Neutral amino acid transporter B(0) OS=Homo sapiens GN=SLC1A5 PE=1 SV=2	Q15758	57 kDa	0	6	3
289	Eukaryotic initiation factor 4A-I OS=Homo sapiens GN=EIF4A1 PE=1 SV=1	P60842	46 kDa	0	5	3
301	Far upstream element-binding protein 2 OS=Homo sapiens GN=KHSRP PE=1 SV=3	Q92945	73 kDa	3	3	3
302	T-complex protein 1 subunit alpha OS=Homo sapiens GN=TCP1 PE=1 SV=1	P17987	60 kDa	3	3	3
305	Hydroxymethylglutaryl-CoA lyase, mitochondrial OS=Homo sapiens GN=HMGCL PE=1 SV=2	P35914	34 kDa	4	0	3
306	Flotillin-1 OS=Homo sapiens GN=FLOT1 PE=1 SV=3	O75955	47 kDa	0	6	3
325	Acyl-protein thioesterase 2 OS=Homo sapiens GN=LYPLA2 PE=1 SV=1	O95372	25 kDa	0	0	3
328	Heterogeneous nuclear ribonucleoprotein A/B OS=Homo sapiens GN=HNRNPAB PE=1 SV=2	Q99729	36 kDa	0	4	3
331	Glycerol-3-phosphate dehydrogenase, mitochondrial OS=Homo sapiens GN=GPD2 PE=1 SV=3	P43304	81 kDa	3	0	3
336	Protein scribble homolog OS=Homo sapiens GN=SCRIB PE=1 SV=4	Q14160	175 kDa	0	4	3
339	C-1-tetrahydrofolate synthase, cytoplasmic OS=Homo sapiens GN=MTHFD1 PE=1 SV=3	P11586	102 kDa	0	5	3
340	PDZ and LIM domain protein 7 OS=Homo sapiens GN=PDLIM7 PE=1 SV=1	Q9NR12	50 kDa	0	4	3
345	Ras GTPase-activating-like protein IQGAP1 OS=Homo sapiens GN=IQGAP1 PE=1 SV=1	P46940	189 kDa	0	4	3
347	TNF receptor-associated factor 2 OS=Homo sapiens GN=TRAF2 PE=1 SV=2	Q12933	56 kDa	0	5	3
352	Drebrin-like protein OS=Homo sapiens GN=DBNL PE=1 SV=1	Q9UJU6	48 kDa	3	3	3
353	Nuclear pore membrane glycoprotein 210 OS=Homo sapiens GN=NUP210 PE=1 SV=3	Q8TEM1	205 kDa	0	3	3
354	Dolichyl-diphosphooligosaccharide--protein glycosyltransferase subunit 2 OS=Homo sapiens GN=RPN2 PE=1 SV=3	P04844	69 kDa	4	0	3
397	GTP-binding protein era homolog OS=Homo sapiens GN=ERAL1 PE=1 SV=2	O75616	48 kDa	3	0	3
398	UBX domain-containing protein 1 OS=Homo sapiens GN=UBXN1 PE=1 SV=2	Q04323	33 kDa	0	3	3
403	Protein lin-7 homolog C OS=Homo sapiens GN=LIN7C PE=1 SV=1	Q9NUP9	22 kDa	0	0	3
404	Actin-related protein 2/3 complex subunit 1A OS=Homo sapiens GN=ARPC1A PE=1 SV=2	Q92747	42 kDa	0	0	3
408	Estradiol 17-beta-dehydrogenase 8 OS=Homo sapiens GN=HSD17B8 PE=1 SV=2	Q92506	27 kDa	3	0	3
409	Coproporphyrinogen-III oxidase, mitochondrial OS=Homo sapiens GN=CPOX PE=1 SV=3	P36551	50 kDa	3	0	3
410	Catenin delta-1 OS=Homo sapiens GN=CTNND1 PE=1 SV=1	O60716	108 kDa	3	0	3
412	Replication factor C subunit 4 OS=Homo sapiens GN=RFC4 PE=1 SV=2	P35249	40 kDa	0	4	3
413	Transmembrane protein 33 OS=Homo sapiens GN=TMEM33 PE=1 SV=2	P57088	28 kDa	0	4	3
423	Alkaline phosphatase, tissue-nonspecific isozyme OS=Homo sapiens GN=ALPL PE=1 SV=4	P05186	57 kDa	0	4	3
425	PCI domain-containing protein 2 OS=Homo sapiens GN=PCID2 PE=1 SV=2	Q5JVF3	46 kDa	0	0	3
427	Twinfilin-2 OS=Homo sapiens GN=TWF2 PE=1 SV=2	Q6IBS0	40 kDa	0	0	3
430	LIM and calponin homology domains-containing protein 1 OS=Homo sapiens GN=LIMCH1 PE=1 SV=4	Q9UPQ0	122 kDa	0	0	3
440	EF-hand domain-containing protein D2 OS=Homo sapiens GN=EFHD2 PE=1 SV=1	Q96C19	27 kDa	0	0	3
445	U5 small nuclear ribonucleoprotein 200 kDa helicase OS=Homo sapiens GN=SNRNP200 PE=1 SV=2	O75643	245 kDa	0	3	3
447	Mitochondrial carrier homolog 1 OS=Homo sapiens GN=MTCH1 PE=1 SV=1	Q9NZJ7	42 kDa	0	0	3
449	26S protease regulatory subunit 6A OS=Homo sapiens GN=PSMC3 PE=1 SV=3	P17980	49 kDa	0	3	3
470	Erlin-2 OS=Homo sapiens GN=ERLIN2 PE=1 SV=1	O94905	38 kDa	0	0	3
474	Catenin alpha-1 OS=Homo sapiens GN=CTNNA1 PE=1 SV=1	P35221	100 kDa	0	0	3
483	TraB domain-containing protein OS=Homo sapiens GN=TRABD PE=2 SV=1	Q9H4I3	42 kDa	0	0	3
484	Tight junction protein ZO-1 OS=Homo sapiens GN=TJP1 PE=1 SV=3	Q07157	195 kDa	0	0	3
487	Programmed cell death 6-interacting protein OS=Homo sapiens GN=PDCD6IP PE=1 SV=1	Q8WUM4	96 kDa	0	0	3
494	Dihydrolipoyl dehydrogenase, mitochondrial OS=Homo sapiens GN=DLD PE=1 SV=2	P09622	54 kDa	0	0	3
499	Histone H4 OS=Homo sapiens GN=HIST1H4A PE=1 SV=2	P62805	11 kDa	0	0	3
510	UPF0465 protein C5orf33 OS=Homo sapiens GN=C5orf33 PE=1 SV=2	Q4G0N4	49 kDa	0	0	3
519	Mixed lineage kinase domain-like protein OS=Homo sapiens GN=MLKL PE=1 SV=1	Q8NB16	54 kDa	0	0	3
520	Ubiquitin carboxyl-terminal hydrolase isozyme L5 OS=Homo sapiens GN=UCHL5 PE=1 SV=3	Q9Y5K5	38 kDa	0	0	3
534	Heterogeneous nuclear ribonucleoprotein A0 OS=Homo sapiens GN=HNRNPA0 PE=1 SV=1	Q13151	31 kDa	0	0	3
552	Exosome complex exonuclease RRP4 OS=Homo sapiens GN=EXOSC2 PE=1 SV=2	Q13868	33 kDa	0	0	3
557	SHC-transforming protein 1 OS=Homo sapiens GN=SHC1 PE=1 SV=4	P29353	63 kDa	0	0	3
558	Signal recognition particle 72 kDa protein OS=Homo sapiens GN=SRP72 PE=1 SV=3	O76094	75 kDa	0	0	3
58	Heterogeneous nuclear ribonucleoprotein M OS=Homo sapiens GN=HNRNPM PE=1 SV=3	P52272	78 kDa	13	14	4
76	Importin subunit beta-1 OS=Homo sapiens GN=KPNB1 PE=1 SV=2	Q14974	97 kDa	8	13	4
83	Heterogeneous nuclear ribonucleoprotein U OS=Homo sapiens GN=HNRNPU PE=1 SV=6	Q00839	91 kDa	11	7	4
94	Emerin OS=Homo sapiens GN=EMD PE=1 SV=1	P50402	29 kDa	11	7	4
126	40S ribosomal protein S6 OS=Homo sapiens GN=RPS6 PE=1 SV=1	P62753	29 kDa	9	5	4
129	Junction plakoglobin OS=Homo sapiens GN=JUP PE=1 SV=3	P14923	82 kDa	5	6	4
134	Exportin-2 OS=Homo sapiens GN=CSE1L PE=1 SV=3	P55060	110 kDa	0	9	4
135	Signal recognition particle receptor subunit beta OS=Homo sapiens GN=SRPRB PE=1 SV=3	Q9Y5M8	30 kDa	8	8	4
137	Thymidine kinase, cytosolic OS=Homo sapiens GN=TK1 PE=1 SV=2	P04183	25 kDa	0	12	4
142	60S ribosomal protein L6 OS=Homo sapiens GN=RPL6 PE=1 SV=3	Q02878	33 kDa	6	6	4
143	60S ribosomal protein L4 OS=Homo sapiens GN=RPL4 PE=1 SV=5	P36578	48 kDa	5	7	4

145	T-complex protein 1 subunit eta OS=Homo sapiens GN=CCT7 PE=1 SV=2	Q99832	59 kDa	3	5	4
146	60S ribosomal protein L10 OS=Homo sapiens GN=RPL10 PE=1 SV=4	P27635	25 kDa	5	6	4
149	Desmoglein-2 OS=Homo sapiens GN=DSG2 PE=1 SV=2	Q14126	122 kDa	5	6	4
153	Sodium/potassium-transporting ATPase subunit alpha-1 OS=Homo sapiens GN=ATP1A1 PE=1 SV=1	P05023	113 kDa	4	8	4
162	Nuclear mitotic apparatus protein 1 OS=Homo sapiens GN=NUMA1 PE=1 SV=2	Q14980	238 kDa	0	7	4
163	Complement decay-accelerating factor OS=Homo sapiens GN=CD55 PE=1 SV=4	P08174	41 kDa	3	9	4
164	Vesicle-trafficking protein SEC22b OS=Homo sapiens GN=SEC22B PE=1 SV=3	O75396	25 kDa	8	6	4
176	Exportin-1 OS=Homo sapiens GN=XPO1 PE=1 SV=1	O14980	123 kDa	8	4	4
177	Erythrocyte band 7 integral membrane protein OS=Homo sapiens GN=STOM PE=1 SV=3	P27105	32 kDa	4	6	4
179	40S ribosomal protein S5 OS=Homo sapiens GN=RPS5 PE=1 SV=4	P46782	23 kDa	6	5	4
191	40S ribosomal protein S8 OS=Homo sapiens GN=RPS8 PE=1 SV=2	P62241	24 kDa	6	6	4
192	Transportin-1 OS=Homo sapiens GN=TNPO1 PE=1 SV=2	Q92973	102 kDa	5	6	4
193	Serine/threonine-protein phosphatase 2A 65 kDa regulatory subunit A alpha isoform OS=Homo sapiens GN=PPP2R1A PE=1 SV=4	P30153	65 kDa	3	7	4
198	Ketosamine-3-kinase OS=Homo sapiens GN=FN3KRP PE=1 SV=2	Q9HA64	34 kDa	0	0	4
199	60S ribosomal protein L15 OS=Homo sapiens GN=RPL15 PE=1 SV=2	P61313	24 kDa	0	4	4
208	Nestin OS=Homo sapiens GN=NES PE=1 SV=2	P48681	177 kDa	3	4	4
209	D-3-phosphoglycerate dehydrogenase OS=Homo sapiens GN=PHGDH PE=1 SV=4	O43175	57 kDa	3	6	4
221	Serine/threonine-protein phosphatase PP1-alpha catalytic subunit OS=Homo sapiens GN=PPP1CA PE=1 SV=1	P62136	38 kDa	4	5	4
222	Protein transport protein Sec24C OS=Homo sapiens GN=SEC24C PE=1 SV=3	P53992	118 kDa	3	5	4
223	Cysteine and histidine-rich domain-containing protein 1 OS=Homo sapiens GN=CHORDC1 PE=1 SV=2	Q9UHD1	37 kDa	0	4	4
224	S-adenosylmethionine synthase isoform type-2 OS=Homo sapiens GN=MAT2A PE=1 SV=1	P31153	44 kDa	0	5	4
225	Mitochondrial ribonuclease P protein 1 OS=Homo sapiens GN=RG9MTD1 PE=1 SV=2	Q7L0Y3	47 kDa	0	3	4
228	Trifunctional enzyme subunit alpha, mitochondrial OS=Homo sapiens GN=HADHA PE=1 SV=2	P40939	83 kDa	0	5	4
235	Multifunctional protein ADE2 OS=Homo sapiens GN=PAICS PE=1 SV=3	P22234	47 kDa	0	5	4
243	Ancient ubiquitous protein 1 OS=Homo sapiens GN=AUP1 PE=1 SV=1	Q9Y679	53 kDa	4	4	4
246	Serine-threonine kinase receptor-associated protein OS=Homo sapiens GN=STRAP PE=1 SV=1	Q9Y3F4	38 kDa	3	4	4
259	Reticulon-4 OS=Homo sapiens GN=RTN4 PE=1 SV=2	Q9NQC3	130 kDa	0	6	4
260	Nucleophosmin OS=Homo sapiens GN=NPM1 PE=1 SV=2	P06748	33 kDa	0	4	4
262	Acetolactate synthase-like protein OS=Homo sapiens GN=ILVBL PE=1 SV=2	A1L0T0	68 kDa	4	0	4
270	Serum albumin OS=Bos taurus GN=ALB PE=1 SV=4	P02769	?	0	0	4
279	Src substrate cortactin OS=Homo sapiens GN=CTTN PE=1 SV=2	Q14247	62 kDa	3	4	4
284	T-complex protein 1 subunit zeta OS=Homo sapiens GN=CCT6A PE=1 SV=3	P40227	58 kDa	3	0	4
287	TAR DNA-binding protein 43 OS=Homo sapiens GN=TARDBP PE=1 SV=1	Q13148	45 kDa	3	0	4
300	Actin-related protein 3 OS=Homo sapiens GN=ACTR3 PE=1 SV=3	P61158	47 kDa	3	3	4
303	Dolichol-phosphate mannosyltransferase OS=Homo sapiens GN=DPM1 PE=1 SV=1	O60762	30 kDa	3	3	4
316	Nck-associated protein 1 OS=Homo sapiens GN=NCKAP1 PE=1 SV=1	Q9Y2A7	129 kDa	0	0	4
330	F-actin-capping protein subunit alpha-2 OS=Homo sapiens GN=CAPZA2 PE=1 SV=3	P47755	33 kDa	6	0	4
333	Alkyldihydroxyacetonephosphate synthase, peroxisomal OS=Homo sapiens GN=AGPS PE=1 SV=1	O00116	73 kDa	0	0	4
357	ATP-dependent DNA helicase Q1 OS=Homo sapiens GN=RECQL PE=1 SV=3	P46063	73 kDa	0	3	4
369	LETM1 and EF-hand domain-containing protein 1, mitochondrial OS=Homo sapiens GN=LETM1 PE=1 SV=1	O95202	83 kDa	0	0	4
386	Presequence protease, mitochondrial OS=Homo sapiens GN=PITRM1 PE=1 SV=2	Q5JRX3	117 kDa	3	0	4
439	Sperm-specific antigen 2 OS=Homo sapiens GN=SSFA2 PE=1 SV=3	P28290	138 kDa	0	0	4
443	Aldehyde dehydrogenase X, mitochondrial OS=Homo sapiens GN=ALDH1B1 PE=1 SV=2	P30837	57 kDa	0	0	4
446	Guanine nucleotide-binding protein G(k) subunit alpha OS=Homo sapiens GN=GNAI3 PE=1 SV=3	P08754	41 kDa	0	6	4
451	Caprin-1 OS=Homo sapiens GN=CAPRIN1 PE=1 SV=2	Q14444	78 kDa	0	0	4
455	NADH-ubiquinone oxidoreductase 75 kDa subunit, mitochondrial OS=Homo sapiens GN=NDUFS1 PE=1 SV=3	P28331	79 kDa	3	0	4
500	NFU1 iron-sulfur cluster scaffold homolog, mitochondrial OS=Homo sapiens GN=NFU1 PE=1 SV=2	Q9UMS0	28 kDa	0	0	4
504	Protein phosphatase methylesterase 1 OS=Homo sapiens GN=PPME1 PE=1 SV=3	Q9Y570	42 kDa	0	0	4
505	Mitochondrial-processing peptidase subunit alpha OS=Homo sapiens GN=PMPCA PE=1 SV=2	Q10713	58 kDa	0	0	4
514	Isocitrate dehydrogenase [NAD] subunit beta, mitochondrial OS=Homo sapiens GN=IDH3B PE=1 SV=2	O43837	42 kDa	0	0	4
52	Clathrin heavy chain 1 OS=Homo sapiens GN=CLTC PE=1 SV=5	Q00610	192 kDa	5	15	5
56	Transferrin receptor protein 1 OS=Homo sapiens GN=TFRC PE=1 SV=2	P02786	85 kDa	9	14	5
67	Calnexin OS=Homo sapiens GN=CANX PE=1 SV=2	P27824	68 kDa	6	12	5
75	40S ribosomal protein S3a OS=Homo sapiens GN=RPS3A PE=1 SV=2	P61247	30 kDa	6	7	5
89	40S ribosomal protein S9 OS=Homo sapiens GN=RPS9 PE=1 SV=3	P46781	23 kDa	10	9	5
102	NADH-cytochrome b5 reductase 3 OS=Homo sapiens GN=CYB5R3 PE=1 SV=3	P00387	34 kDa	9	6	5
112	DNA replication licensing factor MCM5 OS=Homo sapiens GN=MCM5 PE=1 SV=5	P33992	82 kDa	8	5	5
113	Sarcoplasmic/endoplasmic reticulum calcium ATPase 2 OS=Homo sapiens GN=ATP2A2 PE=1 SV=1	P16615	115 kDa	0	9	5
120	B-cell receptor-associated protein 31 OS=Homo sapiens GN=BCAP31 PE=1 SV=3	P51572	28 kDa	5	4	5
122	Hypoxanthine-guanine phosphoribosyltransferase OS=Homo sapiens GN=HPRT1 PE=1 SV=2	P00492	25 kDa	11	4	5
131	Phosphate carrier protein, mitochondrial OS=Homo sapiens GN=SLC25A3 PE=1 SV=2	Q00325	40 kDa	5	5	5
141	Ras-related protein Rab-8A OS=Homo sapiens GN=RAB8A PE=1 SV=1	P61006	24 kDa	11	7	5
148	60S ribosomal protein L7a OS=Homo sapiens GN=RPL7A PE=1 SV=2	P62424	30 kDa	4	4	5
151	Folate receptor alpha OS=Homo sapiens GN=FOLR1 PE=1 SV=3	P15328	30 kDa	8	5	5
155	Cystathionine beta-synthase OS=Homo sapiens GN=CBS PE=1 SV=2	P35520	61 kDa	6	5	5
160	Aspartyl-tRNA synthetase, cytoplasmic OS=Homo sapiens GN=DARS PE=1 SV=2	P14868	57 kDa	4	6	5

161	S-methyl-5'-thioadenosine phosphorylase OS=Homo sapiens GN=MTAP PE=1 SV=2	Q13126	31 kDa	6	5	5
167	Desmoplakin OS=Homo sapiens GN=DSP PE=1 SV=3	P15924	332 kDa	0	0	5
171	Mitochondrial 2-oxoglutarate/malate carrier protein OS=Homo sapiens GN=SLC25A11 PE=1 SV=3	Q02978	34 kDa	8	5	5
172	GTP-binding nuclear protein Ran OS=Homo sapiens GN=RAN PE=1 SV=3	P62826	24 kDa	8	5	5
173	Melanoma-associated antigen D2 OS=Homo sapiens GN=MAGED2 PE=1 SV=2	Q9UNF1	65 kDa	5	6	5
180	tRNA (cytosine-5-)-methyltransferase NSUN2 OS=Homo sapiens GN=NSUN2 PE=1 SV=2	Q08J23	86 kDa	0	6	5
195	Protein disulfide-isomerase OS=Homo sapiens GN=P4HB PE=1 SV=3	P07237	57 kDa	4	3	5
205	Acetyl-CoA carboxylase 1 OS=Homo sapiens GN=ACACA PE=1 SV=2	Q13085	266 kDa	3	5	5
206	Aspartyl aminopeptidase OS=Homo sapiens GN=DNPEP PE=1 SV=1	Q9ULA0	52 kDa	4	6	5
207	Glyceraldehyde-3-phosphate dehydrogenase OS=Homo sapiens GN=GAPDH PE=1 SV=3	P04406	36 kDa	4	6	5
211	Leucine-rich repeat-containing protein 59 OS=Homo sapiens GN=LRRC59 PE=1 SV=1	Q96AG4	35 kDa	3	6	5
213	60S ribosomal protein L13 OS=Homo sapiens GN=RPL13 PE=1 SV=4	P26373	24 kDa	0	4	5
215	Histone deacetylase 6 OS=Homo sapiens GN=HDAC6 PE=1 SV=2	Q9UBN7	131 kDa	0	6	5
218	Cysteine and glycine-rich protein 2 OS=Homo sapiens GN=CSRP2 PE=1 SV=3	Q16527	21 kDa	6	0	5
229	Fascin OS=Homo sapiens GN=FSCN1 PE=1 SV=3	Q16658	55 kDa	0	4	5
230	Clusterin OS=Homo sapiens GN=CLU PE=1 SV=1	P10909	52 kDa	0	6	5
248	6-phosphofructokinase type C OS=Homo sapiens GN=PFKP PE=1 SV=2	Q01813	86 kDa	0	0	5
254	Ras-related protein Rab-34 OS=Homo sapiens GN=RAB34 PE=1 SV=1	Q9BZG1	29 kDa	5	0	5
256	Pyruvate kinase isozymes M1/M2 OS=Homo sapiens GN=PKM2 PE=1 SV=4	P14618	58 kDa	4	4	5
269	Peflin OS=Homo sapiens GN=PEF1 PE=1 SV=1	Q9UBV8	30 kDa	5	0	5
276	Epidermal growth factor receptor OS=Homo sapiens GN=EGFR PE=1 SV=2	P00533	134 kDa	0	6	5
290	Histone-binding protein RBBP7 OS=Homo sapiens GN=RBBP7 PE=1 SV=1	Q16576	48 kDa	0	4	5
292	GMP synthase [glutamine-hydrolyzing] OS=Homo sapiens GN=GMPS PE=1 SV=1	P49915	77 kDa	0	0	5
299	60S ribosomal protein L8 OS=Homo sapiens GN=RPL8 PE=1 SV=2	P62917	28 kDa	0	0	5
315	ES1 protein homolog, mitochondrial OS=Homo sapiens GN=C21orf33 PE=1 SV=3	P30042	28 kDa	4	0	5
335	Complement component 1 Q subcomponent-binding protein, mitochondrial OS=Homo sapiens GN=C1QBP PE=1 SV=1	Q07021	31 kDa	0	0	5
367	ATP-dependent RNA helicase DDX39 OS=Homo sapiens GN=DDX39 PE=1 SV=2	O00148	49 kDa	0	0	5
389	Mitochondrial GTPase 1 OS=Homo sapiens GN=MTG1 PE=1 SV=2	Q9BT17	37 kDa	0	0	5
390	Proteasome activator complex subunit 2 OS=Homo sapiens GN=PSME2 PE=1 SV=4	Q9UL46	27 kDa	0	0	5
431	Putative transferase C1orf69, mitochondrial OS=Homo sapiens GN=C1orf69 PE=1 SV=1	Q5T440	38 kDa	0	0	5
517	Ras-related protein Rab-5B OS=Homo sapiens GN=RAB5B PE=1 SV=1	P61020	24 kDa	0	0	5
49	Heat shock protein beta-1 OS=Homo sapiens GN=HSPB1 PE=1 SV=2	P04792	23 kDa	9	15	6
50	Nucleolin OS=Homo sapiens GN=NCL PE=1 SV=3	P19338	77 kDa	5	14	6
60	Heterogeneous nuclear ribonucleoproteins C1/C2 OS=Homo sapiens GN=HNRNPC PE=1 SV=4	P07910	34 kDa	9	9	6
68	Ras-related protein Rab-14 OS=Homo sapiens GN=RAB14 PE=1 SV=4	P61106	24 kDa	10	11	6
74	Voltage-dependent anion-selective channel protein 2 OS=Homo sapiens GN=VDAC2 PE=1 SV=2	P45880	32 kDa	14	6	6
81	40S ribosomal protein S4, X isoform OS=Homo sapiens GN=RPS4X PE=1 SV=2	P62701	30 kDa	11	5	6
92	Prohibitin-2 OS=Homo sapiens GN=PHB2 PE=1 SV=2	Q99623	33 kDa	8	6	6
114	Transgelin-2 OS=Homo sapiens GN=TAGLN2 PE=1 SV=3	P37802	22 kDa	8	6	6
124	RuvB-like 1 OS=Homo sapiens GN=RUVBL1 PE=1 SV=1	Q9Y265	50 kDa	9	7	6
130	Ras-related protein Rab-5C OS=Homo sapiens GN=RAB5C PE=1 SV=2	P51148	23 kDa	9	6	6
132	Probable ATP-dependent RNA helicase DDX5 OS=Homo sapiens GN=DDX5 PE=1 SV=1	P17844	69 kDa	3	6	6
139	60S acidic ribosomal protein P0 OS=Homo sapiens GN=RPLP0 PE=1 SV=1	P05388	34 kDa	4	5	6
140	T-complex protein 1 subunit delta OS=Homo sapiens GN=CCT4 PE=1 SV=4	P50991	58 kDa	5	6	6
147	Neutral alpha-glucosidase AB OS=Homo sapiens GN=GANAB PE=1 SV=3	Q14697	107 kDa	5	6	6
150	Glutathione S-transferase P OS=Homo sapiens GN=GSTP1 PE=1 SV=2	P09211	23 kDa	5	7	6
152	Elongation factor 1-delta OS=Homo sapiens GN=EEF1D PE=1 SV=5	P29692	31 kDa	5	6	6
159	6-phosphogluconolactonase OS=Homo sapiens GN=PGLS PE=1 SV=2	O95336	28 kDa	6	6	6
175	Tropomodulin-3 OS=Homo sapiens GN=TMOD3 PE=1 SV=1	Q9NYL9	40 kDa	5	4	6
178	Vesicle-associated membrane protein-associated protein B/C OS=Homo sapiens GN=VAPB PE=1 SV=3	O95292	27 kDa	3	5	6
183	Coiled-coil-helix-coiled-coil-helix domain-containing protein 3, mitochondrial OS=Homo sapiens GN=CHCHD3 PE=1 SV=1	Q9NX63	26 kDa	6	3	6
185	Ubiquitin-like modifier-activating enzyme 1 OS=Homo sapiens GN=UBA1 PE=1 SV=3	P22314	118 kDa	6	0	6
196	Cytoskeleton-associated protein 4 OS=Homo sapiens GN=CKAP4 PE=1 SV=2	Q07065	66 kDa	4	5	6
202	Sorting and assembly machinery component 50 homolog OS=Homo sapiens GN=SAMM50 PE=1 SV=3	Q9Y512	52 kDa	6	0	6
217	Calcium-binding mitochondrial carrier protein Aralar2 OS=Homo sapiens GN=SLC25A13 PE=1 SV=2	Q9UJS0	74 kDa	6	0	6
226	ATP synthase subunit b, mitochondrial OS=Homo sapiens GN=ATP5F1 PE=1 SV=2	P24539	29 kDa	3	5	6
237	A-kinase anchor protein 2 OS=Homo sapiens GN=AKAP2 PE=1 SV=3	Q9Y2D5	95 kDa	6	0	6
245	Thioredoxin domain-containing protein 5 OS=Homo sapiens GN=TXNDC5 PE=1 SV=2	Q8NBS9	48 kDa	3	4	6
252	Endoplasmin OS=Homo sapiens GN=HSP90B1 PE=1 SV=1	P14625	92 kDa	0	0	6
321	Cytochrome c1, heme protein, mitochondrial OS=Homo sapiens GN=CYC1 PE=1 SV=2	P08574	35 kDa	0	0	6
323	Haloacid dehalogenase-like hydrolase domain-containing protein 3 OS=Homo sapiens GN=HDHD3 PE=1 SV=1	Q9BSH5	28 kDa	3	0	6
349	Bifunctional coenzyme A synthase OS=Homo sapiens GN=COASY PE=1 SV=4	Q13057	62 kDa	3	0	6
392	Stomatin-like protein 2 OS=Homo sapiens GN=STOML2 PE=1 SV=1	Q9UJZ1	39 kDa	0	0	6
432	Acyl-CoA synthetase family member 3, mitochondrial OS=Homo sapiens GN=ACSF3 PE=1 SV=3	Q4G176	64 kDa	0	0	6
70	Myoferlin OS=Homo sapiens GN=MYOF PE=1 SV=1	Q9NZM1	235 kDa	0	17	7
73	Heterogeneous nuclear ribonucleoprotein H OS=Homo sapiens GN=HNRNPH1 PE=1 SV=4	P31943	49 kDa	10	6	7
80	ATP-citrate synthase OS=Homo sapiens GN=ACLY PE=1 SV=3	P53396	121 kDa	9	9	7
87	Elongation factor 2 OS=Homo sapiens GN=EEF2 PE=1 SV=4	P13639	95 kDa	4	7	7

88	Carbonyl reductase [NADPH] 1 OS=Homo sapiens GN=CBR1 PE=1 SV=3	P16152	30 kDa	10	6	7
93	Plastin-3 OS=Homo sapiens GN=PLS3 PE=1 SV=4	P13797	71 kDa	4	6	7
95	Lamin-B1 OS=Homo sapiens GN=LMNB1 PE=1 SV=2	P20700	66 kDa	11	9	7
103	Vesicle-associated membrane protein-associated protein A OS=Homo sapiens GN=VAPA PE=1 SV=3	Q9P0L0	28 kDa	8	0	7
106	40S ribosomal protein S2 OS=Homo sapiens GN=RPS2 PE=1 SV=2	P15880	31 kDa	11	6	7
107	Protein flightless-1 homolog OS=Homo sapiens GN=FLII PE=1 SV=2	Q13045	145 kDa	5	7	7
111	Elongation factor 1-gamma OS=Homo sapiens GN=EEF1G PE=1 SV=3	P26641	50 kDa	5	7	7
121	Protein disulfide-isomerase A3 OS=Homo sapiens GN=PDIA3 PE=1 SV=4	P30101	57 kDa	9	5	7
123	Cytochrome b-c1 complex subunit 1, mitochondrial OS=Homo sapiens GN=UQCRC1 PE=1 SV=3	P31930	53 kDa	4	0	7
127	Monofunctional C1-tetrahydrofolate synthase, mitochondrial OS=Homo sapiens GN=MTHFD1L PE=1 SV=1	Q6UB35	106 kDa	6	0	7
169	Voltage-dependent anion-selective channel protein 3 OS=Homo sapiens GN=VDAC3 PE=1 SV=1	Q9Y277	31 kDa	15	0	7
188	Serpin B6 OS=Homo sapiens GN=SERPINB6 PE=1 SV=3	P35237	43 kDa	10	0	7
194	Prohibitin OS=Homo sapiens GN=PHB PE=1 SV=1	P35232	30 kDa	3	4	7
212	Polyadenylate-binding protein 1 OS=Homo sapiens GN=PABPC1 PE=1 SV=2	P11940	71 kDa	0	3	7
236	Mitochondrial import receptor subunit TOM40 homolog OS=Homo sapiens GN=TOMM40 PE=1 SV=1	O96008	38 kDa	5	0	7
238	Hydroxysteroid dehydrogenase-like protein 2 OS=Homo sapiens GN=HSDL2 PE=1 SV=1	Q6YN16	45 kDa	3	0	7
264	Peroxiredoxin-4 OS=Homo sapiens GN=PRDX4 PE=1 SV=1	Q13162	31 kDa	0	7	7
277	Succinate dehydrogenase [ubiquinone] flavoprotein subunit, mitochondrial OS=Homo sapiens GN=SDHA PE=1 SV=2	P31040	73 kDa	3	0	7
297	Threonyl-tRNA synthetase, mitochondrial OS=Homo sapiens GN=TARS2 PE=1 SV=1	Q9BW92	81 kDa	5	0	7
298	Mitochondrial-processing peptidase subunit beta OS=Homo sapiens GN=PMPCB PE=1 SV=2	O75439	54 kDa	4	0	7
391	Hornerin OS=Homo sapiens GN=HRNR PE=1 SV=2	Q86YZ3	282 kDa	0	0	7
34	CAD protein OS=Homo sapiens GN=CAD PE=1 SV=3	P27708	243 kDa	11	18	8
69	T-complex protein 1 subunit beta OS=Homo sapiens GN=CCT2 PE=1 SV=4	P78371	57 kDa	3	6	8
72	Glucose-6-phosphate 1-dehydrogenase OS=Homo sapiens GN=G6PD PE=1 SV=4	P11413	59 kDa	8	6	8
78	40S ribosomal protein S3 OS=Homo sapiens GN=RPS3 PE=1 SV=2	P23396	27 kDa	8	7	8
86	Mitochondrial inner membrane protein OS=Homo sapiens GN=IMMT PE=1 SV=1	Q16891	84 kDa	17	0	8
91	Protein DJ-1 OS=Homo sapiens GN=PARK7 PE=1 SV=2	Q99497	20 kDa	6	9	8
96	Protein RCC2 OS=Homo sapiens GN=RCC2 PE=1 SV=2	Q9P258	56 kDa	12	3	8
105	Long-chain-fatty-acid--CoA ligase 3 OS=Homo sapiens GN=ACSL3 PE=1 SV=3	O95573	80 kDa	10	8	8
110	T-complex protein 1 subunit theta OS=Homo sapiens GN=CCT8 PE=1 SV=4	P50990	60 kDa	0	12	8
116	14-3-3 protein theta OS=Homo sapiens GN=YWHAQ PE=1 SV=1	P27348	28 kDa	6	3	8
128	Mitochondrial carrier homolog 2 OS=Homo sapiens GN=MTCH2 PE=1 SV=1	Q9Y6C9	33 kDa	6	3	8
157	Isochorismatase domain-containing protein 2, mitochondrial OS=Homo sapiens GN=ISOC2 PE=1 SV=1	Q96AB3	22 kDa	4	0	8
165	Heat shock protein 75 kDa, mitochondrial OS=Homo sapiens GN=TRAP1 PE=1 SV=3	Q12931	80 kDa	5	4	8
190	Heterogeneous nuclear ribonucleoprotein A1 OS=Homo sapiens GN=HNRNPA1 PE=1 SV=5	P09651	39 kDa	4	9	8
216	Peroxiredoxin-2 OS=Homo sapiens GN=PRDX2 PE=1 SV=5	P32119	22 kDa	5	0	8
227	ATP-dependent RNA helicase DDX3X OS=Homo sapiens GN=DDX3X PE=1 SV=3	O00571	73 kDa	0	4	8
444	Tropomyosin alpha-3 chain OS=Homo sapiens GN=TPM3 PE=1 SV=1	P06753	33 kDa	0	0	8
57	Dolichyl-diphosphooligosaccharide--protein glycosyltransferase subunit 1 OS=Homo sapiens GN=RPN1 PE=1 SV=1	P04843	69 kDa	6	6	9
59	ADP/ATP translocase 2 OS=Homo sapiens GN=SLC25A5 PE=1 SV=6	P05141	33 kDa	13	7	9
61	Glutathione S-transferase Mu 3 OS=Homo sapiens GN=GSTM3 PE=1 SV=3	P21266	27 kDa	11	6	9
62	Heterogeneous nuclear ribonucleoprotein K OS=Homo sapiens GN=HNRNPK PE=1 SV=1	P61978	51 kDa	11	9	9
63	Coronin-1C OS=Homo sapiens GN=CORO1C PE=1 SV=1	Q9ULV4	53 kDa	12	9	9
98	Inosine-5'-monophosphate dehydrogenase 2 OS=Homo sapiens GN=IMPDH2 PE=1 SV=2	P12268	56 kDa	8	8	9
101	Nuclease-sensitive element-binding protein 1 OS=Homo sapiens GN=YBX1 PE=1 SV=3	P67809	36 kDa	5	6	9
109	Methylcrotonoyl-CoA carboxylase beta chain, mitochondrial OS=Homo sapiens GN=MCCC2 PE=1 SV=1	Q9HCC0	61 kDa	9	3	9
119	ATP synthase subunit O, mitochondrial OS=Homo sapiens GN=ATP5O PE=1 SV=1	P48047	23 kDa	6	6	9
125	Protein-L-isoaspartate(D-aspartate) O-methyltransferase OS=Homo sapiens GN=PCMT1 PE=1 SV=3	P22061	25 kDa	9	5	9
189	Supervillin OS=Homo sapiens GN=SVIL PE=1 SV=2	O95425	248 kDa	5	0	9
203	2-amino-3-ketobutyrate coenzyme A ligase, mitochondrial OS=Homo sapiens GN=GCAT PE=2 SV=1	O75600	45 kDa	4	0	9
42	Glutathione reductase, mitochondrial OS=Homo sapiens GN=GSR PE=1 SV=2	P00390	56 kDa	18	6	10
44	ATP synthase subunit alpha, mitochondrial OS=Homo sapiens GN=ATP5A1 PE=1 SV=1	P25705	60 kDa	15	8	10
47	Heterogeneous nuclear ribonucleoproteins A2/B1 OS=Homo sapiens GN=HNRNPA2B1 PE=1 SV=2	P22626	37 kDa	13	14	10
53	HLA class I histocompatibility antigen, A-68 alpha chain OS=Homo sapiens GN=HLA-A PE=1 SV=4	P01891	41 kDa	11	10	10
65	Trifunctional purine biosynthetic protein adenosine-3 OS=Homo sapiens GN=GART PE=1 SV=1	P22102	108 kDa	10	6	10
77	Annexin A1 OS=Homo sapiens GN=ANXA1 PE=1 SV=2	P04083	39 kDa	10	6	10
79	DNA replication licensing factor MCM3 OS=Homo sapiens GN=MCM3 PE=1 SV=3	P25205	91 kDa	9	5	10
82	Guanine nucleotide-binding protein subunit beta-2-like 1 OS=Homo sapiens GN=GNB2L1 PE=1 SV=3	P63244	35 kDa	9	6	10
90	Guanine nucleotide-binding protein G(I)/G(S)/G(T) subunit beta-2 OS=Homo sapiens GN=GNB2 PE=1 SV=3	P62879	37 kDa	8	6	10
99	T-complex protein 1 subunit gamma OS=Homo sapiens GN=CCT3 PE=1 SV=4	P49368	61 kDa	5	8	10
100	CTP synthase 1 OS=Homo sapiens GN=CTPS PE=1 SV=2	P17812	67 kDa	6	4	10
108	40S ribosomal protein SA OS=Homo sapiens GN=RPSA PE=1 SV=4	P08865	33 kDa	8	5	10
337	ADP/ATP translocase 3 OS=Homo sapiens GN=SLC25A6 PE=1 SV=4	P12236	33 kDa	0	0	10
31	Brain acid soluble protein 1 OS=Homo sapiens GN=BASP1 PE=1 SV=2	P80723	23 kDa	15	22	11

51	Voltage-dependent anion-selective channel protein 1 OS=Homo sapiens GN=VDAC1 PE=1 SV=2	P21796	31 kDa	12	6	11
66	Protein disulfide-isomerase A6 OS=Homo sapiens GN=PDIA6 PE=1 SV=1	Q15084	48 kDa	10	6	11
104	LIM domain and actin-binding protein 1 OS=Homo sapiens GN=LIMA1 PE=1 SV=1	Q9UHB6	85 kDa	10	0	11
41	4F2 cell-surface antigen heavy chain OS=Homo sapiens GN=SLC3A2 PE=1 SV=3	P08195	68 kDa	11	15	12
46	3-hydroxyacyl-CoA dehydrogenase type-2 OS=Homo sapiens GN=HSD17B10 PE=1 SV=3	Q99714	27 kDa	12	9	12
97	Drebrin OS=Homo sapiens GN=DBN1 PE=1 SV=4	Q16643	71 kDa	8	0	12
117	Protein transport protein Sec23A OS=Homo sapiens GN=SEC23A PE=1 SV=2	Q15436	86 kDa	9	3	12
38	Poly(rC)-binding protein 1 OS=Homo sapiens GN=PCBP1 PE=1 SV=2	Q15365	37 kDa	19	11	13
48	Tropomyosin alpha-4 chain OS=Homo sapiens GN=TPM4 PE=1 SV=3	P67936	29 kDa	8	11	13
55	Caldesmon OS=Homo sapiens GN=CALD1 PE=1 SV=2	Q05682	93 kDa	9	6	13
156	Serpin H1 OS=Homo sapiens GN=SERPINH1 PE=1 SV=2	P50454	46 kDa	3	0	13
265	Spectrin beta chain, brain 2 OS=Homo sapiens GN=SPTBN2 PE=1 SV=2	O15020	271 kDa	0	0	13
28	LIM domain only protein 7 OS=Homo sapiens GN=LMO7 PE=1 SV=2	Q8WWI1	193 kDa	14	21	14
30	Epiplakin OS=Homo sapiens GN=EPPK1 PE=1 SV=2	P58107	556 kDa	10	39	14
39	Heat shock protein HSP 90-beta OS=Homo sapiens GN=HSP90AB1 PE=1 SV=4	P08238	83 kDa	18	10	14
64	Phenylalanyl-tRNA synthetase beta chain OS=Homo sapiens GN=FARSB PE=1 SV=3	Q9NSD9	66 kDa	11	0	14
25	Lamin-A/C OS=Homo sapiens GN=LMNA PE=1 SV=1	P02545	74 kDa	24	19	15
35	Heat shock 70 kDa protein 1A/1B OS=Homo sapiens GN=HSPA1A PE=1 SV=5	P08107	70 kDa	17	22	15
54	F-actin-capping protein subunit alpha-1 OS=Homo sapiens GN=CAPZA1 PE=1 SV=3	P52907	33 kDa	10	6	15
36	Elongation factor Tu, mitochondrial OS=Homo sapiens GN=TUFM PE=1 SV=2	P49411	50 kDa	19	4	16
37	Myosin-Ic OS=Homo sapiens GN=MYO1C PE=1 SV=3	O00159	122 kDa	12	13	16
43	Phenylalanyl-tRNA synthetase alpha chain OS=Homo sapiens GN=FARSA PE=1 SV=3	Q9Y285	58 kDa	16	6	16
71	Very long-chain specific acyl-CoA dehydrogenase, mitochondrial OS=Homo sapiens GN=ACADVL PE=1 SV=1	P49748	70 kDa	10	0	16
26	Elongation factor 1-alpha 1 OS=Homo sapiens GN=EEF1A1 PE=1 SV=1	P68104 (+1)	50 kDa	17	21	17
45	Carbamoyl-phosphate synthase [ammonia], mitochondrial OS=Homo sapiens GN=CPS1 PE=1 SV=2	P31327	165 kDa	12	6	18
312	Myosin-10 OS=Homo sapiens GN=MYH10 PE=1 SV=3	P35580	229 kDa	0	13	18
20	78 kDa glucose-regulated protein OS=Homo sapiens GN=HSPA5 PE=1 SV=2	P11021	72 kDa	28	29	19
29	Stress-70 protein, mitochondrial OS=Homo sapiens GN=HSPA9 PE=1 SV=2	P38646	74 kDa	14	17	20
23	Neuroblast differentiation-associated protein AHNAK OS=Homo sapiens GN=AHNAK PE=1 SV=2	Q09666	629 kDa	16	22	21
33	F-actin-capping protein subunit beta OS=Homo sapiens GN=CAPZB PE=1 SV=4	P47756	31 kDa	14	10	21
22	ATP synthase subunit beta, mitochondrial OS=Homo sapiens GN=ATP5B PE=1 SV=3	P06576	57 kDa	28	21	24
21	Importin-5 OS=Homo sapiens GN=IPO5 PE=1 SV=4	O00410	124 kDa	21	21	25
14	Heat shock cognate 71 kDa protein OS=Homo sapiens GN=HSPA8 PE=1 SV=1	P11142	71 kDa	30	41	27
15	Tubulin alpha-1B chain OS=Homo sapiens GN=TUBA1B PE=1 SV=1	P68363	50 kDa	30	28	28
40	Alpha-actinin-1 OS=Homo sapiens GN=ACTN1 PE=1 SV=2	P12814	103 kDa	30	33	28
16	Filamin-B OS=Homo sapiens GN=FLNB PE=1 SV=2	O75369	278 kDa	32	33	29
13	Tubulin beta-2C chain OS=Homo sapiens GN=TUBB2C PE=1 SV=1	P68371	50 kDa	37	32	30
24	Dynamin-like 120 kDa protein, mitochondrial OS=Homo sapiens GN=OPA1 PE=1 SV=3	O60313	112 kDa	29	0	30
17	Annexin A2 OS=Homo sapiens GN=ANXA2 PE=1 SV=2	P07355	39 kDa	30	26	31
19	Peroxiredoxin-1 OS=Homo sapiens GN=PRDX1 PE=1 SV=1	Q06830	22 kDa	33	14	31
247	Tubulin beta chain OS=Homo sapiens GN=TUBB PE=1 SV=2	P07437	50 kDa	39	33	31
18	Nuclear pore complex protein Nup155 OS=Homo sapiens GN=NUP155 PE=1 SV=1	O75694	155 kDa	32	9	37
9	DNA-dependent protein kinase catalytic subunit OS=Homo sapiens GN=PRKDC PE=1 SV=3	P78527	469 kDa	28	74	40
12	60 kDa heat shock protein, mitochondrial OS=Homo sapiens GN=HSPD1 PE=1 SV=2	P10809	61 kDa	30	33	43
10	Alpha-actinin-4 OS=Homo sapiens GN=ACTN4 PE=1 SV=2	O43707	105 kDa	54	40	46
11	Fatty acid synthase OS=Homo sapiens GN=FASN PE=1 SV=3	P49327	273 kDa	48	30	52
7	Spectrin beta chain, brain 1 OS=Homo sapiens GN=SPTBN1 PE=1 SV=2	Q01082	275 kDa	65	67	81
5	Filamin-A OS=Homo sapiens GN=FLNA PE=1 SV=4	P21333	281 kDa	95	76	92
6	Spectrin alpha chain, brain OS=Homo sapiens GN=SPTAN1 PE=1 SV=3	Q13813	285 kDa	82	75	93
3	Vimentin OS=Homo sapiens GN=VIM PE=1 SV=4	P08670	54 kDa	173	98	125
4	Actin, cytoplasmic 1 OS=Homo sapiens GN=ACTB PE=1 SV=1	P60709	42 kDa	147	71	139
2	Myosin-9 OS=Homo sapiens GN=MYH9 PE=1 SV=4	P35579	227 kDa	168	89	171
1	Plectin-1 OS=Homo sapiens GN=PLEC1 PE=1 SV=3	Q15149	532 kDa	197	127	191

Appendix F: List of the 348 potential hSUN1 binding partners analysed from both experimental repeats.

Strong (blue) and weak (yellow) candidates are indicated.

	Accession No.	M/W	Repeat 1			Repeat 2		
			1. Async	2. Mitotic	3. GFP	1. Async	2. Mitotic	3. GFP
STRONG: present in both samples, absent from both negatives								
Splicing factor, proline- and glutamine-rich OS=Homo sapiens GN=SFPQ PE=1 SV=2	P23246	76 kDa	6	12	0	3	0	0
Protein ERGIC-53 OS=Homo sapiens GN=LMAN1 PE=1 SV=2	P49257	58 kDa	4	7	0	0	4	0
BAG family molecular chaperone regulator 2 OS=Homo sapiens GN=BAG2 PE=1 SV=1	O95816	24 kDa	4	4	0	10	5	0
60S ribosomal protein L5 OS=Homo sapiens GN=RPL5 PE=1 SV=3	P46777	34 kDa	5	4	0	0	6	0
Plasminogen activator inhibitor 1 RNA-binding protein OS=Homo sapiens GN=SERBP1 PE=1 SV=2	Q8NC51	45 kDa	5	0	0	0	3	0
Trans-2,3-enoyl-CoA reductase OS=Homo sapiens GN=TECR PE=1 SV=1	Q9NZ01	36 kDa	5	0	0	4	0	0
Ras-related protein Rab-7a OS=Homo sapiens GN=RAB7A PE=1 SV=1	P51149	23 kDa	2	0	0	4	8	0
Nurim OS=Homo sapiens GN=NRM PE=2 SV=1	Q8IXM6	29 kDa	4	6	0	9	7	0
Mitochondrial import inner membrane translocase subunit TIM50 OS=Homo sapiens GN=TIMM50 PE=1 SV=2	Q3ZCQ8	40 kDa	2	6	0	4	0	0
Importin subunit alpha-2 OS=Homo sapiens GN=KPNA2 PE=1 SV=1	P52292	58 kDa	2	0	0	0	6	0
Membrane-associated progesterone receptor component 1 OS=Homo sapiens GN=PGRMC1 PE=1 SV=3	O00264	22 kDa	0	9	0	6	5	0
60S ribosomal protein L17 OS=Homo sapiens GN=RPL17 PE=1 SV=3	P18621	21 kDa	2	4	0	0	4	0
CD44 antigen OS=Homo sapiens GN=CD44 PE=1 SV=2	P16070	82 kDa	0	4	0	0	7	0
Large neutral amino acids transporter small subunit 1 OS=Homo sapiens GN=SLC7A5 PE=1 SV=2	Q01650	55 kDa	4	0	0	4	7	0
DnaJ homolog subfamily A member 3, mitochondrial OS=Homo sapiens GN=DNAJA3 PE=1 SV=1	Q96EY1	53 kDa	2	0	0	0	3	0
Probable ATP-dependent RNA helicase DDX17 OS=Homo sapiens GN=DDX17 PE=1 SV=1	Q92841	72 kDa	6	0	0	5	6	0
Heterogeneous nuclear ribonucleoprotein R OS=Homo sapiens GN=HNRNPR PE=1 SV=1	O43390	71 kDa	2	0	0	0	4	0
Aminoacyl tRNA synthase complex-interacting multifunctional protein 2 OS=Homo sapiens GN=AIMP2 PE=1 SV=2	Q13155	35 kDa	0	7	0	0	4	0
LIM and SH3 domain protein 1 OS=Homo sapiens GN=LASP1 PE=1 SV=2	Q14847	30 kDa	0	4	0	0	5	0
Nesprin-1 OS=Homo sapiens GN=SYNE1 PE=1 SV=3	Q8NF91	1011 kDa	0	6	0	6	41	0
Translational activator GCN1 OS=Homo sapiens GN=GCN1L1 PE=1 SV=6	Q92616	293 kDa	0	6	0	0	11	0
Protein CYR61 OS=Homo sapiens GN=CYR61 PE=1 SV=1	O00622	42 kDa	0	6	0	0	6	0
Interleukin enhancer-binding factor 3 OS=Homo sapiens GN=ILF3 PE=1 SV=3	Q12906	95 kDa	2	0	0	4	0	0
NADH dehydrogenase [ubiquinone] 1 alpha subcomplex subunit 9, mitochondrial OS=Homo sapiens GN=NDUFA9 PE=1 SV=2	Q16795	43 kDa	3	0	0	0	4	0
Protein transport protein Sec16A OS=Homo sapiens GN=SEC16A PE=1 SV=3	O15027	234 kDa	0	4	0	0	6	0
Aminoacyl tRNA synthase complex-interacting multifunctional protein 1 OS=Homo sapiens GN=AIMP1 PE=1 SV=2	Q12904	34 kDa	2	0	0	0	6	0
WEAK: present in both samples, absent from one negative								
Emerin OS=Homo sapiens GN=EMD PE=1 SV=1	P50402	29 kDa	8	0	0			
D-3-phosphoglycerate dehydrogenase OS=Homo sapiens GN=PHGDH PE=1 SV=4	O43175	57 kDa	7	13	0			
60S ribosomal protein L15 OS=Homo sapiens GN=RPL15 PE=1 SV=2	P61313	24 kDa	5	4	0			
Polyadenylate-binding protein 1 OS=Homo sapiens GN=PABPC1 PE=1 SV=2	P11940	71 kDa	3	7	0			
40S ribosomal protein S5 OS=Homo sapiens GN=RPS5 PE=1 SV=4	P46782	23 kDa	5	7	0			
Importin subunit beta-1 OS=Homo sapiens GN=KPNB1 PE=1 SV=2	Q14974	97 kDa	2	9	0			
Brain acid soluble protein 1 OS=Homo sapiens GN=BASP1 PE=1 SV=2	P80723	23 kDa	0	18	0			
Glyceraldehyde-3-phosphate dehydrogenase OS=Homo sapiens GN=GAPDH PE=1 SV=3	P04406	36 kDa	6	6	0			
Protein RCC2 OS=Homo sapiens GN=RCC2 PE=1 SV=2	Q9P258	56 kDa	5	6	0			
Glucose-6-phosphate 1-dehydrogenase OS=Homo sapiens GN=G6PD PE=1 SV=4	P11413	59 kDa	7	0	0			
Vesicle-trafficking protein SEC22b OS=Homo sapiens GN=SEC22B PE=1 SV=3	O75396	25 kDa	3	9	0			
Sorting and assembly machinery component 50 homolog OS=Homo sapiens GN=SAMM50 PE=1 SV=3	Q9Y512	52 kDa	10	0	0			
Tubulin alpha-1B chain OS=Homo sapiens GN=TUBA1B PE=1 SV=1	P68363	50 kDa	31	0	0			
Tropomyosin alpha-3 chain OS=Homo sapiens GN=TPM3 PE=1 SV=1	P06753	33 kDa	7	0	0			
NADH-cytochrome b5 reductase 3 OS=Homo sapiens GN=CYB5R3 PE=1 SV=3	P00387	34 kDa	4	4	0			
Cytoplasmic dynein 1 heavy chain 1 OS=Homo sapiens GN=DYNC1H1 PE=1 SV=5	Q14204	532 kDa	0	10	0			
Ras-related protein Rab-5C OS=Homo sapiens GN=RAB5C PE=1 SV=2	P51148	23 kDa	2	6	0			
Folate receptor alpha OS=Homo sapiens GN=FOLR1 PE=1 SV=3	P15328	30 kDa	5	0	0			
Exportin-2 OS=Homo sapiens GN=CSE1L PE=1 SV=3	P55060	110 kDa	0	4	0			
Inosine-5'-monophosphate dehydrogenase 2 OS=Homo sapiens GN=IMPDH2 PE=1 SV=2	P12268	56 kDa	3	6	0			
Sarcoplasmic/endoplasmic reticulum calcium ATPase 2 OS=Homo sapiens GN=ATP2A2 PE=1 SV=1	P16615	115 kDa	0	13	0			
60S ribosomal protein L10 OS=Homo sapiens GN=RPL10 PE=1 SV=4	P27635	25 kDa	2	0	0			
Cytoskeleton-associated protein 4 OS=Homo sapiens GN=CKAP4 PE=1 SV=2	Q07065	66 kDa	5	0	0			
Elongation factor 2 OS=Homo sapiens GN=EEF2 PE=1 SV=4	P13639	95 kDa	0	4	0			
Nuclear pore complex protein Nup155 OS=Homo sapiens GN=NUP155 PE=1 SV=1	O75694	155 kDa	0	7	0			

Vesicle-associated membrane protein-associated protein B/C OS=Homo sapiens GN=VAPB PE=1 SV=3	O95292	27 kDa	0	4	0			
Signal recognition particle receptor subunit beta OS=Homo sapiens GN=SRPRB PE=1 SV=3	Q9Y5M8	30 kDa	3	4	0			
Phenylalanyl-tRNA synthetase alpha chain OS=Homo sapiens GN=FARSA PE=1 SV=3	Q9Y285	58 kDa	4	0	0			
Twinfilin-2 OS=Homo sapiens GN=TWF2 PE=1 SV=2	Q6IBS0	40 kDa	4	0	0			
Heterogeneous nuclear ribonucleoprotein A/B OS=Homo sapiens GN=HNRNPAB PE=1 SV=2	Q99729	36 kDa	3	0	0			
Elongation factor 1-delta OS=Homo sapiens GN=EEF1D PE=1 SV=5	P29692	31 kDa	0	4	0			
Tight junction protein ZO-1 OS=Homo sapiens GN=TJP1 PE=1 SV=3	Q07157	195 kDa	3	0	0			
Four and a half LIM domains protein 2 OS=Homo sapiens GN=FHL2 PE=1 SV=3	Q14192	32 kDa	0	4	0			
Drebrin-like protein OS=Homo sapiens GN=DBNL PE=1 SV=1	Q9UJU6	48 kDa	4	0	0			
Ras-related protein Rab-2A OS=Homo sapiens GN=RAB2A PE=1 SV=1	P61019	24 kDa	0	4	0			
Carbonyl reductase [NADPH] 1 OS=Homo sapiens GN=CBR1 PE=1 SV=3	P16152	30 kDa	3	0	0			
Long-chain-fatty-acid--CoA ligase 3 OS=Homo sapiens GN=ACSL3 PE=1 SV=3	O95573	80 kDa	3	0	0			
Isochorismatase domain-containing protein 2, mitochondrial OS=Homo sapiens GN=ISOC2 PE=1 SV=1	Q96AB3	22 kDa	2	0	0			
Protein disulfide-isomerase A3 OS=Homo sapiens GN=PDIA3 PE=1 SV=4	P30101	57 kDa	2	0	0			
Neutral amino acid transporter B(0) OS=Homo sapiens GN=SLC1A5 PE=1 SV=2	Q15758	57 kDa	0	7	0			
Glutathione reductase, mitochondrial OS=Homo sapiens GN=GSR PE=1 SV=2	P00390	56 kDa	5	0	0			
T-complex protein 1 subunit beta OS=Homo sapiens GN=CCT2 PE=1 SV=4	P78371	57 kDa	3	0	0			
ATP-dependent RNA helicase DDX3X OS=Homo sapiens GN=DDX3X PE=1 SV=3	O00571	73 kDa	0	6	0			
Alkaline phosphatase, tissue-nonspecific isozyme OS=Homo sapiens GN=ALPL PE=1 SV=4	P05186	57 kDa	0	4	0			
Trifunctional enzyme subunit alpha, mitochondrial OS=Homo sapiens GN=HADHA PE=1 SV=2	P40939	83 kDa	0	4	0			
Glutathione S-transferase P OS=Homo sapiens GN=GSTP1 PE=1 SV=2	P09211	23 kDa	2	0	0			
Lamin-B1 OS=Homo sapiens GN=LMNB1 PE=1 SV=2	P20700	66 kDa	0	4	0			
Thymidine kinase, cytosolic OS=Homo sapiens GN=TK1 PE=1 SV=2	P04183	25 kDa	0	6	0			
Sodium/potassium-transporting ATPase subunit alpha-1 OS=Homo sapiens GN=ATP1A1 PE=1 SV=1	P05023	113 kDa	0	6	0			
40S ribosomal protein S27a OS=Homo sapiens GN=RPS27A PE=1 SV=1	P62979 (+3)	9 kDa				9	5	0
60S ribosomal protein L18 OS=Homo sapiens GN=RPL18 PE=1 SV=2	Q07020	22 kDa				6	4	0
60S ribosomal protein L14 OS=Homo sapiens GN=RPL14 PE=1 SV=4	P50914	23 kDa				5	5	0
Histone H1.2 OS=Homo sapiens GN=HIST1H1C PE=1 SV=2	P16403	21 kDa				4	4	0
Ras-related protein Rab-1A OS=Homo sapiens GN=RAB1A PE=1 SV=3	P62820	23 kDa				6	6	0
Interleukin enhancer-binding factor 2 OS=Homo sapiens GN=ILF2 PE=1 SV=2	Q12905	43 kDa				4	4	0
60S ribosomal protein L10a OS=Homo sapiens GN=RPL10A PE=1 SV=2	P62906	25 kDa				4	4	0
Polypeptide N-acetylgalactosaminyltransferase 2 OS=Homo sapiens GN=GALNT2 PE=1 SV=1	Q10471	65 kDa				0	6	0
Calcyclin-binding protein OS=Homo sapiens GN=CACYBP PE=1 SV=2	Q9HB71	26 kDa				0	3	0
Heterogeneous nuclear ribonucleoprotein A3 OS=Homo sapiens GN=HNRNPA3 PE=1 SV=2	P51991	40 kDa				0	6	0
Guanine nucleotide-binding protein G(I)/G(S)/G(T) subunit beta-1 OS=Homo sapiens GN=GNB1 PE=1 SV=3	P62873	37 kDa				6	0	0
Isoamyl acetate-hydrolyzing esterase 1 homolog OS=Homo sapiens GN=IAH1 PE=1 SV=1	Q2TAA2	28 kDa				4	0	0
Myosin-Ib OS=Homo sapiens GN=MYO1B PE=1 SV=3	O43795	132 kDa				0	4	0
Transforming protein RhoA OS=Homo sapiens GN=RHOA PE=1 SV=1	P61586	22 kDa				0	3	0
UPF0568 protein C14orf166 OS=Homo sapiens GN=C14orf166 PE=1 SV=1	Q9Y224	28 kDa				0	4	0
Prostaglandin E synthase 2 OS=Homo sapiens GN=PTGES2 PE=1 SV=1	Q9H7Z7	42 kDa				0	3	0
60S ribosomal protein L24 OS=Homo sapiens GN=RPL24 PE=1 SV=1	P83731	18 kDa				0	4	0
X-ray repair cross-complementing protein 6 OS=Homo sapiens GN=XRCC6 PE=1 SV=2	P12956	70 kDa				0	3	0
Cellular nucleic acid-binding protein OS=Homo sapiens GN=CNBP PE=1 SV=1	P62633	19 kDa				0	3	0
WEAK: present in one sample, absent from negative								
Tubulin alpha-1C chain OS=Homo sapiens GN=TUBA1C PE=1 SV=1	Q9BQE3	50 kDa	28	0	0			
40S ribosomal protein S17 OS=Homo sapiens GN=RPS17 PE=1 SV=2	P08708	16 kDa	8	0	0			
40S ribosomal protein S10 OS=Homo sapiens GN=RPS10 PE=1 SV=1	P46783	19 kDa	3	10	0			
NADPH--cytochrome P450 reductase OS=Homo sapiens GN=POR PE=1 SV=2	P16435	77 kDa	0	18	0			
60S ribosomal protein L36a OS=Homo sapiens GN=RPL36A PE=1 SV=2	P83881	12 kDa	4	9	0			
40S ribosomal protein S26 OS=Homo sapiens GN=RPS26 PE=1 SV=3	P62854	13 kDa	0	10	0			
60S ribosomal protein L30 OS=Homo sapiens GN=RPL30 PE=1 SV=2	P62888	13 kDa	5	7	0			
60S ribosomal protein L23 OS=Homo sapiens GN=RPL23 PE=1 SV=1	P62829	15 kDa	5	0	0			
60S ribosomal protein L13a OS=Homo sapiens GN=RPL13A PE=1 SV=2	P40429	24 kDa	2	0	0			
Transmembrane emp24 domain-containing protein 10 OS=Homo sapiens GN=TMED10 PE=1 SV=2	P49755	25 kDa	3	0	0			
60S ribosomal protein L31 OS=Homo sapiens GN=RPL31 PE=1 SV=1	P62899	14 kDa	2	0	0			
40S ribosomal protein S11 OS=Homo sapiens GN=RPS11 PE=1 SV=3	P62280	18 kDa	3	0	0			
Actin-binding LIM protein 1 OS=Homo sapiens GN=ABLIM1 PE=1 SV=3	O14639	88 kDa	3	0	0			
Non-POU domain-containing octamer-binding protein OS=Homo sapiens GN=NONO PE=1 SV=4	Q15233	54 kDa	0	15	0			
60S ribosomal protein L21 OS=Homo sapiens GN=RPL21 PE=1 SV=2	P46778	19 kDa	0	4	0			
Casein kinase I isoform alpha OS=Homo sapiens GN=CSNK1A1 PE=1 SV=2	P48729	39 kDa	0	7	0			
Histone-binding protein RBBP4 OS=Homo sapiens GN=RBBP4 PE=1 SV=3	Q09028	48 kDa	5	4	0			
Uncharacterized protein C19orf21 OS=Homo sapiens GN=C19orf21 PE=1 SV=1	Q8IVT2	75 kDa	4	0	0			
60S ribosomal protein L11 OS=Homo sapiens GN=RPL11 PE=1 SV=2	P62913	20 kDa	4	0	0			
Tropomyosin beta chain OS=Homo sapiens GN=TPM2 PE=1 SV=1	P07951	33 kDa	8	0	0			
Eukaryotic translation initiation factor 5A-1 OS=Homo sapiens GN=EIF5A PE=1	P63241	17 kDa	2	0	0			

SV=2								
60S ribosomal protein L9 OS=Homo sapiens GN=RPL9 PE=1 SV=1	P32969	22 kDa	3	0	0			
Eukaryotic translation initiation factor 2 subunit 1 OS=Homo sapiens GN=EIF2S1 PE=1 SV=3	P05198	36 kDa	0	6	0			
Cytochrome c oxidase subunit 2 OS=Homo sapiens GN=MT-CO2 PE=1 SV=1	P00403	26 kDa	4	0	0			
60S ribosomal protein L32 OS=Homo sapiens GN=RPL32 PE=1 SV=2	P62910	16 kDa	3	0	0			
Aspartyl/asparaginyl beta-hydroxylase OS=Homo sapiens GN=ASPH PE=1 SV=3	Q12797	86 kDa	2	4	0			
Transmembrane protein 43 OS=Homo sapiens GN=TMEM43 PE=1 SV=1	Q9BTV4	45 kDa	3	0	0			
CDGSH iron-sulfur domain-containing protein 2 OS=Homo sapiens GN=CISD2 PE=1 SV=1	Q8N5K1	15 kDa	0	4	0			
Inositol 1,4,5-trisphosphate receptor type 3 OS=Homo sapiens GN=ITPR3 PE=1 SV=2	Q14573	304 kDa	5	0	0			
Actin-related protein 2/3 complex subunit 4 OS=Homo sapiens GN=ARPC4 PE=1 SV=3	P59998	20 kDa	2	0	0			
Lysophosphatidylcholine acyltransferase 1 OS=Homo sapiens GN=LPCAT1 PE=1 SV=2	Q8NF37	59 kDa	2	0	0			
Minor histocompatibility antigen H13 OS=Homo sapiens GN=HM13 PE=1 SV=1	Q8TCT9	41 kDa	0	7	0			
Core histone macro-H2A.1 OS=Homo sapiens GN=H2AFY PE=1 SV=4	O75367	40 kDa	3	0	0			
Metallothionein-2 OS=Homo sapiens GN=MT2A PE=1 SV=1	P02795	6 kDa	0	6	0			
ADP-ribosylation factor 4 OS=Homo sapiens GN=ARF4 PE=1 SV=3	P18085	21 kDa	3	0	0			
Transketolase OS=Homo sapiens GN=TKT PE=1 SV=3	P29401	68 kDa	3	0	0			
Beta-1,4-galactosyltransferase 1 OS=Homo sapiens GN=B4GALT1 PE=1 SV=5	P15291	44 kDa	2	0	0			
Tubulin alpha-4A chain OS=Homo sapiens GN=TUBA4A PE=1 SV=1	P68366	50 kDa	21	0	0			
Bone marrow stromal antigen 2 OS=Homo sapiens GN=BST2 PE=1 SV=1	Q10589	20 kDa	2	0	0			
Poly(rC)-binding protein 2 OS=Homo sapiens GN=PCBP2 PE=1 SV=1	Q15366	39 kDa	4	0	0			
Protein FAM162A OS=Homo sapiens GN=FAM162A PE=1 SV=2	Q96A26	17 kDa	0	4	0			
Myosin phosphatase Rho-interacting protein OS=Homo sapiens GN=MPRIP PE=1 SV=3	Q6WCQ1	117 kDa	0	4	0			
Prostaglandin E synthase OS=Homo sapiens GN=PTGES PE=1 SV=2	O14684	17 kDa	0	4	0			
RNA-binding protein 4 OS=Homo sapiens GN=RBM4 PE=1 SV=1	Q9BWF3	40 kDa	3	0	0			
Tricarboxylate transport protein, mitochondrial OS=Homo sapiens GN=SLC25A1 PE=1 SV=2	P53007	34 kDa	2	0	0			
Surfeit locus protein 4 OS=Homo sapiens GN=SURF4 PE=1 SV=3	O15260	30 kDa	0	4	0			
Leucine-rich repeat flightless-interacting protein 2 OS=Homo sapiens GN=LRRFIP2 PE=1 SV=1	Q9Y608	82 kDa	2	0	0			
Metaxin-1 OS=Homo sapiens GN=MTX1 PE=1 SV=2	Q13505	51 kDa	2	0	0			
Signal peptidase complex subunit 2 OS=Homo sapiens GN=SPCS2 PE=1 SV=3	Q15005	25 kDa	0	4	0			
ATPase family AAA domain-containing protein 1 OS=Homo sapiens GN=ATAD1 PE=1 SV=1	Q8NBU5	41 kDa	2	0	0			
Actin, alpha cardiac muscle 1 OS=Homo sapiens GN=ACTC1 PE=1 SV=1	P68032 (+1)	42 kDa				0	47	0
Nesprin-2 OS=Homo sapiens GN=SYNE2 PE=1 SV=3	Q8WXH0	796 kDa				11	7	0
Basigin OS=Homo sapiens GN=BSG PE=1 SV=2	P35613	42 kDa				4	10	0
Hsp70-binding protein 1 OS=Homo sapiens GN=HSPBP1 PE=1 SV=1	Q9NZL4	39 kDa				10	6	0
Importin-7 OS=Homo sapiens GN=IPO7 PE=1 SV=1	O95373	120 kDa				0	11	0
Thrombospondin-1 OS=Homo sapiens GN=THBS1 PE=1 SV=2	P07996	129 kDa				0	16	0
Mitotic checkpoint protein BUB3 OS=Homo sapiens GN=BUB3 PE=1 SV=1	O43684	37 kDa				3	6	0
Protein arginine N-methyltransferase 1 OS=Homo sapiens GN=PRMT1 PE=1 SV=2	Q99873	42 kDa				0	7	0
Proteasome activator complex subunit 1 OS=Homo sapiens GN=PSME1 PE=1 SV=1	Q06323	29 kDa				8	5	0
Ribonucleoside-diphosphate reductase large subunit OS=Homo sapiens GN=RRM1 PE=1 SV=1	P23921	90 kDa				3	7	0
Transcription intermediary factor 1-beta OS=Homo sapiens GN=TRIM28 PE=1 SV=5	Q13263	89 kDa				3	9	0
Microtubule-associated protein 4 OS=Homo sapiens GN=MAP4 PE=1 SV=3	P27816	121 kDa				0	6	0
Cell division protein kinase 9 OS=Homo sapiens GN=CDK9 PE=1 SV=3	P50750	43 kDa				3	3	0
Ras-related protein Rab-11B OS=Homo sapiens GN=RAB11B PE=1 SV=4	Q15907	24 kDa				4	4	0
Polypyrimidine tract-binding protein 1 OS=Homo sapiens GN=PTBP1 PE=1 SV=1	P26599	57 kDa				0	5	0
DnaJ homolog subfamily C member 10 OS=Homo sapiens GN=DNAJC10 PE=1 SV=2	Q8IXB1	91 kDa				0	11	0
Heat shock protein 105 kDa OS=Homo sapiens GN=HSPH1 PE=1 SV=1	Q92598	97 kDa				4	6	0
Adenosylhomocysteinase OS=Homo sapiens GN=AHCY PE=1 SV=4	P23526	48 kDa				4	4	0
U2 small nuclear ribonucleoprotein A' OS=Homo sapiens GN=SNRPA1 PE=1 SV=2	P09661	28 kDa				0	5	0
T-complex protein 1 subunit epsilon OS=Homo sapiens GN=CCT5 PE=1 SV=1	P48643	60 kDa				0	5	0
Matrin-3 OS=Homo sapiens GN=MATR3 PE=1 SV=2	P43243	95 kDa				4	5	0
Palladin OS=Homo sapiens GN=PALLD PE=1 SV=2	Q8WX93	151 kDa				8	4	0
LanC-like protein 1 OS=Homo sapiens GN=LANCL1 PE=1 SV=1	O43813	45 kDa				0	4	0
26S proteasome non-ATPase regulatory subunit 13 OS=Homo sapiens GN=PSMD13 PE=1 SV=1	Q9UNM6	43 kDa				5	4	0
Apoptosis-inducing factor 1, mitochondrial OS=Homo sapiens GN=AIFM1 PE=1 SV=1	O95831	67 kDa				0	5	0
Ras-related protein Rab-6A OS=Homo sapiens GN=RAB6A PE=1 SV=3	P20340	24 kDa				0	5	0
Carnitine O-palmitoyltransferase 1, liver isoform OS=Homo sapiens GN=CPT1A PE=1 SV=2	P50416	88 kDa				0	5	0
Peroxiredoxin-6 OS=Homo sapiens GN=PRDX6 PE=1 SV=3	P30041	25 kDa				0	4	0
Zinc finger CCCH-type antiviral protein 1-like OS=Homo sapiens GN=ZC3HAV1L PE=1 SV=2	Q96H79	33 kDa				4	0	0
Heterogeneous nuclear ribonucleoprotein G OS=Homo sapiens GN=RBMX PE=1 SV=3	P38159	42 kDa				0	4	0
Isoleucyl-tRNA synthetase, cytoplasmic OS=Homo sapiens GN=IARS PE=1 SV=2	P41252	145 kDa				0	4	0
Opioid growth factor receptor OS=Homo sapiens GN=OGFR PE=1 SV=3	Q9NZT2	73 kDa				3	4	0

Basic leucine zipper and W2 domain-containing protein 2 OS=Homo sapiens GN=BZW2 PE=1 SV=1	Q9Y6E2	48 kDa				0	3	0
rRNA 2'-O-methyltransferase fibrillarin OS=Homo sapiens GN=FBL PE=1 SV=2	P22087	34 kDa				0	6	0
Developmentally-regulated GTP-binding protein 1 OS=Homo sapiens GN=DRG1 PE=1 SV=1	Q9Y295	41 kDa				0	5	0
Protein transport protein Sec61 subunit alpha isoform 1 OS=Homo sapiens GN=SEC61A1 PE=1 SV=2	P61619	52 kDa				0	4	0
Guanine nucleotide-binding protein G(s) subunit alpha isoforms short OS=Homo sapiens GN=GNAS PE=1 SV=1	P63092 (+1)	46 kDa				0	5	0
Peroxisomal 2,4-dienoyl-CoA reductase OS=Homo sapiens GN=DECR2 PE=1 SV=1	Q9NUI1	31 kDa				6	0	0
Guanine deaminase OS=Homo sapiens GN=GDA PE=1 SV=1	Q9Y2T3	51 kDa				0	3	0
Aminopeptidase B OS=Homo sapiens GN=RNPEP PE=1 SV=2	Q9H4A4	73 kDa				0	3	0
Cytosolic phospholipase A2 OS=Homo sapiens GN=PLA2G4A PE=1 SV=1	P47712	85 kDa				0	4	0
Cytochrome b5 type B OS=Homo sapiens GN=CYB5B PE=1 SV=2	O43169	16 kDa				0	4	0
Probable glutathione peroxidase 8 OS=Homo sapiens GN=GPX8 PE=1 SV=2	Q8TED1	24 kDa				0	3	0
Ras-related protein Rap-1b OS=Homo sapiens GN=RAP1B PE=1 SV=1	P61224	21 kDa				0	5	0
Histone deacetylase 10 OS=Homo sapiens GN=HDAC10 PE=1 SV=1	Q969S8	71 kDa				0	3	0
Heat shock protein HSP 90-alpha OS=Homo sapiens GN=HSP90AA1 PE=1 SV=5	P07900	85 kDa				0	8	0
Membrane-associated progesterone receptor component 2 OS=Homo sapiens GN=PGRMC2 PE=1 SV=1	O15173	24 kDa				3	4	0
Ras-related protein Rab-18 OS=Homo sapiens GN=RAB18 PE=1 SV=1	Q9NP72	23 kDa				3	4	0
Lamina-associated polypeptide 2, isoforms beta/gamma OS=Homo sapiens GN=TMPO PE=1 SV=2	P42167	51 kDa				3	3	0
NADH dehydrogenase [ubiquinone] iron-sulfur protein 3, mitochondrial OS=Homo sapiens GN=NDUFS3 PE=1 SV=1	O75489	30 kDa				5	0	0
Arginyl-tRNA synthetase, cytoplasmic OS=Homo sapiens GN=RARS PE=1 SV=2	P54136	75 kDa				0	4	0
Dolichyl-diphosphooligosaccharide--protein glycosyltransferase 48 kDa subunit OS=Homo sapiens GN=DDOST PE=1 SV=4	P39656	51 kDa				0	5	0
Methyltransferase-like protein 11A OS=Homo sapiens GN=METTL11A PE=1 SV=3	Q9BV86	25 kDa				4	0	0
14-3-3 protein zeta/delta OS=Homo sapiens GN=YWHAZ PE=1 SV=1	P63104	28 kDa				6	0	0
Monocarboxylate transporter 4 OS=Homo sapiens GN=SLC16A3 PE=1 SV=1	O15427	49 kDa				0	4	0
Tubulin beta-3 chain OS=Homo sapiens GN=TUBB3 PE=1 SV=2	Q13509	50 kDa				0	20	0
Ataxin-10 OS=Homo sapiens GN=ATXN10 PE=1 SV=1	Q9UBB4	53 kDa				0	5	0
Succinate dehydrogenase [ubiquinone] iron-sulfur subunit, mitochondrial OS=Homo sapiens GN=SDHB PE=1 SV=3	P21912	32 kDa				4	0	0
Growth factor receptor-bound protein 2 OS=Homo sapiens GN=GRB2 PE=1 SV=1	P62993	25 kDa				5	0	0
Endoplasmic reticulum-Golgi intermediate compartment protein 1 OS=Homo sapiens GN=ERGIC1 PE=1 SV=1	Q969X5	33 kDa				0	4	0
26S protease regulatory subunit 8 OS=Homo sapiens GN=PSMC5 PE=1 SV=1	P62195	46 kDa				0	4	0
Ras-related protein Ral-A OS=Homo sapiens GN=RALA PE=1 SV=1	P11233	24 kDa				0	5	0
Perilipin-3 OS=Homo sapiens GN=PLIN3 PE=1 SV=2	O60664	47 kDa				0	6	0
Myristoylated alanine-rich C-kinase substrate OS=Homo sapiens GN=MARCKS PE=1 SV=4	P29966	32 kDa				0	6	0
HLA class I histocompatibility antigen, B-55 alpha chain OS=Homo sapiens GN=HLA-B PE=1 SV=1	P30493 (+1)	40 kDa				0	8	0
26S protease regulatory subunit 10B OS=Homo sapiens GN=PSMC6 PE=1 SV=1	P62333	44 kDa				3	0	0
Ras-related protein Rab-10 OS=Homo sapiens GN=RAB10 PE=1 SV=1	P61026	23 kDa				0	6	0
Serine/threonine-protein phosphatase 2A 55 kDa regulatory subunit B alpha isoform OS=Homo sapiens GN=PPP2R2A PE=1 SV=1	P63151	52 kDa				0	6	0
Thyroid receptor-interacting protein 13 OS=Homo sapiens GN=TRIP13 PE=1 SV=2	Q15645	49 kDa				0	5	0
AH receptor-interacting protein OS=Homo sapiens GN=AIP PE=1 SV=2	O00170	38 kDa				0	6	0
26S proteasome non-ATPase regulatory subunit 2 OS=Homo sapiens GN=PSMD2 PE=1 SV=3	Q13200	100 kDa				4	0	0
Cell division protein kinase 1 OS=Homo sapiens GN=CDK1 PE=1 SV=2	P06493	34 kDa				0	6	0
Serine/threonine-protein kinase 6 OS=Homo sapiens GN=AURKA PE=1 SV=2	O14965	46 kDa				0	5	0
Aminopeptidase N OS=Homo sapiens GN=ANPEP PE=1 SV=4	P15144	110 kDa				0	6	0
Actin-binding protein anillin OS=Homo sapiens GN=ANLN PE=1 SV=2	Q9NQW6	124 kDa				0	5	0
ADP-ribosylation factor-like protein 15 OS=Homo sapiens GN=ARL15 PE=1 SV=1	Q9NXU5	23 kDa				3	0	0
UDP-N-acetylglucosamine--peptide N-acetylglucosaminyltransferase 110 kDa subunit OS=Homo sapiens GN=OGT PE=1 SV=3	O15294	117 kDa				4	0	0
Plasma membrane calcium-transporting ATPase 1 OS=Homo sapiens GN=ATP2B1 PE=1 SV=3	P20020	139 kDa				0	4	0
Thioredoxin-related transmembrane protein 1 OS=Homo sapiens GN=TMX1 PE=1 SV=1	Q9H3N1	32 kDa				0	3	0
Ras-related protein Rab-32 OS=Homo sapiens GN=RAB32 PE=1 SV=3	Q13637	25 kDa				0	4	0
Epoxide hydrolase 1 OS=Homo sapiens GN=EPHX1 PE=1 SV=1	P07099	53 kDa				0	3	0
Proteasome subunit beta type-5 OS=Homo sapiens GN=PSMB5 PE=1 SV=3	P28074	28 kDa				3	4	0
Proteasome subunit alpha type-1 OS=Homo sapiens GN=PSMA1 PE=1 SV=1	P25786	30 kDa				0	3	0
Extended synaptotagmin-2 OS=Homo sapiens GN=ESYT2 PE=1 SV=1	A0FGR8	102 kDa				3	3	0
Proteasome subunit alpha type-5 OS=Homo sapiens GN=PSMA5 PE=1 SV=3	P28066	26 kDa				3	0	0
Splicing factor, arginine/serine-rich 7 OS=Homo sapiens GN=SFRS7 PE=1 SV=1	Q16629	27 kDa				0	3	0
Glucosidase 2 subunit beta OS=Homo sapiens GN=PRKCSH PE=1 SV=2	P14314	59 kDa				0	4	0
Pyrroline-5-carboxylate reductase 3 OS=Homo sapiens GN=PYCRL PE=1 SV=2	Q53H96	29 kDa				5	0	0
Histone acetyltransferase type B catalytic subunit OS=Homo sapiens GN=HAT1 PE=1 SV=1	O14929	50 kDa				0	4	0
Putative pre-mRNA-splicing factor ATP-dependent RNA helicase DHX15 OS=Homo sapiens GN=DHX15 PE=1 SV=2	O43143	91 kDa				0	5	0
X-ray repair cross-complementing protein 5 OS=Homo sapiens GN=XRCC5 PE=1 SV=3	P13010	83 kDa				0	3	0

ADP-ribosylation factor-like protein 6-interacting protein 6 OS=Homo sapiens GN=ARL6IP6 PE=1 SV=1	Q8N6S5	25 kDa				4	4	0
Cytospin-A OS=Homo sapiens GN=CYTSA PE=1 SV=2	Q69YQ0	125 kDa				0	3	0
Tubulin beta-6 chain OS=Homo sapiens GN=TUBB6 PE=1 SV=1	Q9BUF5	50 kDa				13	0	0
Lamin-B2 OS=Homo sapiens GN=LMNB2 PE=1 SV=3	Q03252	68 kDa				6	0	0
Nicalin OS=Homo sapiens GN=NCLN PE=1 SV=2	Q969V3	63 kDa				0	4	0
N(2),N(2)-dimethylguanosine tRNA methyltransferase OS=Homo sapiens GN=TRMT1 PE=1 SV=1	Q9NXH9	72 kDa				0	3	0
Eukaryotic translation initiation factor 4E OS=Homo sapiens GN=EIF4E PE=1 SV=2	P06730	25 kDa				3	0	0
Leukocyte elastase inhibitor OS=Homo sapiens GN=SERPINB1 PE=1 SV=1	P30740	43 kDa				3	0	0
Proteasome subunit alpha type-4 OS=Homo sapiens GN=PSMA4 PE=1 SV=1	P25789	29 kDa				3	0	0
28S ribosomal protein S22, mitochondrial OS=Homo sapiens GN=MRPS22 PE=1 SV=1	P82650	41 kDa				3	0	0
Glutathione peroxidase 1 OS=Homo sapiens GN=GPX1 PE=1 SV=3	P07203	22 kDa				4	0	0
E3 SUMO-protein ligase RanBP2 OS=Homo sapiens GN=RANBP2 PE=1 SV=2	P49792	358 kDa				0	5	0
Heterogeneous nuclear ribonucleoprotein F OS=Homo sapiens GN=HNRNPF PE=1 SV=3	P52597	46 kDa				0	5	0
Atlastin-3 OS=Homo sapiens GN=ATL3 PE=1 SV=1	Q6DD88	61 kDa				0	5	0
Tyrosine-protein phosphatase non-receptor type 1 OS=Homo sapiens GN=PTPN1 PE=1 SV=1	P18031	50 kDa				0	4	0
Signal transducer and activator of transcription 3 OS=Homo sapiens GN=STAT3 PE=1 SV=2	P40763	88 kDa				0	4	0
Secretory carrier-associated membrane protein 3 OS=Homo sapiens GN=SCAMP3 PE=1 SV=3	O14828	38 kDa				0	5	0
Ras-related C3 botulinum toxin substrate 1 OS=Homo sapiens GN=RAC1 PE=1 SV=1	P63000	21 kDa				3	0	0
Adenylate kinase 2, mitochondrial OS=Homo sapiens GN=AK2 PE=1 SV=2	P54819	26 kDa				4	0	0
Myeloid differentiation primary response protein MyD88 OS=Homo sapiens GN=MYD88 PE=1 SV=1	Q99836	33 kDa				5	0	0
Uncharacterized protein C2orf47, mitochondrial OS=Homo sapiens GN=C2orf47 PE=1 SV=1	Q8WWC4	33 kDa				4	0	0
Myosin-X OS=Homo sapiens GN=MYO10 PE=1 SV=3	Q9HD67	237 kDa				0	5	0
Heme oxygenase 2 OS=Homo sapiens GN=HMOX2 PE=1 SV=2	P30519	36 kDa				0	4	0
Calumenin OS=Homo sapiens GN=CALU PE=1 SV=2	O43852	37 kDa				0	5	0
Retinoic acid-induced protein 3 OS=Homo sapiens GN=GPRC5A PE=1 SV=2	Q8NFJ5	40 kDa				0	5	0
G2/mitotic-specific cyclin-B1 OS=Homo sapiens GN=CCNB1 PE=1 SV=1	P14635	48 kDa				0	6	0
Enoyl-CoA hydratase, mitochondrial OS=Homo sapiens GN=ECHS1 PE=1 SV=4	P30084	31 kDa				3	0	0
Thyroid receptor-interacting protein 6 OS=Homo sapiens GN=TRIP6 PE=1 SV=3	Q15654	50 kDa				3	0	0
Cytokine receptor-like factor 1 OS=Homo sapiens GN=CRLF1 PE=1 SV=1	O75462	46 kDa				3	0	0
Translin OS=Homo sapiens GN=TSN PE=1 SV=1	Q15631	26 kDa				0	3	0
DNA damage-binding protein 1 OS=Homo sapiens GN=DDB1 PE=1 SV=1	Q16531	127 kDa				0	3	0
Oxidoreductase HTATIP2 OS=Homo sapiens GN=HTATIP2 PE=1 SV=1	Q9BUP3	27 kDa				0	3	0
Exosome complex exonuclease RRP41 OS=Homo sapiens GN=EXOSC4 PE=1 SV=3	Q9NPD3	26 kDa				0	3	0
NAD-dependent deacetylase sirtuin-5 OS=Homo sapiens GN=SIRT5 PE=1 SV=2	Q9NXA8	34 kDa				0	3	0
Eukaryotic translation initiation factor 3 subunit H OS=Homo sapiens GN=EIF3H PE=1 SV=1	O15372	40 kDa				0	3	0
Ribose-phosphate pyrophosphokinase 1 OS=Homo sapiens GN=PRPS1 PE=1 SV=2	P60891	35 kDa				0	3	0
Integrin beta-1 OS=Homo sapiens GN=ITGB1 PE=1 SV=2	P05556	88 kDa				0	3	0
UBX domain-containing protein 4 OS=Homo sapiens GN=UBXN4 PE=1 SV=2	Q92575	57 kDa				0	3	0
28S ribosomal protein S29, mitochondrial OS=Homo sapiens GN=DAP3 PE=1 SV=1	P51398	46 kDa				3	0	0
GTP-binding protein SAR1a OS=Homo sapiens GN=SAR1A PE=1 SV=1	Q9NR31	22 kDa				0	3	0
Signal recognition particle receptor subunit alpha OS=Homo sapiens GN=SRPR PE=1 SV=2	P08240	70 kDa				0	3	0
ATPase ASNA1 OS=Homo sapiens GN=ASNA1 PE=1 SV=2	O43681	39 kDa				0	3	0
Calponin-3 OS=Homo sapiens GN=CNN3 PE=1 SV=1	Q15417	36 kDa				0	4	0
Cob(I)yrinic acid a,c-diamide adenosyltransferase, mitochondrial OS=Homo sapiens GN=MMAB PE=1 SV=1	Q96EY8	27 kDa				3	0	0
HCLS1-associated protein X-1 OS=Homo sapiens GN=HAX1 PE=1 SV=2	O00165	32 kDa				3	0	0
Cytospin-B OS=Homo sapiens GN=CYTSB PE=1 SV=1	Q5M775	119 kDa				0	3	0
L-lactate dehydrogenase B chain OS=Homo sapiens GN=LDHB PE=1 SV=2	P07195	37 kDa				0	4	0
Ran GTPase-activating protein 1 OS=Homo sapiens GN=RANGAP1 PE=1 SV=1	P46060	64 kDa				0	3	0
Phospholipid scramblase 1 OS=Homo sapiens GN=PLSCR1 PE=1 SV=1	O15162	35 kDa				0	3	0
Alpha-internexin OS=Homo sapiens GN=INA PE=1 SV=2	Q16352	55 kDa				5	0	0
Tubulin--tyrosine ligase-like protein 12 OS=Homo sapiens GN=TTLL12 PE=1 SV=2	Q14166	74 kDa				3	0	0
PDZ and LIM domain protein 5 OS=Homo sapiens GN=PDLIM5 PE=1 SV=4	Q96HC4	64 kDa				0	5	0
Cysteine-rich protein 2 OS=Homo sapiens GN=CRIP2 PE=1 SV=1	P52943	22 kDa				0	4	0
Heterogeneous nuclear ribonucleoprotein Q OS=Homo sapiens GN=SYNCRIP PE=1 SV=2	O60506	70 kDa				0	6	0
Sequestosome-1 OS=Homo sapiens GN=SQSTM1 PE=1 SV=1	Q13501	48 kDa				0	5	0
Cell division protein kinase 6 OS=Homo sapiens GN=CDK6 PE=1 SV=1	Q00534	37 kDa				0	6	0
Insulin-like growth factor-binding protein 7 OS=Homo sapiens GN=IGFBP7 PE=1 SV=1	Q16270	29 kDa				0	5	0
mRNA export factor OS=Homo sapiens GN=RAE1 PE=1 SV=1	P78406	41 kDa				3	0	0
Proteasome assembly chaperone 1 OS=Homo sapiens GN=PSMG1 PE=1 SV=1	O95456	33 kDa				0	3	0
E3 ubiquitin-protein ligase HUWE1 OS=Homo sapiens GN=HUWE1 PE=1 SV=3	Q7Z6Z7	482 kDa				0	3	0
26S proteasome non-ATPase regulatory subunit 11 OS=Homo sapiens GN=PSMD11 PE=1 SV=3	O00231	47 kDa				0	3	0

DNA-directed RNA polymerases I and III subunit RPAC1 OS=Homo sapiens GN=POLR1C PE=1 SV=1	O15160	39 kDa				0	3	0
Ras-related protein R-Ras OS=Homo sapiens GN=RRAS PE=1 SV=1	P10301	23 kDa				0	3	0
Sodium/potassium-transporting ATPase subunit beta-3 OS=Homo sapiens GN=ATP1B3 PE=1 SV=1	P54709	32 kDa				0	3	0
Transitional endoplasmic reticulum ATPase OS=Homo sapiens GN=VCP PE=1 SV=4	P55072	89 kDa				3	0	0
Inorganic pyrophosphatase 2, mitochondrial OS=Homo sapiens GN=PPA2 PE=1 SV=2	Q9H2U2	38 kDa				0	3	0
28S ribosomal protein S23, mitochondrial OS=Homo sapiens GN=MRPS23 PE=1 SV=2	Q9Y3D9	22 kDa				3	0	0
14-3-3 protein gamma OS=Homo sapiens GN=YWHAG PE=1 SV=2	P61981	28 kDa				6	0	0
Sepiapterin reductase OS=Homo sapiens GN=SPR PE=1 SV=1	P35270	28 kDa				0	3	0
RNA-binding protein Raly OS=Homo sapiens GN=RALY PE=1 SV=1	Q9UKM9	32 kDa				0	3	0
Testisin OS=Homo sapiens GN=PRSS21 PE=2 SV=1	Q9Y6M0	35 kDa				3	0	0
Spermidine synthase OS=Homo sapiens GN=SRM PE=1 SV=1	P19623	34 kDa				3	0	0
Phosphatidylinositol transfer protein beta isoform OS=Homo sapiens GN=PITPNB PE=1 SV=2	P48739	32 kDa				0	4	0
Alpha-soluble NSF attachment protein OS=Homo sapiens GN=NAPA PE=1 SV=3	P54920	33 kDa				0	4	0
Exportin-T OS=Homo sapiens GN=XPOT PE=1 SV=2	O43592	110 kDa				0	3	0
DnaJ homolog subfamily C member 11 OS=Homo sapiens GN=DNAJC11 PE=1 SV=2	Q9NVH1	63 kDa				3	0	0
Triple functional domain protein OS=Homo sapiens GN=TRIO PE=1 SV=2	O75962	347 kDa				0	3	0
CCR4-NOT transcription complex subunit 1 OS=Homo sapiens GN=CNOT1 PE=1 SV=2	A5YKK6	267 kDa				0	3	0
26S proteasome non-ATPase regulatory subunit 5 OS=Homo sapiens GN=PSMD5 PE=1 SV=3	Q16401	56 kDa				0	4	0
Syntenin-1 OS=Homo sapiens GN=SDCBP PE=1 SV=1	O00560	32 kDa				0	5	0
Connective tissue growth factor OS=Homo sapiens GN=CTGF PE=1 SV=2	P29279	38 kDa				0	5	0
Myb-binding protein 1A OS=Homo sapiens GN=MYBBP1A PE=1 SV=2	Q9BQG0	149 kDa				0	5	0
Coagulation factor V OS=Homo sapiens GN=F5 PE=1 SV=3	P12259	252 kDa				0	4	0
Suppressor of G2 allele of SKP1 homolog OS=Homo sapiens GN=SUGT1 PE=1 SV=3	Q9Y2Z0	41 kDa				3	0	0
Thioredoxin-like protein 1 OS=Homo sapiens GN=TXNL1 PE=1 SV=3	O43396	32 kDa				0	4	0
Heat shock 70 kDa protein 4 OS=Homo sapiens GN=HSPA4 PE=1 SV=4	P34932	94 kDa				0	3	0
Thioredoxin-dependent peroxide reductase, mitochondrial OS=Homo sapiens GN=PRDX3 PE=1 SV=3	P30048	28 kDa				3	0	0
Mitochondrial import inner membrane translocase subunit TIM44 OS=Homo sapiens GN=TIMM44 PE=1 SV=2	O43615	51 kDa				0	3	0
Calpastatin OS=Homo sapiens GN=CAST PE=1 SV=4	P20810	77 kDa				0	3	0
ADP-ribosylation factor GTPase-activating protein 1 OS=Homo sapiens GN=ARFGAP1 PE=1 SV=2	Q8N6T3	45 kDa				0	3	0
Coatomer subunit alpha OS=Homo sapiens GN=COPA PE=1 SV=2	P53621	138 kDa				0	3	0
Zinc finger ZZ-type and EF-hand domain-containing protein 1 OS=Homo sapiens GN=ZZEF1 PE=1 SV=6	O43149	331 kDa				0	4	0
Transforming growth factor beta-1-induced transcript 1 protein OS=Homo sapiens GN=TGFB1I1 PE=1 SV=2	O43294	50 kDa				0	4	0
A-kinase anchor protein 12 OS=Homo sapiens GN=AKAP12 PE=1 SV=3	Q02952	191 kDa				0	4	0
Proteasome-associated protein ECM29 homolog OS=Homo sapiens GN=ECM29 PE=1 SV=2	Q5VYK3	204 kDa				0	4	0
Testin OS=Homo sapiens GN=TES PE=1 SV=1	Q9UGI8	48 kDa				0	4	0
Multidrug resistance-associated protein 1 OS=Homo sapiens GN=ABCC1 PE=1 SV=3	P33527	172 kDa				0	4	0
CD97 antigen OS=Homo sapiens GN=CD97 PE=1 SV=4	P48960	92 kDa				0	4	0
Nexilin OS=Homo sapiens GN=NEXN PE=1 SV=1	Q0ZGT2	81 kDa				3	0	0
Transmembrane emp24 domain-containing protein 1 OS=Homo sapiens GN=TMED1 PE=1 SV=1	Q13445	25 kDa				0	4	0
Mitochondrial Rho GTPase 2 OS=Homo sapiens GN=RHOT2 PE=1 SV=2	Q8IXI1	68 kDa				3	0	0
Tetratricopeptide repeat protein 1 OS=Homo sapiens GN=TTC1 PE=1 SV=1	Q99614	34 kDa				0	4	0
Mitochondrial import receptor subunit TOM70 OS=Homo sapiens GN=TOMM70A PE=1 SV=1	O94826	67 kDa				0	3	0
DNA topoisomerase 2-alpha OS=Homo sapiens GN=TOP2A PE=1 SV=3	P11388	174 kDa				0	3	0
Tubulin gamma-1 chain OS=Homo sapiens GN=TUBG1 PE=1 SV=2	P23258 (+1)	51 kDa				0	3	0
EGF-containing fibulin-like extracellular matrix protein 1 OS=Homo sapiens GN=EFEMP1 PE=1 SV=2	Q12805	55 kDa				0	3	0
Chromobox protein homolog 3 OS=Homo sapiens GN=CBX3 PE=1 SV=4	Q13185	21 kDa				0	3	0
Protein LYRIC OS=Homo sapiens GN=MTDH PE=1 SV=2	Q86UE4	64 kDa				0	3	0
Retinol dehydrogenase 11 OS=Homo sapiens GN=RDH11 PE=1 SV=2	Q8TC12	35 kDa				0	3	0
39S ribosomal protein L4, mitochondrial OS=Homo sapiens GN=MRPL4 PE=1 SV=1	Q9BYD3	35 kDa				3	0	0
Phospholipase A-2-activating protein OS=Homo sapiens GN=PLAA PE=1 SV=2	Q9Y263	87 kDa				0	3	0
Endoplasmic reticulum-Golgi intermediate compartment protein 3 OS=Homo sapiens GN=ERGIC3 PE=1 SV=1	Q9Y282	43 kDa				0	3	0
Kinesin-like protein KIF20A OS=Homo sapiens GN=KIF20A PE=1 SV=1	O95235	100 kDa				0	3	0